URS 709-11

Final Report

STRUCTURAL RESPONSE and LOADING OF WALL PANELS

Contract No. DAHC20-67-C-0136

OCD Work Unit 1123E

Prepared for

OFFICE OF CIVIL DEFENSE
Office of the Secretary of the Army
Washington, D.C. 20310

URS RESEARCH COMPANY
155 Bovet Road, San Mateo, California 94402

Approved for public release; distribution unlimited.

Unclassified
Security Classification

DOCUMENT CONTROL DATA - R & D

(Security classification of title, body of abstract and indexing annotation must be entered when the overall report is classified)

1. ORIGINATING ACTIVITY (Corporate author) URS Research Company, 155 Bovet Road San Mateo, California 94402	2a. REPORT SECURITY CLASSIFICATION Unclassified 2b. GROUP

3. REPORT TITLE

STRUCTURAL RESPONSE AND LOADING OF WALL PANELS

4. DESCRIPTIVE NOTES (Type of report and inclusive dates)

Final Report

5. AUTHOR(S) (First name, middle initial, last name)

C. Wilton, B. Gabrielsen, P. Morris

6. REPORT DATE	7a. TOTAL NO. OF PAGES	7b. NO. OF REFS
July 1971	202	8

8a. CONTRACT OR GRANT NO.	9a. ORIGINATOR'S REPORT NUMBER(S)
DAHC20-67-C-0136 b. PROJECT NO. c. Work Unit 1123E d.	URS 709-11 9b. OTHER REPORT NO(S) (Any other numbers that may be assigned this report)

10. DISTRIBUTION STATEMENT

Approved for public release; distribution unlimited.

11. SUPPLEMENTARY NOTES	12. SPONSORING MILITARY ACTIVITY
	Office of Civil Defense

13. ABSTRACT

The objective of the program was to study the loading and structural response of wall panels. This report describes technical progress and reports the data from numerous loading study tests with a range of test geometries. Correlations between theory and test results for panel failure phenomena are presented and discussed. Also provided are appendices on the shock tunnel and its instrumentation. The work to date was summarized on the development of a theory of the dynamic failure of brittle materials.

DD FORM 1 NOV 68 1473 REPLACES DD FORM 1473, 1 JAN 64, WHICH IS OBSOLETE FOR ARMY USE.

Unclassified
Security Classification

URS 709-11

Final Report

STRUCTURAL RESPONSE and LOADING OF WALL PANELS

Contract No. DAHC20-67-C-0136

OCD Work Unit 1123E

Prepared for

OFFICE OF CIVIL DEFENSE
Office of the Secretary of the Army
Washington, D.C. 20310

Prepared by

C. Wilton, B. Gabrielsen, P. Morris
URS Research Company

July 1971

URS RESEARCH COMPANY
155 Bovet Road, San Mateo, California 94402

A URS Systems Affiliate

14. KEY WORDS	LINK A		LINK B		LINK C	
	ROLE	WT	ROLE	WT	ROLE	WT

BLANK PAGE

URS 709-11

Final Report Summary

STRUCTURAL RESPONSE and LOADING OF WALL PANELS

Contract No. DAHC20-67-C-0136

OCD Work Unit 1123E

Prepared for

OFFICE OF CIVIL DEFENSE
Office of the Secretary of the Army
Washington, D.C. 20310

Prepared by

C. Wilton, B. Gabrielsen, P. Morris
URS Research Company

July 1971

URS RESEARCH COMPANY
155 Bovet Road, San Mateo, California 94402

A URS Systems Affiliate

Summary Report

of

LOADING AND STRUCTURAL RESPONSE OF WALL PANELS

The work reported on herein stems from a recognition some years ago that there was a complete lack of information on full-scale structural response to blast loadings — information such as element failure times, energy or impulse transmitted to a building frame, and the influences of support conditions and other geometric factors — required by the Office of Civil Defense for such things as casualty and injury predictions, debris predictions, etc. During this part of the continuing comprehensive investigation of the loading and response of full-scale structural building wall panels, work has been concentrated on panels of brittle materials, notably nonreinforced brick.

In the course of the program, which consisted of parallel theoretical and experimental efforts, loading tests (on nonfailing walls) have been conducted on walls which completely closed the tunnel, on walls with 17.5 percent doorway openings, and on walls with 16.7 and 27 percent window openings. Pressure data taken during these tests in general show oscillations of about 2 msec frequency with a magnitude of about 15 percent of the signal size, which appears to be typical of Primacord-powered shock tubes. To provide sufficient input data to analytical programs in the most efficient manner and at the least cost, smoothing techniques were employed on the basis of an analysis of errors that would be encountered with various techniques. The reduced pressure data, and data from load cells located at the four corners of the wall support were processed through a series of computer programs which gave values of net pressure at each wall location, overpressure impulse, total load cell reading, and impulse derived from load cell readings for the first 25 msec of the pulse (a time longer than required for wall failure to occur).

Among the data from loading studies analyzed was that relating to the influence of back pressure (pressure on the back side of a wall with openings caused by loading through the openings) on net loading of the wall in the case

of an "infinitely long" room (a room long enough that rear wall effects cannot influence front wall failure). It was found, in general, that net load as a percent of front load at various distances from a doorway was never reduced below about 80 percent and generally was over 90 percent, and that much of the influence of back pressure was over within about 20 msec. In the infinitely long room case, therefore, back pressure has only a small influence on net load, although the influence increases with the size of the opening.

Additional loading tests conducted with and without glass in window openings indicate that the glass decreases the back pressure at early times to a very significant degree (in one case, for a gage 7 in. from the opening, from an early peak of about 4.5 psi without glass to one of about 1.5 psi with glass). As a result, early-time load cell readings were increased by factors as large as 3. Thus it appears that the presence of glass can have a major effect at very early times on the reaction transmitted to a support structure.

The analytical portion of the program has concentrated on the use of a finite-element computer program known as the Structural Analysis and Matrix Interpretive System (SAMIS). The program was applied to a (modelled) simple beam wall 8-ft high x 12-ft wide, for both a static loading of 2.0 psi, and a step pulse dynamic loading of 1.0 psi. Comparison of the SAMIS output with experimental load cell information for a nonfailing wall showed that SAMIS predicted a dynamic load factor (DLF, the ratio of peak load cell reading to applied load) of 2.0 while the experimental value was about 1.87, only about 7 percent below the SAMIS prediction.

For a failing simple beam wall, displacements, velocities, and stresses were computed, and failure times were predicted. (It should be noted that such calculations must take into account statistical distributions of material properties.) For the failure time, a URS crack gage which indicated failure at about 8 msec roughly confirmed the SAMIS values of 6 to 7 msec.

Additional effort was applied to using SAMIS as an aid in determining post-crack behavior through the use of a simple model (a two lump system that becomes a one lump system at the time of failure). This work will be extended during the next reporting period.

SAMIS was also used to predict the elastic response of a wall with a doorway in which the loading over the wall face was modified by diffraction effects from the simple step loading adopted for walls which completely close the shock tunnel. There was good general agreement of SAMIS predicted peak load cell readings (92,800 lbs) with experimental information from a nonfailing wall (98,000 lbs).

In general, our ability to predict — and then experimentally confirm — the behavior of simple beam supported nonreinforced, nonbearing walls, containing various openings (and of a simple plate support wall with no openings) gives us confidence that similar success can be expected for other support and opening configurations. As a result, test programs can be minimized in extent (and cost) being used principally for confirming theoretical predictions. With enough data on variations in wall and material properties (on, perhaps, a regional basis) statistically sound predictions of wall failure — of the sort useful in making casualty predictions — can also be made.

In the future — once brittle materials other than brick, load bearing walls, and arching are investigated — attention will be concentrated on reinforced concrete walls.

CONTENTS

Section		Page
	SUMMARY	ii
	ILLUSTRATIONS	vi
	TABLES	ix
	NOTATION	x
1	INTRODUCTION	1-1
2	BACKGROUND	2-1
	Discussion	2-1
	Approach to the Research Program	2-5
3	EXPERIMENTAL TEST PROGRAM	3-1
	Loading Tests	3-1
	General Discussion of Data and Data Reduction	3-8
	Data Reduction Technique	3-12
	Data Analysis	3-19
	Wall Panel Failure Tests	3-50
4	ANALYTICAL PROGRAM	4-1
	Structural Modeling	4-1
	Application of SAMIS	4-1
	Simple Beam Wall	4-7
	Simple Beam Wall with Door	4-28
5	LOADING AND STRUCTURAL RESPONSE OF WALL PANELS SUMMARY OF PROGRESS TO DATE	5-1
	Nonreinforced Brittle Materials	5-1
	Other Wall Types	5-10
6	REFERENCES	6-1
Appendix A	THE URS SHOCK TUNNEL	A-1
Appendix B	BRITTLE STRUCTURES — DYNAMIC FAILURE AND STATISTICAL THEORY	B-1

ILLUSTRATIONS

Figure		Page
3-1	Sketch of Nonfailing Wall	3-2
3-2	Experimental Arrangement for Test 01207001 — Loading Study Test with 17.5 Percent Open Doorway	3-9
3-3	Tracing of Analog Data from Test 01207001 — Loading Study Test	3-10
3-4	Displacement in In. as a Function of Time	3-15
3-5	Displacement in In. as a Function of Natural Period	3-16
3-6	Net Pressure Data from One-Strand, Case Two Tests	3-20
3-7	Net Impulse Data from One-Strand, Case Two Tests	3-21
3-8	Net Pressure Data from Three-Strand, Case Two Tests	3-22
3-9	Net Impulse Data from Three-Strand, Case Two Tests	3-23
3-10	Net Pressure Data from Five-Strand, Case Two Tests	3-24
3-11	Net Impulse Data from Five-Strand, Case Two Tests	3-25
3-12	Net Pressure Data from One-Strand, Case Three Tests	3-26
3-13	Net Impulse Data from One-Strand, Case Three Tests	3-27
3-14	Net Pressure Data from Three-Strand, Case Three Tests	3-28
3-15	Net Impulse Data from Three-Strand, Case Three Tests	3-29
3-16	Net Pressure Data from Five-Strand, Case Three Tests	3-30
3-17	Net Impulse Data from Five-Strand, Case Three Tests	3-31
3-18	Net Pressure Data from One-Strand, Case Four Tests	3-32
3-19	Net Impulse Data from One-Strand, Case Four Tests	3-33
3-20	Net Pressure Data from Three-Strand, Case Four Tests	3-34
3-21	Net Impulse Data from Three-Strand, Case Four Tests	3-35
3-22	Net Pressure Data from Five-Strand, Case Four Tests	3-36
3-23	Net Impulse Data from Five-Strand, Case Four Tests	3-37
3-24	Net Load as a Percent of Front Load — Three- and Five-Strand, Case Two Tests	3-38
3-25	Load Cell Data, Case Two	3-41
3-26	Load Cell Data, Case Three	3-42
3-27	Load Cell Data, Case Four	3-43
3-28	Net Pressure Data from Three-Strand Test, Case Four with Glass	3-44

ILLUSTRATIONS (cont.)

Figure		Page
3-29	Net Impulse Data from Three-Strand, Case Four with Glass	3-45
3-30	Net Pressure Data from Five-Strand, Case Four with Glass	3-46
3-31	Net Impulse Data from Five-Strand, Case Four with Glass	3-47
3-32	Load Cell Data from Tests With and Without Glass, Case Four	3-48
3-33	Average Pressure-Time Curves for Gage H on Back Face of Wall, 7 in. from Edge of Window, With and Without Glass, Case Four	3-49
4-1	Trial Model of Brick Wall Panel for SAMIS	4-3
4-2	Dynamic Displacements as Calculated by SAMIS	4-6
4-3	Cutaway View of Shock Tunnel Showing Test Panel and Location of Horizontal and Vertical Plate Girders, Wall Blocks, and Load Cells	4-8
4-4	Final SAMIS Model Configuration	4-9
4-5	Typical Pressure Gage Data, Nonfailing Wall, Closed Tunnel Test	4-10
4-6	Typical Load Cell Trace, Nonfailing Wall, Close-Tunnel Test	4-13
4-7	Computed Load Trace, Nonfailing Wall	4-13
4-8	Contour Display of Maximum Deflection of Wall Surface at T/2	4-14
4-9	Node 360 Displacement and Velocity vs Time	4-15
4-10	Typical Stress/Time Relation for Facet on Structure Centerline	4-16
4-11	Apparent Fiber Stress vs Overload Ratio	4-18
4-12	Normalized Load Factors vs Failure Time	4-21
4-13	Half-Panel Moment	4-23
4-14	Half-Panel Shear at t = 0	4-24
4-15	Half-Panel Reaction vs Time	4-26
4-16	Brick "Beam" Wall Panels	4-27
4-17	Basic Grid and Line Elements	4-29
4-18	Structural Response vs Sinusoidal Forcing Functions	4-32
4-19	Displacement in In. as a Function of Time	4-34
4-20	Displacement in In. as a Function of Natural Period	4-35

ILLUSTRATIONS, cont.

Figure		Page
4-21	SAMIS Input Loads	4-36
4-22	Wall with Doorway Deflection Contour at 12 msec	4-38
4-23	Wall with Doorway Deflection Contour at 13 msec	4-39
4-24	Wall with Doorway Deflection Contour at 14 msec	4-40
4-25	Wall with Doorway Deflection Contour at 15 msec	4-41
4-26	Wall with Doorway Deflection Contour at 16 msec	4-42
4-27	Wall with Doorway Deflection Contour at 17 msec	4-43
4-28	Displacement vs Time Plot for Wall with Doorway	4-44
4-29	Load vs Time for Load Cells 58 and 658	4-45
4-30	Displacement and Velocity vs Time for Wall with Doorway	4-47
4-31	Stress vs Time for Wall with Doorway	4-48
5-1	Predicted Strength Distribution for 8-ft x 12-ft x 8-in. Brick Wall Panel	5-3
5-2	Extreme Probability Plot of Fracture for 8-ft x 12-ft x 8-in. Walls with Various Loadings and Support Conditions	5-5
5-3	Extreme Probability Plot of Fracture for 8-ft x 12-ft x 8-in. Walls with Various Support Conditions and a 3-ft x 8-ft Doorway	5-6
5-4	Wall Loads	5-7
5-5	Displacement vs Time	5-8
5-6	Doorway Wall Panel Stress Area of Node 10	5-9

TABLES

Table		Page
2-1	NFSS Structural Data	2-3
2-2	NFSS Structural Character of Exterior Walls	2-4
2-3	NFSS Structural Data for Large Buildings	2-5
3-1	Doorway – Net Pressure Data, Average Values for Three Tests, Three Strands Primacord	3-17
3-2	Doorway – Load Cell Data, Average Values for Three Tests, Three Strands Primacord	3-18
3-3	Comparison of Glass/No-Glass Impulses on Back Face, Five Strand Tests, 27 Percent Window	3-50
3-4	Summary of Loading Tests	3-51
3-5	Summary of Loading and Response Data for Wall Panels . . .	3-52
4-1	Displacements for Trial Beam Due to a 2-psi Static Load .	4-4
4-2	Summary of Loading and Response Data for Nonfailing Test Walls that Provide 100-Percent Closure	4-11

NOTATION

$d/dt = \dot{x}$	Differential with respect to time (L/T)
E	Energy (FL)
E	Modulus of elasticity (F/L^2)
F	Force (F)
$F_1[f(t)]$	Force, time variant (F)
$\bar{F}$	Fracture force (F)
g	Gravity (F/T^2)
H	Centerline shear at fracture
I	Area moment of inertia (L^4)
k	Stiffness (F/L)
L	Length (L)
ℓ	Length (L)
m	Mass ($F \cdot T^2/L$)
M	Bending moment (FL)
m,n	Integers
p	Probability of failure, flaw theory dominated
q	Probability of failure, parallel system dominated
p_i	Incident pressure (F/L^2)
p_r	Reflected pressure (F/L^2)
P_f	Probability of failure
P_s	Probability of success
P_v	Vertical load (F)
R	Resistance (F)
s	Measure of dispersion
S	Standard deviation
t	Time, variable (T)
T	Period (T)
V	Shear (F)
V	Velocity (L/T)
W	Weight (F)
x,y,z	Coordinate axes (L)

NOTATION, cont.

$\bar{x}$	Mean value
$\bar{\alpha}$	Normalized coefficient
$1/\alpha$	Measure of dispersion
β	Normalized coefficient
δ	Virtual displacement (L)
η	Coordinate axis (L)
Θ	Angle (rad)
μ	Modal value
ρ	Mass density ($F \cdot T^2/L^4$)
ρ	Correlation coefficient
σ	Standard deviation
σ_c	Compressive allowable shear (F/L^2)
σ_r	Rupture module (F/L^2)
σ_t	Tensile allowable shear (F/L^2)
τ	Time, variable (T)
ω	Natural frequency (rad/T)
Ω	Frequency (rad/T)

Section 1
INTRODUCTION

This report is one of a series describing the progress on a long-range program of shock tunnel research on the loading, structural response, and debris characteristics of wall panels. This work was started in 1966 and has been conducted for the Office of Civil Defense under Subcontract Nos. 11229 (6300A-320), 11618 (6300A-250), and 12671 (6300A-290) from the Stanford Research Institute which has been acting as technical monitor on the program. This current subcontract concludes this phase of the effort for SRI.

Since the technical monitoring of the follow-on work on this program will be performed directly by OCD, this seemed like an excellent time to review the progress on the program to date, reassess the philosophy behind the program and establish the guidelines for the follow-on work. Thus, the organization of this report is as follows: The background and philosophy behind the program is discussed briefly in Section 2, the progress to date in the experimental portion of the program is presented in Section 3, and the analytical portion of the program in Section 4. A summary of progress to date is presented in Section 5.

Section 2
BACKGROUND

DISCUSSION

Since the development of nuclear weapons, voluminous information has been accumulated (from weapons tests, bombing surveys, and theoretical work) on the effects of these weapons on buildings and their structural elements. A review of much of this material at the start of this program revealed an almost complete lack of certain types of information which were needed to make the refined structural damage predictions required by OCD for a variety of purposes, including:

- Casualty and injury predictions
- Debris predictions
- Predictions of blast effects on fire development and spread
- Prediction of damage to equipment and property in structures
- Guidance in construction design for protection from all weapons effects

Some of the specific types of information found to be lacking were: element failure times; the amount of energy and/or impulse transmitted by a failing element to its supporting frame; and the effect of a variety of geometric considerations such as openings, support conditions, building orientation, and building size on the loading function. At about the time this literature review was completed, URS acquired a facility which included a 163-ft-long, heavily reinforced concrete tunnel. The tunnel could inexpensively be converted into a large shock tunnel uniquely suited for full-scale tests of structural elements, such as wall panels.

In November 1966, conversion work was begun to transform this tunnel into a shock tube configuration. Instrumentation was installed, tested, and calibrated, and a series of tests conducted to determine the ranges of air

blast characteristics that could be obtained in the facility. The results of this program were sufficiently encouraging that a second phase was initiated which included further tunnel evaluation tests, additional facility improvements necessary for fabrication and handling of wall panels, and initial tests of brick panels and timber stud walls. A third phase has since been initiated – a comprehensive investigation of loading, response, and failure characteristics (including debris production) of full-sized structural building wall panels, and a program to obtain blast-slanting information to aid in the design of new shelter facilities.

The main emphasis to date under Phase 3 has been the study of brittle materials, particularly wall panels constructed of nonreinforced brick. The rationale behind this choice of structural material was set out in URS Proposal 67P37, dated October 1967, and was based on data collected during a survey of 309 National Fallout Shelter Survey Buildings (Ref. 1) in which it was determined that nonreinforced brick accounted for the largest percentage of exterior walls (approximately 38 percent of the total) and that brittle materials in general accounted for approximately 59 percent of all exterior partitions. These data, as presented in 67P37, are shown in Tables 2-1 and 2-2.

During the present contract and the preparation of this report, these data were briefly reanalyzed to determine if the emphasis on the types of structural materials was warranted. For example, although the majority of buildings identified in the NFSS survey were constructed of brick or other brittle materials, it was thought possible that the majority of shelter spaces might be in a relatively small number of large buildings which are not constructed of brittle materials. Thus, the heavy emphasis which had been placed on brittle materials because of their common occurrence might not be justified if shelter spaces, rather than shelter buildings, were used to establish priorities. Information on the construction materials of buildings as a function of shelter sizes was not directly available from the data presented in Ref. 1. However, since it can be assumed that the larger shelters (> 1,000 people) will most likely be in the larger buildings, it is assumed that an analysis of only the larger buildings would reveal the construction materials used in the majority of large shelter areas.

Table 2-1

NFSS STRUCTURAL DATA

BUILDING DESCRIPTION	EXTERIOR WALLS	
	PERCENTAGE OF WALLS	CUMULATIVE PERCENTAGE OF WALLS
1. Nonreinforced brick - bearing wall	23	
2. Cast in place concrete - bearing wall	15	38
3. Nonreinforced brick - curtain wall	11	49
4. Tile - curtain wall - masonry veneer	08	57
5. Nonreinforced concrete block - curtain wall	06	63
6. Cast in place concrete - curtain wall	04	67
7. Nonreinforced concrete block - bearing wall	04	71
8. Nonreinforced brick - bearing wall - masonry veneer	04	75
9. Nonreinforced concrete block - curtain wall - masonry veneer	03	78
OTHER WALL TYPES IN ORDER OF OCCURRENCE		
10. Nonreinforced brick - curtain wall - masonry veneer		
11. Cast in place concrete - bearing wall - masonry veneer		
12. Nonreinforced concrete block - bearing wall		
13. Tile - curtain wall		
14. Reinforced concrete block - bearing wall - masonry veneer		
15. Studwall - timber - bearing wall		
16. Stone - bearing wall		
17. Cast in place concrete - curtain wall - masonry veneer		
18. Reinforced brick - bearing wall		
19. Studwall - timber - curtain wall - masonry veneer		
20. Metal panel - curtain wall		
21. Precast concrete - bearing wall - masonry veneer		
22. Reinforced concrete block - bearing wall		
23. Structural tile - bearing wall - masonry veneer		
24. Precast concrete - curtain wall		
25. Reinforced concrete block - curtain wall - masonry veneer		
26. Reinforced brick - bearing wall - masonry veneer		
27. Stone - bearing wall - masonry veneer		
28. Precast concrete - curtain wall - masonry veneer		
29. Precast concrete - bearing wall		
30. Reinforced brick - curtain wall		
31. Studwall - timber - curtain wall		
32. Metal panel - curtain wall - masonry veneer		

Table 2-2

NFSS STRUCTURAL CHARACTER OF EXTERIOR WALLS

STRUCTURAL CHARACTER OF EXTERIOR WALLS	PERCENTAGE OF WALLS	CUMULATIVE PERCENTAGE OF WALLS
I. Nonreinforced brick wall with and without veneer, Types 1, 3, 8	38	
II. Reinforced concrete wall, Types 2, 6	19	57
III. Nonreinforced concrete block wall with and without veneer, Types 5, 7, 9	13	70
IV. Structural tile wall, Type 4	08	78

NOTE: The above wall types would account for 50 percent of all partition walls also.

For this analysis, the information contained in Appendix A of Ref. 1 was extracted for those buildings in which the floor areas designated as containing shelters were in excess of 12,000 sq ft. From a total of 308 buildings, 46 were found to have a total of 60 floors which exceeded 12,000 sq ft floor area and contained shelters. Forty-three of these were basements and 17 were above ground. The data collected for these larger buildings are presented in Table 2-3. From recent information obtained from OCD, most shelter spaces were found to be in the larger buildings. Although the data are insufficient to support the findings from the survey reported in Ref. 1, the problem is under continuing study by OCD.

These data indicated that brittle materials accounted for 82 percent of all above-ground exterior walls (over 50 percent of these being nonreinforced brick) and from 42 to 47 percent of all interior partitions. It was, therefore, concluded that the study of brittle wall materials outlined in the original statement of work was not only still valid, but of even greater importance than originally presumed.

Table 2-3

NFSS STRUCTURAL DATA FOR LARGE BUILDINGS

TYPE	PERCENT
Exterior Walls (above ground floors)	
• Brittle materials*	82
• Reinforced concrete	18
Interior Walls (above ground floors)	
• Brittle materials	47
• Reinforced concrete	35
• Wood partitions (various types)	18
Interior Walls (basements)	
• Brittle materials	42
• Reinforced concrete	35
• Wood partitions (various types)	16
• No partitions	7

* Brittle materials included nonreinforced brick, concrete blocks and tile. Over 50 percent of these walls were of nonreinforced brick.

APPROACH TO THE RESEARCH PROGRAM

Since the beginning of the panel test program, analytical and experimental efforts have been closely coordinated. Preliminary analytical work is first used to design and predict the results of experimental tests. The experimental program is conducted on selected types of exterior and interior wall panels and partitions, with panel types studied being selected as representative of a class of panels whose general structural response characteristics are expected to be similar. The results of the experimental tests are then combined with additional analytical work and existing test information to develop theories of loading, response and debris formation in sufficient detail, and with sufficient reliability to be used for personnel casualty and building damage estimates.

It was anticipated that predictions could be made for a wide variety of other types of panels in the same class without the need for additional extensive experimental tests by carefully studying the wall panel types selected, and by using this combination of experimentation and analysis.

Section 3
EXPERIMENTAL TEST PROGRAM

The experimental tests that have been conducted in the URS Shock Tunnel in support of this program have included:

- Calibration tests
- Loading study tests using a variety of instrumented nonfailing wall geometries
- Failure tests using full-scale structural wall panels and open tunnel calibration tests

A brief description of the shock tunnel facility, a discussion of the operating concepts, descriptions of the instrumentation, test hardware and support equipment available at the facility, and the results of the calibration tests are presented in Appendix A.

LOADING TESTS

Definition

Loading tests are defined as those shock tunnel tests which are conducted with one or two nonfailing test walls to obtain loading information needed for designing the structural wall panel tests and interpreting the data from the wall panel failure tests. Figure 3-1 is a sketch showing one of the nonfailing walls.

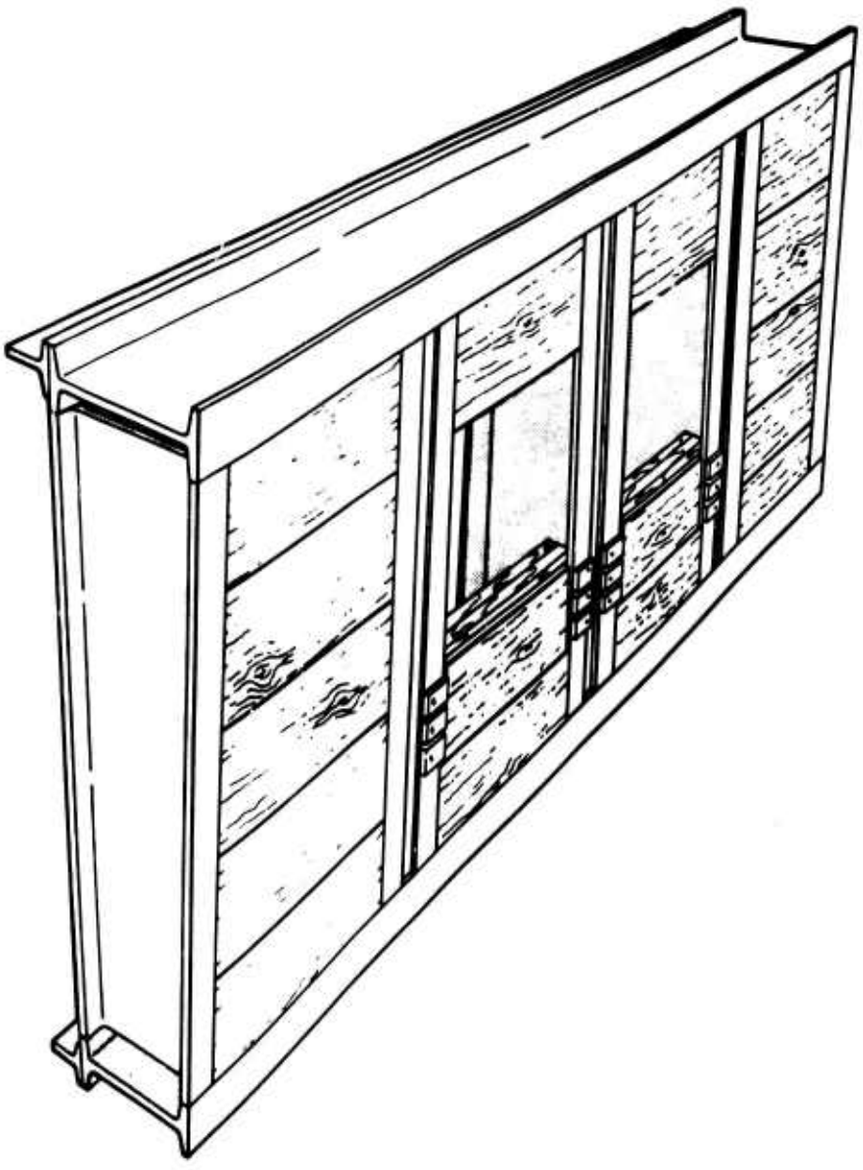

Fig. 3-1. Sketch of Nonfailing Wall

Test Geometries

A total of seven different loading study test geometries have been investigated to date. These are as follows:

- Case One - Nonfailing instrumented wall completely closing the tunnel

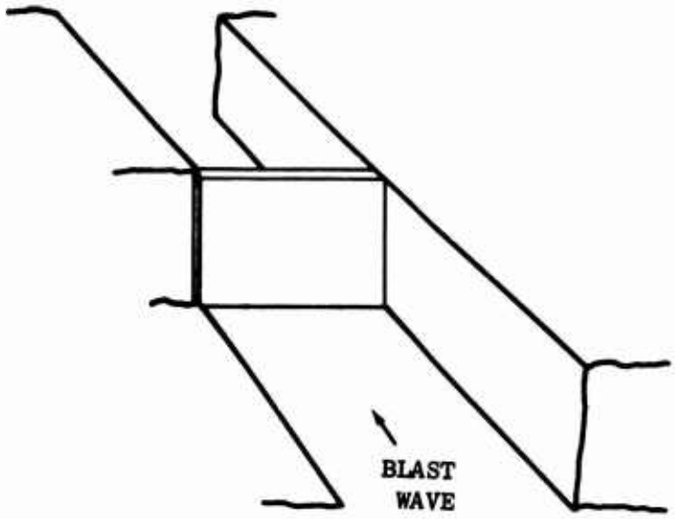

- Case Two - Nonfailing instrumented wall with 17.5 percent open doorway

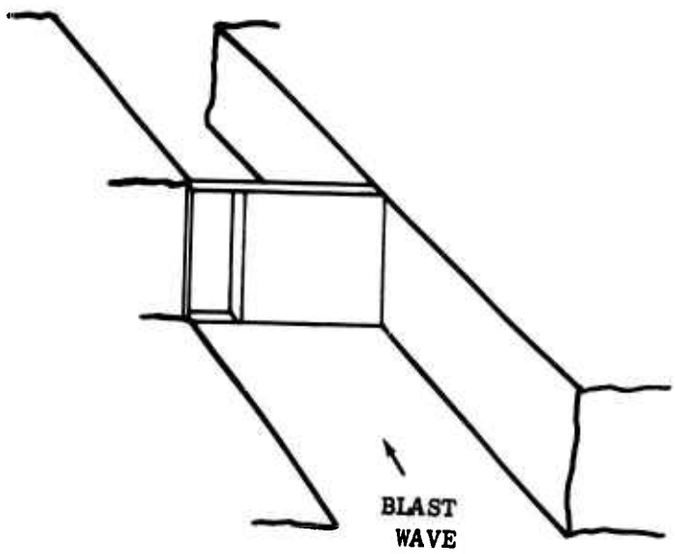

- Case Three - Nonfailing instrumented wall with 16.7 percent open window

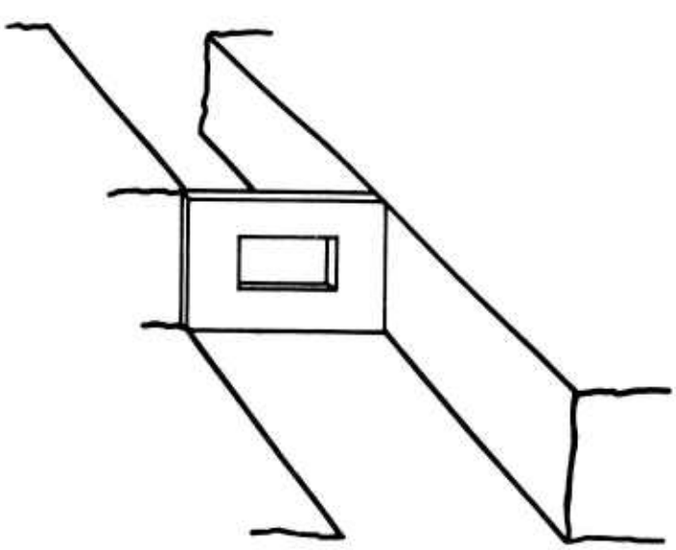

- Case Four - Nonfailing instrumented wall with 27 percent open window

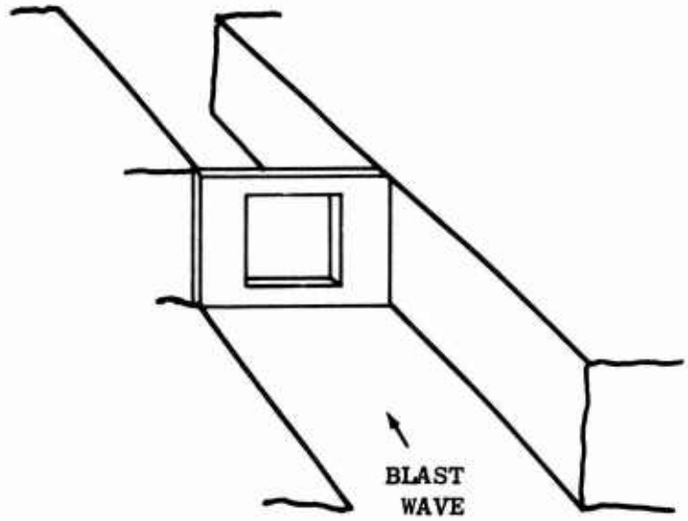

- Case Five - Two nonfailing instrumented walls: Front with 16.7 percent open window, back wall instrumented and 100 percent closed

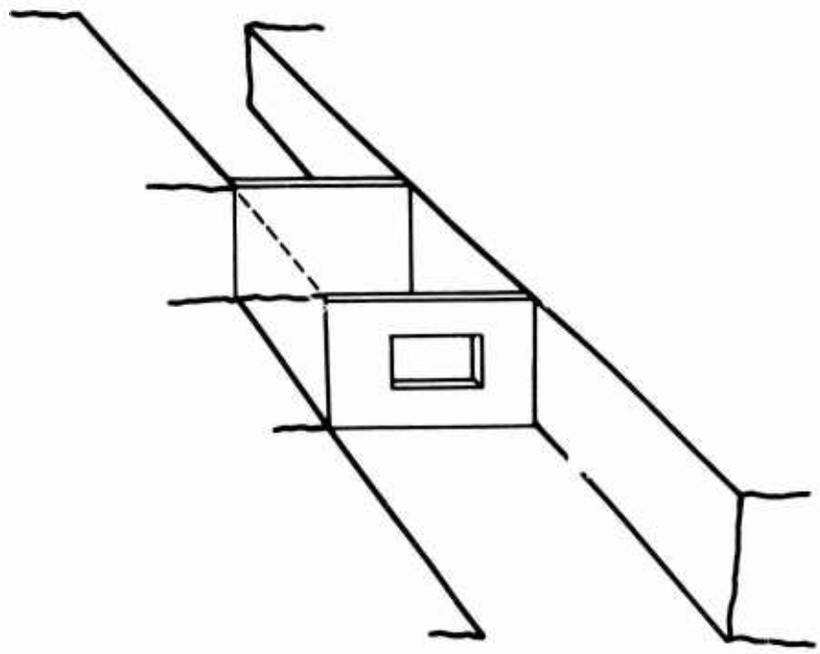

- Case Six - Two nonfailing instrumented walls: Front with 27 percent open window, back wall instrumented and 100 percent closed

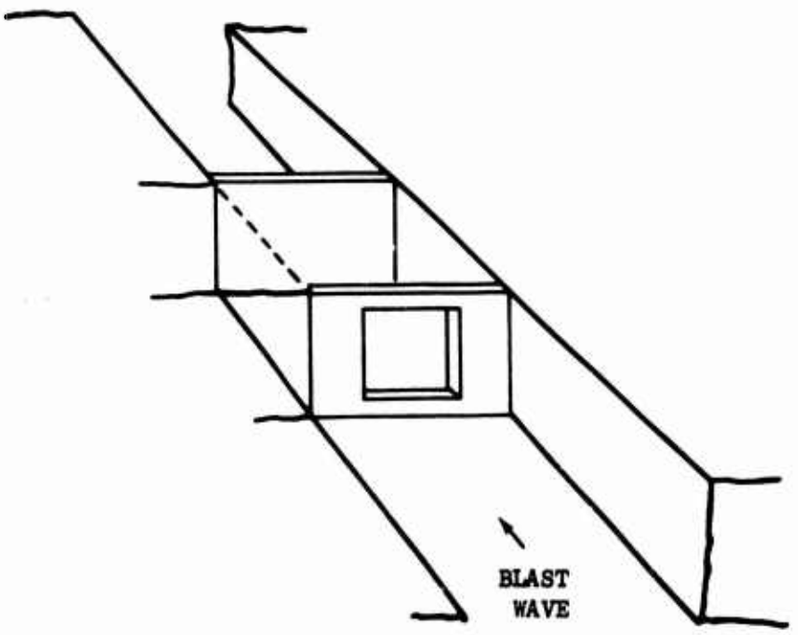

- Case Seven - Two nonfailing instrumented walls: Front with 17.5 percent open doorway, back wall instrumented and 100 percent closed

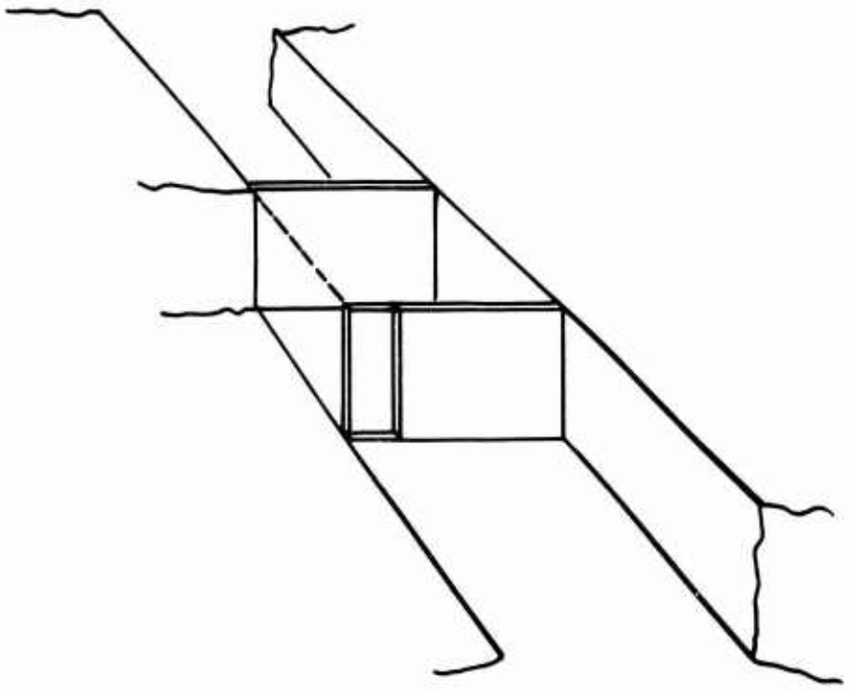

Instrumentation

The instrumentation used during a typical loading test includes pressure gages located on the shock tunnel wall and on the nonfailing wall or walls, and load cells located on the support structure to monitor the total load imparted to the support structure. Occasionally this instrumentation is supplemented with time-of-arrival gages, strain gages, and motion picture cameras. For a description of the various components of the instrumentation system, refer to Appendix A.

One typical instrumentation arrangement for a test with a 17.5 percent open doorway (Case Two) is sketched in Fig. 3-2. Note that pressure gages for this test were located back-to-back on both sides of the wall as well as on the tunnel wall.

GENERAL DISCUSSION OF DATA AND DATA REDUCTION

Typical Data

Tracings of the analog data from a test (No. 01207001) with a 17.5 percent open doorway is shown in Fig. 3-3. The explosive used for this test consisted of five strands of Primacord approximately 60 ft long (approximately 2.14 lbs PETN) detonated simultaneously at the open end of the compression chamber. The peak overpressures at the wall location for this test were 6.1 psi incident 14.3 psi reflected. It will be noted that oscillations appear on all traces with a period on the order of 2 msec and with a magnitude of the order of 15 percent of the signal size. This noise is typical of Primacord-powered shock tubes and is most likely associated with the waves that radiate from the Primacord line charges and bounce off the compression chamber walls. The extremely short period of these oscillations is not significant in relation to the response periods of the structural wall panels tested in this program and hence the generated wave shapes are entirely adequate for this purpose.

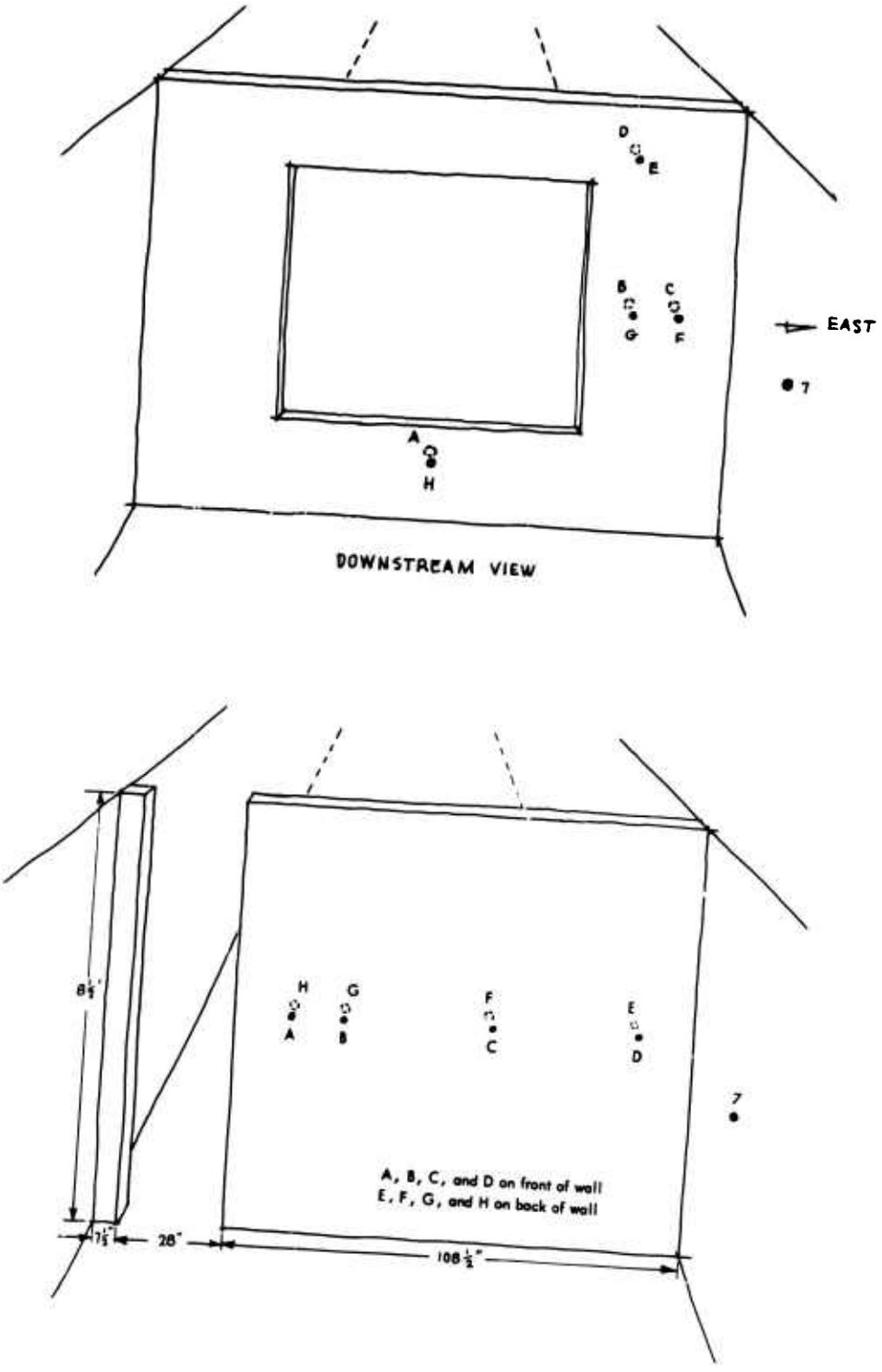

Fig. 3-2. Experimental Arrangement for Test 01207001 – Loading Study Test with 17.5 percent Doorway (Case Two)

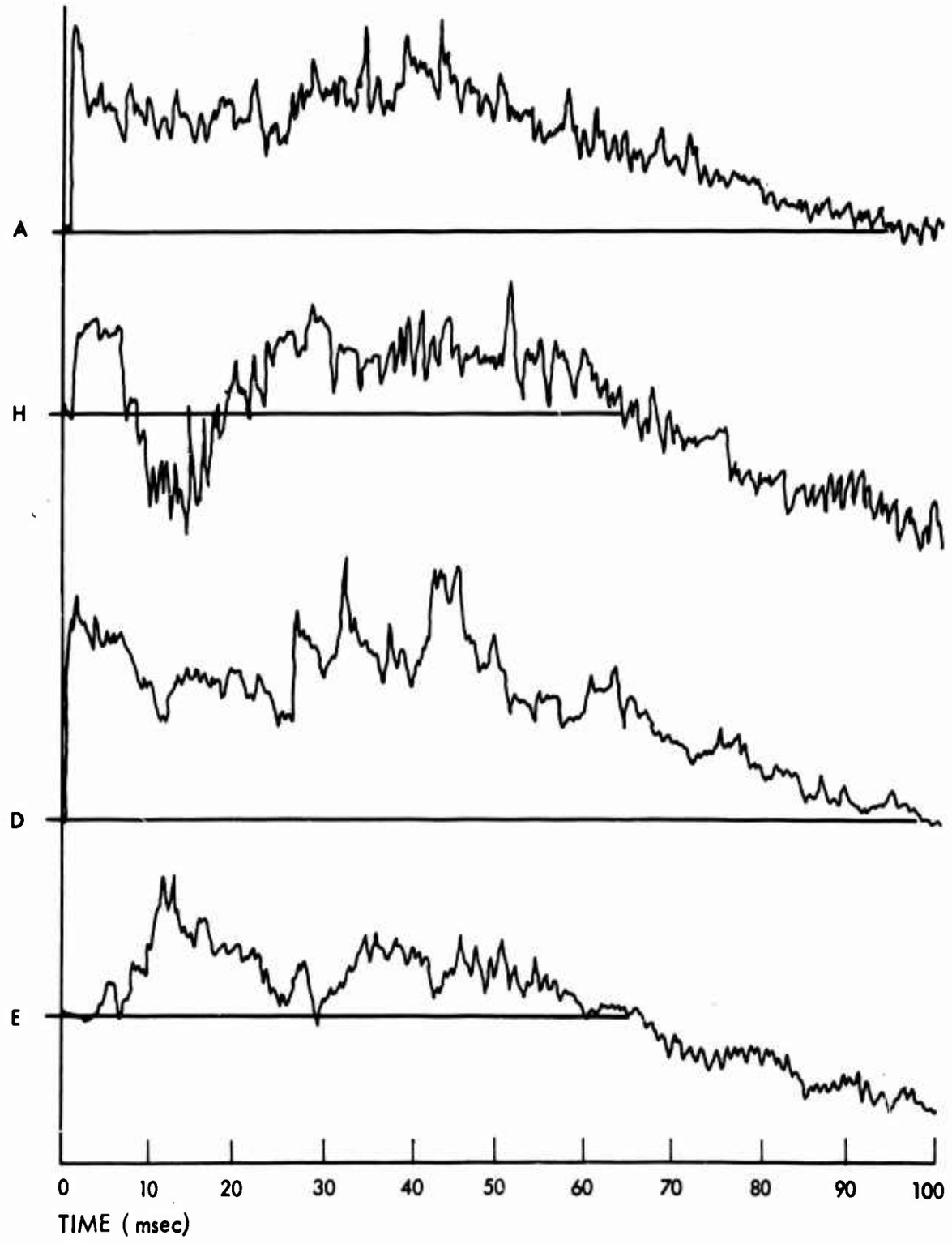

Fig. 3-3. Tracing of Analog Data from Test 01207001 — Loading Study Test Case Two (17.5 percent open doorway)

The primary purpose of these tests was to obtain loading information for use in predicting the response and failure characteristics for the structural wall panel tests. Of particular interest in a wall geometry with an opening is the net load as a function of time. For example, note the difference in pulse shape between the tracings from gage D and those from gage E in Fig. 3-3. These gages are placed back-to-back and are 8 ft from the edge of the door. Gage D measured a peak reflected overpressure of 14.8 psi when the shock wave first struck the nonfailing wall. This gradually decayed to a stagnation value of 9.4 psi as the flow pattern was established through the doorway. Gage E, on the other hand, saw a gradual buildup of pressure and finally reached a peak of 4.3 psi at approximately 12 msec. The net pressure difference between the two gages at this point in time (12 msec) was 5.2 psi.

DATA REDUCTION TECHNIQUE

One major data requirement needed as input to the analytical portion of the program was a curve of net load as a function of time for a particular wall geometry. In the failure theory development so far, emphasis has been on the elastic phase (up to the time of first crack); therefore, the data analysis effort has been concentrated on the first 25 msec of each trace with lesser emphasis on the total trace. This time (25 msec) was an arbitrary value chosen as likely to be longer than the failure (cracking) time of any brittle wall panels planned for testing.

Probably the most desirable method of obtaining net load as a function of time would be a complete digitizing of the two traces (one taken from a gage on the front of the wall and the other from a gage at a corresponding location on the back of the wall) at very close time intervals, and then computing the pressure difference at each sampling interval. As noted earlier, however, the noise oscillations (which would be extremely difficult and expensive to digitize) do not have a significant influence on the response of a structural wall panel. Thus, it seemed desirable to adopt a simpler data reduction technique with an accuracy commensurate with the requirements imposed by the analytical program.

The method used was to smooth the traces by fitting straight line segments to the various portions of the trace by eye (a typical example is shown on the next page). The end point coordinates in terms of pressure and time were then recorded on data sheets for further analysis.

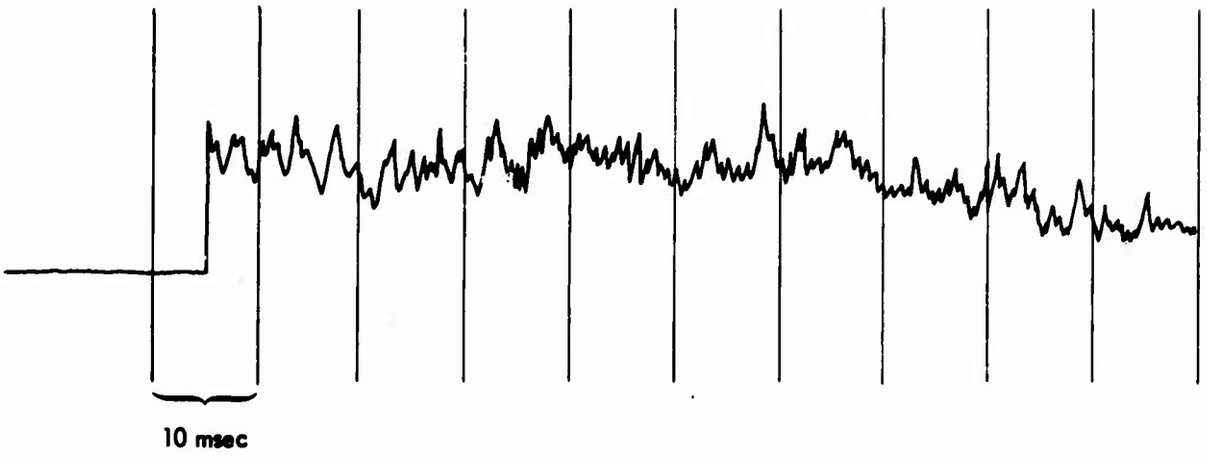

To check the accuracy of this particular data reduction technique, sample records from three- and five-strand tests on the doorway configuration of the nonfailing wall were analyzed. The front and back face gage pair examined was located 7 ft from the doorway. A grid was drawn at 1-msec intervals from time 0 to 25 msec on the original traces. The pressure reading at each point where the grid intersected the trace was then read, yielding a digitized gage record. The back face loading was then subtracted from the front face load to yield a digitized net pressure time record for comparison with the straight line segment method of obtaining net pressure vs time. The deviation of the straight line method from the digitized record was then determined. A similar procedure was also carried out to obtain net impulse as a function of time. The results of this analysis indicated an average deviation of 5 percent for both pressure and impulse.

To further increase our confidence in the data reduction procedure used, a structural response-sensitivity study was performed (for additional discussion, see Section 4). A one-lump system with a mass similar to that of an 8-in. brick wall and with natural periods of 15 to 40 msec (the natural period of an 8-in. brick wall is approximately 33 msec) was subjected (numerically) to each of the following pulses:

1. The best average fit curve through the data with straight line fits of as little as 1 msec.

2. A 1-msec sampling technique with an averaging or fitting of the trace.

3. The smoothing technique shown provided as a typical example.

The results of this study are shown in Fig. 3-4, a plot of displacement in inches as a function of time for a wall similar to brick in mass and natural period and Fig. 3-5, a plot of displacement in inches as a function of natural period. It can be seen that the results from the three pulses are very similar. It was concluded, therefore, that for the present at least, the simplified data reduction technique is completely adequate. (For additional discussion, see Section 4.)

Loading Study Data

The reduced pressure data and the data from the load cells* located at the four corners of the wall support framework were processed through a series of computer programs which yielded sets of tables of net pressure at each wall location, overpressure impulse, total load cell reading, and pressure impulse derived from load cell readings for each of the first 25 msec. Tables 3-1 and 3-2 are examples of this printout. Time zero on the load cell readings was taken as the time that a load was first registered rather than the time of arrival of the shock at the wall. (The delay between the two usually amounted to about 2 msec.) The pressure impulse derived from the load cell readings was computed to provide a simple check of the internal consistency of the data — the pressure impulse determined from pressure readings, and the impulse derived from the load cell readings — should both follow the same general trend with time.** The excitation of the basic response frequency of the wall was not taken into account.

---

* For discussion of load cells and test arrangements see Appendix A.

** The Integral of Duhamel Solution(s) to the differential equation(s) of motion require this type of internal consistency.

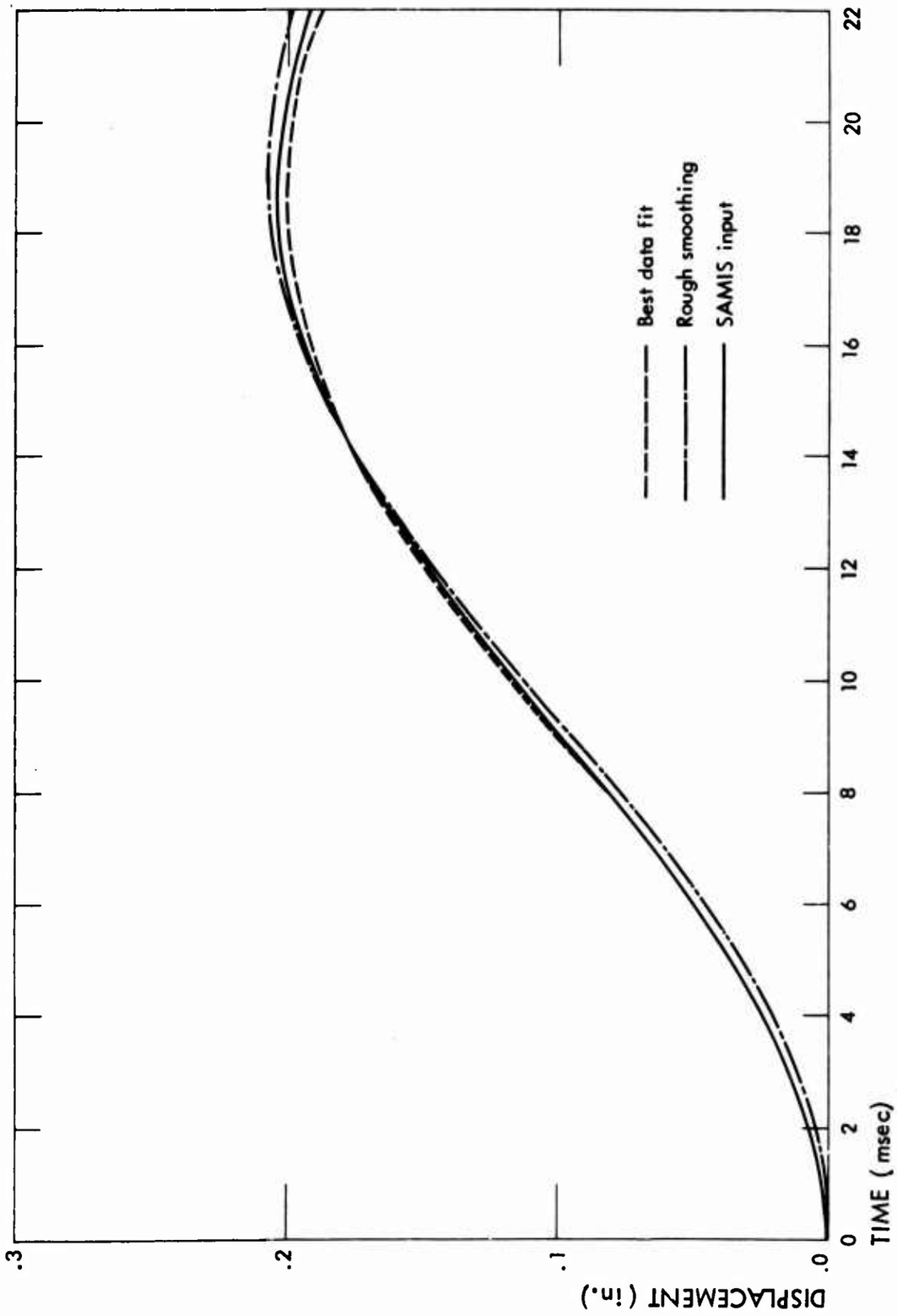

Fig. 3-4. Displacement in In. as a Function of Time

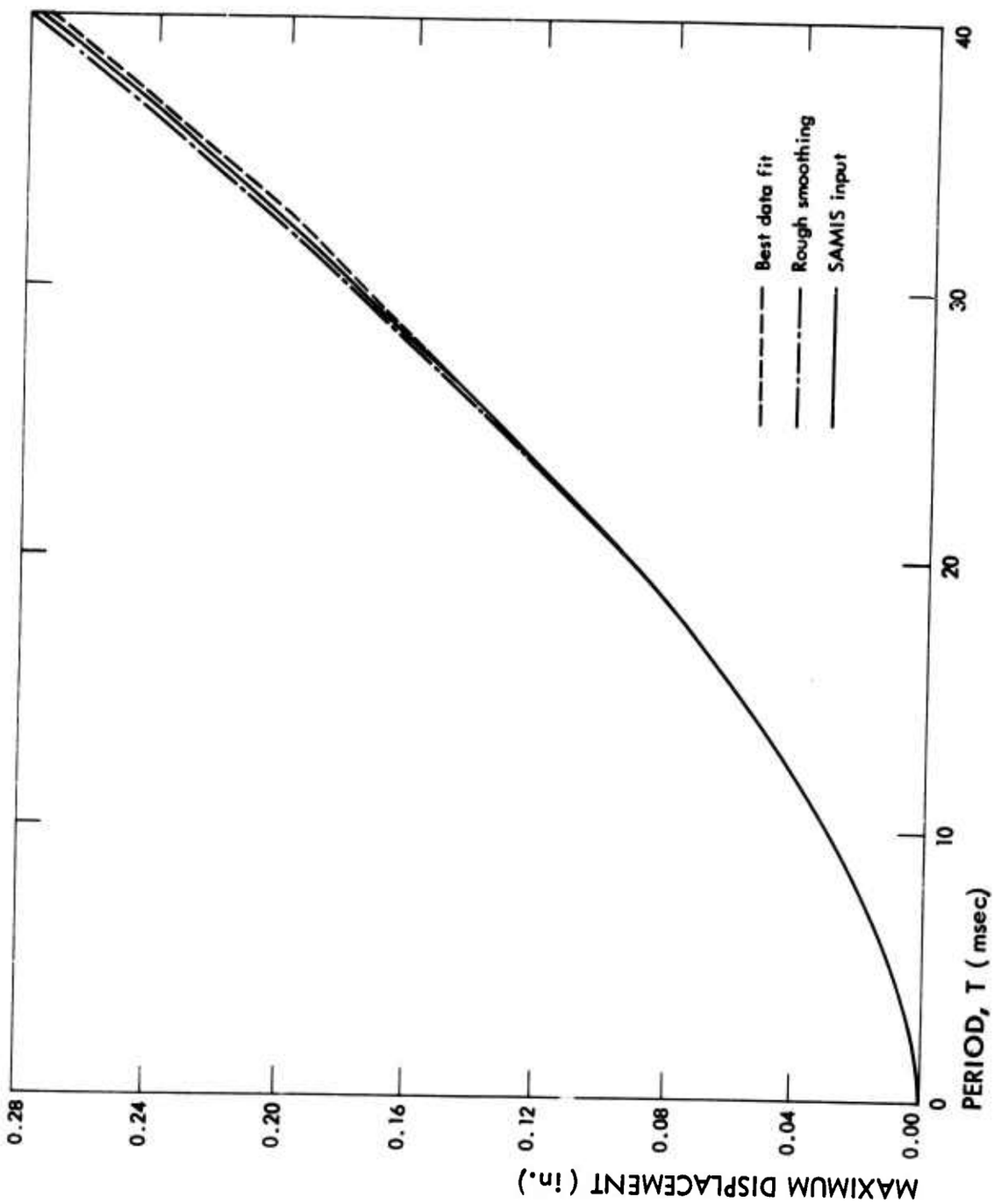

Fig. 3-5. Displacement in In. as a Function of Natural Period

Table 3-1

DOORWAY – NET PRESSURE DATA, AVERAGE VALUES FOR THREE TESTS, THREE STRANDS PRIMACORD
(Case Two, 17.5 percent open doorway)

TIME (msec)	GAGE PAIR RESULTS							
	A-H PAIR		B-G PAIR		C-F PAIR		D-E PAIR	
	PRESSURE (psi)	IMPULSE (psi/msec)	PRESSURE (psi)	IMPULSE (psi/msec)	PRESSURE (psi)	IMPULSE (psi/msec)	PRESSURE (psi)	IMPULSE (psi/msec)
0	7.43	.00	8.40	.00	6.31	.00	4.42	.00
1	6.37	6.90	7.38	7.89	6.20	6.26	6.71	5.57
2	3.94	12.05	6.36	14.76	6.08	12.40	7.31	12.58
3	3.32	15.68	4.58	20.24	5.97	18.42	7.40	19.94
4	3.05	18.86	3.86	24.45	5.85	24.34	7.50	27.39
5	3.01	21.89	3.68	28.22	5.17	29.85	7.27	34.77
6	2.98	24.89	3.51	31.82	5.06	34.97	6.88	41.85
7	2.95	27.86	3.51	35.32	4.71	39.85	6.80	48.69
8	3.06	30.86	3.51	38.83	4.35	44.38	6.72	55.45
9	3.33	34.06	3.51	42.34	4.00	48.56	5.89	61.75
10	3.73	37.59	3.51	45.84	3.65	52.38	5.06	67.23
11	4.13	41.51	3.62	49.41	3.56	55.99	3.73	71.62
12	4.48	45.82	3.74	53.08	3.48	59.51	3.27	75.11
13	4.82	50.47	3.85	56.88	3.49	62.99	3.12	78.31
14	5.17	55.47	3.96	60.78	3.51	66.49	3.20	81.46
15	5.52	60.81	4.08	64.81	3.55	70.03	3.28	84.70
16	5.76	66.46	4.14	68.92	3.62	73.61	3.28	87.98
17	5.66	72.17	4.21	73.10	3.68	77.26	3.28	91.25
18	5.55	77.77	4.28	77.34	3.85	81.03	3.28	94.53
19	5.38	83.24	4.30	81.63	4.01	84.96	3.28	97.81
20	5.23	88.54	4.30	85.93	4.17	89.05	3.38	101.14
21	5.07	93.69	4.30	90.24	4.32	93.29	3.38	104.52
22	4.97	98.71	4.37	94.57	4.46	97.69	3.50	107.96
23	4.86	103.62	4.44	98.98	4.61	102.22	3.63	111.53
24	4.76	108.44	4.50	103.45	4.64	106.85	3.90	115.29
25	4.69	113.16	4.57	107.98	4.66	111.49	4.55	119.52

Table 3-2

DOORWAY – LOAD CELL DATA, AVERAGE VALUES FOR THREE TESTS, THREE STRANDS PRIMACORD

TIME (msec)	LC1 (kips)	LC2 (kips)	LC3 (kips)	LC4 (kips)	TOTAL (kips)	DERIVED PRESSURE IMPULSE (psi-msec)
0	.00	.00	.00	.00	.00	.00
1	1.33	5.15	15.90	5.64	28.02	1.30
2	2.66	10.31	31.81	11.28	56.05	5.20
3	3.98	15.46	47.71	16.91	84.07	11.69
4	5.31	20.61	50.28	22.55	98.75	20.17
5	6.64	25.77	42.47	24.94	99.82	29.38
6	7.97	30.92	34.67	23.93	97.48	38.53
7	9.16	36.07	26.86	22.91	95.01	47.45
8	10.35	41.23	19.06	21.90	92.53	56.15
9	10.52	46.38	11.26	20.88	89.04	64.57
10	12.05	41.21	3.45	17.05	73.75	72.12
11	13.57	31.71	-4.35	13.21	54.15	78.05
12	13.72	22.22	-2.63	9.38	42.69	82.54
13	10.26	12.73	-0.90	7.13	29.21	85.87
14	6.79	7.74	0.83	6.81	22.16	88.26
15	3.32	2.75	2.55	6.48	15.10	89.98
16	1.63	1.07	2.94	6.16	11.79	91.23
17	1.43	3.18	1.69	4.54	10.84	92.28
18	2.36	5.29	0.45	2.92	11.02	93.29
19	2.19	7.40	-0.80	3.41	12.20	94.37
20	0.49	4.37	3.22	5.39	13.47	95.56
21	-1.21	1.35	7.24	7.37	14.74	96.87
22	-1.58	-1.68	11.26	9.34	17.34	98.36
23	-0.76	-0.67	15.28	9.69	23.54	100.25
24	1.04	2.29	19.29	10.03	32.66	102.86
25	2.83	5.25	23.31	10.38	41.77	106.31

The results from this computer analysis are displayed graphically in Figs. 3-6 through 3-23. Unless otherwise noted these graphs present the combined data for three to six repeat tests.

DATA ANALYSIS

It is obvious that wall panels with openings "feel" a different net load when subjected to blast waves than those without openings. In general, for structural response, one is interested in the net loading, not in front face or back face loading. Hence, the analysis of data was concentrated on the pressure (load) difference between front and back face, i.e., net loading. Of course, only a finite number of gage locations are practical, hence "net loads" are considered to act uniformly on a region, i.e., in the case of the doorway, 2 ft wide strips were used.

In this report, the simplest case of net loading from an "infinitely long" room is considered.* Most attention was concentrated on the doorway configuration because it provided the best opportunity to examine the effect of distance from an opening on back loading.

The average net and front impulse at 10 msec, 25 msec, and 100 msec was determined for the wall exposed to a shock wave from three and five strands of Primacord. A smooth curve was then fitted through the points to give an indication of the net load as a percentage of the front load and as a function of time for various distances from the opening (see Fig. 3-24). This figure

* For practical purposes, an "infinitely long" room is defined as a room long enough that shock wave reflection and filling phenomena caused by the presence of a rear wall occur too late to affect wall failure. Net loadings from rooms of finite lengths will be considered in a later report.

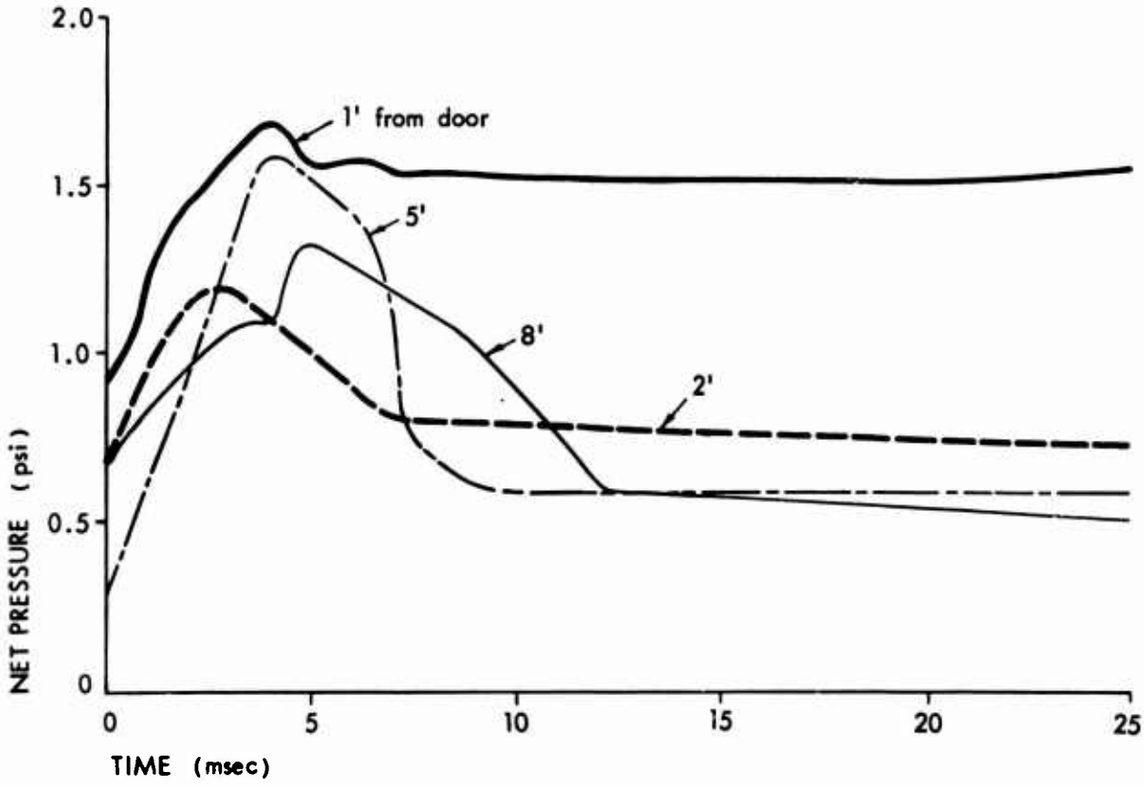

Fig. 3-6. Net Pressure Data from One-Strand, Case Two Tests (17.5 percent open doorway)

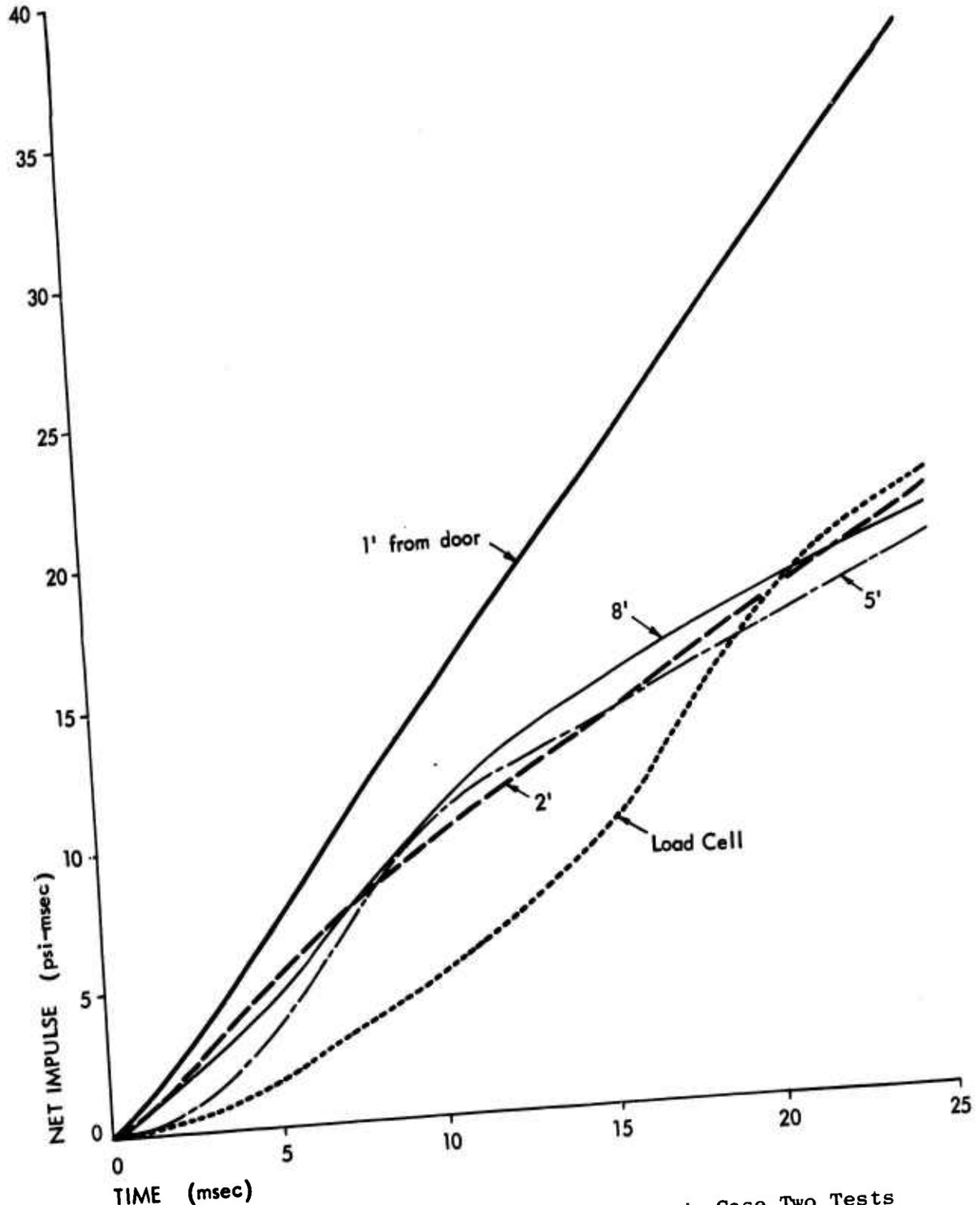

Fig. 3-7. Net Impulse Data from One-Strand, Case Two Tests (17.5 percent open doorway)

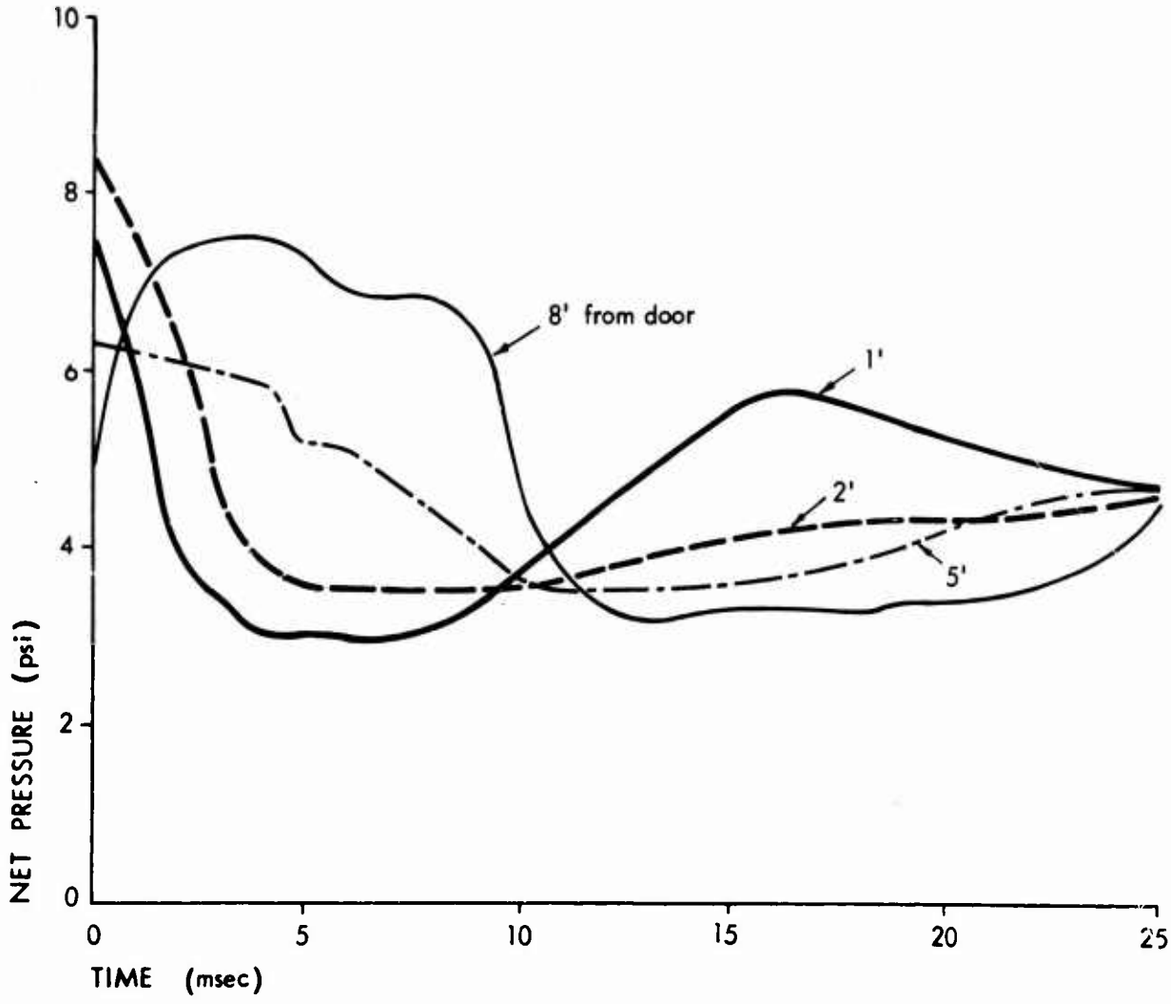

Fig. 3-8. Net Pressure Data from Three-Strand, Case Two Tests (17.5 percent open doorway)

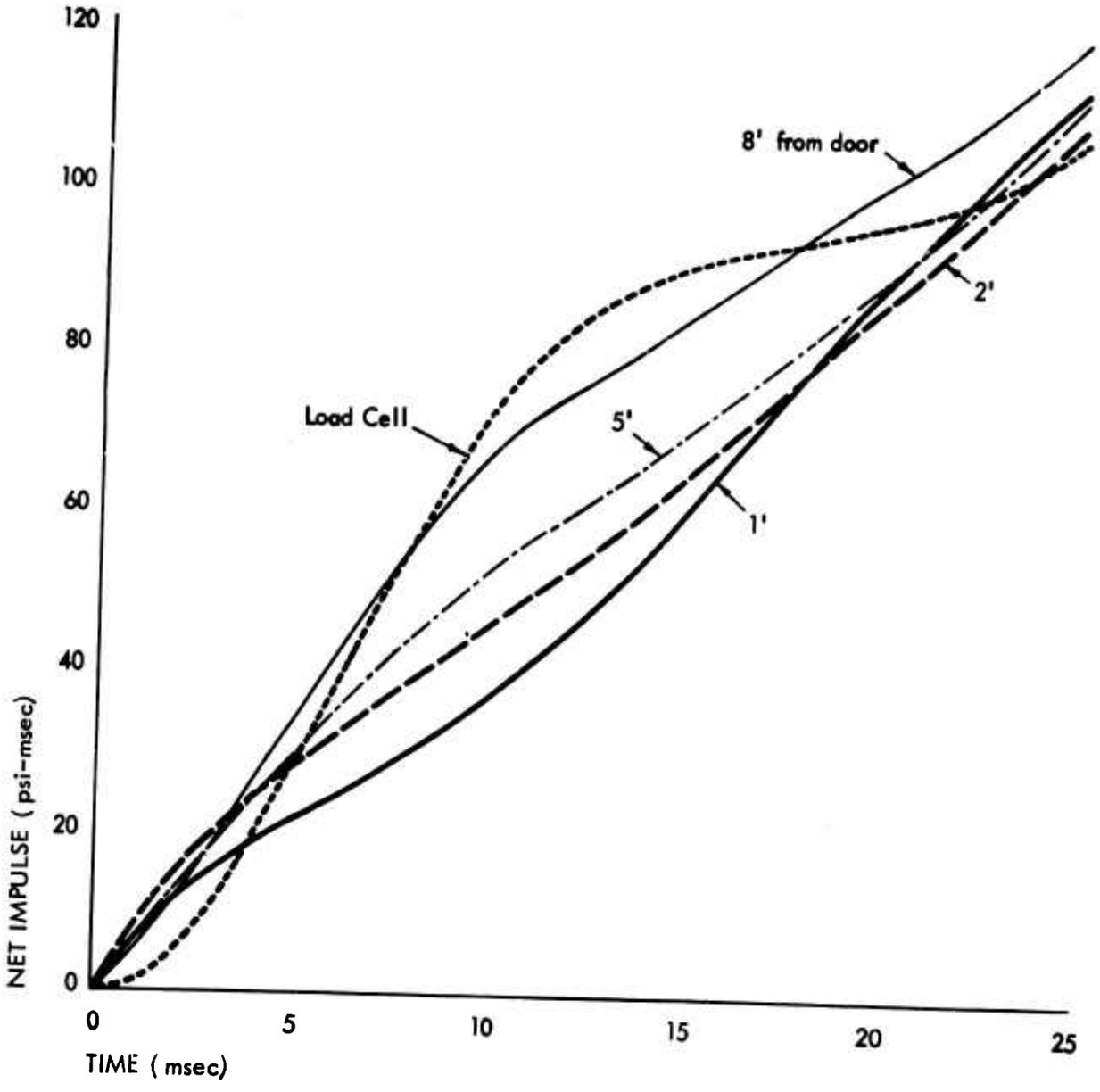

Fig. 3-9. Net Impulse Data from Three-Strand, Case Two Tests (17.5 percent open doorway)

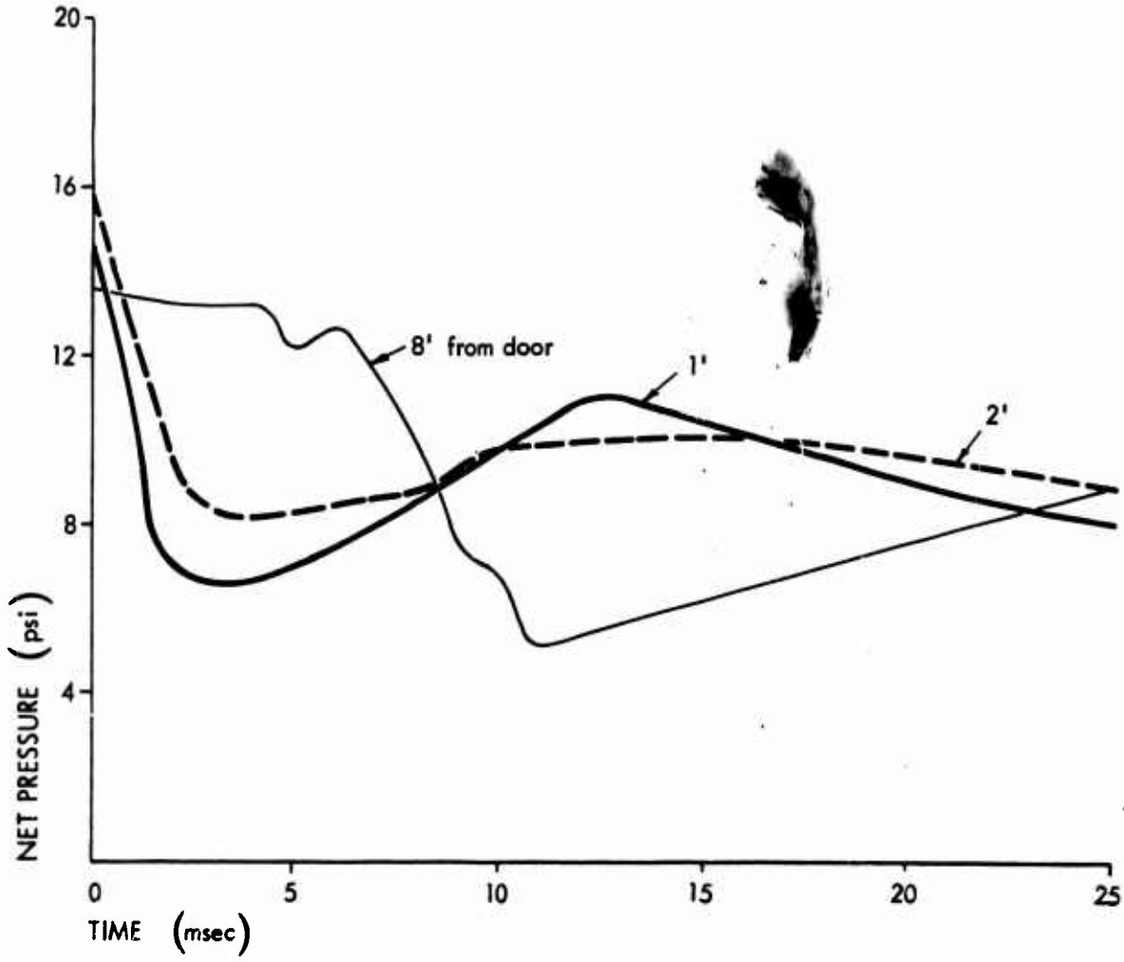

Fig. 3-10. Net Pressure Data from Five-Strand, Case Two Tests (17.5 percent open doorway)

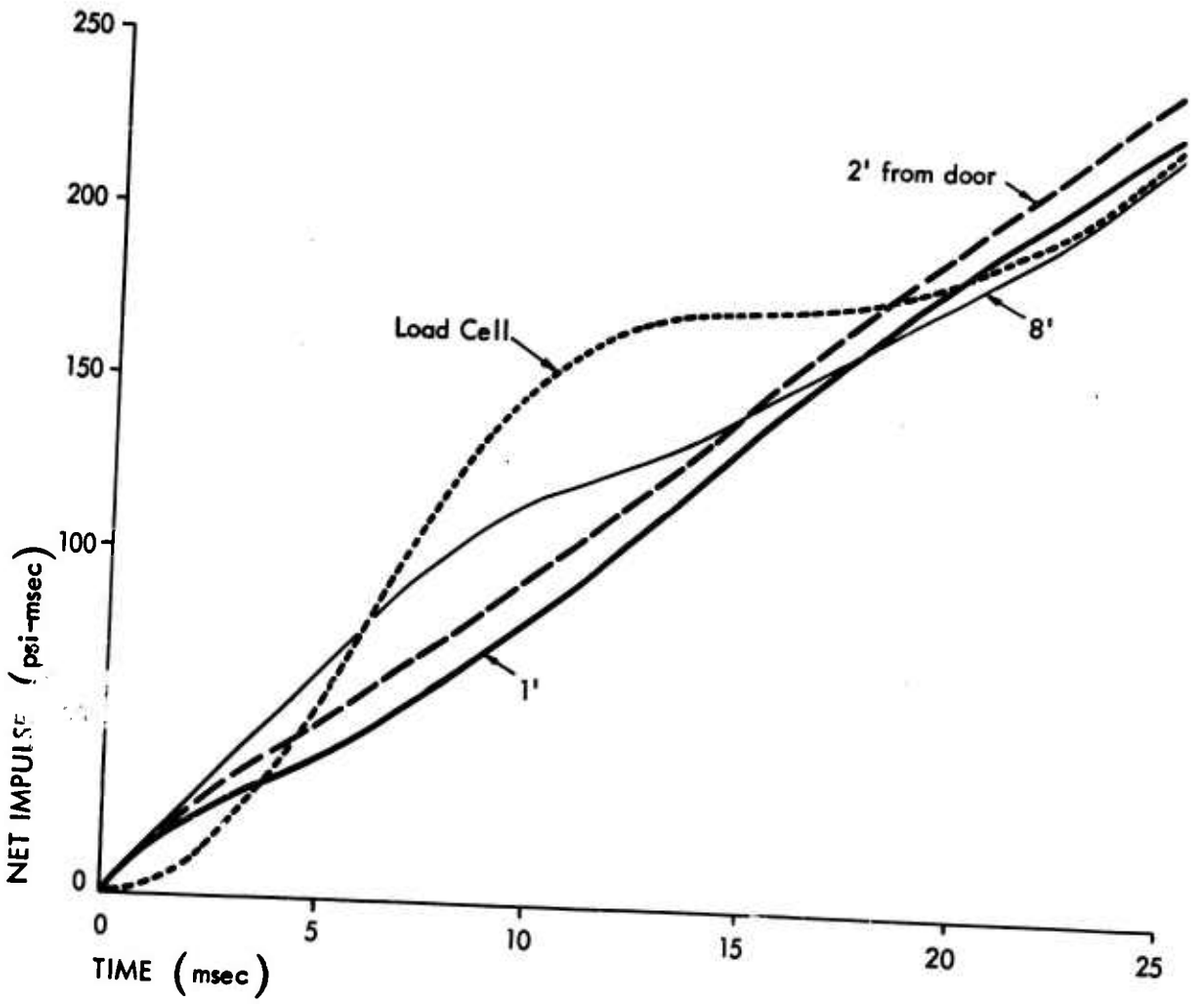

Fig. 3-11. Net Impulse Data from Five-Strand, Case Two Tests (17.5 percent open doorway)

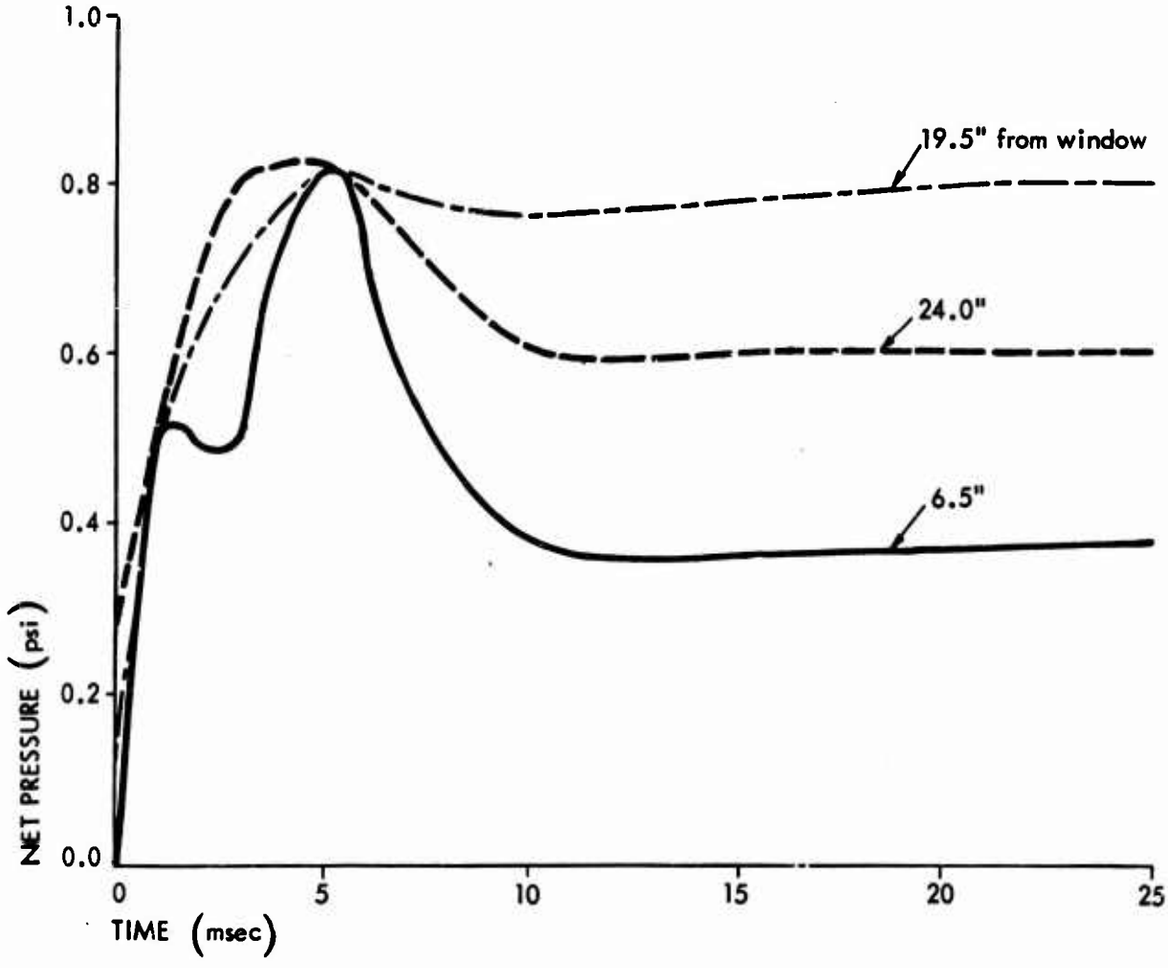

Fig. 3-12. Net Pressure Data from One-Strand, Case Three Tests (16.7 percent open window)

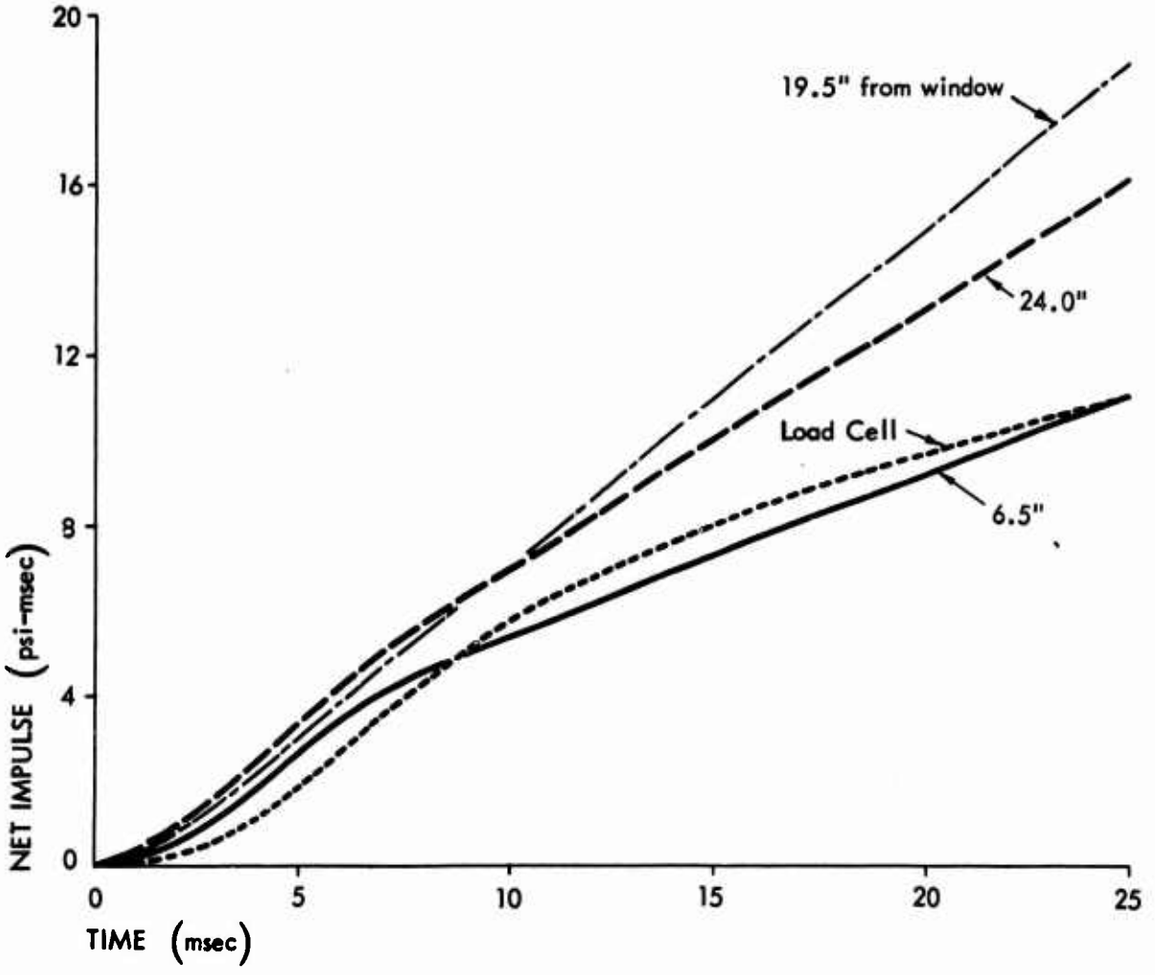

Fig. 3-13. Net Impulse Data from One-Strand, Case Three Tests (16.7 percent open window)

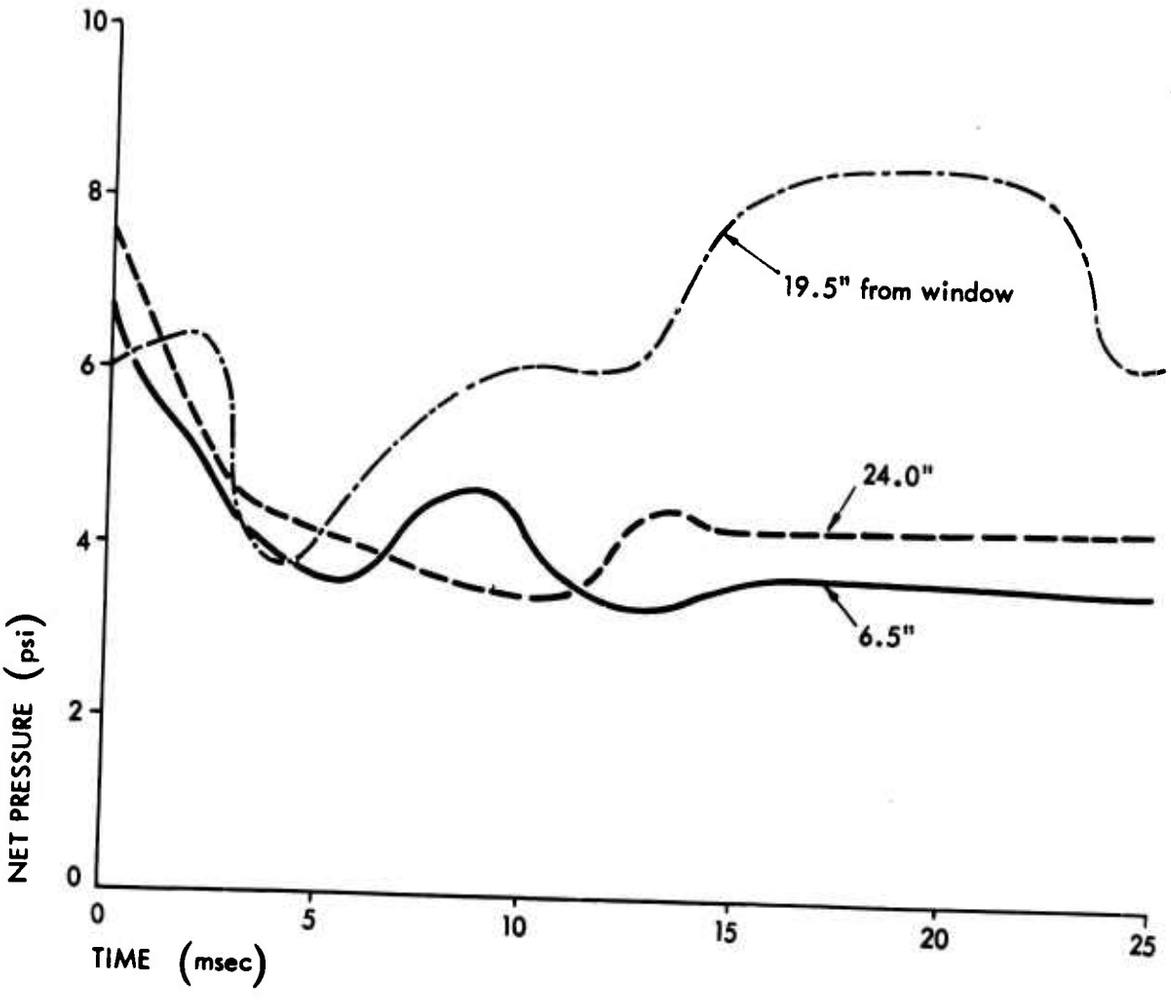

Fig. 3-14. Net Pressure Data from Three-Strand, Case Three Tests (16.7 percent open window)

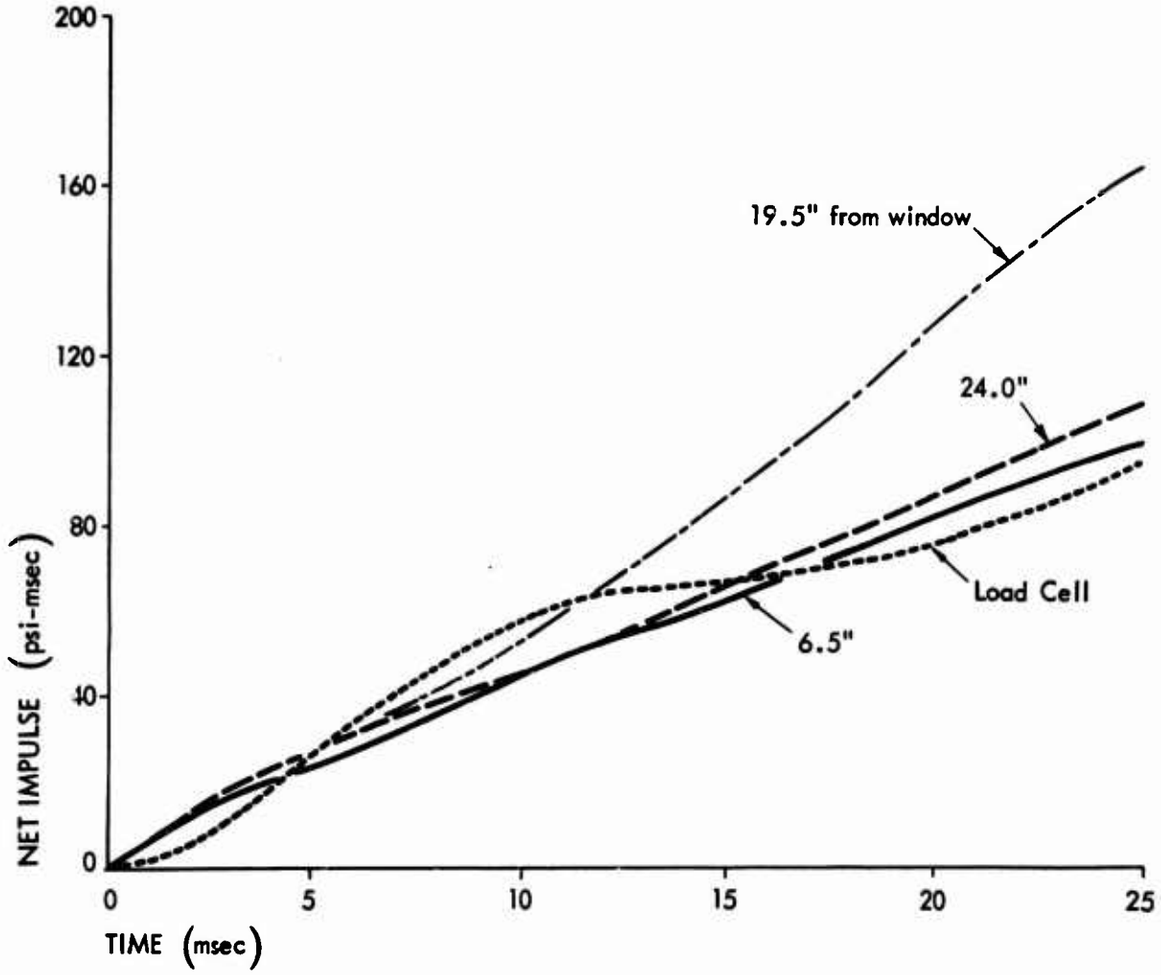

Fig. 3-15. Net Impulse Data from Three-Strand, Case Three Tests (16.7 percent open window)

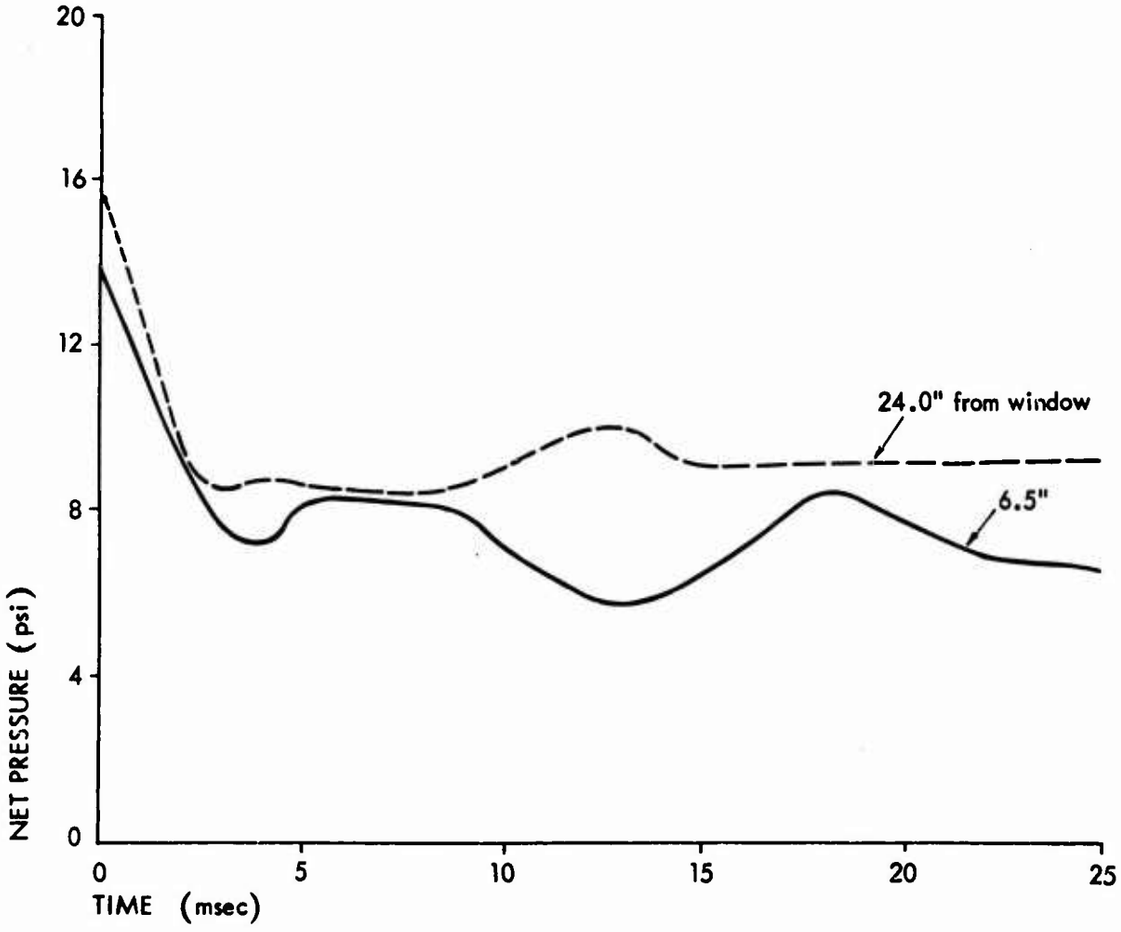

Fig. 3-16. Net Pressure Data from Five-Strand, Case Three Tests (16.7 percent open window)

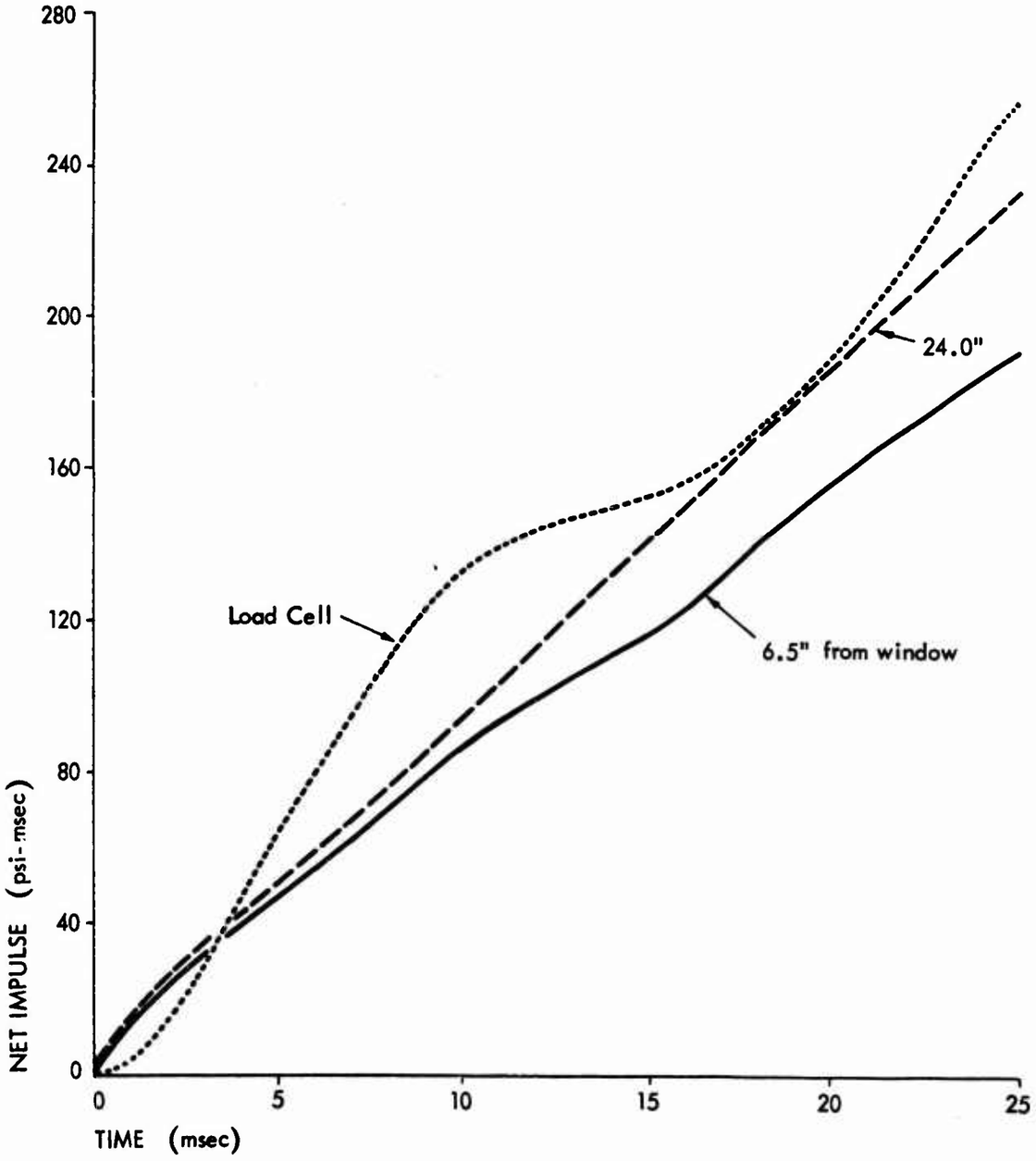

Fig. 3-17. Net Impulse Data from Five-Strand, Case Three Tests (16.7 percent open window)

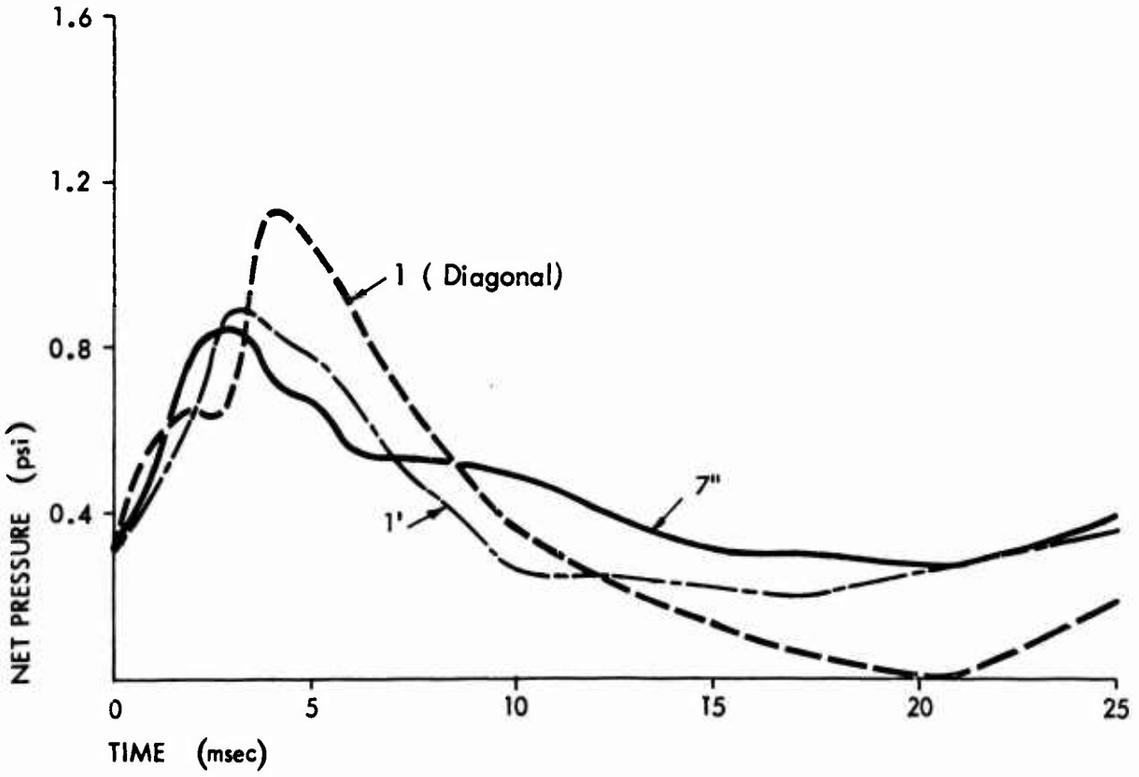

Fig. 3-18. Net Pressure Data from One-Strand, Case Four Tests (27 percent open window) (see sketch, pg. 3-9)

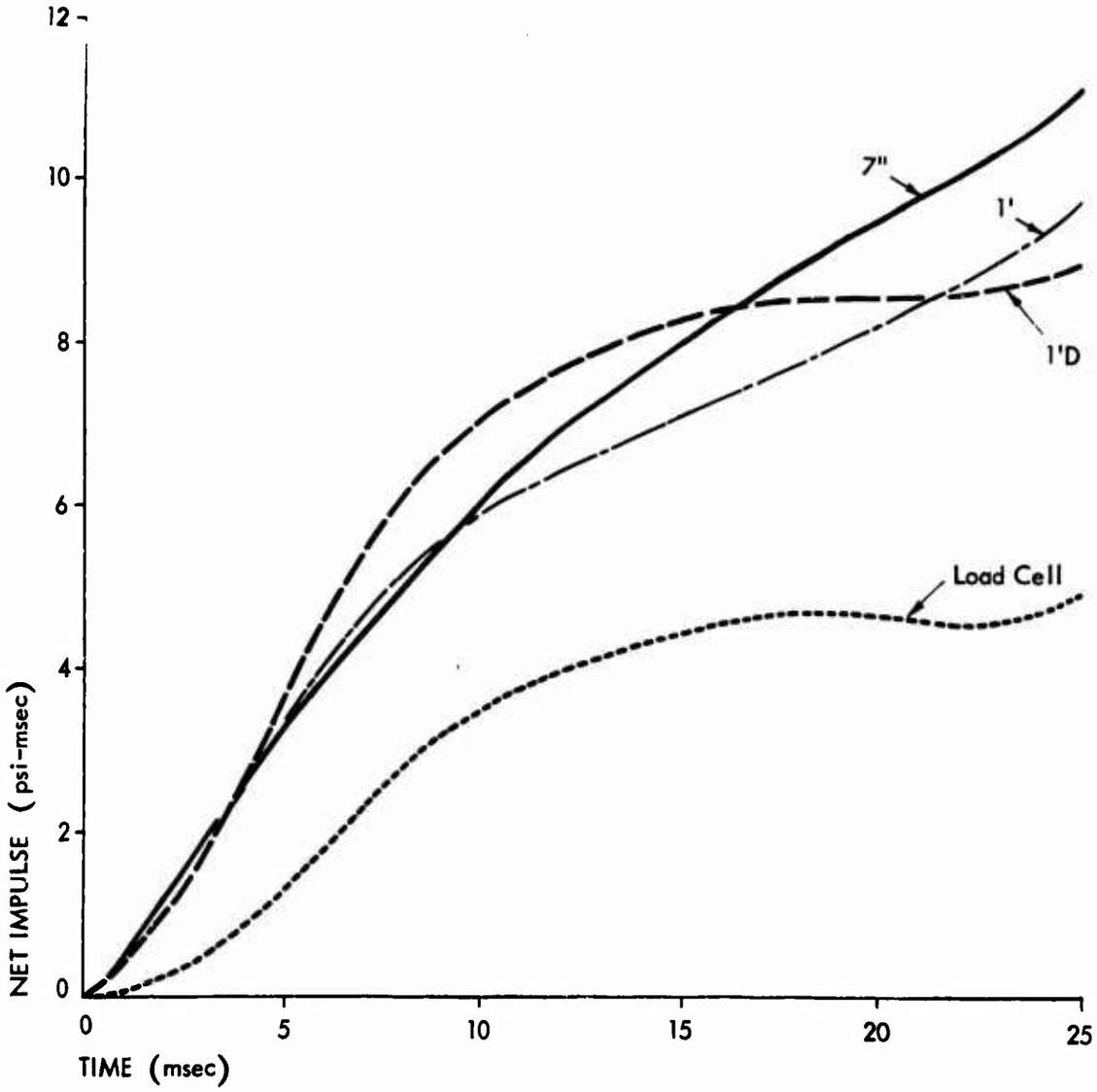

Fig. 3-19. Net Impulse Data from One-Strand, Case Four Tests (27 percent open window)

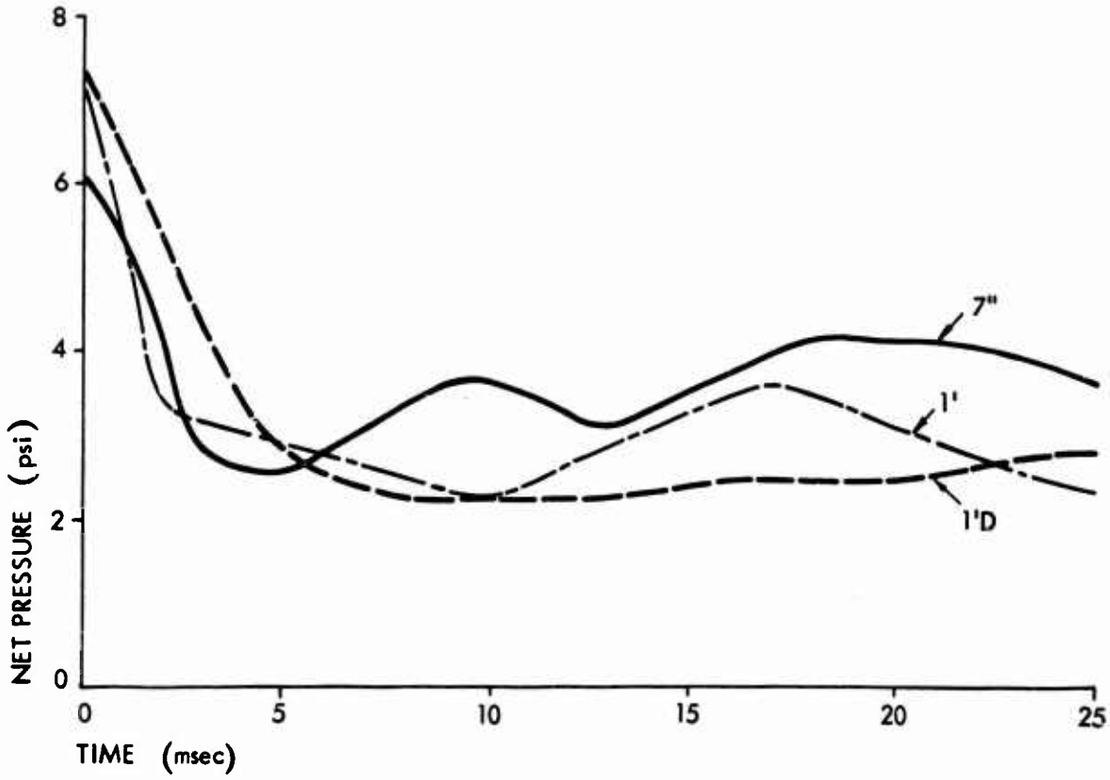

Fig. 3-20. Net Pressure Data from Three-Strand, Case Four Tests (27 percent open window)

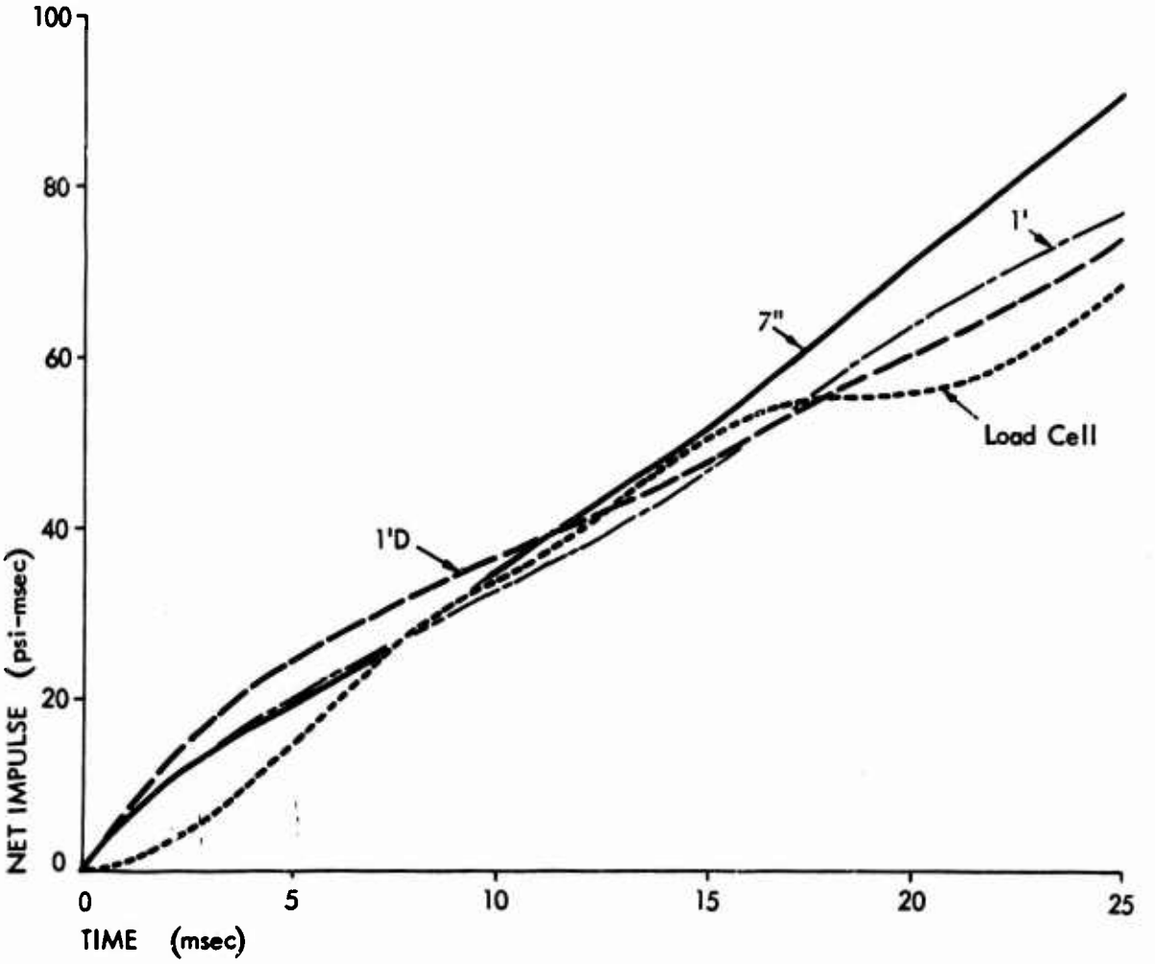

Fig. 3-21. Net Impulse Data from Three-Strand, Case Four Tests (27 percent open window)

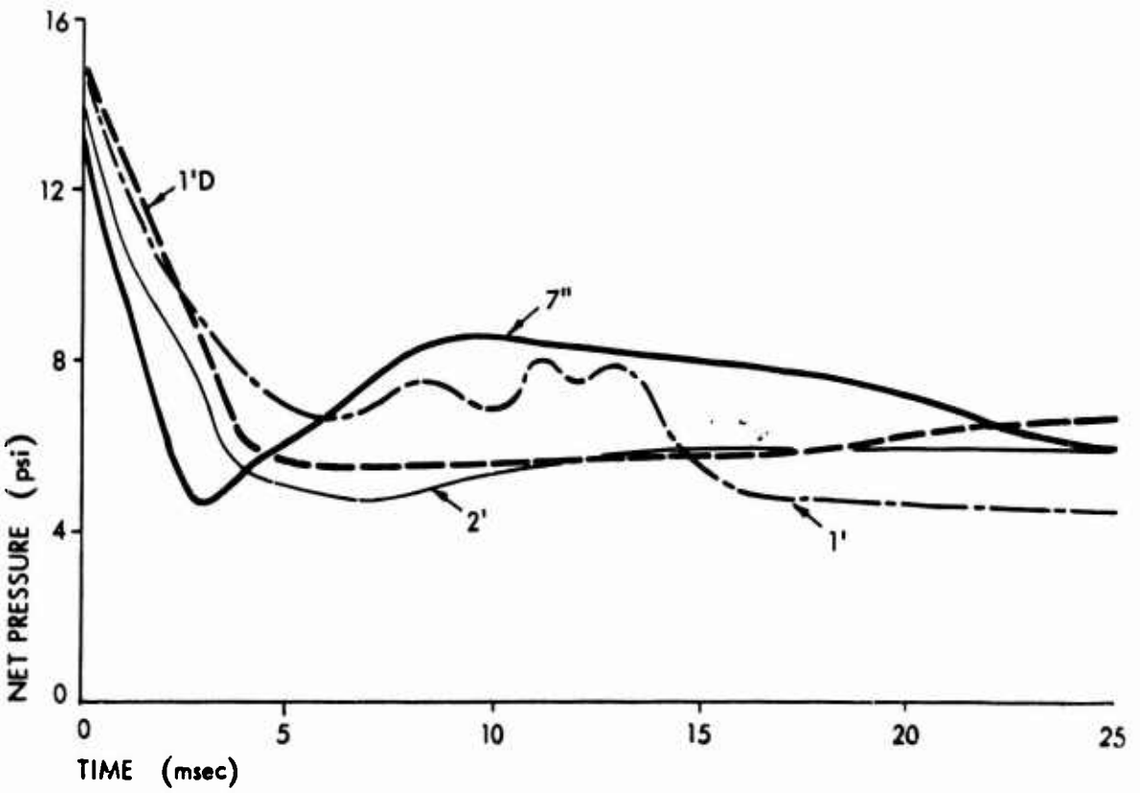

Fig. 3-22. Net Pressure Data from Five-Strand, Case Four Tests (27 percent open window)

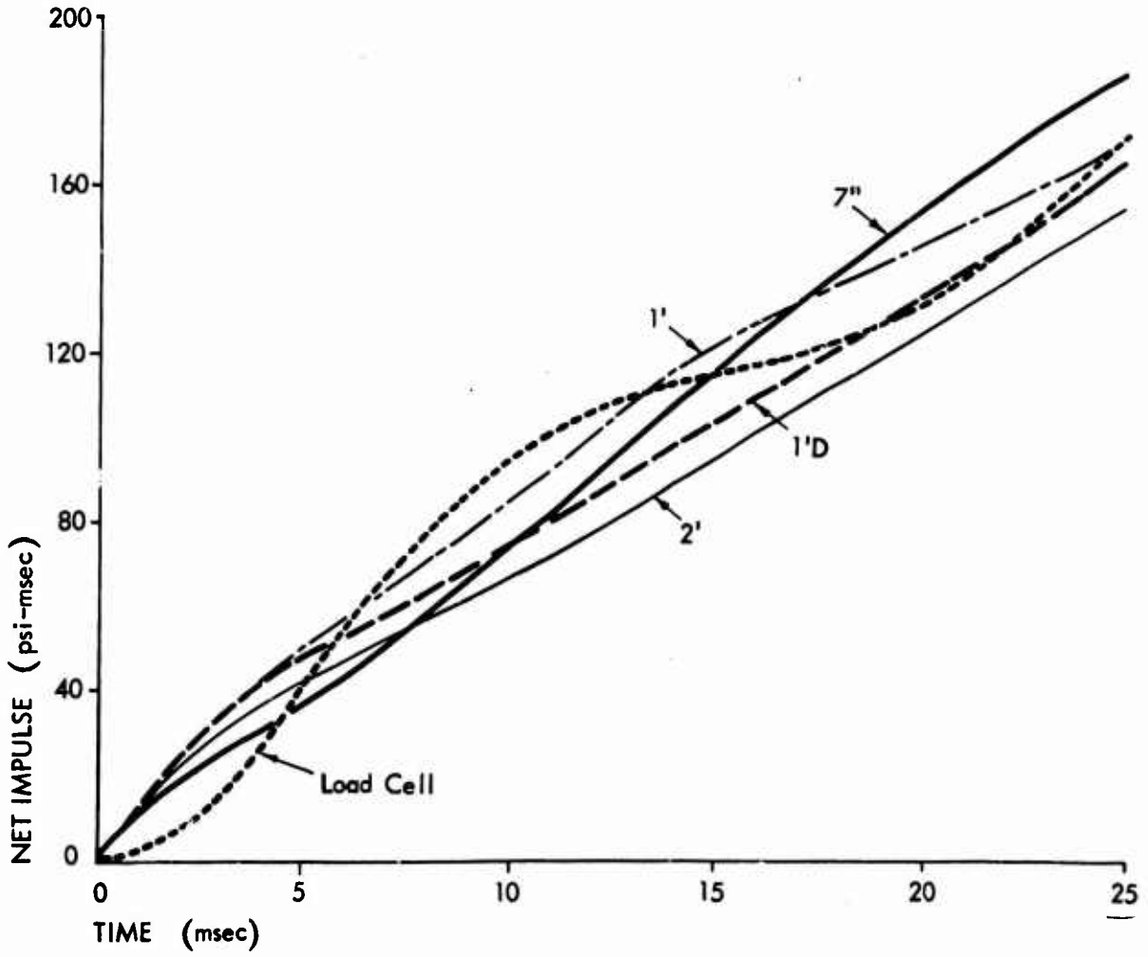

Fig. 3-23. Net Impulse Data from Five-Strand, Case Four Tests (27 percent open window)

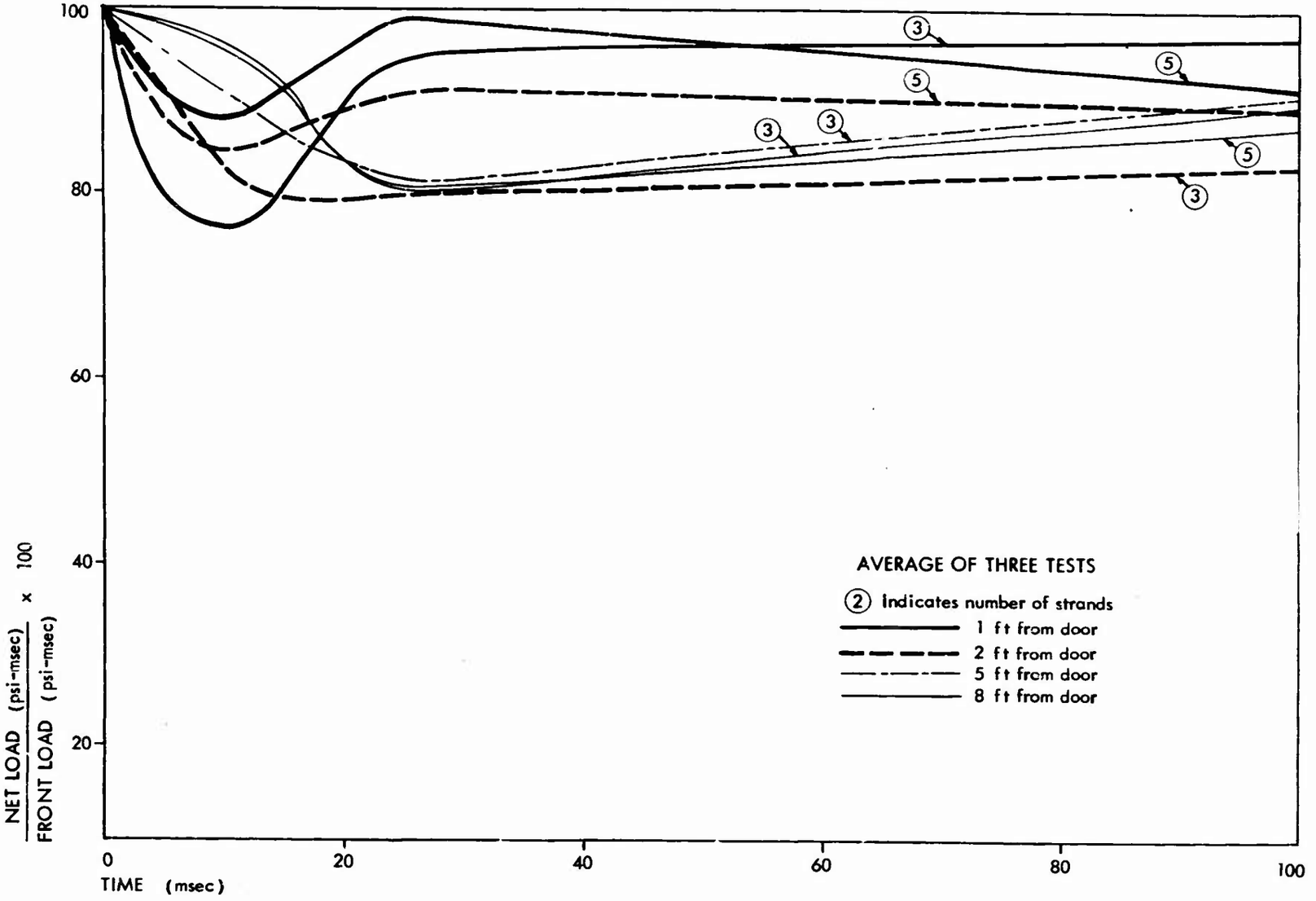

Fig. 3-24. Net Load as a Percent of Front Load — Three- and Five-Strand, Case Two Tests (17.5 percent open doorway)

indicates that backloading has little significance beyond 20 msec and that the net load is generally 80 to 95 percent of the front load. Figure 3-24 also shows how the effect of the back loading wave changes as it travels across the wall; at short distances from the opening, the effect is seen very early, while at greater distances, the effect is not as abrupt and is somewhat delayed. This figure also indicates that the distribution of net impulse across the wall will vary with time, such that peak stress is likely to occur first at the greatest distance from the opening with some reversal of this condition occurring at later times, not considering wall behavior. In general, Fig. 3-24 indicates that back loading in an infinite room with a doorway has relatively little significance, although if loadings at early times (between 5 and 20 msec) are of importance it should be noted that back loadings can account for as much as 20 percent of the net load.

In none of the doorway tests did the net pressure become negative, meaning that the overpressure on the front always exceeded the pressure on the back. The maximum back pressure always occurred at a distance of 8 ft from the opening and amounted to a maximum of 2.39 and 4.7 psi for three- and five-strand tests. There were consistent occurrences of a negative back pressure, pressure in the same direction as the front pressure, at a distance of 1 ft from the opening on the three- and five-strand tests which amounted to a maximum of 1.36 and 2.2 psi, respectively. Also, a small negative back pressure at the 2-ft distance occurred on the five-strand tests. This negative pressure at the 1-ft distance occurred generally at 15 msec on the three-strand tests and at 12 msec on the five-strand tests.

An examination of data for the large and small window loading tests yields the same general results except the importance of back loading is greater for the large window of 27-percent opening (Case Four) than for the doorway (Case Two) or the 16.7 percent opening window (Case Three). The importance of the back load for the window configurations is generally greater because the back loading wave can completely cover the back surface of the wall in a shorter time. For equivalent distances from the opening, for the 16.7 percent window

and the doorway (which was about 17.5 percent-open), the amount of reduction of the front load by the back load is about the same. However, for the 27-percent window, the reduction was greater at the same distance from the opening. It is apparent, therefore, that both the size of the opening and its placement in the wall influence the amount of net loading.

The variation of total reaction with time as measured by the load cells is shown in Fig. 3-25 for the doorway test (Case 2), Fig. 3-26 for the 16.7 percent window (Case 3), and Fig. 3-27 for the 27-percent window (Case 4). These figures are averages of the three tests conducted at each pressure level, as indicated. The natural period of the three configurations, calculated as twice the average time between the first peak and the first trough, were approximately 18 msec, 16 msec, and 20 msec for the doorway, 16-percent window, and 27-percent window, respectively. All traces shown are shifted 2 msec because there was a consistent delay of 2 msec between arrival of the shock at the front of the wall and the first registration of load by the load cells.

One very interesting series of loading tests was conducted with glass windows installed in the 27-percent opening on a nonfailing wall. The data from one three-strand and two five-strand tests are presented in Figs. 3-28 through 3-31. The load cell data from these tests, which are presented in Fig. 3-32 along with load cell data from window tests without glass, show a considerable difference between the glass and no-glass tests. In fact, the peak load indicated for windows with glass is nearly as great at early times as one would expect from a solid wall (70 to 90 percent of solid wall load vs 30 to 45 percent of solid wall load for windows without glass). The effect of the presence of glass on back loading is illustrated in Fig. 3-33 where the average pressure-time curves for the two test conditions are shown for a gage located 7 in. from the window on the back face. For the no-glass condition, there is a rapid rise to a peak pressure of almost 4.5 psi, whereas for the with-glass test condition, there is a 5-msec rise time to a peak pressure of only about 1.5 psi. The impulse under each curve at various times is given below in Table 3-3.

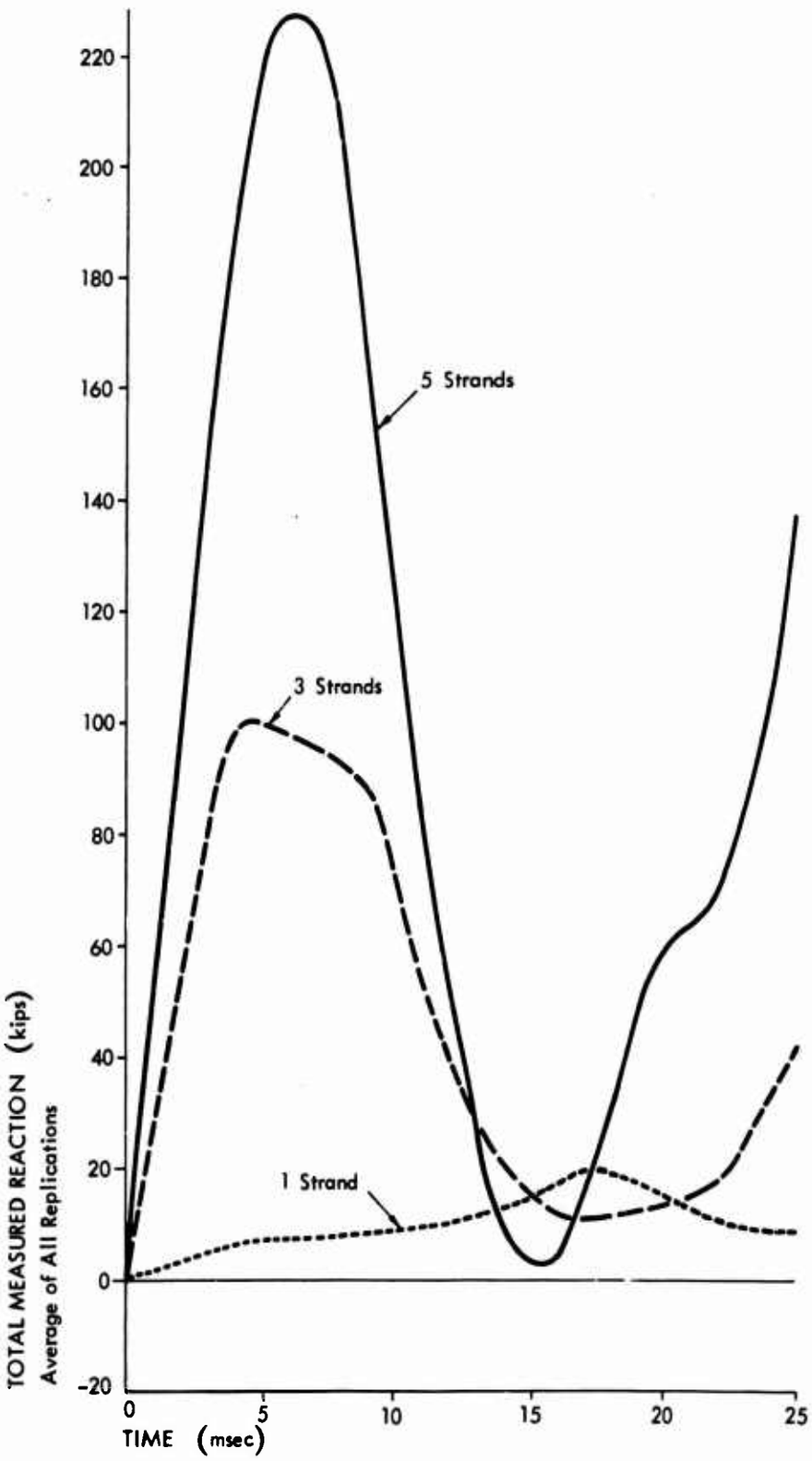

Fig. 3-25. Load Cell Data, Case Two
(17.5 percent open doorway)

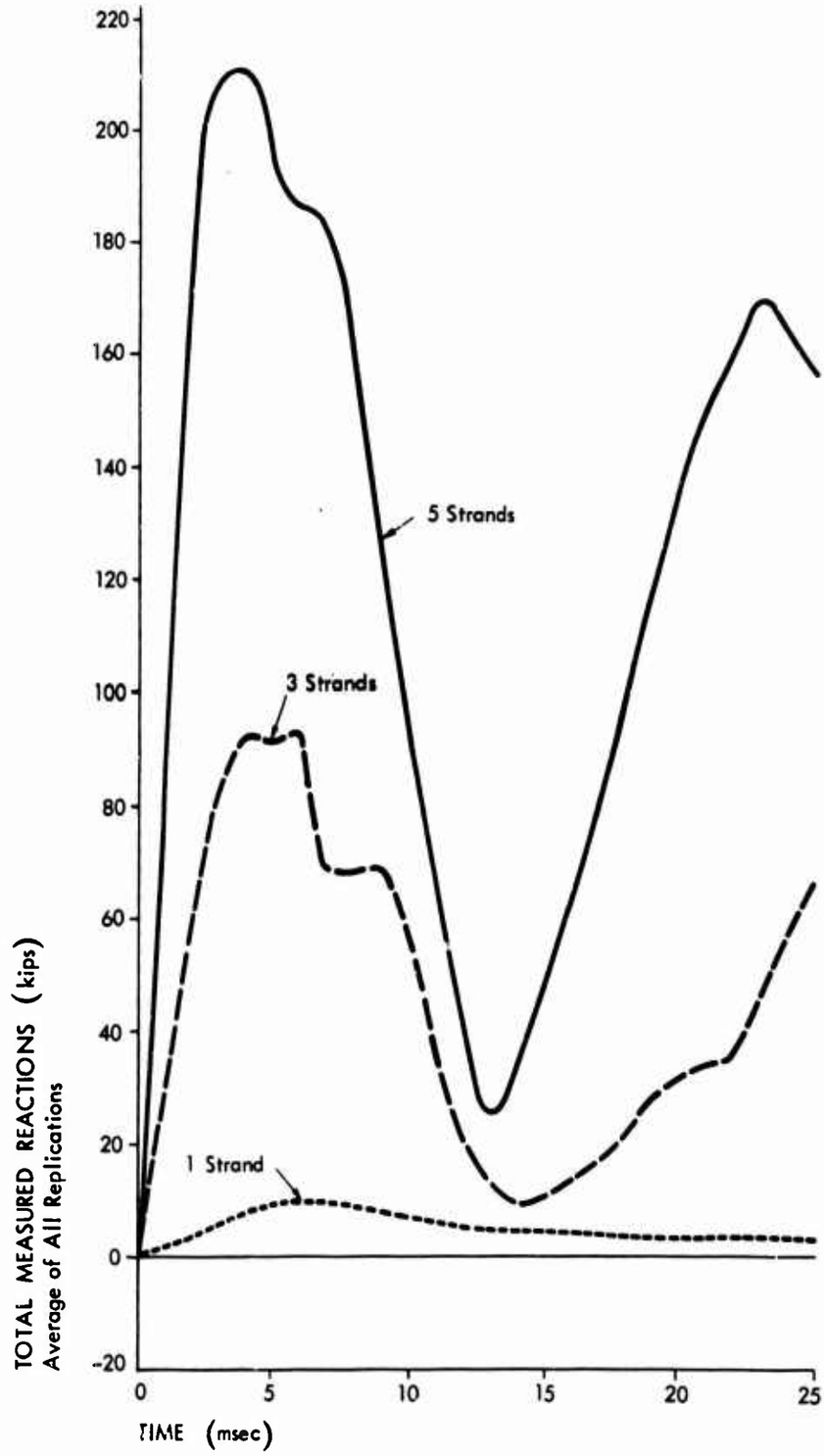

Fig. 3-26. Load Cell Data, Case Three (16.7 percent open window)

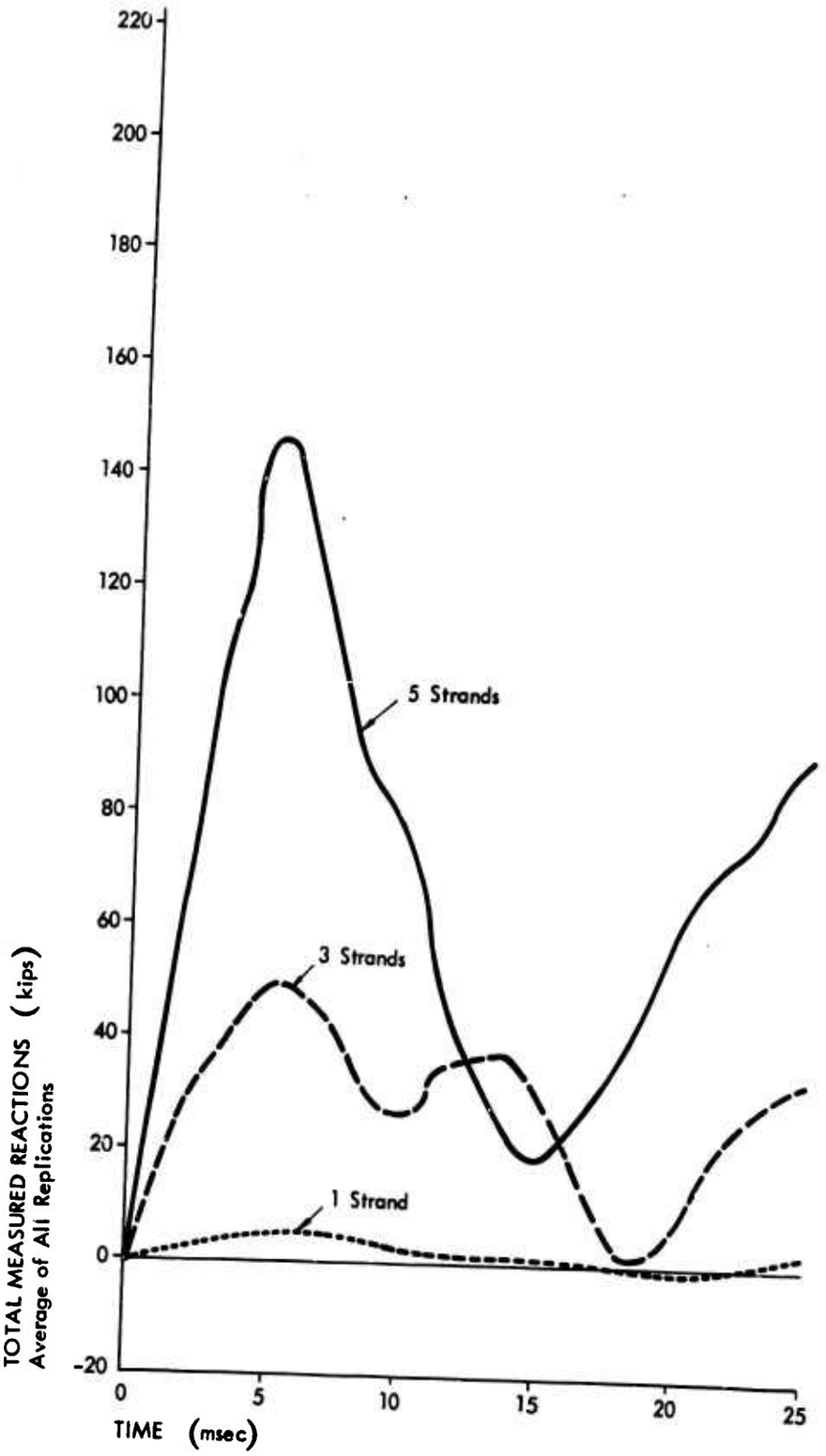

Fig. 3-27. Load Cell Data, Case Four (27 percent open window)

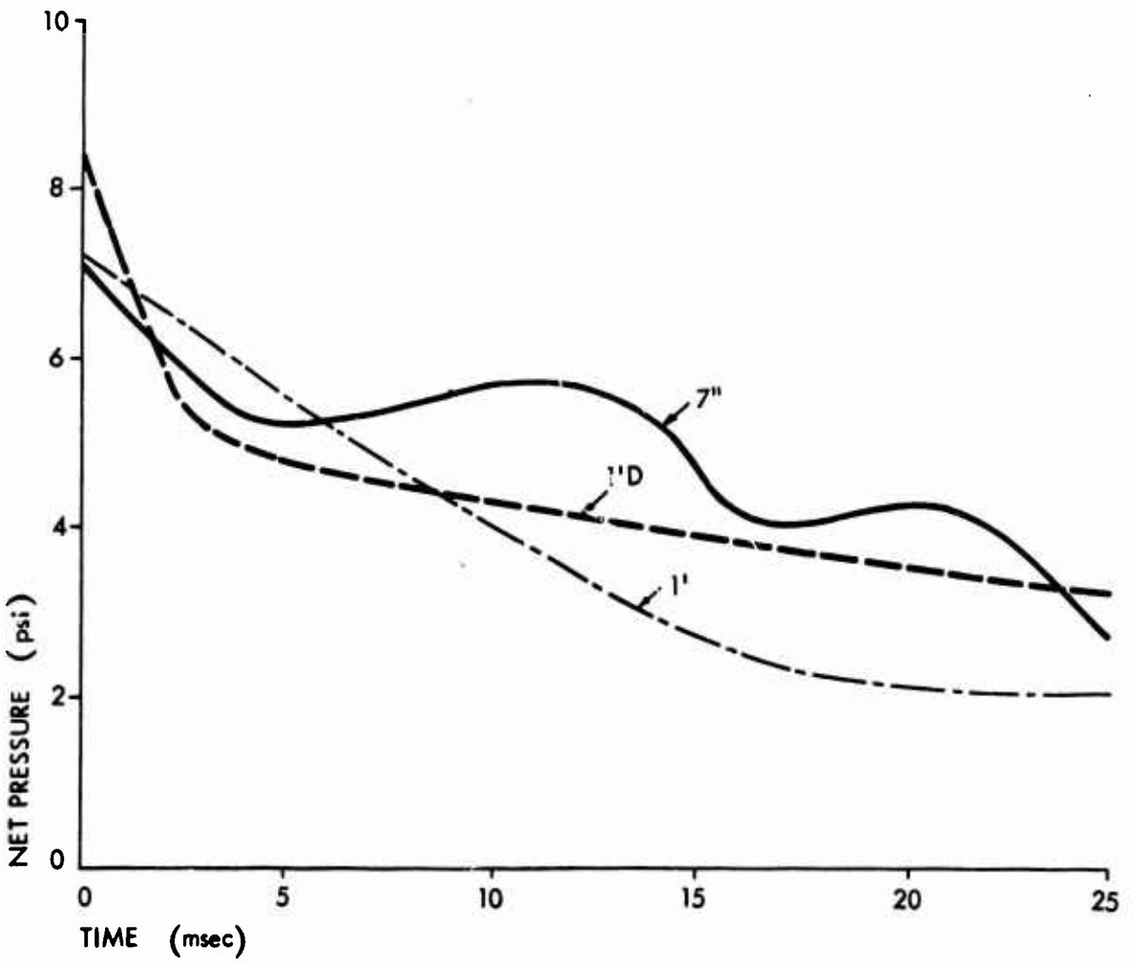

Fig. 3-28. Net Pressure Data from Three-Strand Test, Case Four with Glass (27 percent open window)

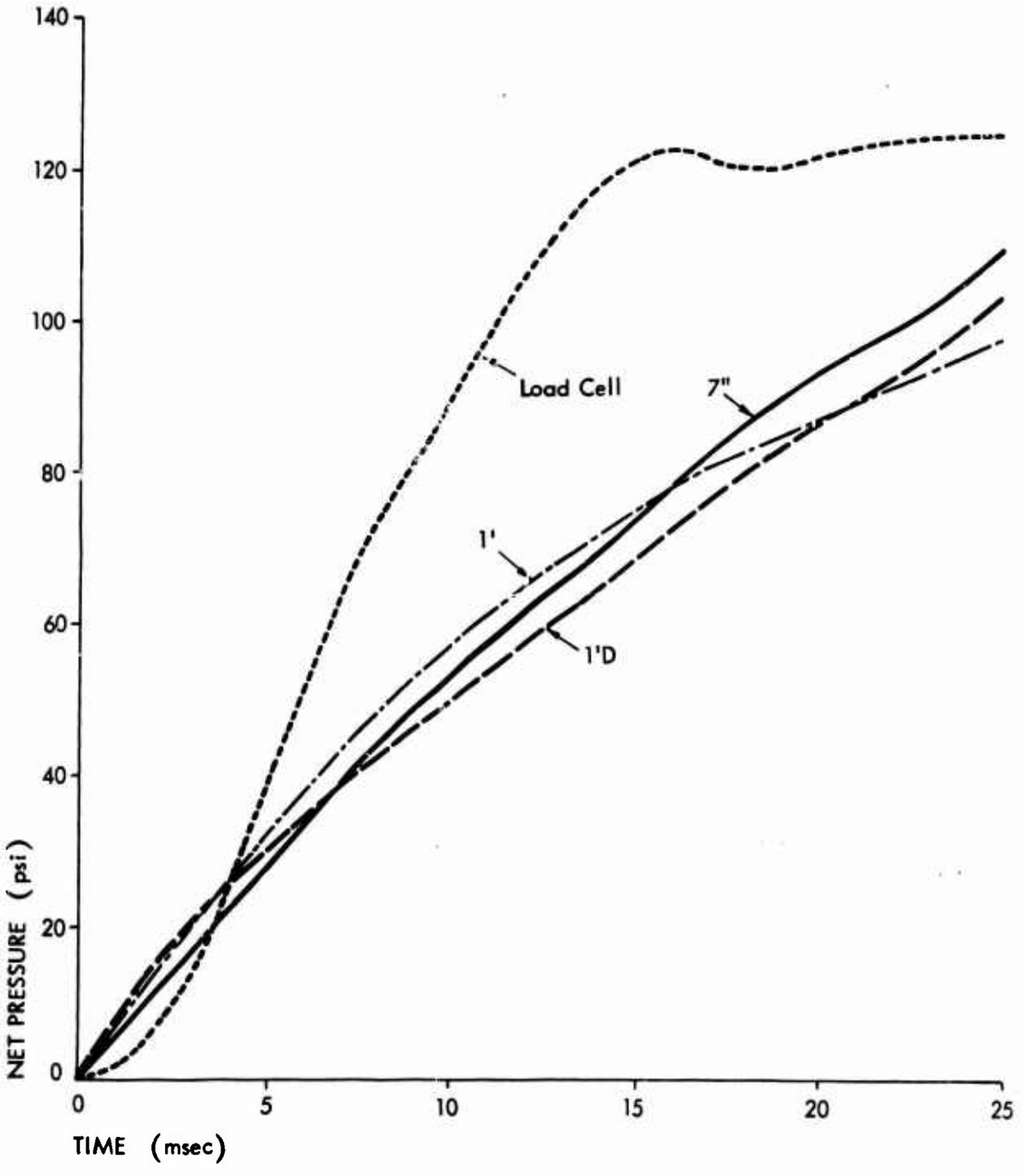

Fig. 3-29. Net Impulse Data from Three-Strand Test, Case Four with Glass (27 percent open window)

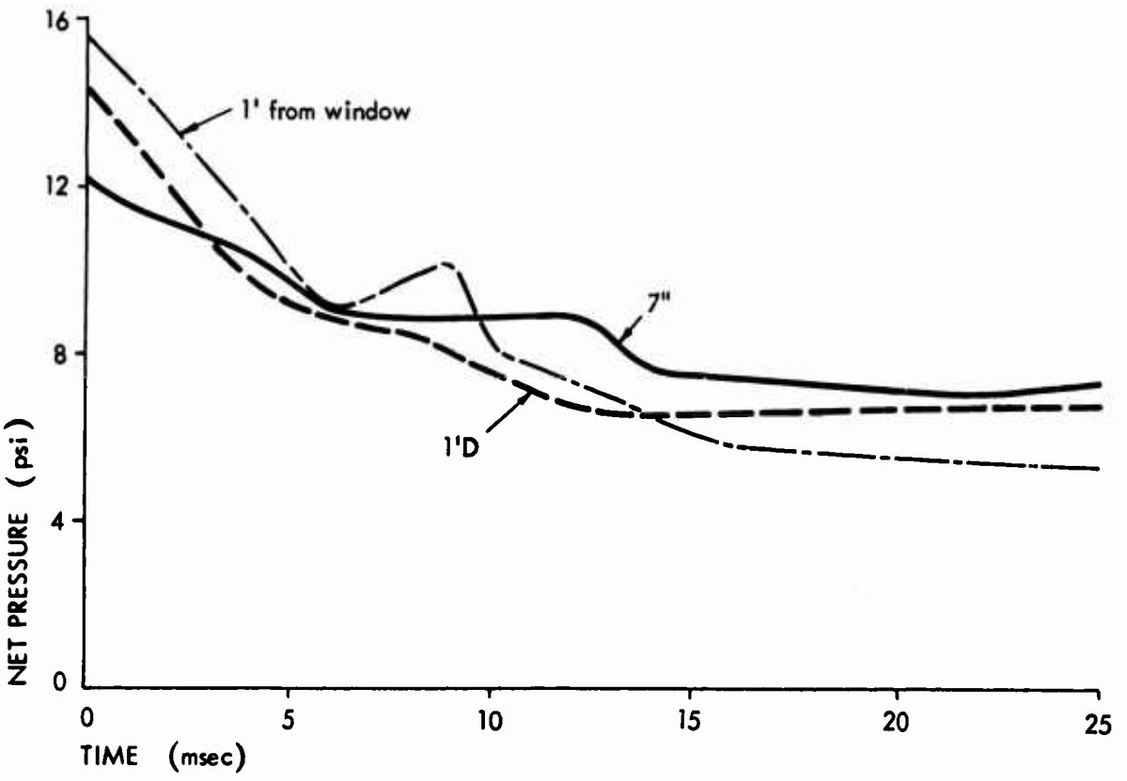

Fig. 3-30. Net Pressure Data from Five-Strand Test, Case Four With Glass (27 percent open window)

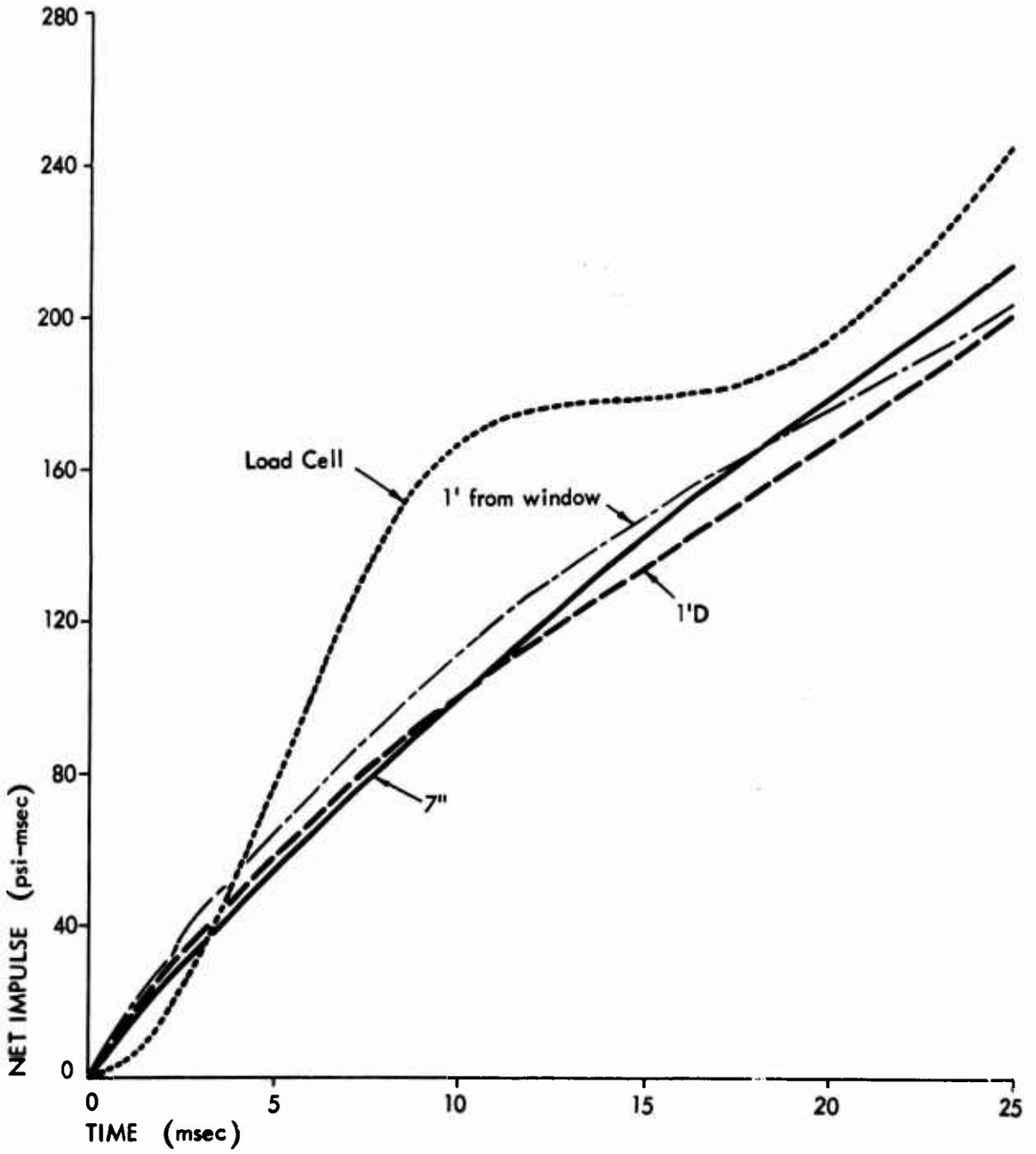

Fig. 3-31. Net Impulse Data from Five-Strand Test, Case Four with Glass (27 percent open window)

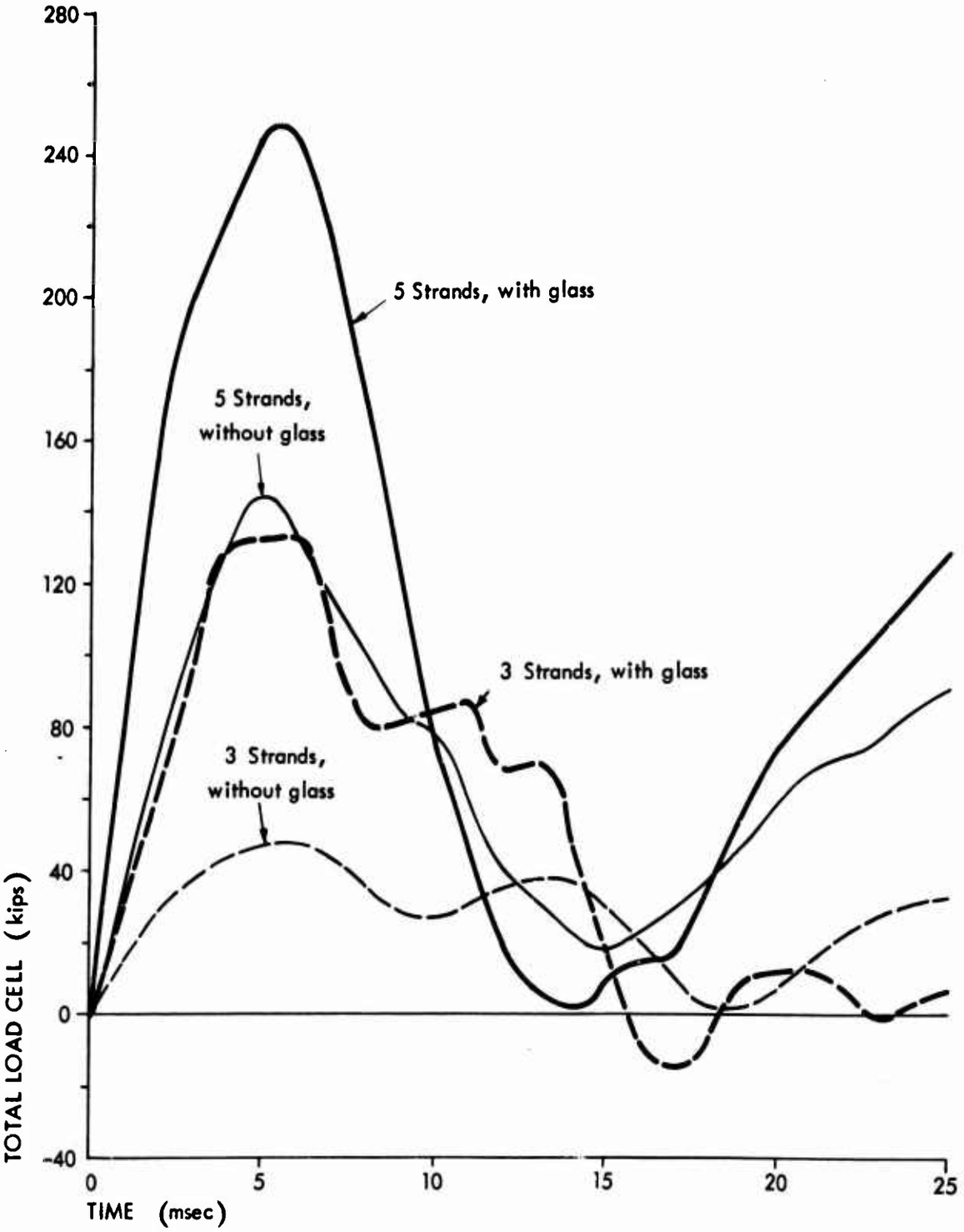

Fig. 3-32. Load Cell Data from Tests with and without Glass, Case Four (27 percent open window)

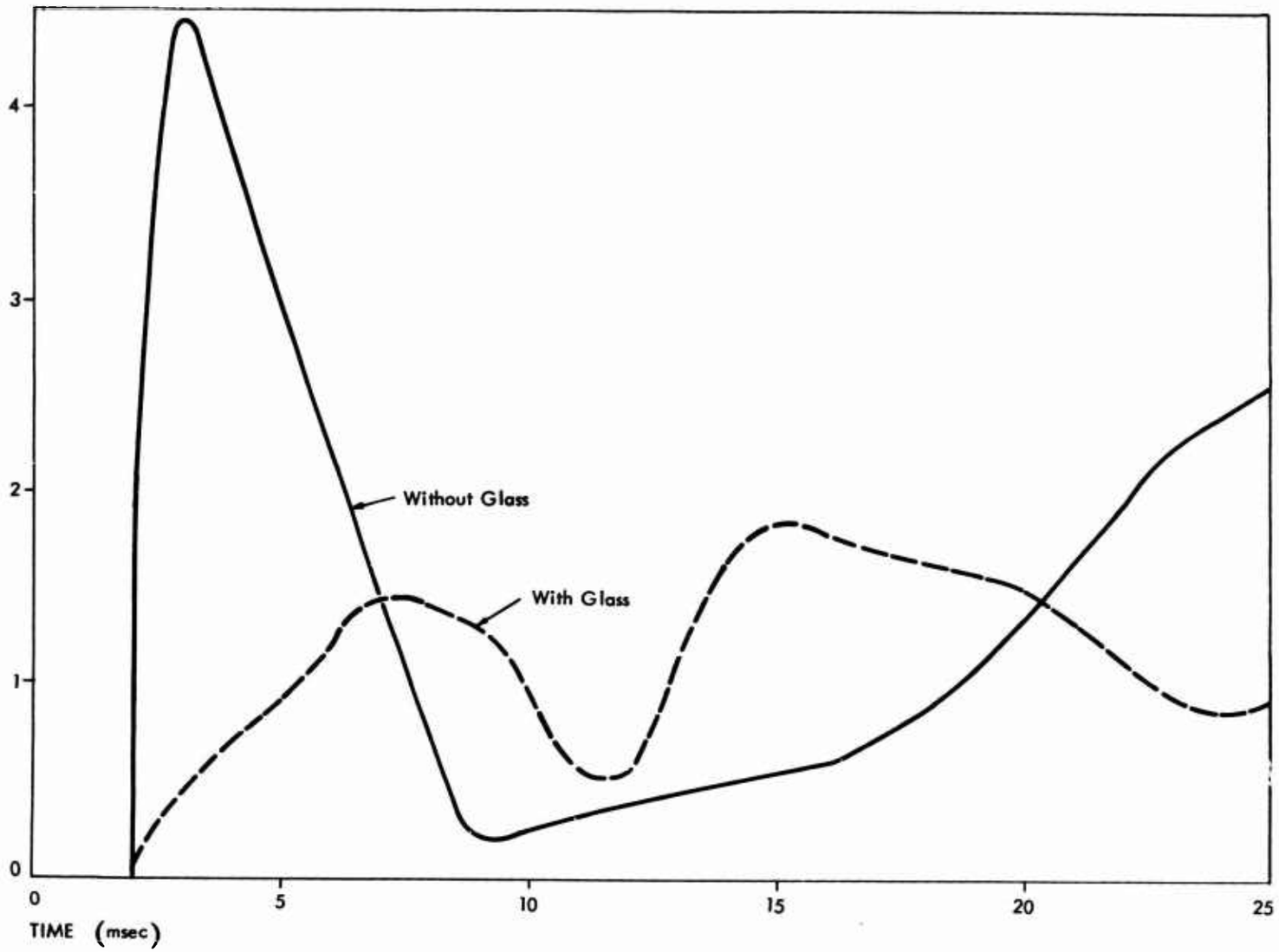

Fig. 3-33. Average Pressure-Time Curves for Gage H on Back Face of Wall, 7 in. from Edge of Window, with and without Glass, Case Four (27 percent open window)

Table 3-3

COMPARISON OF GLASS/NO-GLASS IMPULSES ON BACK FACE, 5 STRAND TESTS, 27 PERCENT WINDOW

TIME (msec)	IMPULSE (psi-msec)		PERCENT OF DIFFERENCE
	WITH GLASS	WITHOUT GLASS	
10	7.9	16.8	- 53
15	13.1	18.8	- 30
20	21.6	23.0	- 6
25	27.0	33.2	- 19

From this small amount of preliminary data, it appears that the presence of glass in the window opening could have a significant effect on the magnitude of the reaction transferred to the supporting structure, particularly at early times.

Summary of Loading Tests

The data presented in Figs. 3-6 through 3-33 are primarily that which was required as input to the computer work described in Section 4 and thus constitutes only a portion of the loading study data that are available. To indicate the scope of the loading program, a summary of the loading tests conducted to date is presented in Table 3-4.

WALL PANEL FAILURE TESTS

A summary of the wall panel failure tests conducted to date is presented in Table 3-5. Included in this table are the number of strands of Primacord, the measured peak reflected overpressure, and the total load as measured by the load cells.

Table 3-4

SUMMARY OF LOADING TESTS

TEST GEOMETRY		NUMBER OF TESTS
Case One	Nonfailing wall completely closing tunnel	28
Case Two	Nonfailing wall with 17.5 percent open door	21
Case Three	Nonfailing wall with 16.7 percent open window	9
Case Four	Nonfailing wall with 27 percent open window	29
Case Five	2 nonfailing walls, front with 16.7 percent open window, back closed	2
Case Six	2 nonfailing walls, front with 27 percent open window, back closed	9
Case Seven	2 nonfailing walls, front with 17.5 percent open doorway, back closed	6
Case Eight	2 nonfailing walls, front with 17.5 percent open doorway, back with 17.5 percent open doorway	7

Table 3-5

SUMMARY OF LOADING AND RESPONSE DATA FOR WALL PANELS

WALL NO.	LOADING STRANDS*	LOADING P_r (psi)	MEASURED PEAK AT LOAD CELLS (lb)	REMARKS
Brick Simple Beam Walls (8 in. thick)				
1	2	3	-	
2	2	3.5	-	
3	2	3.5	-	
5	2	3.6	92,000	
7	2	3.6	120,000	
21	2	3.4	82,000	
46	2	3.5	34,000	20 percent open door
47	4	10.1	116,000	20 percent open door
4	4	10	-	
6	4	10.1	42,000	
20	4	10.3	105,000	
22	4	7.6	126,000	
44	4	9.5	116,000	20 percent open door
Brick Simple Beam Walls (12 in. thick)				
50	2	4.0	-	
51	2	4.3	-	
Sheetrock Simple Beam Walls (4 in. thick)				
8	2	3.3	47,000	
10	2	2.4	46,000	
9	4	7.0	70,000	
39	2	1.5	55,000	behind nonfailing wall with window
40	4	5.4	67,000	behind nonfailing wall with window
41	2	1.5	62,000	behind nonfailing wall with doorway
42	4	5.4	49,000	behind nonfailing wall with doorway
43	4	5.4	86,000	behind nonfailing wall with doorway

* Of Primacord.

Table 3-5 (cont.)

WALL NO.	LOADING STRANDS*	LOADING P_r (psi)	MEASURED PEAK AT LOAD CELLS (lb)	REMARKS
		Brick Simple Plate Walls (8 in. thick)		
24a	2	3.2	-	wall did not collapse
24b	2	3.0	43,000	second loading
25	2	3.5	74,000	wall did not collapse
29a	2	3.8	86,000	wall did not collapse
29b	2	4.2	90,000	second loading
28	2-1/2	4.0	62,000	
23	4	10.9	235,000	
32	4	9.3	166,000	
33	4	9.3	189,000	
26	6	19.3	-	
30	6	16.3	235,000	
31	6	15.0	304,000	
		Concrete Simple Beam Walls (8 in. thick)		
36	2	3.5	76,000	

These tests were conducted over a period ranging from early 1967 to October 1970. As noted earlier in the report, the fundamental philosophy used throughout this long-range program has been to conduct tests primarily to furnish specific data imputs to the theoretical efforts which have been proceeding in parallel with the experimental program.

Section 4
ANALYTICAL PROGRAM

The major effort in the analytical portion of the program has been devoted to expansion of our computer analysis and prediction capability. As our knowledge of the failure process matured, there was an increased need for more sophisticated mathematical models, particularly as we expanded our analysis capability to more complex wall forms (doorways and window openings) where the loading was much more complex than that on walls with no openings, i.e., every point on the wall has a different load-time history.

STRUCTURAL MODELING

In recent years, an analytical procedure known as the finite-element method for analyzing continuums (such as plates and shells) has been perfected. This method is based upon the assumption that a continuum with a infinite number of degrees of freedom can be quite accurately approximated by an equivalent continuum with a finite number of degrees of freedom. This equivalent continuum is divided into elements which are interconnected at a finite number of points, known as nodal points. The total degrees of freedom is the sum of the degrees of freedom of each node. A number of computer codes have been developed using this computational procedure. The one presently being used on this program is the Structural Analysis and Matrix Interpretive System (SAMIS), developed by the Western Development Laboratories (WDL) of the Philco-Ford Corporation under contract to and in association with the Jet Propulsion Laboratory. This is a very powerful and complex code, capable of handling either triangular elements (e.g., plates and shells) or line elements (e.g., trusses and frames).

APPLICATION OF SAMIS

The solution of a typical structural problem using this computer code involves the following steps. First, the mechanical properties of the materials of interest are defined. Then a listing is made of the element data

defining the local geometry (thickness, cross-sectional area, moment of inertia), gridpoint (numbers and locations) coordinate systems, temperatures, weight, and pressure on each element. Matrix input is used to define boundary and loading conditions. Finally, a set of pseudo instructions are used to direct the operation of the program.

As a trial run, a model segment of a simply supported nonfailing brick wall panel was analyzed with SAMIS. The dimensions chosen were 2 ft wide by 8 ft long (due to symmetry about the centerline, only about 4 ft are analyzed) by 8 in. thick.* The 2-ft width was chosen as a convenience, since it could be repeated many times. For example, by repeating it six times, a complete 12-ft-wide panel as used in the tunnel tests could be studied. The horizontal girder was not modeled for this problem, since it would have unnecessarily complicated this first trial. The computer model is shown in Fig. 4-1. It has 18 joints and 19 elements (16 triangular and 3 line). The triangular elements represent the brick wall, and the line elements are steel rods representing the horizontal support members. The connections at joints 5, 11, and 17 are pinned and those at 6, 12, and 18 are fixed. The connections at joints 1, 7, and 13 are modeled such that they are capable of translation in the z-direction only, i.e., perpendicular to the face of the wall. This effectively models the panel as if it were half of an 8-ft panel. The material properties of brick were a modulus of elasticity of 1×10^6 psi, and a Poisson's ratio of 0.1.

Two example problems were chosen. One was a static solution, using a uniform 2.0-psi loading; the other was a dynamic solution, using a uniform 1.0-psi step pulse of infinite duration (although only 40 msec of the loading history was used).

*For a detailed description of this initial effort, see Ref. 2.

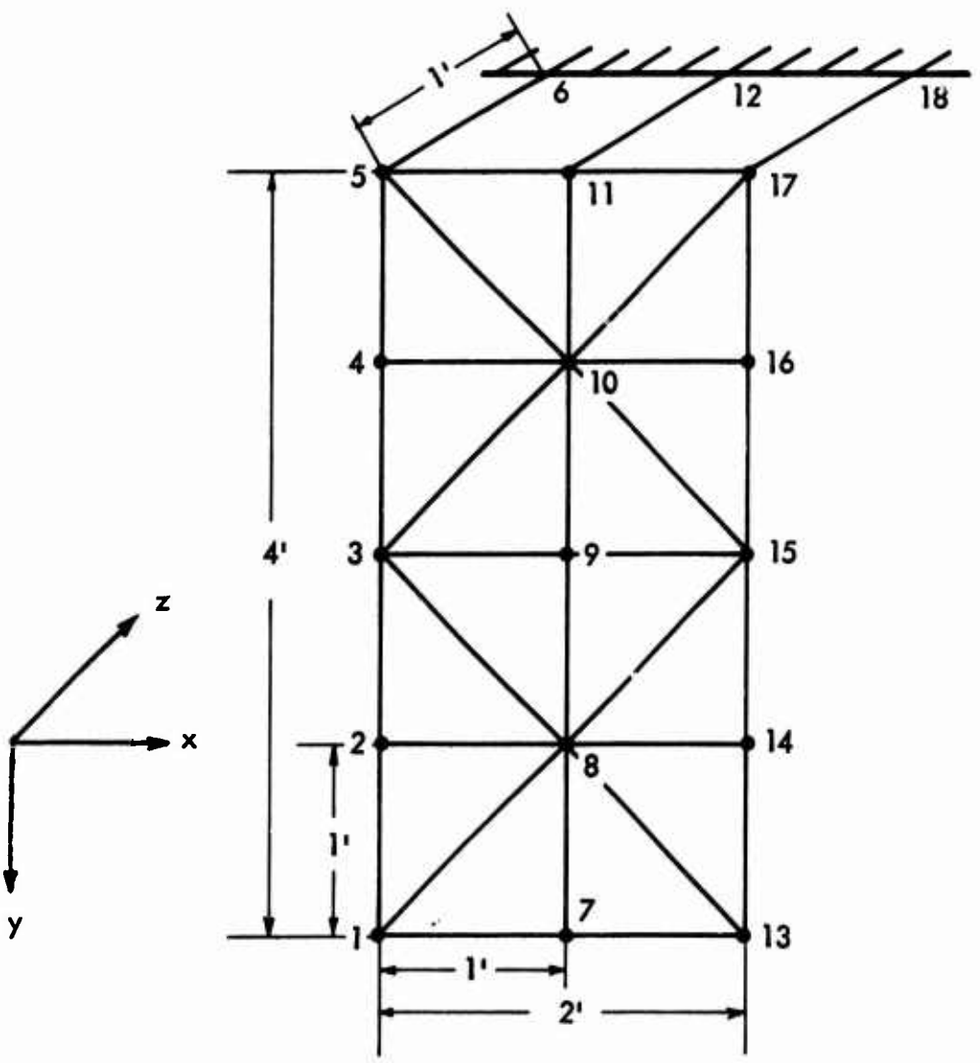

Fig. 4-1. Trial Model of Brick Wall Panel for SAMIS

Static Problem

The uniform load of 2.0 psi was included as input for each facet. The output of SAMIS for this static case included the displacements for each of the 15 nodal points, and the stresses associated with each of the 19 elements. These computed displacements are listed in Table 4-1. It will be noted that there are differences between the edge and center displacements. These are caused by the fact that the fibers on the loaded face are in compression while the fibers on the unloaded face are in tension, thus causing a convex curvature of the surface (antielastic bending), which is changed to concave at the supports due to their restraining effect. This effect is caused by Poisson's ratio for the material and is more pronounced in metal plates or wide beams when Poisson's ratio is near 0.3. In masonry it tends to be 0.1 or less.

Table 4-1

DISPLACEMENTS FOR TRIAL BEAM DUE TO A 2-PSI STATIC LOAD (in inches)*

NODE	5	11	17
DISPLACEMENT	0.0001473	0.0001806	0.0001473
NODE	4	10	16
DISPLACEMENT	0.02045	0.02033	0.02045
NODE	3	9	15
DISPLACEMENT	0.03745	0.03718	0.03744
NODE	2	8	14
DISPLACEMENT	0.04862	0.04830	0.04862
NODE	1	7	13
DISPLACEMENT	0.05252	0.05216	0.05252

* From Table 3-2, Ref. 2.

Dynamic Problem

The dynamic portion of SAMIS uses a loading matrix and computes stresses and deflections at the end of each time step. The time interval is predetermined by the program user and, for program stability, must be on the order of one-twentieth the highest natural period for the structure in question.

This time requirement created some problems with our application because the highest natural period for our model of the brick wall was quite short, being on the order of 2 msec, which means a time step of 0.01 msec. Further, the model of the beam was simplified so that the panel was represented by having the total mass concentrated at the five center nodal points, rather than all 15. This had the effect of decreasing the highest natural period, thus increasing the minimum time interval by a factor of 10. A plot of the displacements versus time (Fig. 4-2) indicates that the maximum dynamic displacements at the center is 0.05202 in., which is almost identical to the static displacement of 0.05216.

Although the modeling (computer-wise) is rather briefly discussed herein, it should be noted that a good deal of engineering judgement and experience is required to achieve an adequate, yet economical computer model. That is why it seemed important to the authors to experiment with a small portion of the system before moving to the more complex and complete system. For example, it is possible to lump the masses on alternate nodes to decrease the number of steps required in the dynamic solution, which, of course, saves computer time at some cost of accuracy. This particular simplification led to no detectable error in the displacement calculations while still simpler models did indeed prove inadequate.

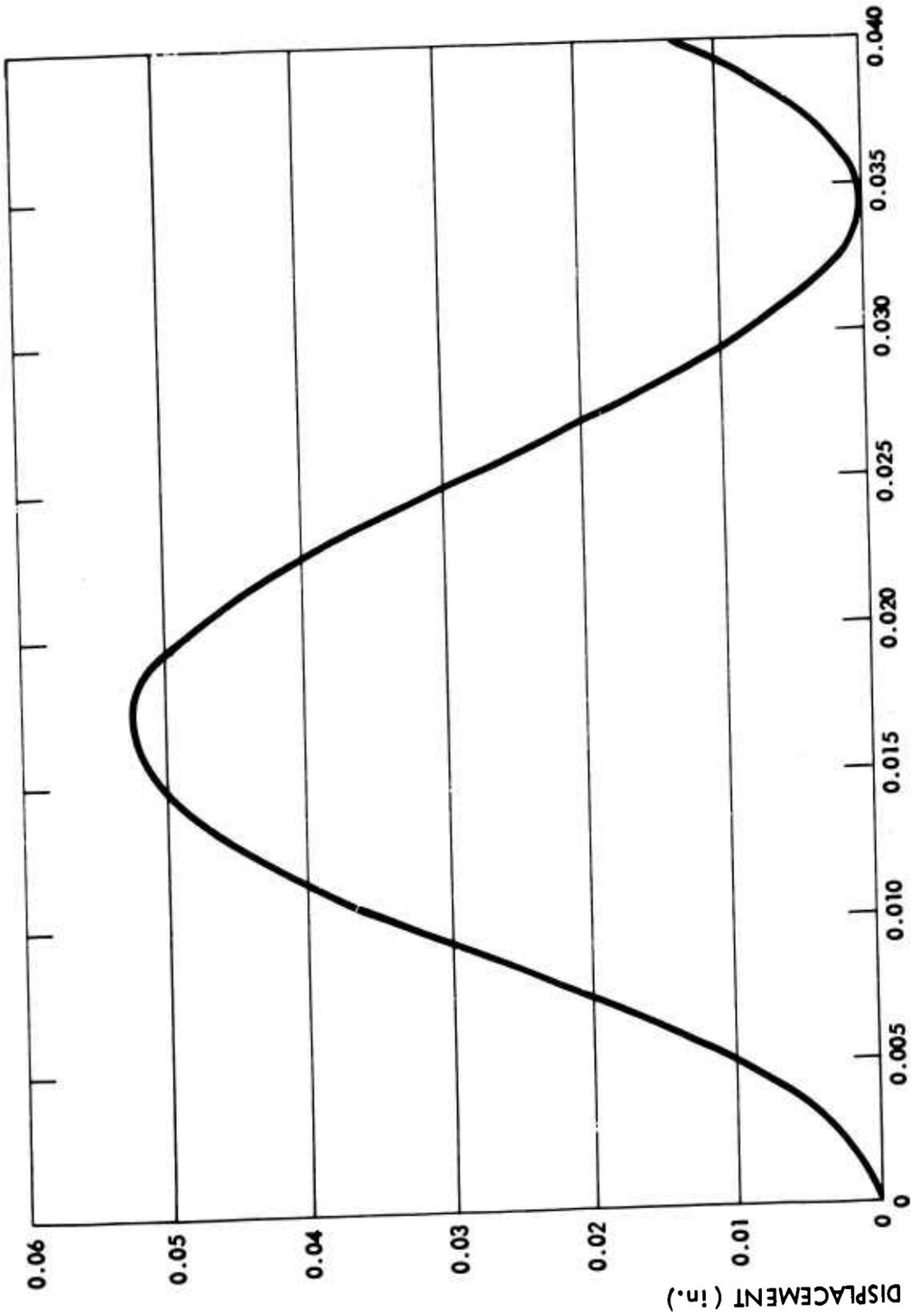

Fig. 4-2. Dynamic Displacements as Calculated by SAMIS

SIMPLE BEAM WALL

The first modeling task attempted was the simple beam wall, i.e., an 8-ft by 12-ft brick wall with only the horizontal girders in place (see Fig. 4-3). SAMIS has the capability of duplicating elements so the trial wall model was simply repeated to form the configuration shown in Fig. 4-4. Note that nodes 1, 7 and 13 of the trial model are replaced by 10, 60 and 110, respectively, of the simple beam model.

This increasing of the nodal numbers allows the addition of boundary conditions in a zone of the wall without recoding of the entire system. For example, the horizontal girder is modeled by line element (beam) 55, 105, ... 605, 655. Geometric similitude is maintained by placing the member along its center of gravity and connecting 55 to 50, 105 to 100, etc., by nondeformable elements (this is done within the computer program on a remote joint). Care must be exercised at all levels of modeling; for example, the horizontal girder is a very short, deep beam (3:1) which means shear deformations are important as well as shear stresses. It is also important to properly account for and lump the mass of the girders since they weigh approximately as much as the wall itself. The material properties used as input were:

For steel: $E = 30 \times 10^6$

$\mu = 0.3$ from AISC Manual

For brick: $E = 1 \times 10^6$ from Static Test Program

$\mu = 0.1$ (estimate)

Loadings used for the Simple Beam Wall were a 2-psi static load and a 1-psi step dynamic load, uniformly distributed across the surface. Since the typical shock tunnel loading pulse (shown in Fig. 4-5) is essentially uniform for about 40 to 50 msec, and since we need less than 20 msec of computation (because failure should take place before that time), this pulse is more than adequate to provide a comparison of SAMIS results with actual results. The 1-psi value was chosen to make arithmetic simple, i.e., the output need merely be multiplied by the actual reflected pressure applied to the wall for the corrected output for any load.

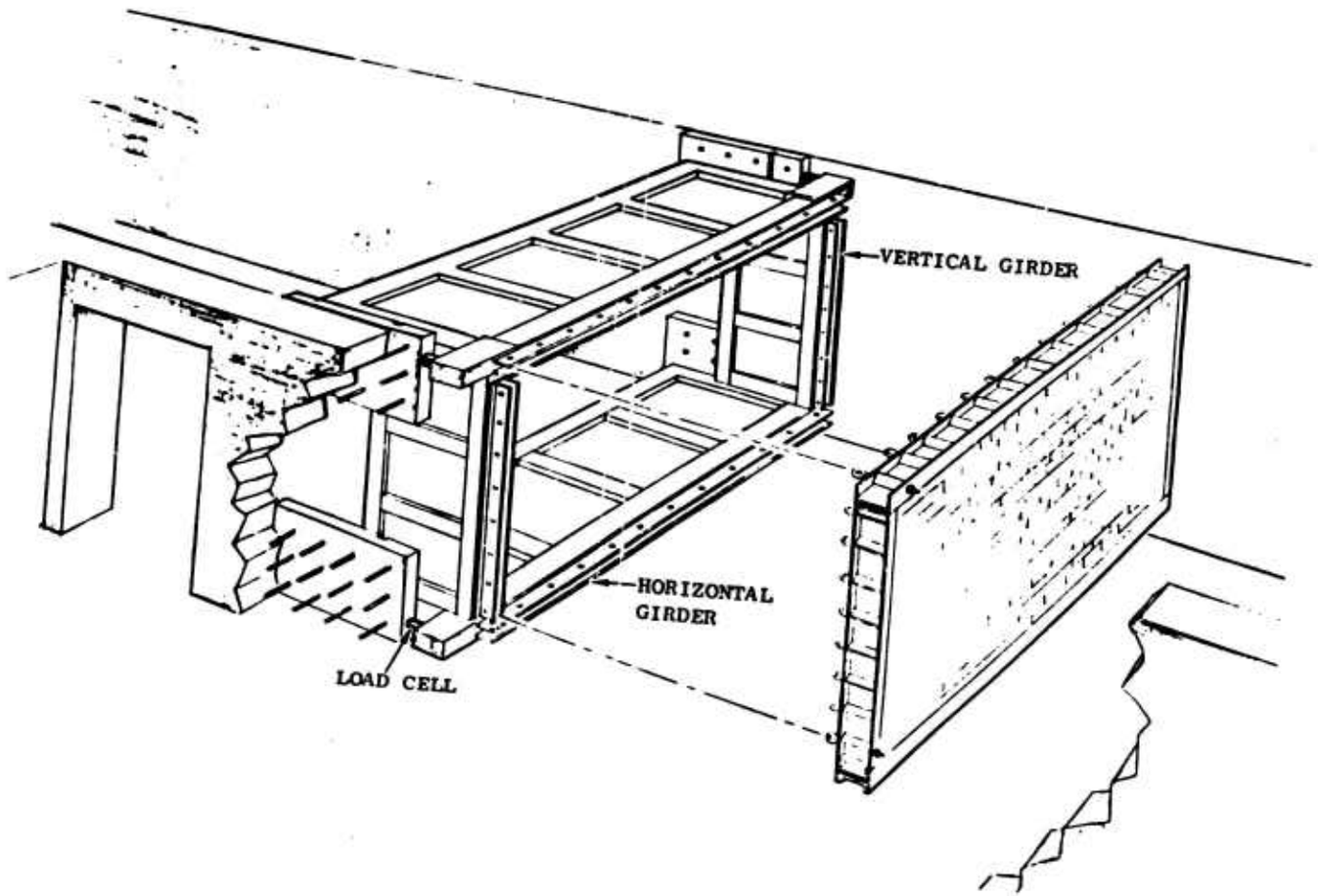

Fig. 4-3. Cutaway View of Shock Tunnel Showing Test Panel and Location of Horizontal and Vertical Plate Girders, Wall Blocks, and Load Cells

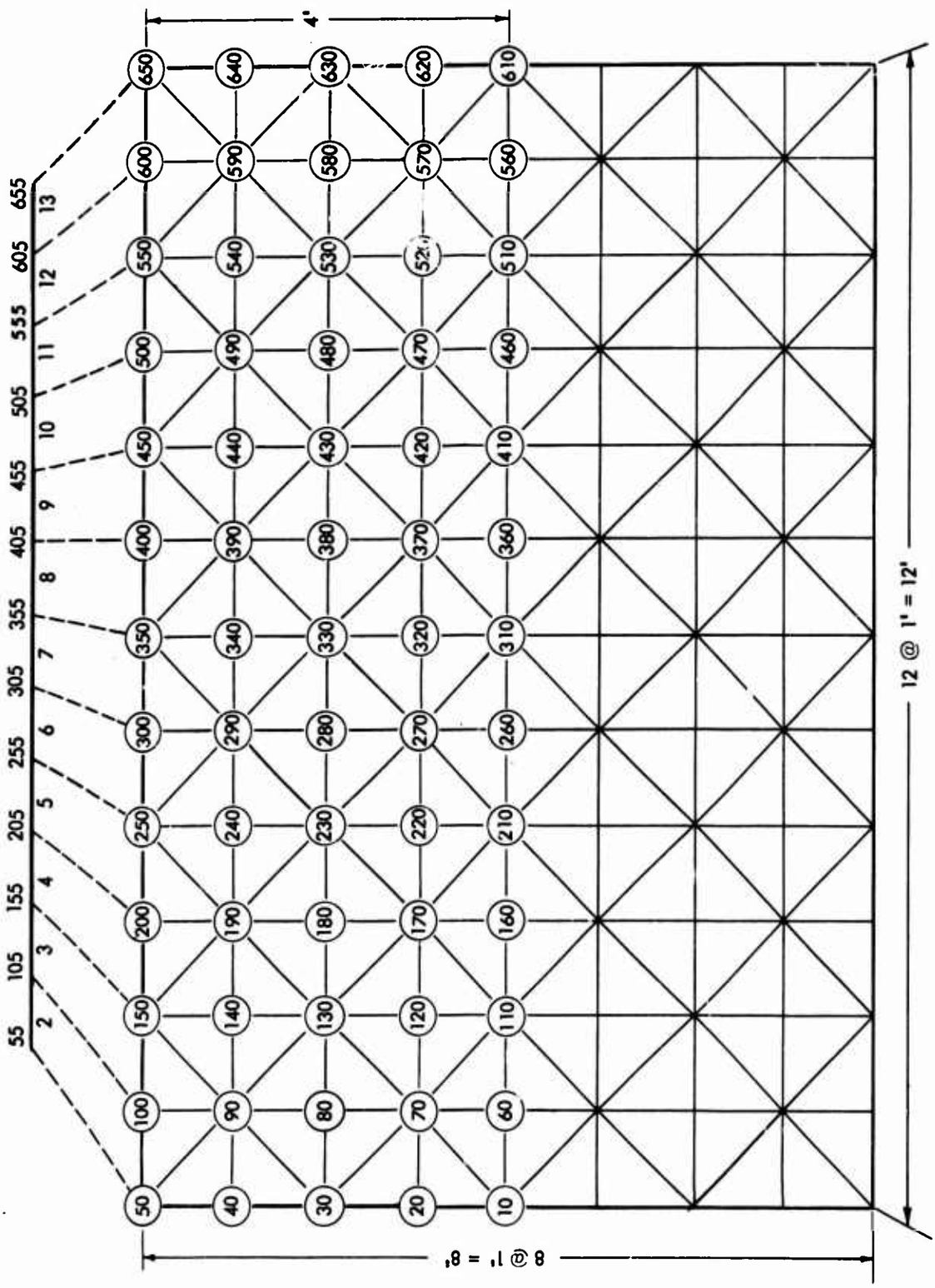

Fig. 4-4. Final SAMIS Model Configuration

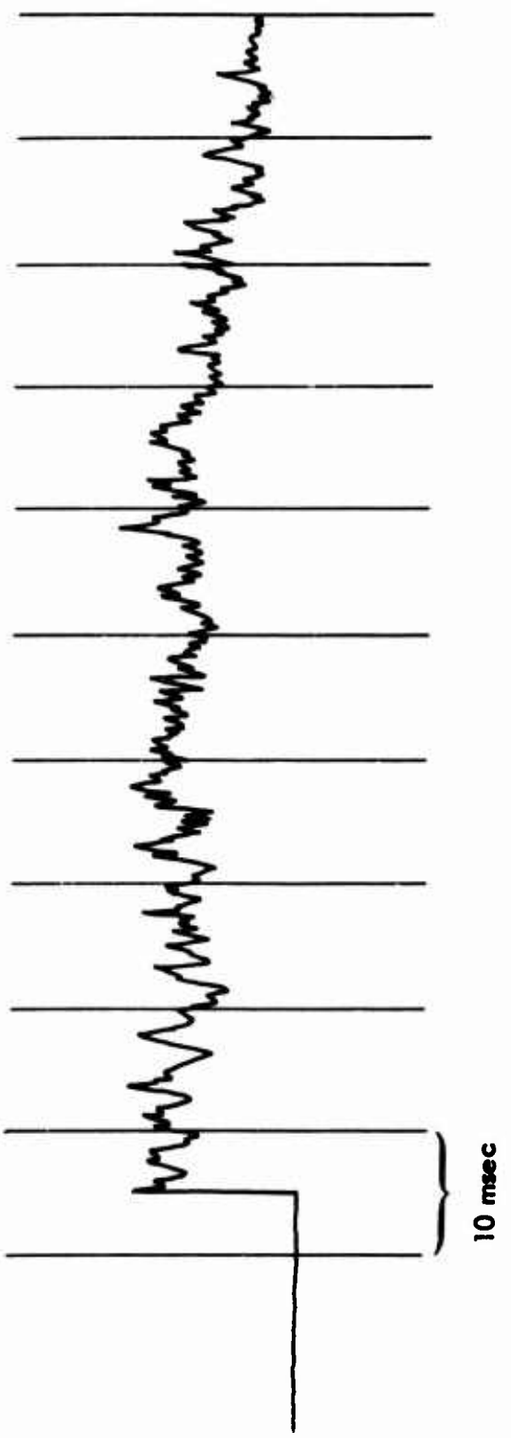

Fig. 4-5. Typical Pressure Gage Data, Nonfailing Wall, Closed Tunnel Test

Checks on Validity of SAMIS

Basically the SAMIS analysis provides information for a nonfailing elastic wall and support structure (or, at least, information up to the failure point). As an early gross check on the validity of this analysis, its output was compared to load cell data (Table 4-2) from the nonfailing wall in the tunnel. (There seemed to be little purpose in making a detailed response analysis for the anomalous steel and plywood nonfailing wall itself, but load cell data from such a wall does give information on gross responses, such as the peak reading expected from a system subjected to a step loading.)

The SAMIS analysis, with zero damping, predicts a peak load cell reading of twice the applied load at T/2 [a dynamic load factor (DLF) of 2 at the half period time]. Table 4-2 indicates that measured values were close to theoretical values, with the median DLF being 1.87, or about 7 percent below the theoretical 2.0. An assumption of only 5 percent structural damping (not an unreasonable value) would have lead to predictions of a DLF almost exactly equal

Table 4-2

SUMMARY OF LOADING AND RESPONSE DATA FOR NONFAILING TEST WALLS THAT PROVIDE 100-PERCENT CLOSURE
(All load values in thousands of pounds)

TEST NO.*	PEAK REFLECTED OVERPRESSURE (psi)	APPLIED PEAK LOAD	MEASURED PEAK AT LOAD CELLS	DYNAMIC LOAD FACTOR**
3 Strand				
08226802	6.2	89	156	1.8
08226801	6.1	88	157	1.8
08276801	5.3	77	148	1.9
08276802	5.5	81	148	1.8
4 Strand				
08276803	7.9	113	228	2.0
08286801	8.1	117	233	2.0
08286802	9.2	130	238	1.8

* Ref. 4.

** Ratio of Column 4/3.

to those observed. Note especially that the scatter of test data is extremely small in spite of the rather noisy pressure pulse created by Primacord, indicating again that the rapidly fluctuating noise has little effect on the structure's dynamic reponse.

It should be noted that the nonfailing wall in the shock tunnel actually has a period T of about 24 msec (Fig. 4-6), while the period T of the SAMIS calculation, for a brick wall, was 34 msec (Fig. 4-7). There is no loss of generality because of this difference; in either case, maximum response occurred at about T/2.

To further validate the SAMIS procedure, it should also be noted that measured brick and concrete wall periods (approximately 32 msec) compare favorably with those from SAMIS.

Panel Behavior to Failure

Next we will consider the failing simple beam wall panel, which is a brick wall 8 ft by 12 ft by 8 in. thick, simply supported at the top and bottom. Figure 4-8 is a contour display of the maximum deflection of the wall surface at T/2 (17 msec) as predicted by the SAMIS code for a 1 psi step-loading pressure input. The computer output actually provides a displacement, velocity, acceleration, etc., for every nodal point at any time interval desired; in this case one printout per millisecond was deemed to be sufficiently often.

Figure 4-9 shows a point-by-point plot of both the displacement and the velocity of node 360 as a function of time. Figure 4-10 is the plot of a typical stress/time relation for a facet on the centerline of the structure. It is obvious from the displacement plot (Fig. 4-8) that the stress across the center of the beam is essentially the same for every facet so the above-mentioned plots are deemed adequate to describe the behavior. More comprehensive plots are needed for more complex walls.

In order to utilize the foregoing response information in failure prediction, we need some additional information on material properties. As discussed at considerable length in Appendix B, the material properties are not simple

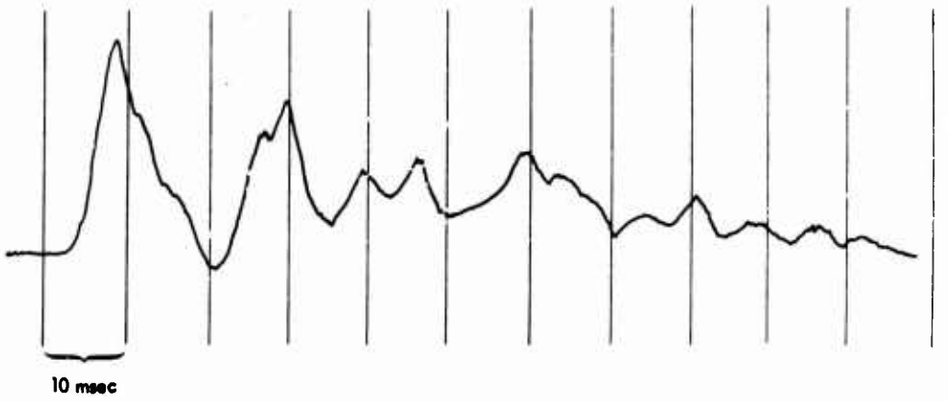

Fig. 4-6. Typical Load Cell Trace, Nonfailing Wall, Close-Tunnel Test

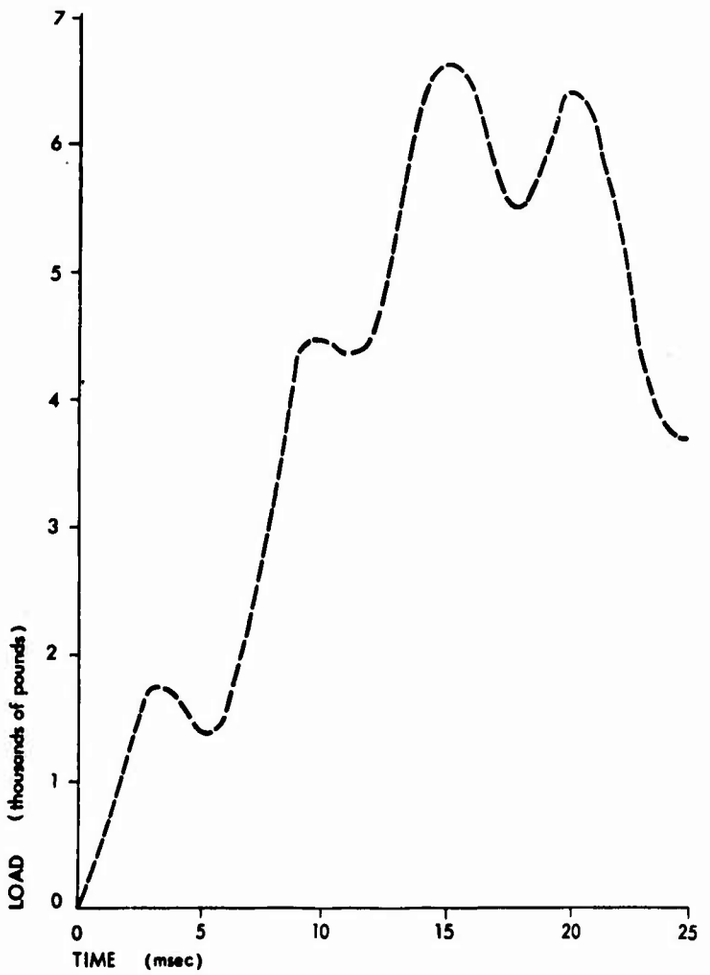

Fig. 4-7. Computed Load Trace, Nonfailing Wall

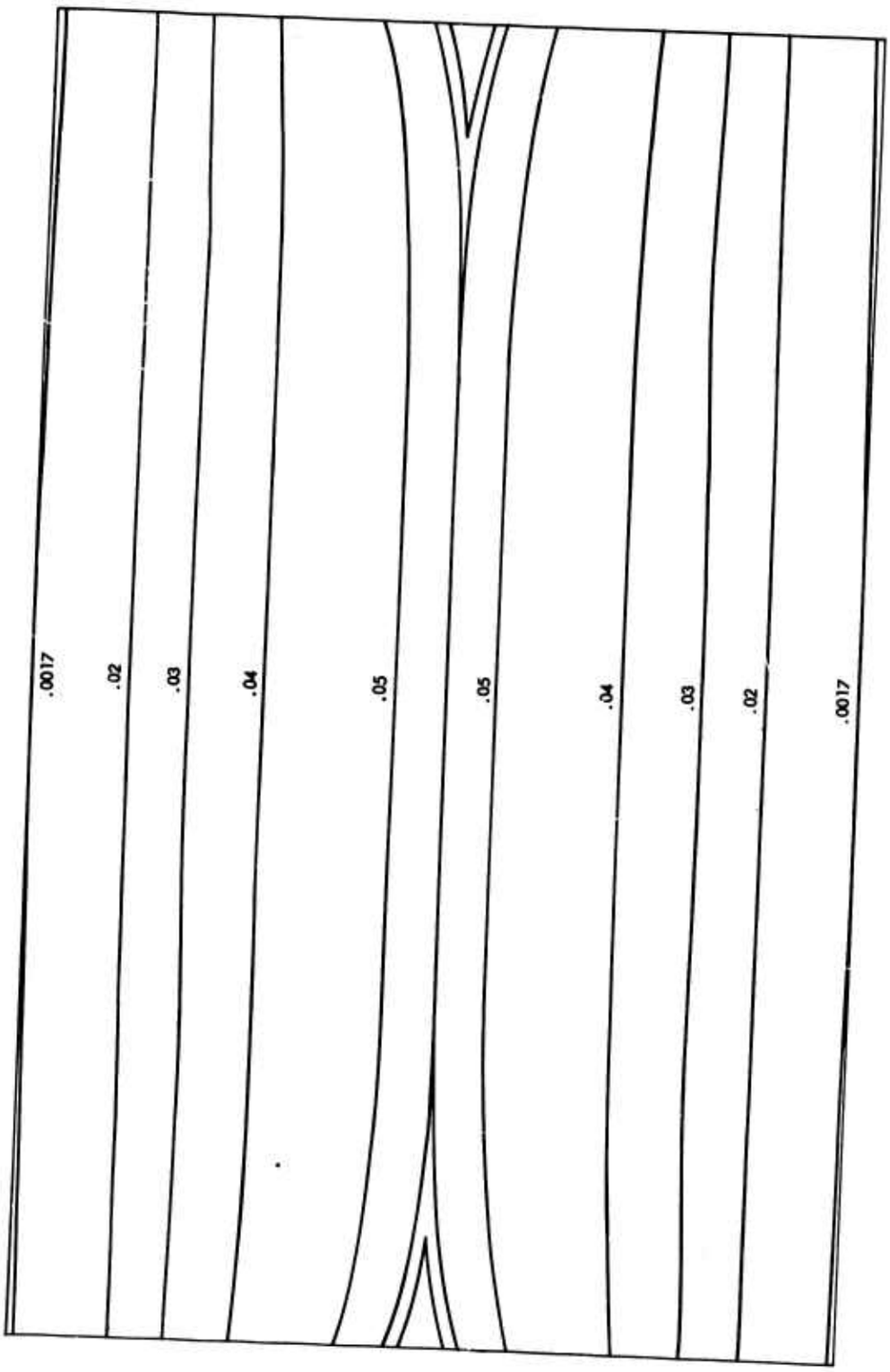

Fig. 4-8. Contour Display of Maximum Deflection of Wall Surface at T/2 (SAMIS)

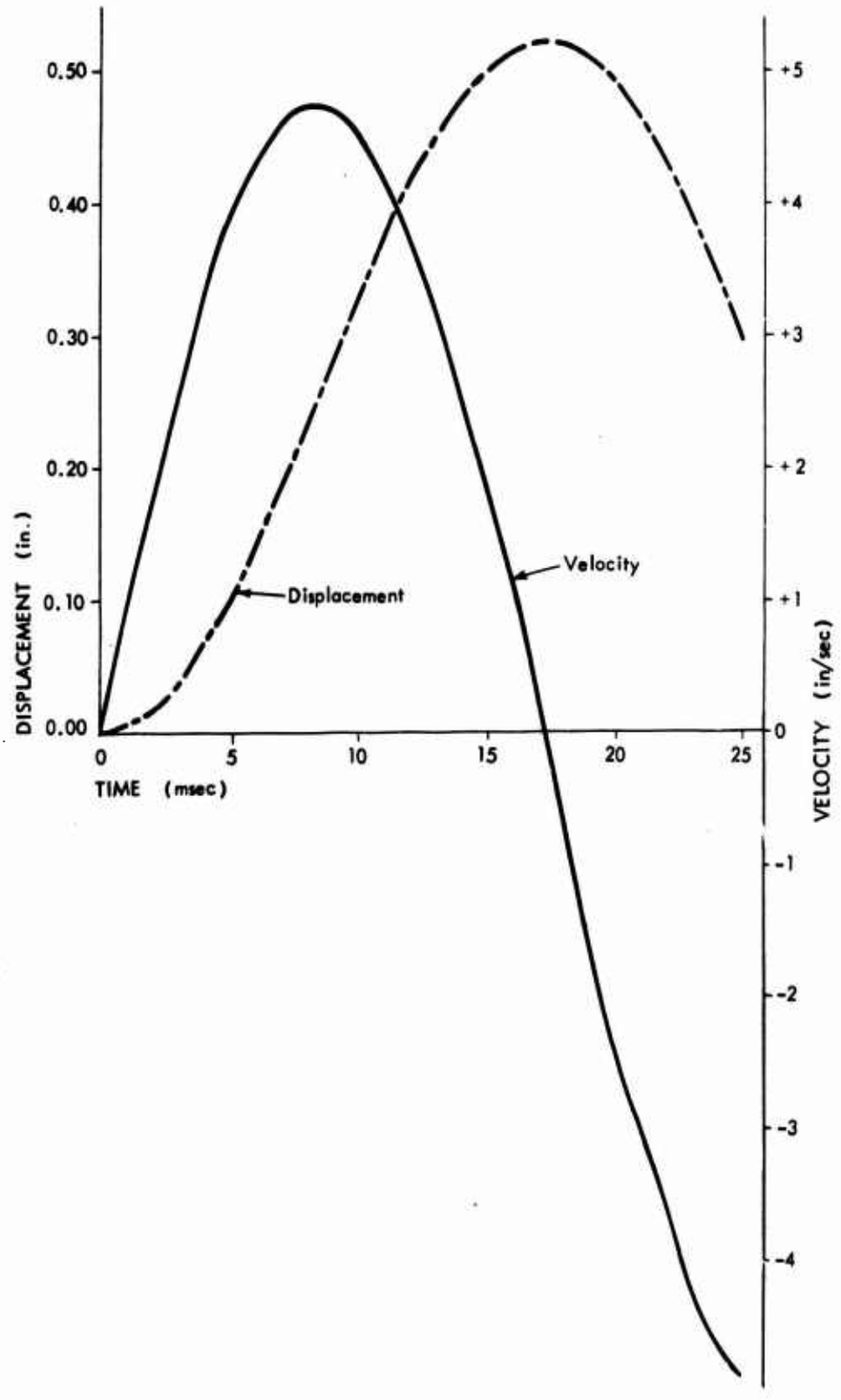

Fig. 4-9. Node 360 Displacement and Velocity vs Time

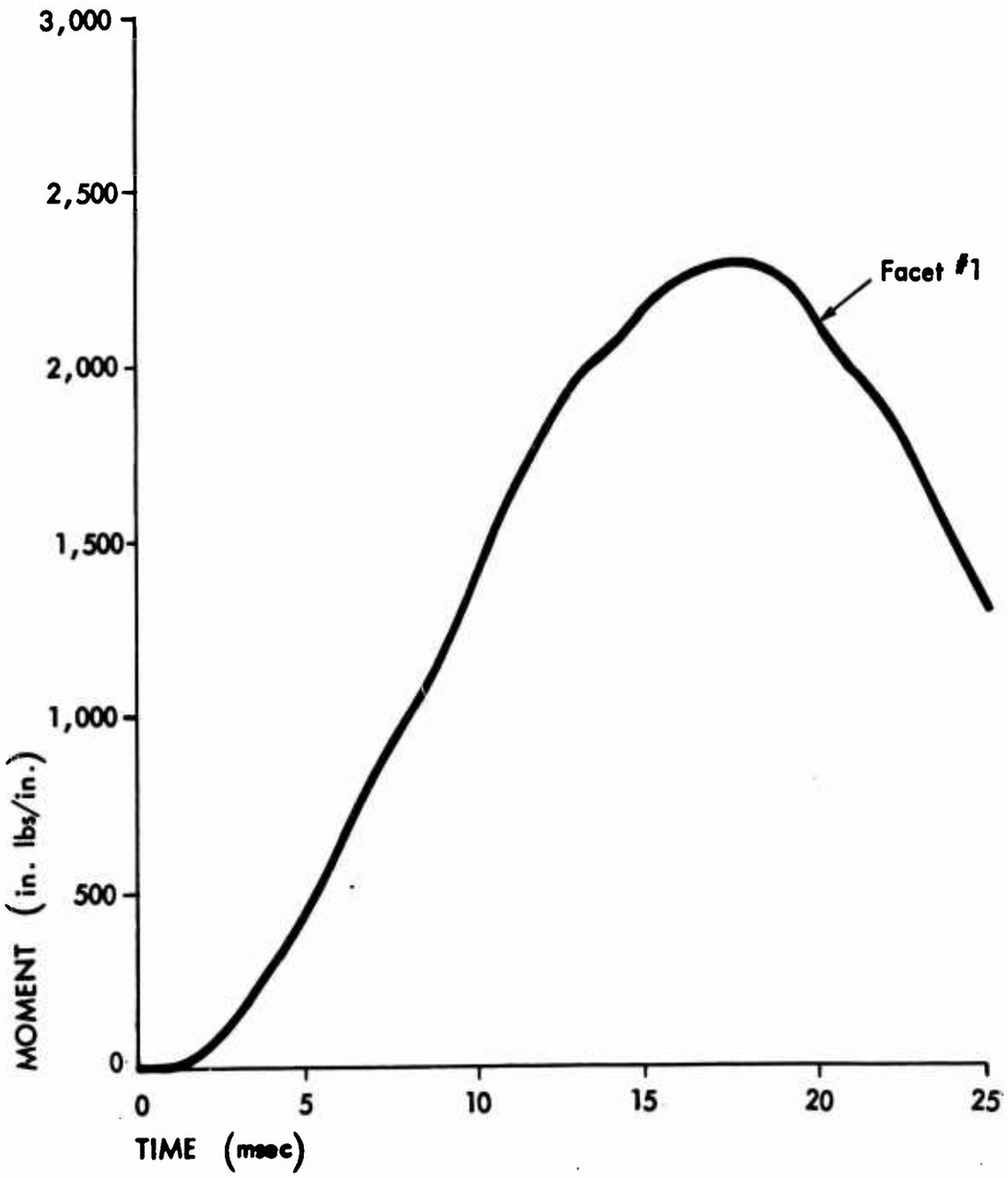

Fig. 4-10. Typical Stress/Time Relation for Facet on Structure Centerline

to predict for a brittle structure of finite size when the properties are both size and load-rate sensitive. Figure 4-11 is developed in Appendix B and is presented here as input without theory or discussion.*

For a typical case, the ratio of applied to fracture force $F_1/\bar{F}$ is 3.1/0.54 = 5.1. From Fig. 4-11, the apparent failure fiber stress is 182 psi ± 10 percent for 90 percent of the time. Obviously, considerable variation from test to test of "identical" fracture and the pressure will greatly increase our knowledge of this apparent failure stress, which in turn should tend to eliminate any weaknesses in the failure theory.

URS has been using experimental crack gages, which seem to verify the foregoing technique for predicting failure times. For two strands of Primacord (about 3.1 psi reflected) one would predict — from the static test data, via failure theory and the computer response calculations — a failure time (cracking) of 6 to 7 msec. The gages indicated a time of about 8 msec (see Ref. 2).

Panel Behavior After Failure

Another, and perhaps even more interesting, facet of the wall test program is the post-crack structural behavior. Work by SRI (Ref. 3) has addressed the rigid-body aspects of the problem with some interesting results; these results are, however, insufficient to describe the complete response of a particular wall panel accurately, or to interpret the test data and predict wall response in other situations. In previous URS work (Refs. 4 and 2) some effort was expended in studying the behavior of a failing system to help in the interpretation of other test data.

One of the first models studied was a changing-mass system, i.e., one in which part of the structure is thrown clear (as a wall panel eventually behaves). This model is briefly discussed below.

A simple two-phase system was assumed, in which the wall panel fractures and falls away immediately, principally to provide a simple analytical model with which to gain insight into the complete process. (In reality, of course,

* Preliminary development and discussion appear in Refs. 2 and 4.

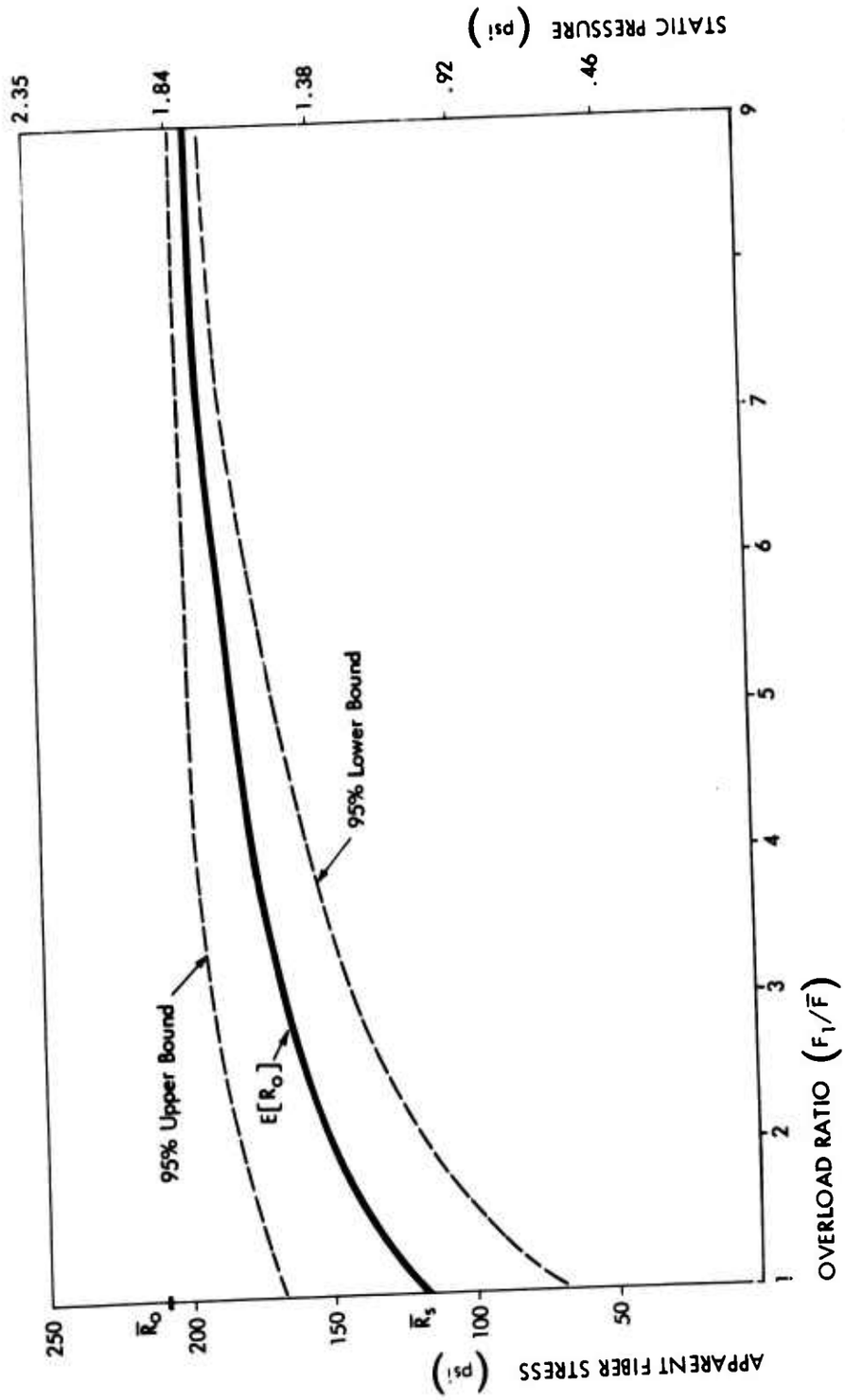

Fig. 4-11. Apparent Fiber Stress vs Overload Ratio

the wall does not behave in this way; actually the wall fractures and remains in the system for some time — for about 8 in. of travel at the centerline.)

One of the primary objectives of this changing-mass model was to interpret the load cell data from the wall panel tests conducted in the URS Shock Tunnel. These load cells are positioned between the wall panel support hardware and blocks fastened to the tunnel wall. The load cells, in effect, sense the motion of the support hardware.

To a first approximation, the behavior of the wall and support hardware can be simulated as follows: Let M_1 = the wall mass, and M_2 the mass of the support hardware. A forcing function F is applied to a two-lump system (System 1) up to a time of failure $t_f < T_1/2$, where T_1 is the fundamental period of the system. At t_f, M_1 is disconnected and the system reduced to a one-lump system (System 2) with the initial conditions derived from the two-lump system at t_f (see sketches below).

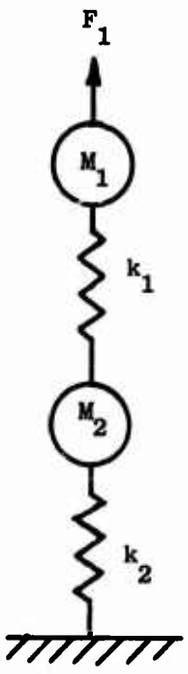

System 1

M_2 = 155 Slugs

M_2 = 247 Slugs (brick wall)

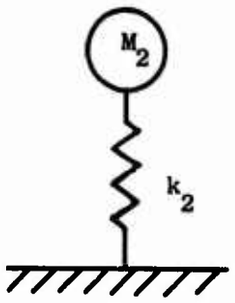

System 2

M_2 = 155 Slugs

As usual, we define $\bar{F}$ as the load that just causes failure cracking. Threshold failure will then occur at $t_f = T_1/2 = \pi/\omega_1$, where ω_1 is the fundamental frequency of System 1.

Now, let:

$$\bar{\alpha} = \frac{F_1}{\bar{F}_1}$$

$$\beta = \frac{A_1}{\bar{F}_1/k_2}$$

and

$$DLF = \frac{A_2}{F_1/k_2}$$

where:

A_1 = amplitude of System 2 in terms of $\bar{F}$

A_2 = amplitude of System 2 in terms of F_1

Curves of $\bar{\alpha}$, β, and DLF are shown in Fig. 4-12. The $\bar{\alpha}$ curve shows the increase in loading necessary to cause failure at various fractions of the specified period T, e.g., if a reflected pressure p_r of 1 psi were the threshold failure strength, it would take 6.83 psi to fail the wall in one-quarter the threshold failure time of T/2.

The β curve illustrates the load cell factor as a function of excess load and failure strength, i.e., for the above example, the load cell would record 3.08 psi.

The DLF curve illustrates the more conventional dynamic load factor as a function of applied load, i.e., $\beta/\bar{\alpha}$.

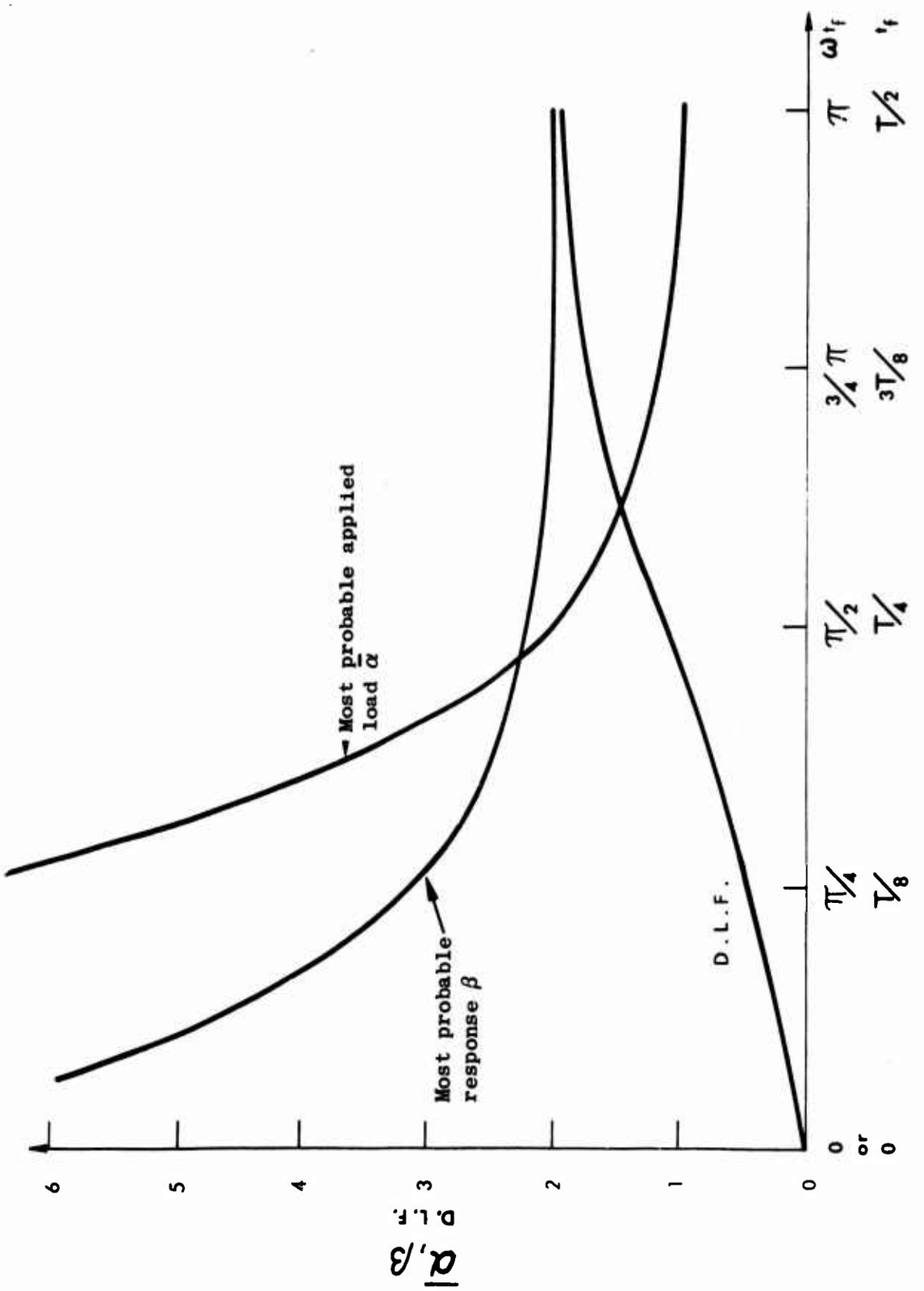

Fig. 4-12. Normalized Load Factors vs Failure Time

Obviously, the foregoing is a crude approximation to the real system response, for the wall panel does not fracture and fall away immediately as previously mentioned. Instead, the wall panel fractures across the center, and each half slowly rotates about and out of its support. To get a feel for this behavior, the vibrations of a half-beam were studied in some detail in Ref. 4.

For example, the cases illustrated below were studied to help our understanding of the problem.

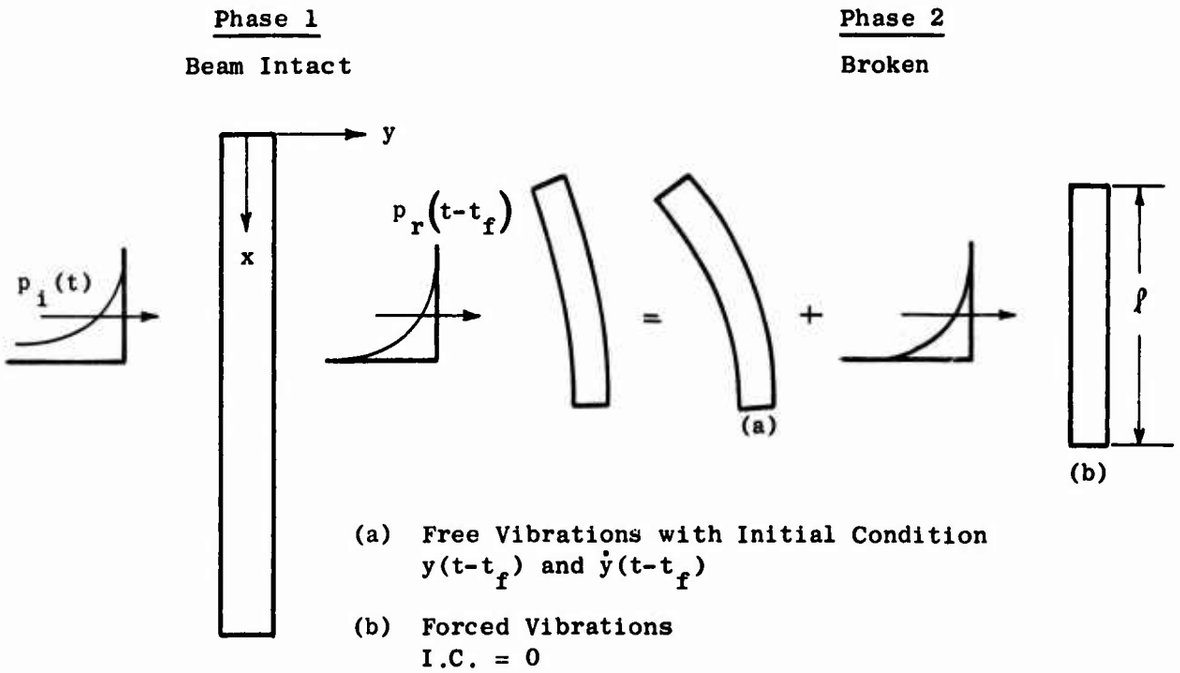

(a) Free Vibrations with Initial Condition $y(t-t_f)$ and $\dot{y}(t-t_f)$

(b) Forced Vibrations
I.C. = 0

From the free-vibration portion one can study the transient response of the half-wall caused by the initial condition at fracture and gain knowledge of the shear, moment, deflection, etc., during the motion of the half-beam. Typical values are illustrated in Figs. 4-13 and 4-14.

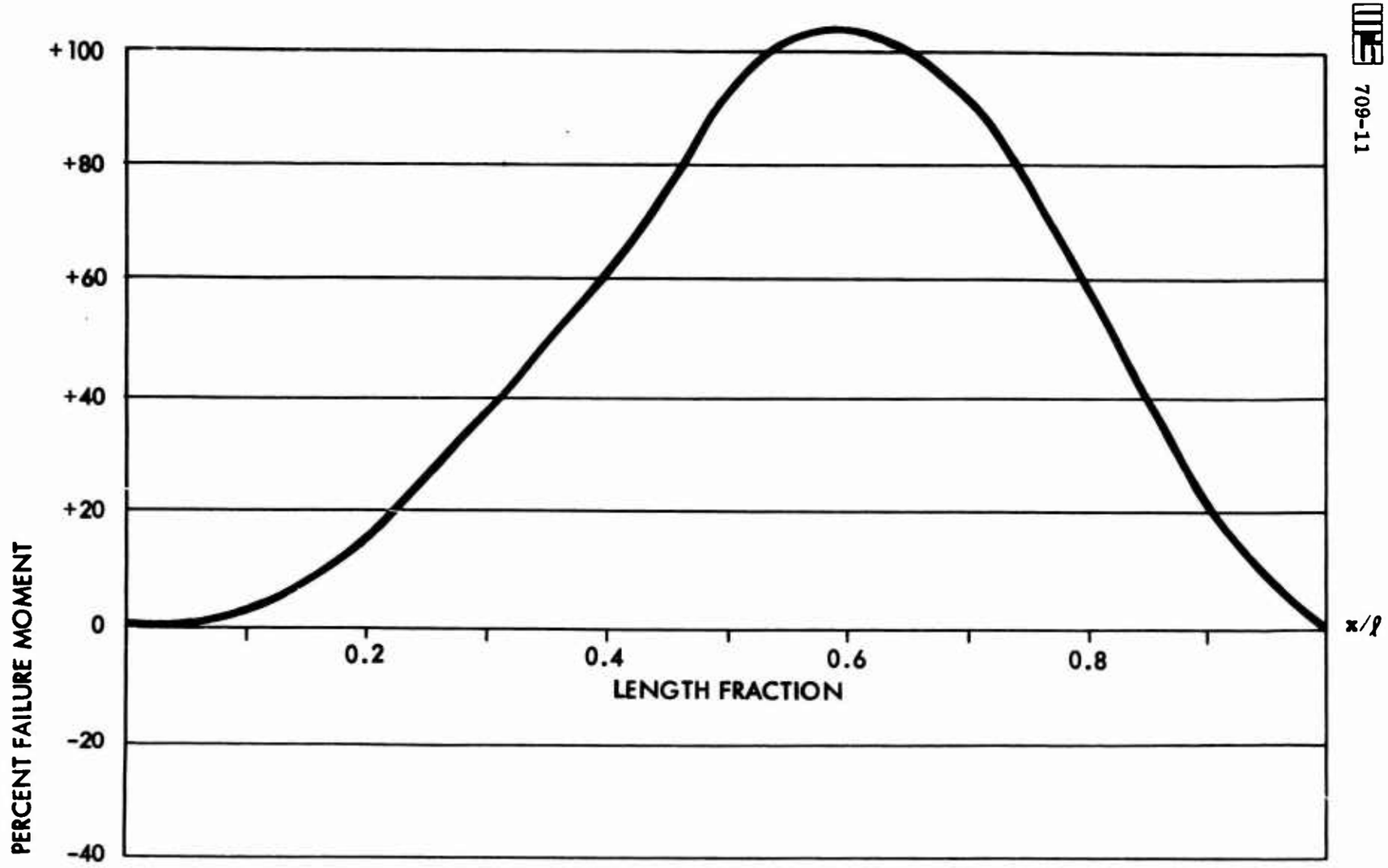

Fig. 4-13. Half-Panel Moment

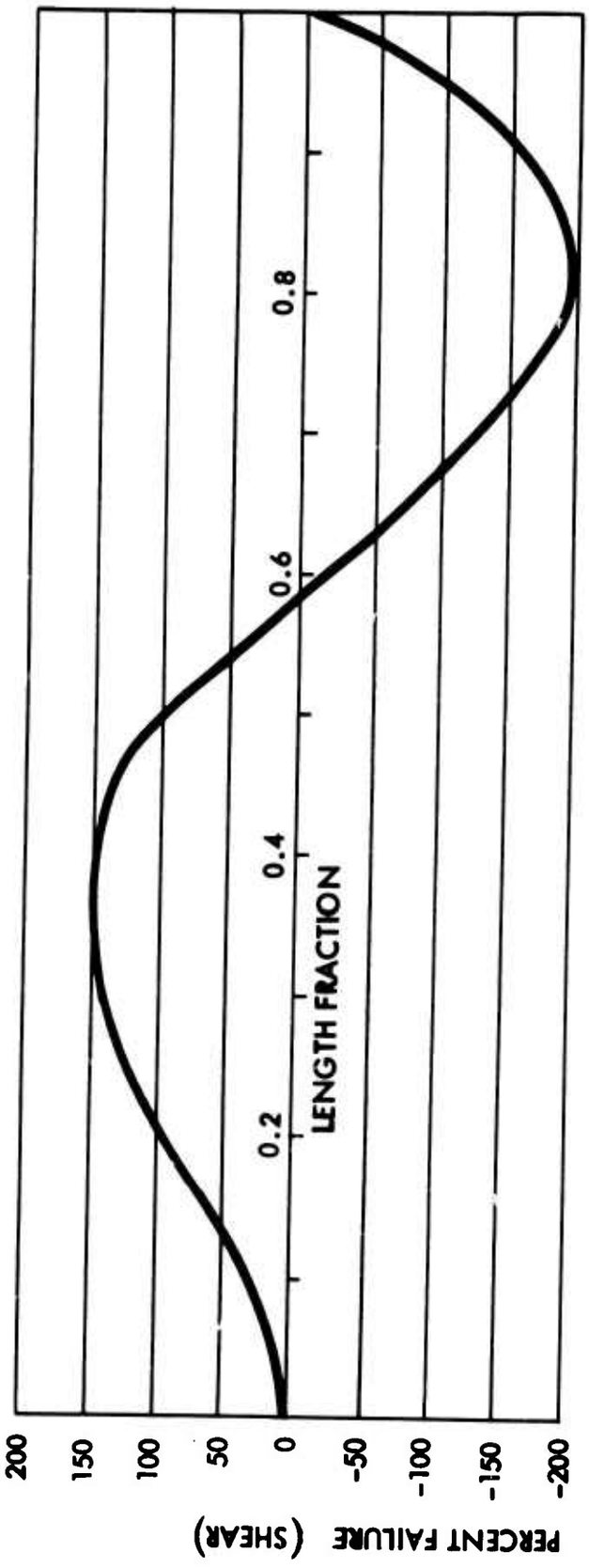

Fig. 4-14. Half-Panel Shear at t = 0

Interestingly enough, the forced vibrations (an elastic solution of a half-panel under shear load) portion produced mainly rigid-body motion and very little panel vibration compared to the fracture-induced initial conditions.

Another type of information extracted from this analysis was the reaction (shear at the support) for the vibrating half-panel. One case examined in Ref. 4 is shown in Fig. 4-15. In the previous report (Ref. 4), this was combined with the two-lump approximation shown earlier to give an estimate of the maximum system response. This is illustrated in Fig. 4-16 in which load cell readings shown for six brick wall panel tests are compared with results using the simplified model.

Obviously, the foregoing approach was a simplified analysis, but it provided the groundwork for a more meaningful interpretation of test data and for building better and more complete analytical models. During the next phase of the program, the load cell peak curve will be predicted to a much greater degree of accuracy by using the SAMIS computer code. From the analyses completed during the current period, we have the initial velocity and displacement for every node on the wall panel which will be used on input data (initial conditions) to the forced vibrations of a half-panel previously analyzed by hand for one set of initial conditions. An additional refinement easily achievable with the computer will be the inclusion of a trajectory of the centerline elements (at the crack) which is dictated by the lower half-panel. This will account for any energy used in lifting the wall mass as it translates and rotates out of its support structure. Of course, this more accurate modeling should provide a far better after-crack response prediction, which in turn will supply much better information on the load transferred to the building frame and allow for a much more complete understanding of data gathered at the shock tube.

To evaluate the predictive capability of the SAMIS program, URS has constructed three wall panels with pre-formed cracks. With these walls, the time of cracking (zero) and the precise initial conditions are available to us. This type of test program, whose results would be used to prediction-

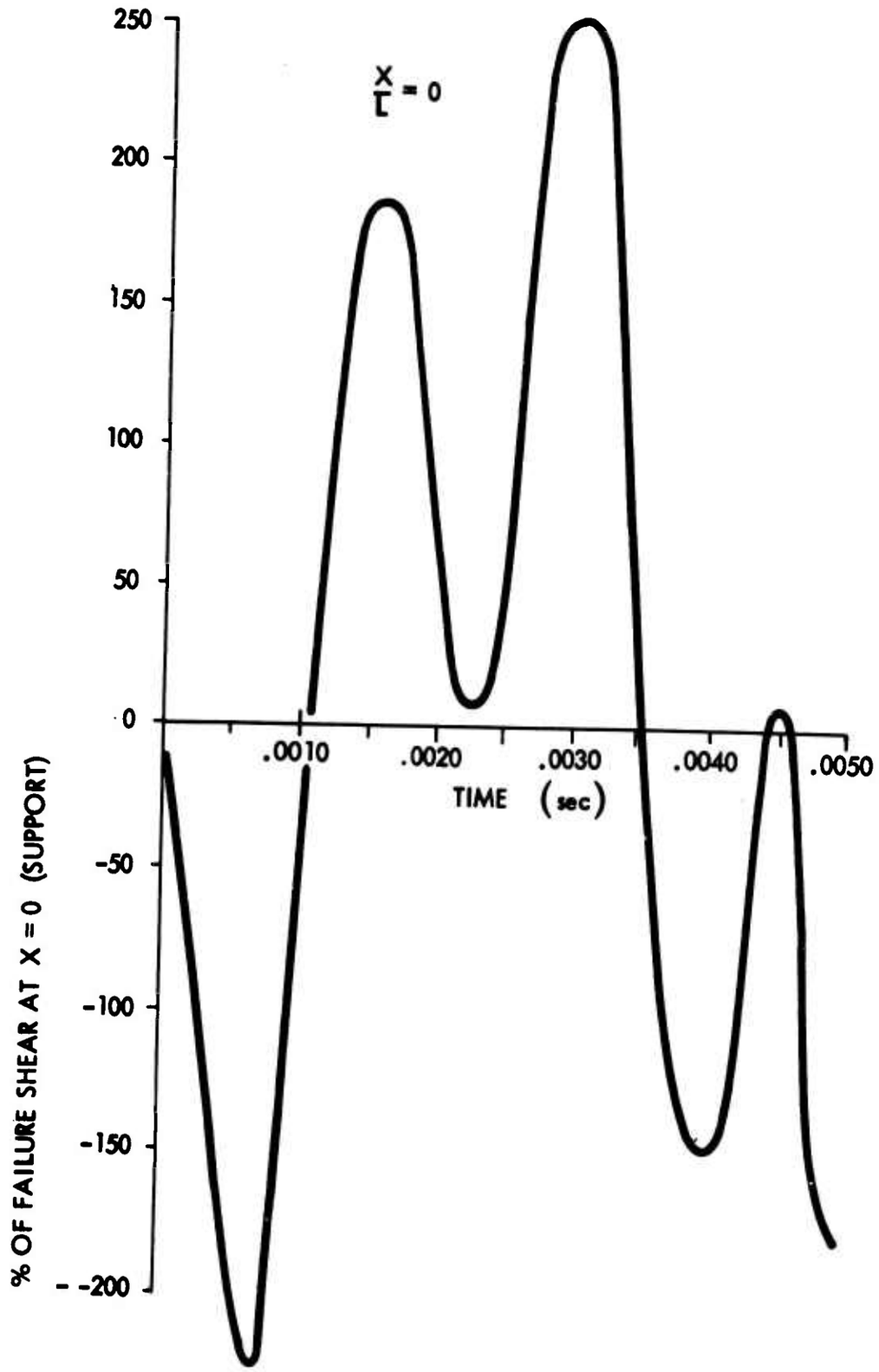

Fig. 4-15. Half-Panel Reaction vs Time

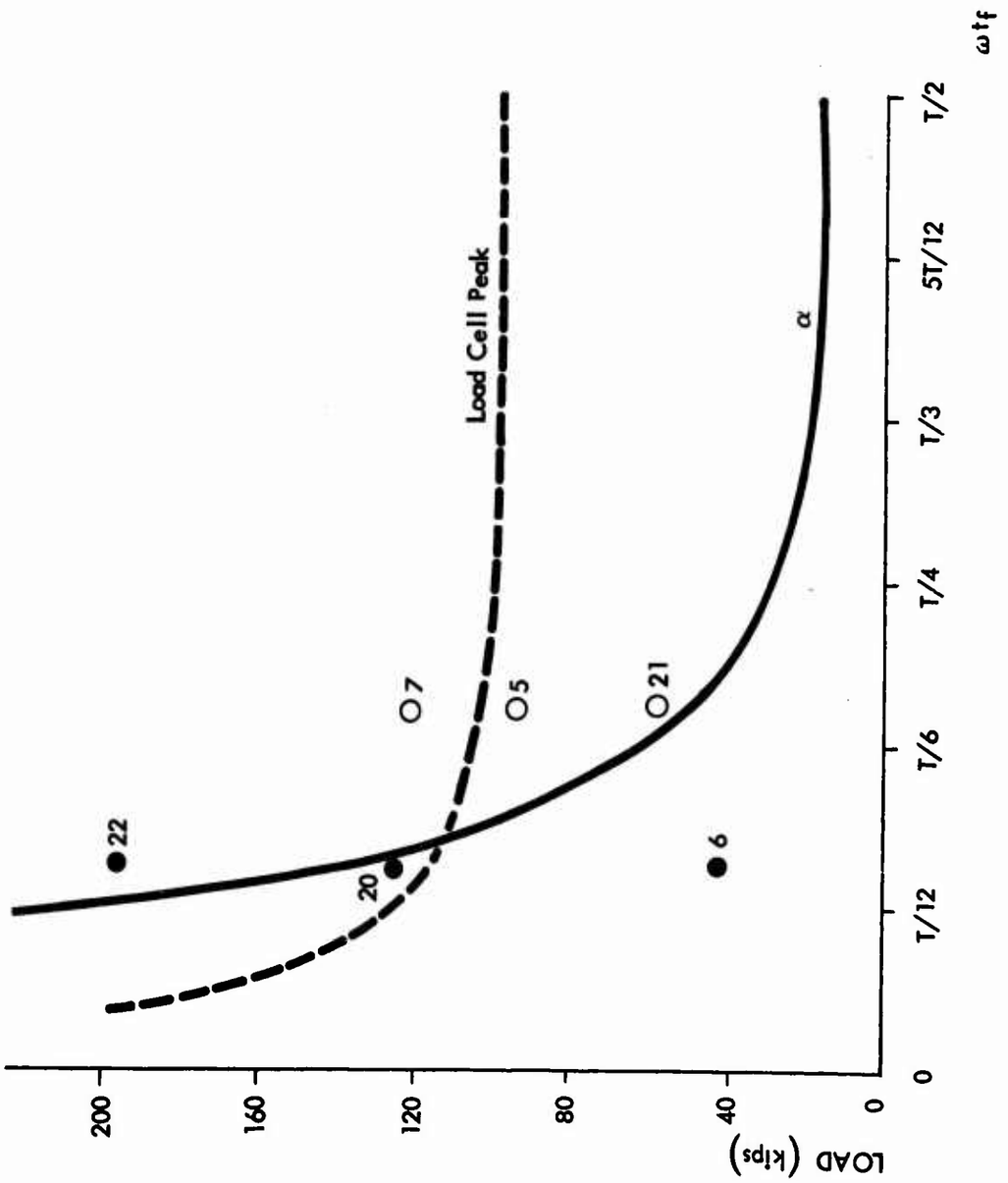

Fig. 4-16. Brick "Beam" Wall Panels

test-improve the prediction technique, should increase the value of previous and future data. Further, it would most likely reduce the number of future tests required.

SIMPLE BEAM WALL WITH DOOR

In this section of the report the value of the more advanced and complete analysis procedures made available to us with SAMIS becomes obvious. When an opening (such as a door) is made in a wall panel, not only does the structure and its response change, but the loading function changes even more dramatically. With changes such as this, manual analysis becomes almost impossible.

The structural modeling for a brick wall with a doorway to be used in the SAMIS computer code involved only the removal of the facets shown in Fig. 4-17. With such a minor change in the structural modeling, a static loading structural analysis was not required prior to the dynamic response analysis. The wall is the basic 8-ft by 12-ft by 8-in. brick wall with a 3-ft doorway cut from the right-hand side.

A good deal of effort was expended trying to determine an acceptably accurate loading for the computer code. The dynamic response prediction is a step-by-step numerical integration of structural behavior; hence, loading must be supplied to each facet at each time increment used in the numerical integration. This was not necessary in the first problem as each facet was loaded identically and each time step receives the same load. The computer was merely told this and it generated its own loads.

In the case of the doorway, however, each facet is loaded differently at each time period, hence the loading is more complex (for a description of loadings with openings, see Section 3). Input loads must be supplied at an interval between 1/10 and 1/20 the highest period of the structure. For our system this meant one load every 0.1 msec or 250 input loads per mass for a 25-msec response prediction. However, the computer code has a built-in feature whereby it can generate linearly interpolated loads between points supplied. For example, the four points shown in the following sketch would replace 250 input bits of data — an obvious saving.

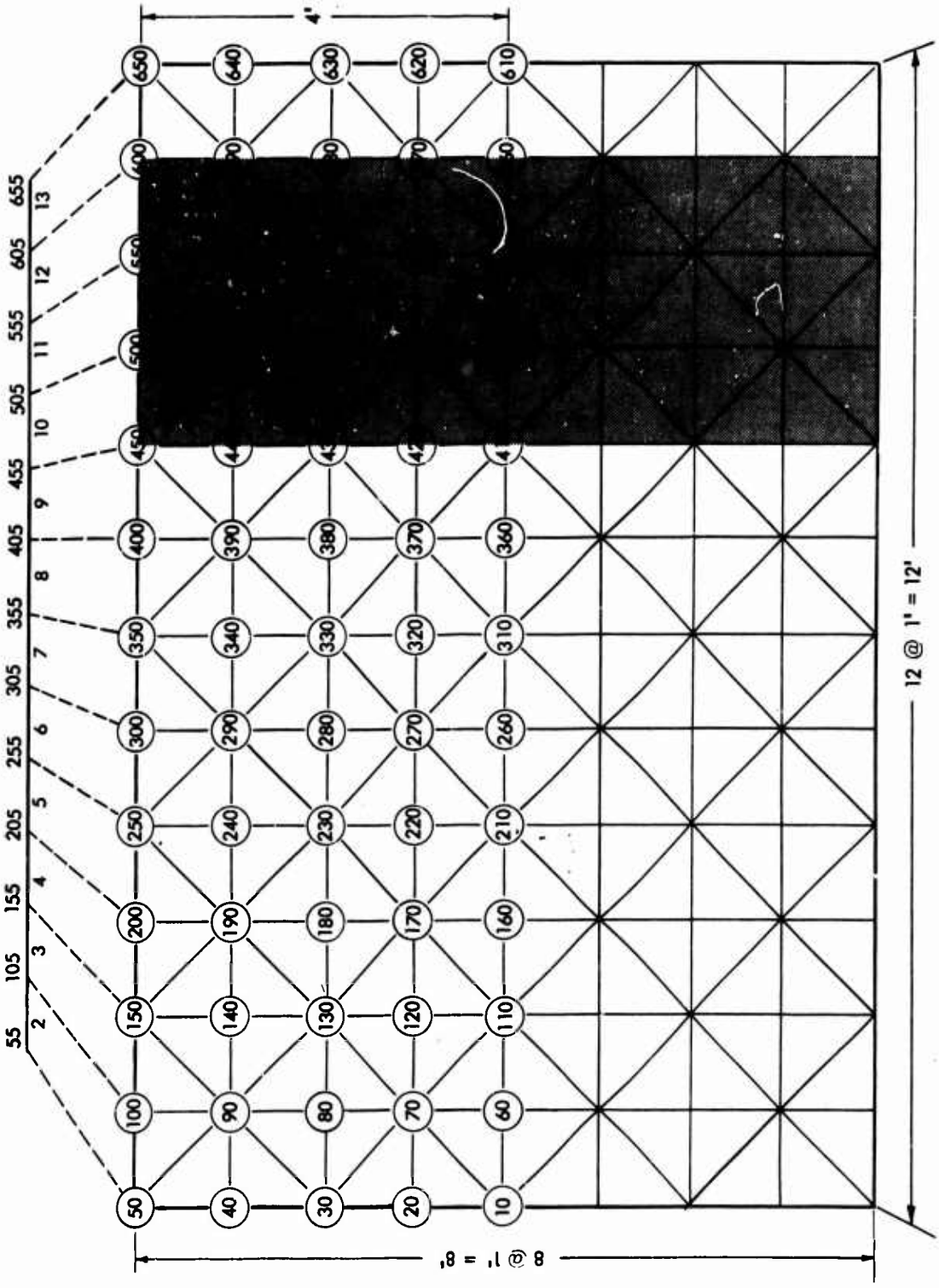

Fig. 4-17. Basic Grid and Line Elements

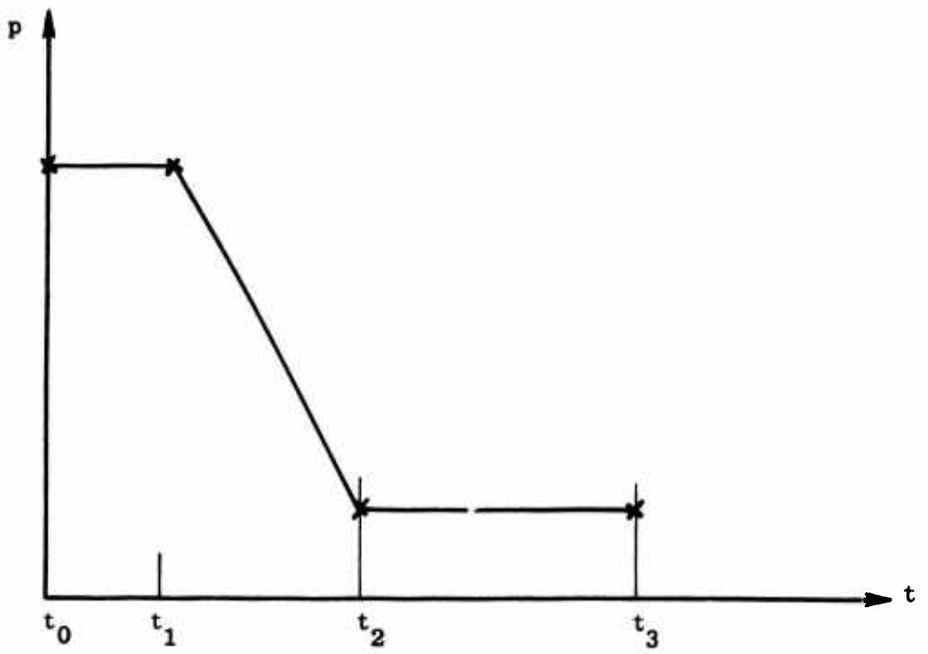

Obviously, then, many factors entered into the selection of a data reduction technique, including

1. The use to which the data will be put (input to SAMIS)
2. The cost (in time and money) to reduce the data adequately
3. The quality of the data (its reproducibility)
4. The equipment available to perform this reduction.

The primary use made of the pressure data was to predict the structural response of wall panels, in particular, the response of the test wall and its support hardware. A way of thinking about structural response from a loading input is to visualize a structural system as a filter, borrowing an analogy from electrical engineering. This filter may be visualized as a "black box" with an input signal p(t), pressure, and an output signal X(t), displacement, shown on the next page:

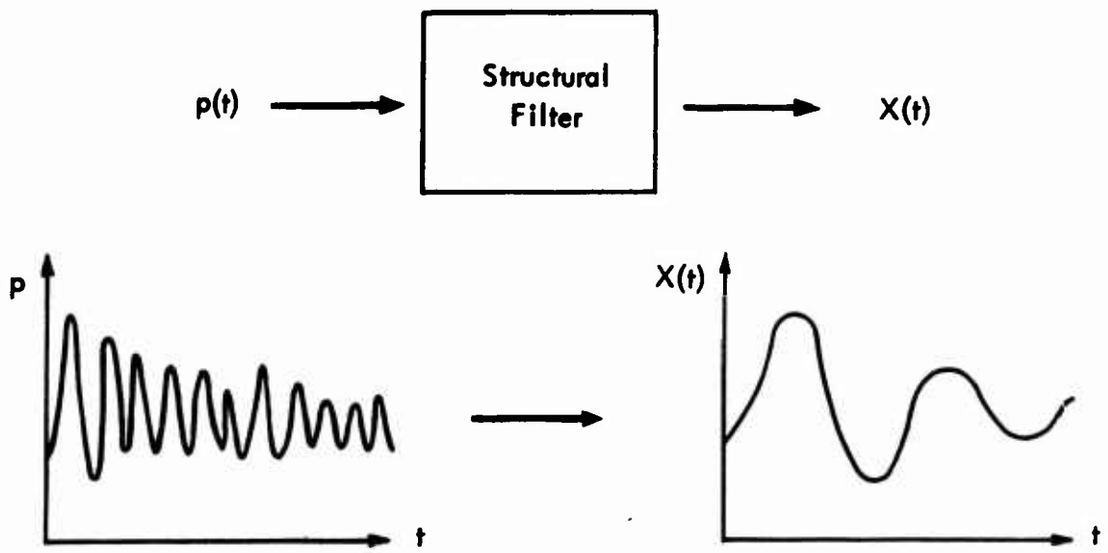

To illustrate the validity of this point, one may observe the actual pressure input recorded, shown in Fig. 4-5, and a typical load cell trace shown in Fig. 4-6 for the same load input.

Because of this filtering capability, and because of our wish to use the most cost-effective form of data, the loading pulses were approximated by a series of straight lines. The walls' response to such loads would be essentially the same as their responses to the noisier loadings actually experienced in the tube. However, it is first necessary to establish the level of approximation that is adequate for our purposes; that is, the prediction of structural response.

To do this, we first turn to classical mechanics to get some feeling of the structural response vs sinusoidal forcing functions (which are the Fourier components of any load) in the manner illustrated in Fig. 4-18. When we look at a typical trace we observe some very high frequency noise, with periods of about 0.3 msec compared to the 25- to 35-msec period for the structural systems. Obviously, if real, this would contribute nothing to the structural response. In fact, if we neglected sinusoidal noise with periods less than 5 to 6 msec and a magnitude of 25 percent of the average loading p(t), we would introduce

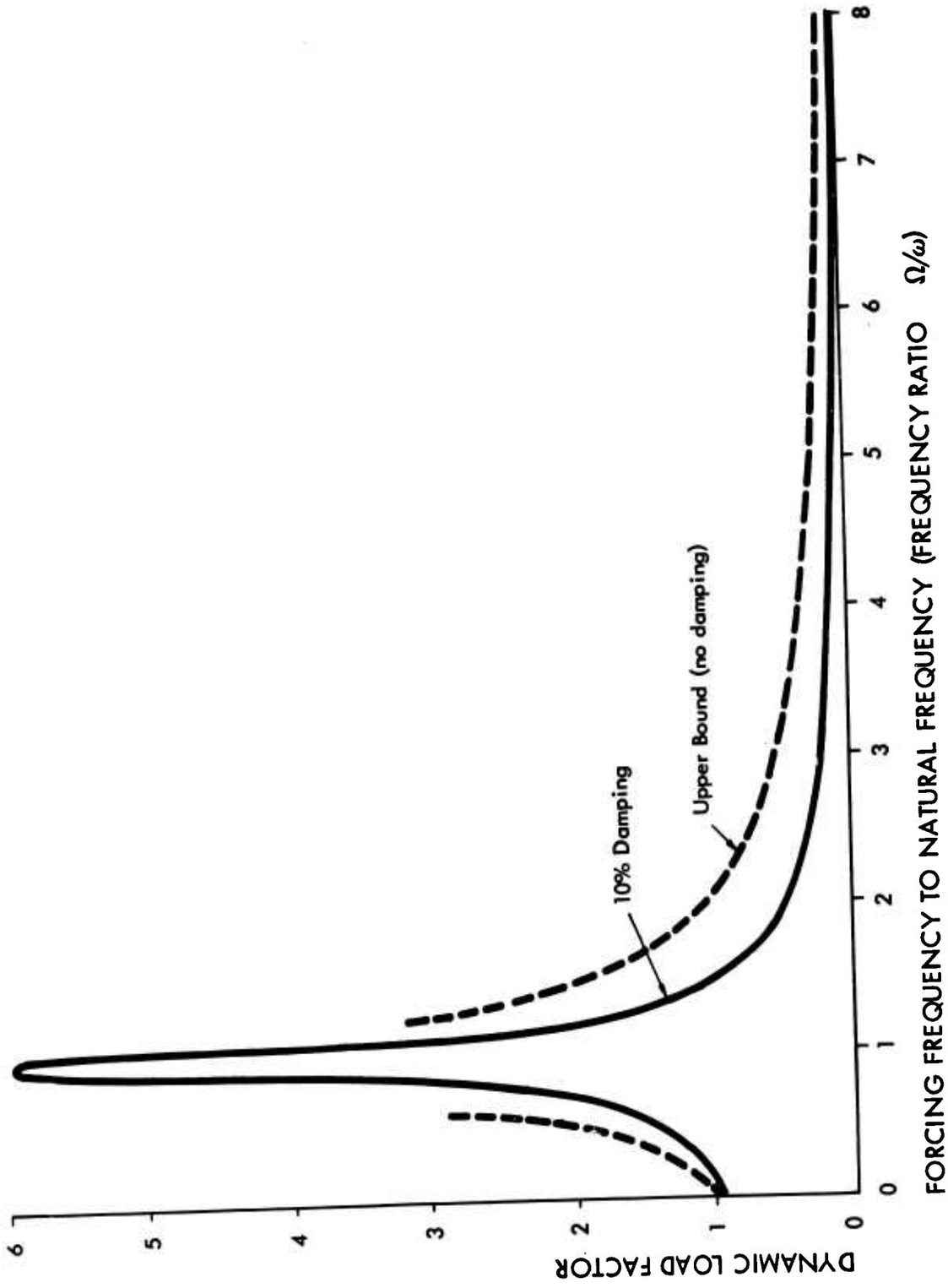

Fig. 4-18. Structural Response vs Sinusoidal Forcing Functions

an upperbound DLF error of 0.06, or only a 6 percent upperbound error. This was the criterion adopted to aid in reducing (approximating) pressure traces to loading functions; for any sinusoidal noise with a period less than 6 msec and a magnitude less than 25 percent, the average pressure was smoothed.

In addition, several other tests of the approximation was made. Since Primacord itself has a deviation on the order of 10 percent, several replications (at least three) of each test series were conducted and averaged (discussed in Section 3).

To further increase our confidence in the reduction procedure and minimize the reduction effort, a structural response-sensitivity study was performed. That is, a one-lump system of mass similar to that of the walls (200 slugs) and with periods of from 15 to 40 msec (brick wall period = 33 msec) were subjected numerically to

1. The best average-fit curve through the data, i.e., straight-line fits in time steps as small as 1 msec
2. A rough smoothing, i.e., smoothing 5- to 6-msec oscillations; and
3. The SAMIS input approximation (described later in this section).

Figure 4-19 illustrates the differences for a structure with a period T of 33 msec during the first 20 msec of response. The maximum error difference in response is only about three percent. Figure 4-20 displays the peak response differences for various periods from 15 to 45 msec and also indicates extremely small errors (± 3 percent).

Armed with the foregoing results, for SAMIS input we used the loads shown in Fig. 4-21. Curve "7-ft" is the loading used on the facets bounded by nodes 50, 150, 110 and 10; curve "5-ft" on the facets bounded by nodes 150, 250, 210 and 110; curve "3-ft" on the facets bounded by nodes 250, 350, 310 and 210; and curve "1-ft" on the facets bounded by nodes 350, 450, 410 and 310 and nodes 600, 650, 610 and 560. This zoning further simplified input and is certainly valid in light of the shot-to-shot variations when compared to region-to-region

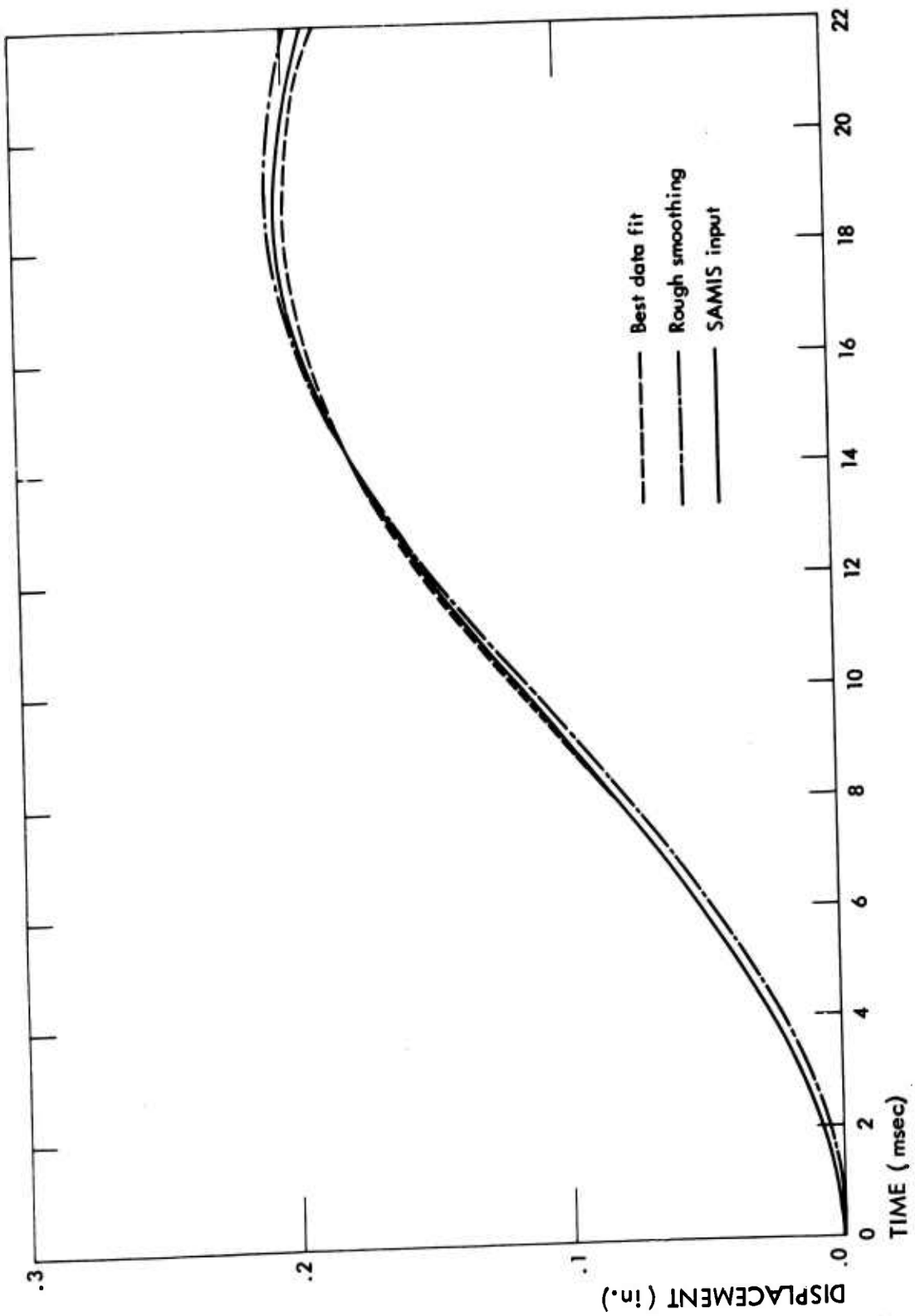

Fig. 4-19. Displacement in In. as a Function of Time

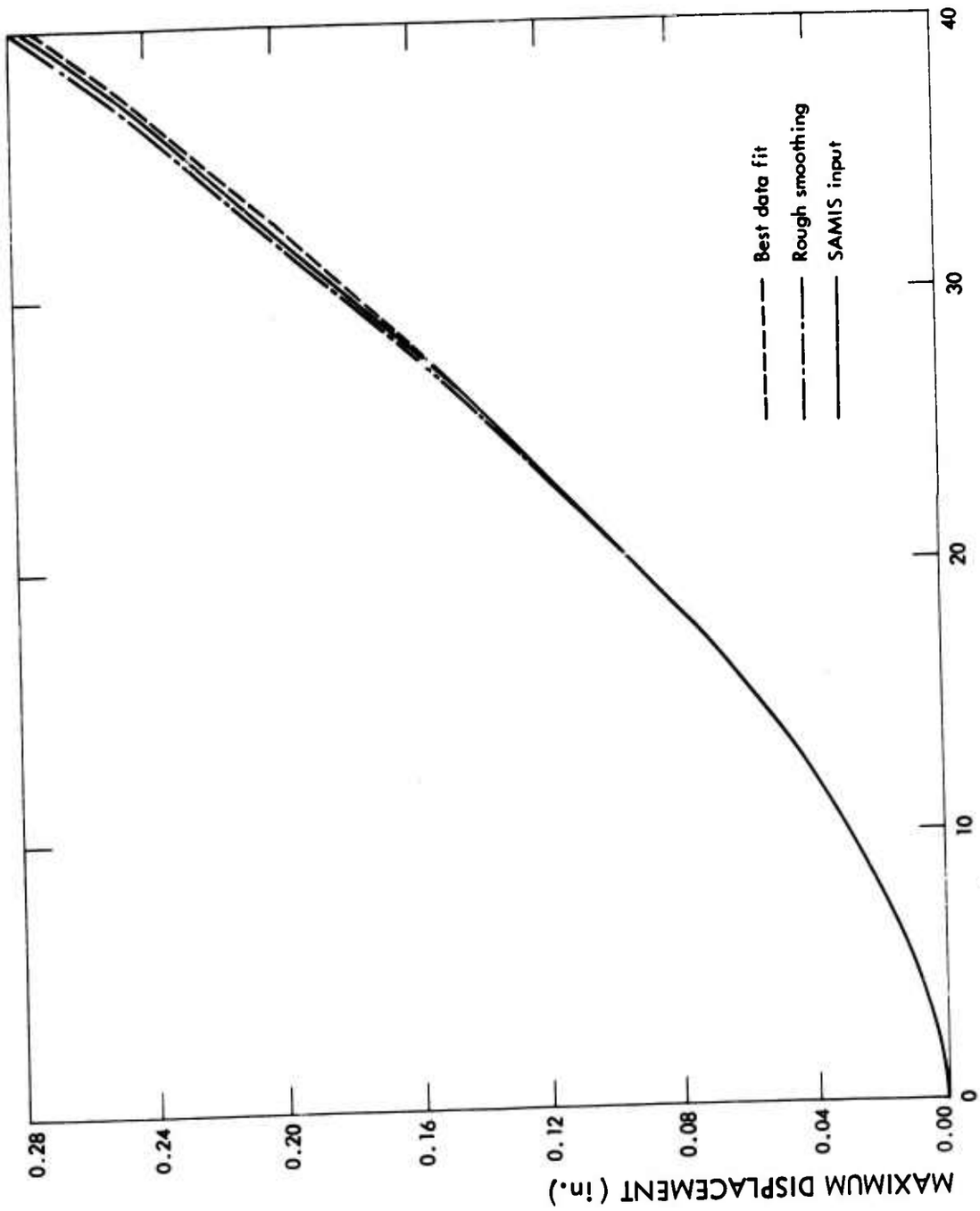

Fig. 4-20. Displacement in In. as a Function of Natural Period

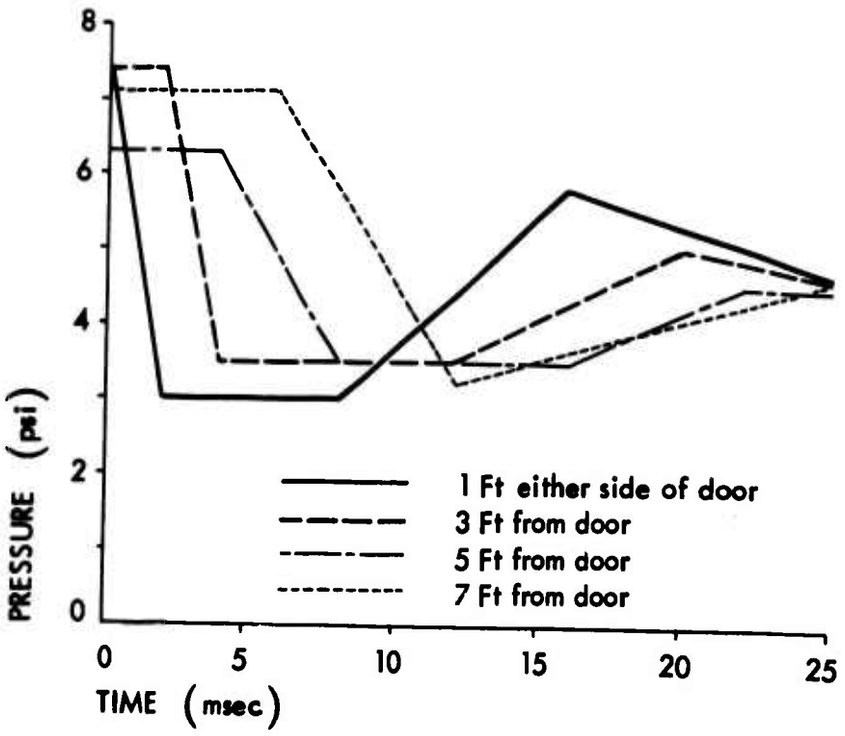

Fig. 4-21. SAMIS Input Loads

variation used as input. Further, little variation is noted in the vertical direction since the doorway is the full height of the shock tunnel.

The computer supplies more than enough nonfailing wall response data, some of which seems appropriate to print herein to illustrate the added insight that can be developed. As further evaluation of data and tests are performed, some revision of this information will certainly be in order.

Figures 4-22 through 4-27 illustrate the deflection contours for the wall with doorway every millisecond for times from 12 msec through 17 msec.

In Fig. 4-22, the deflection nearest the tunnel wall is greater than that near the door (25 percent greater). This is intuitively pleasing because the higher loads remain longer near the wall; that is, the rarefaction wave relieves the load near the door. Moving forward in time, a uniformly deflected wall is approached at about 14 msec, which might be called the fundamental half period, i.e., T = 28 msec. As time progresses, we observe that at t = 17 msec a peak displacement is achieved adjacent to the doorway. This interesting phenomenon is further illustrated in Fig. 4-28 on a time vs displacement plot for Nodes 10 (at wall), 210 (center of panel) and 410 (next to the doorway). From this graph it is apparent that failure is expected to begin adjacent to the wall more often than adjacent to the doorway — an interesting thing to look for in future tests. Another important observation is that the movement of the shock across the wall excites a mode other than the fundamental of the n x m modes available in a structure of this kind. This should be observable in the load cell responses, i.e., in the supporting structure behavior.

Figure 4-29 is a plot of the load cell nodes 58 and 658, respectively. This plot clearly shows the influence of this higher mode (T = 6 msec) on the fundamental mode (T = 28).

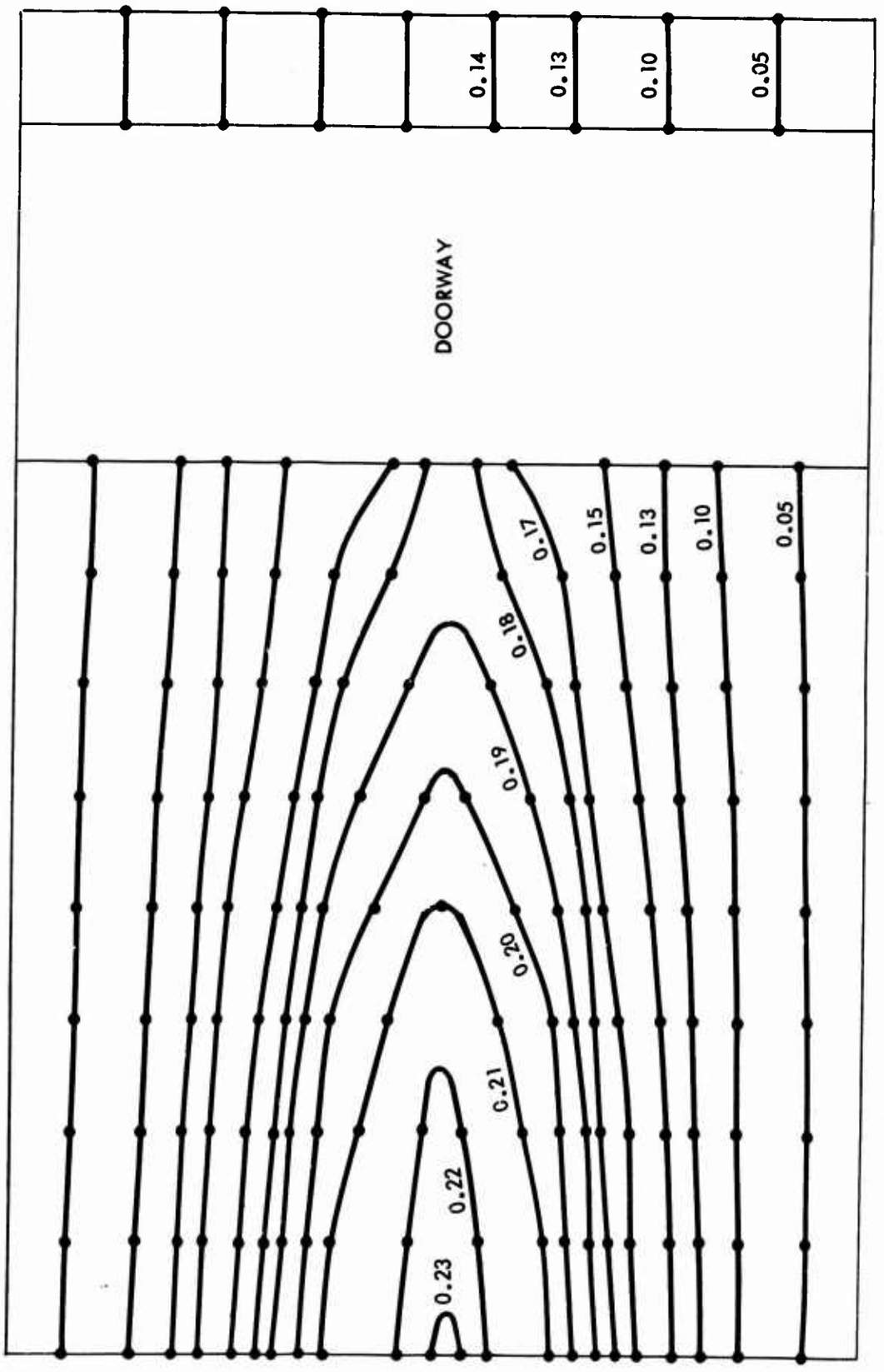

Fig. 4-22. Wall With Doorway Deflection Contour at 12 msec

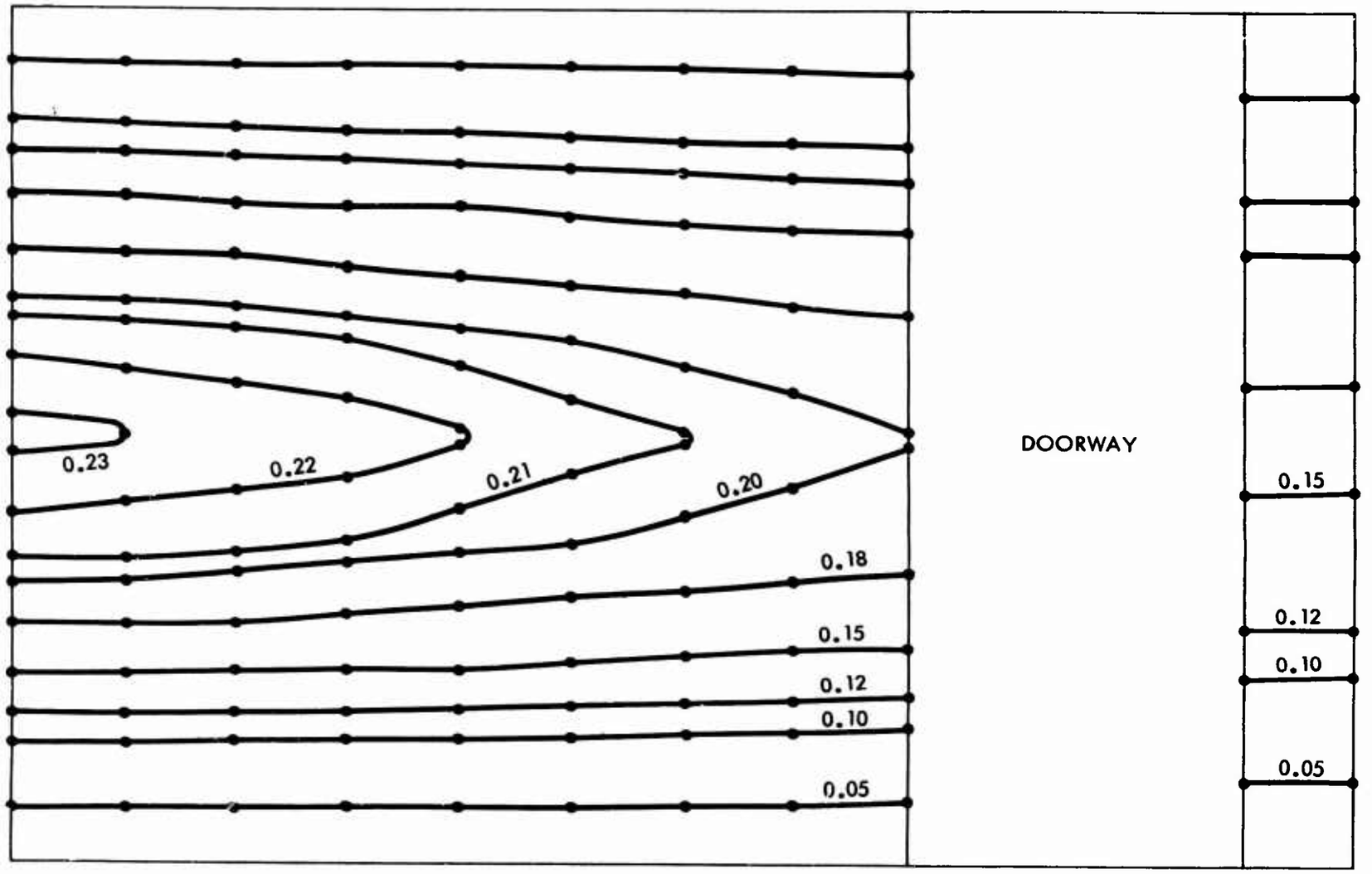

Fig. 4-23. Wall With Doorway Deflection Contour at 13 msec

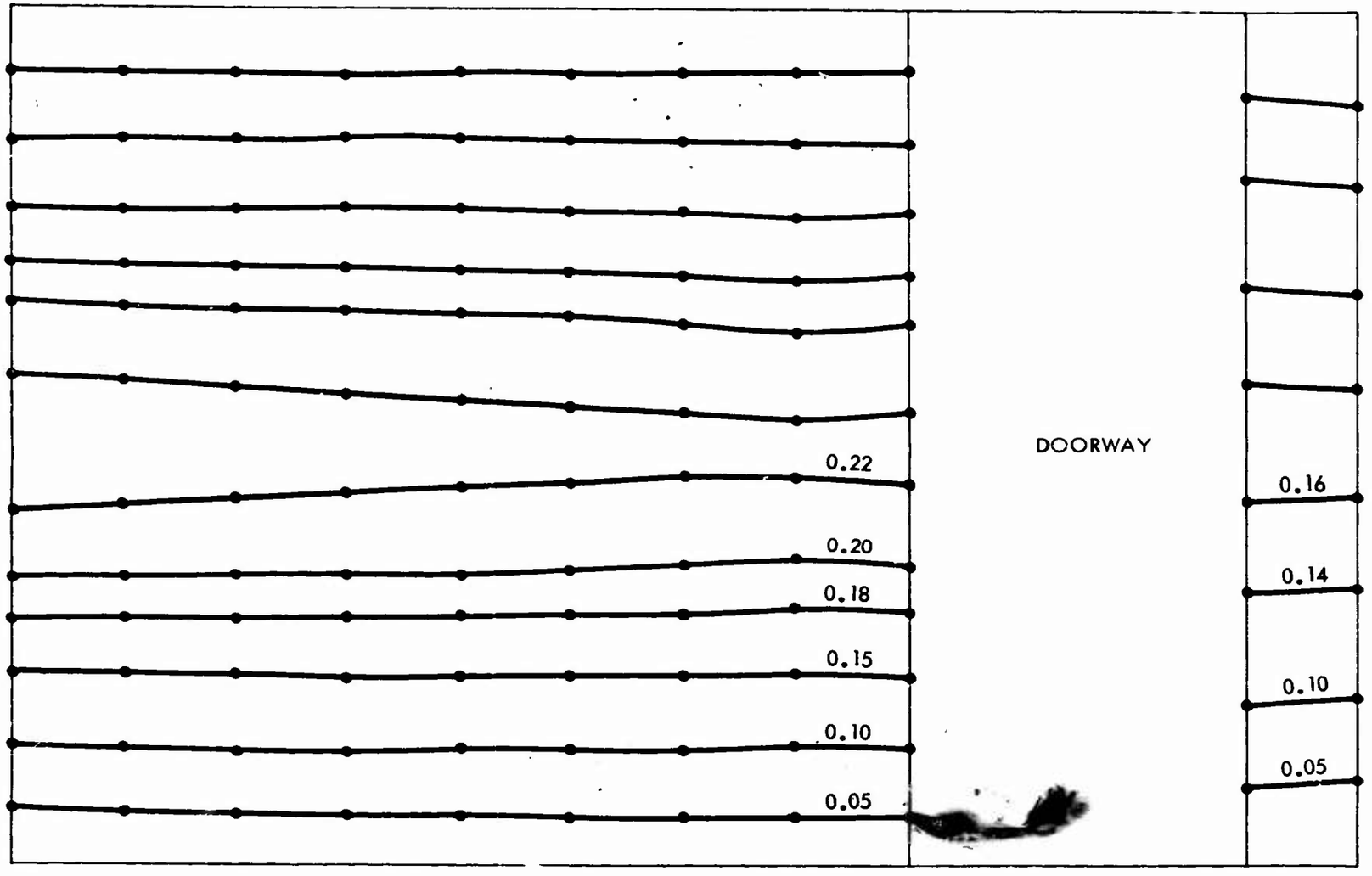

Fig. 4-24. Wall With Doorway Deflection Contour at 14 msec

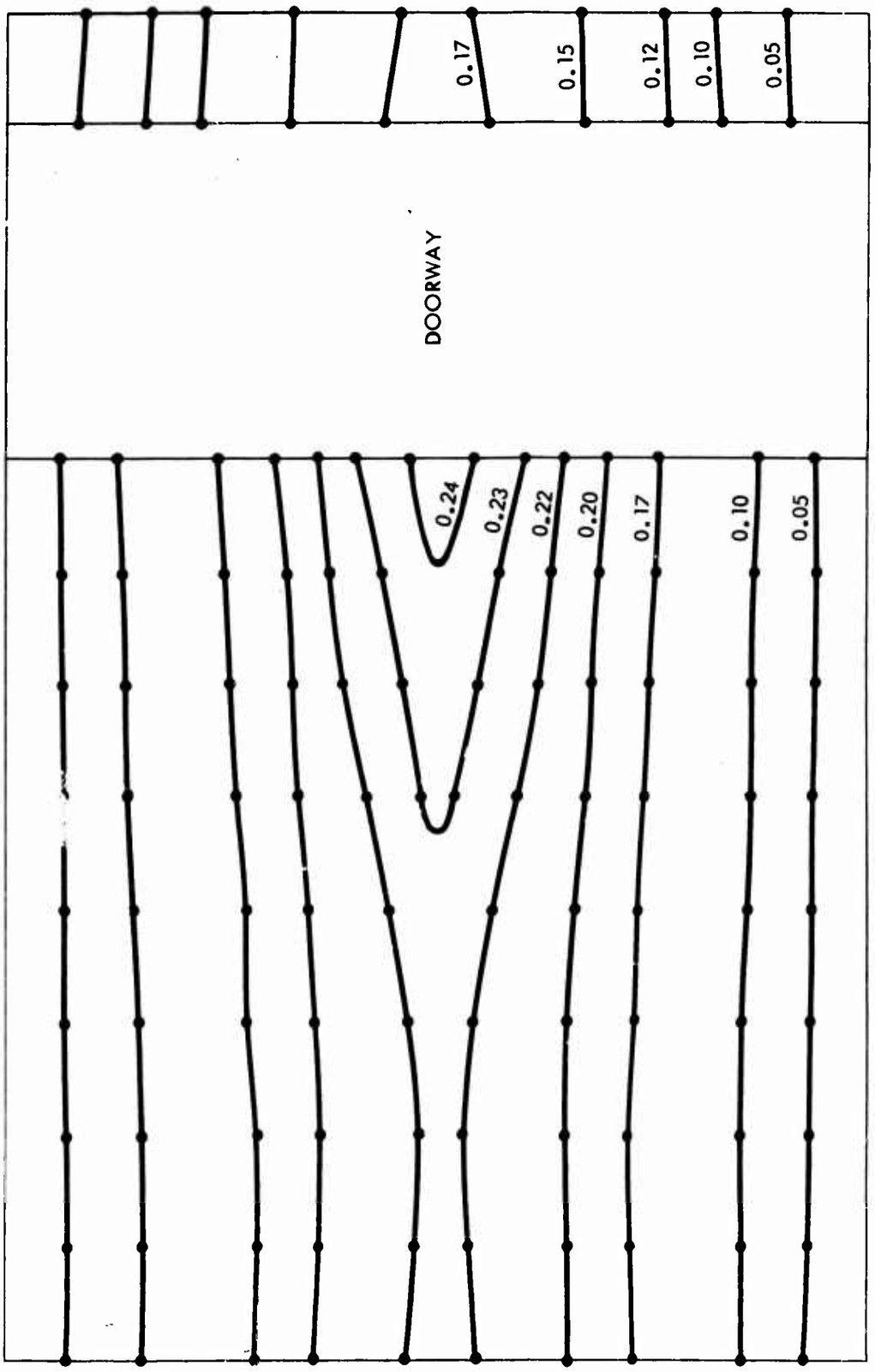

Fig. 4-25. Wall With Doorway Deflection Contour at 15 msec

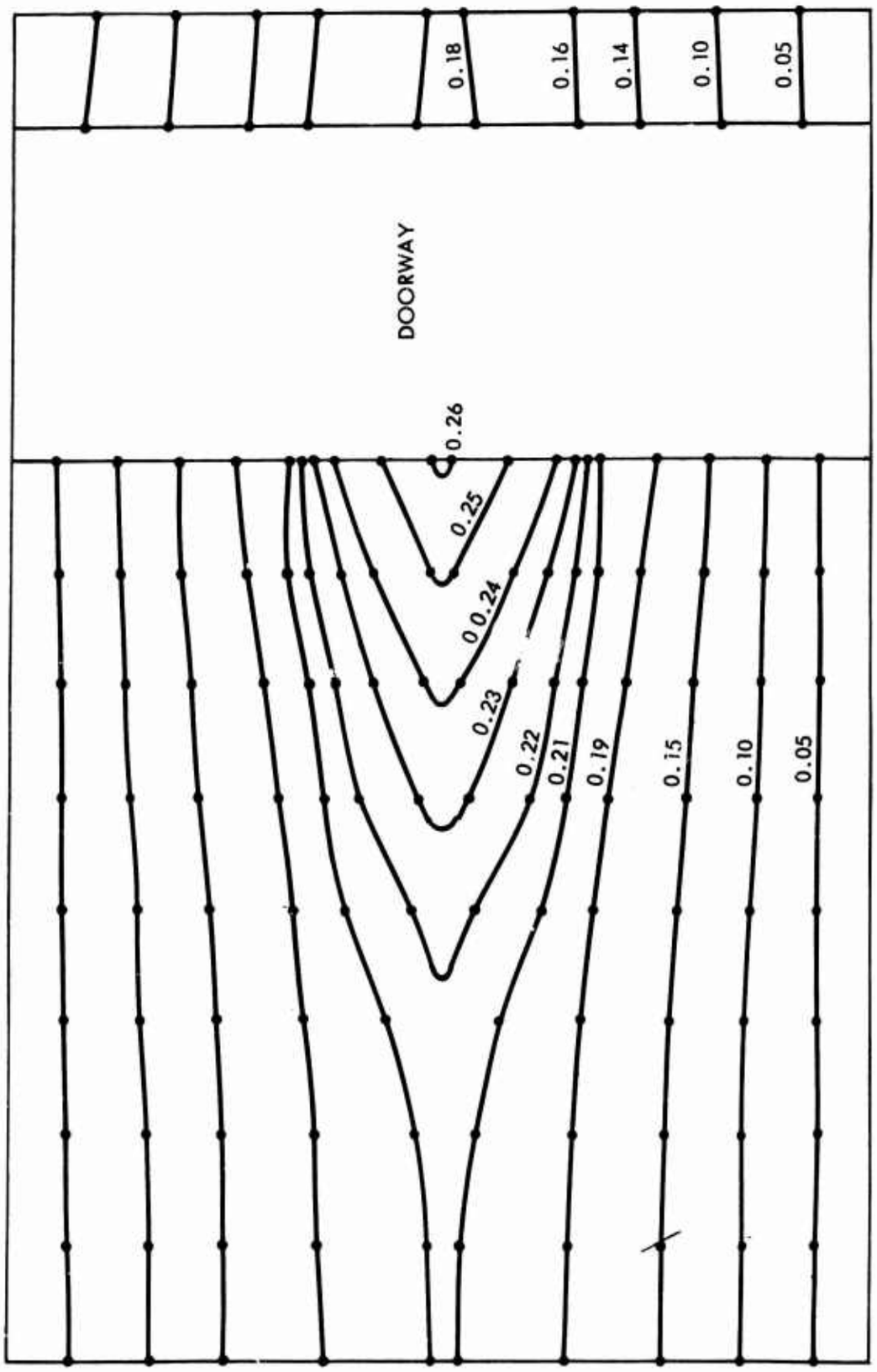

Fig. 4-26. Wall With Doorway Deflection Contour at 16 msec

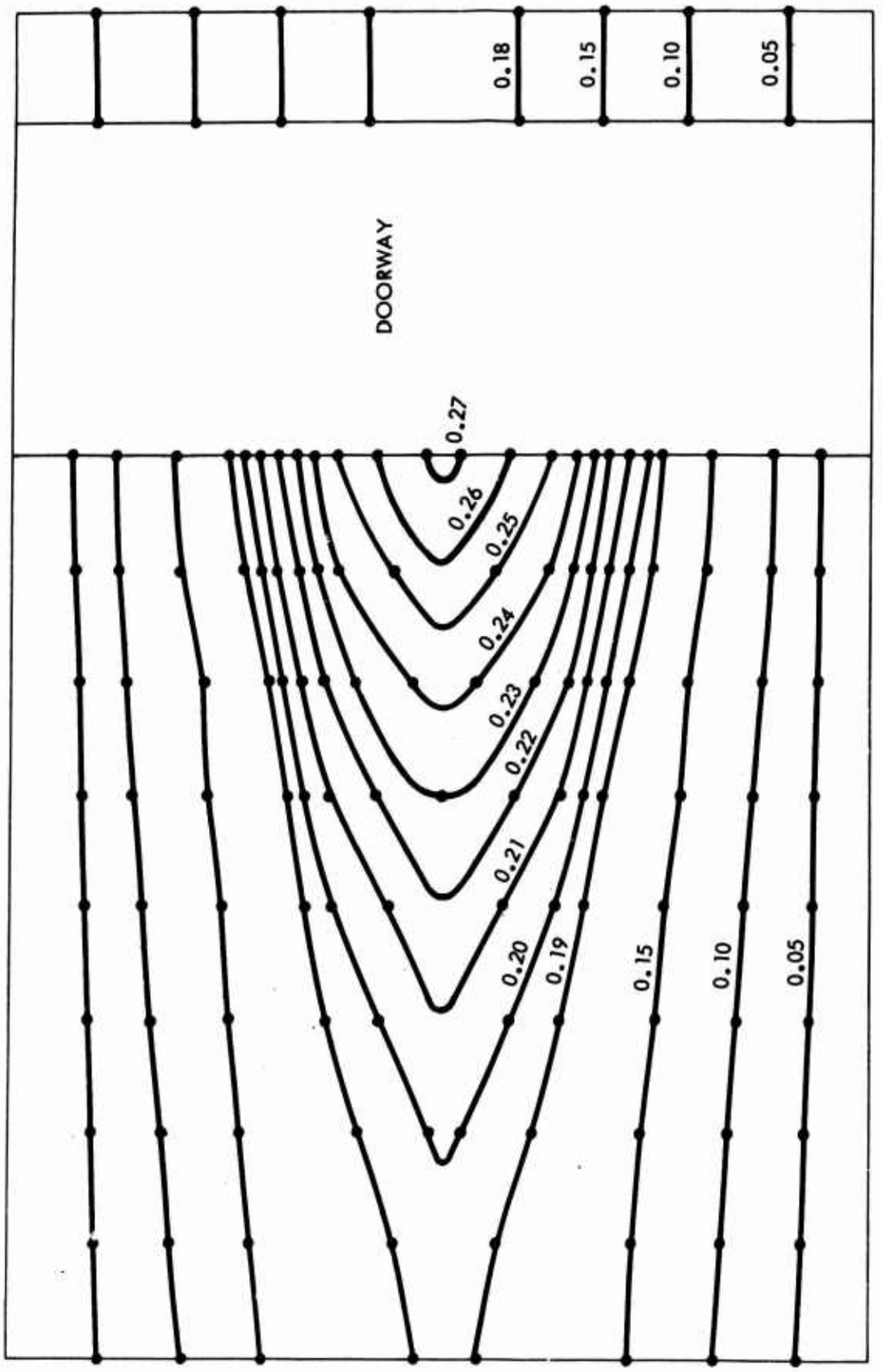

Fig. 4-27. Wall With Doorway Deflection Contour at 17 msec

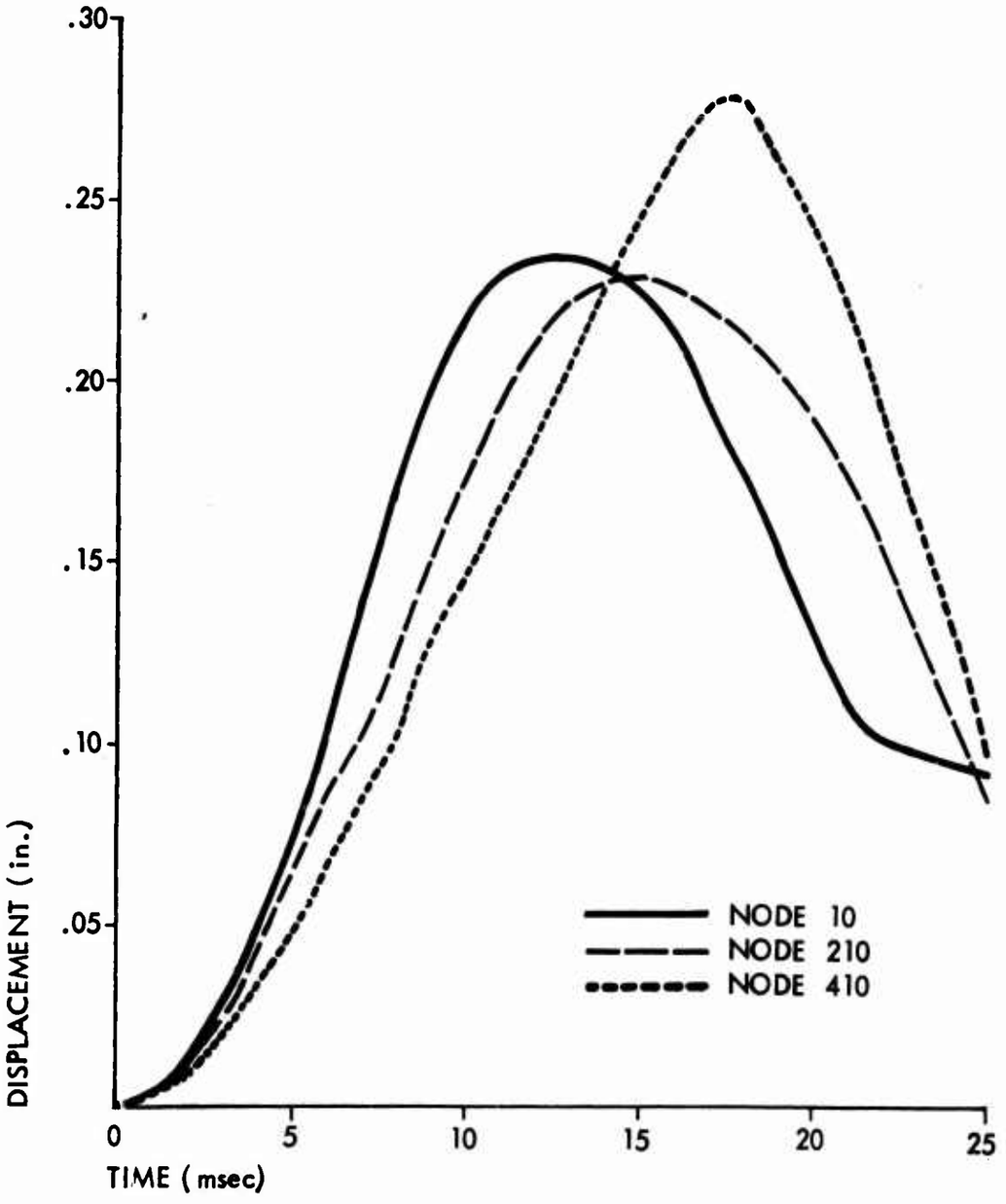

Fig. 4-28. Displacement vs Time Plot for Wall with Doorway

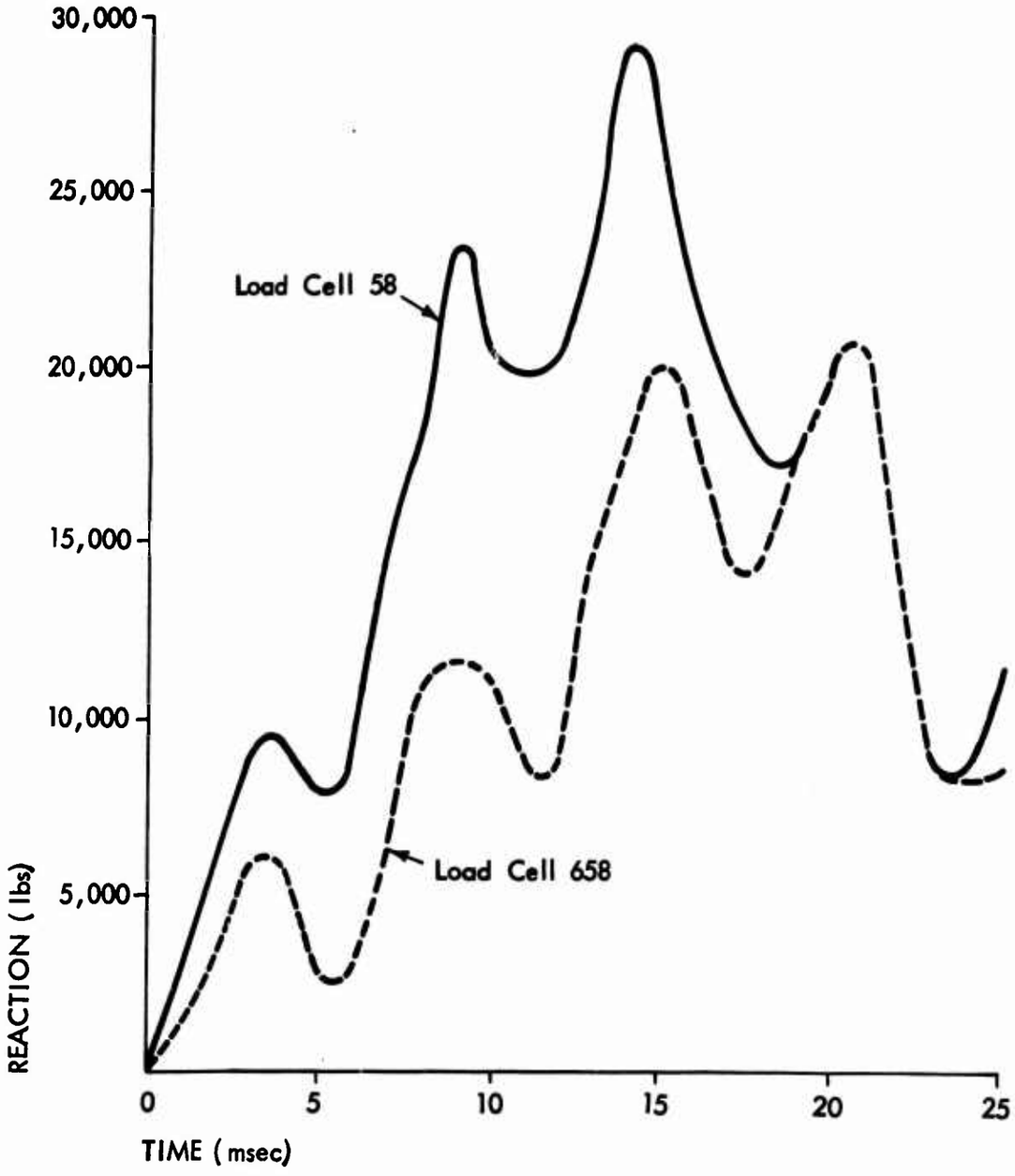

Fig. 4-29. Load vs Time for Load Cells 58 and 658

As described earlier, this precise type of phenomenon cannot be expected from the URS nonfailing wall due to its unusual construction (modular) and material difference (steel and wood vs brick). However, the total peak load cell reading is 92,800 lbs from the computer and 98,000 lbs from the loading study, which is very good agreement although the form of the trace (see Fig. 4-7) is somewhat different. It is hoped that in future tests a nonfailing masonry wall or a concrete wall can be recorded.

As with the simple beam wall panel, other data are available, such as velocity-time and displacement-time for each node as shown in Fig. 4-30. This data will be valuable as input to the second phase study of structural response vs time after cracking. Also available is data for stress vs time as shown in Fig. 4-31, which, when combined with an apparent-failure stress prediction from the brittle failure theory section should provide a rather complete failure-response prediction and analysis scheme for walls with doorways, which, of course, will be extendable to other openings.

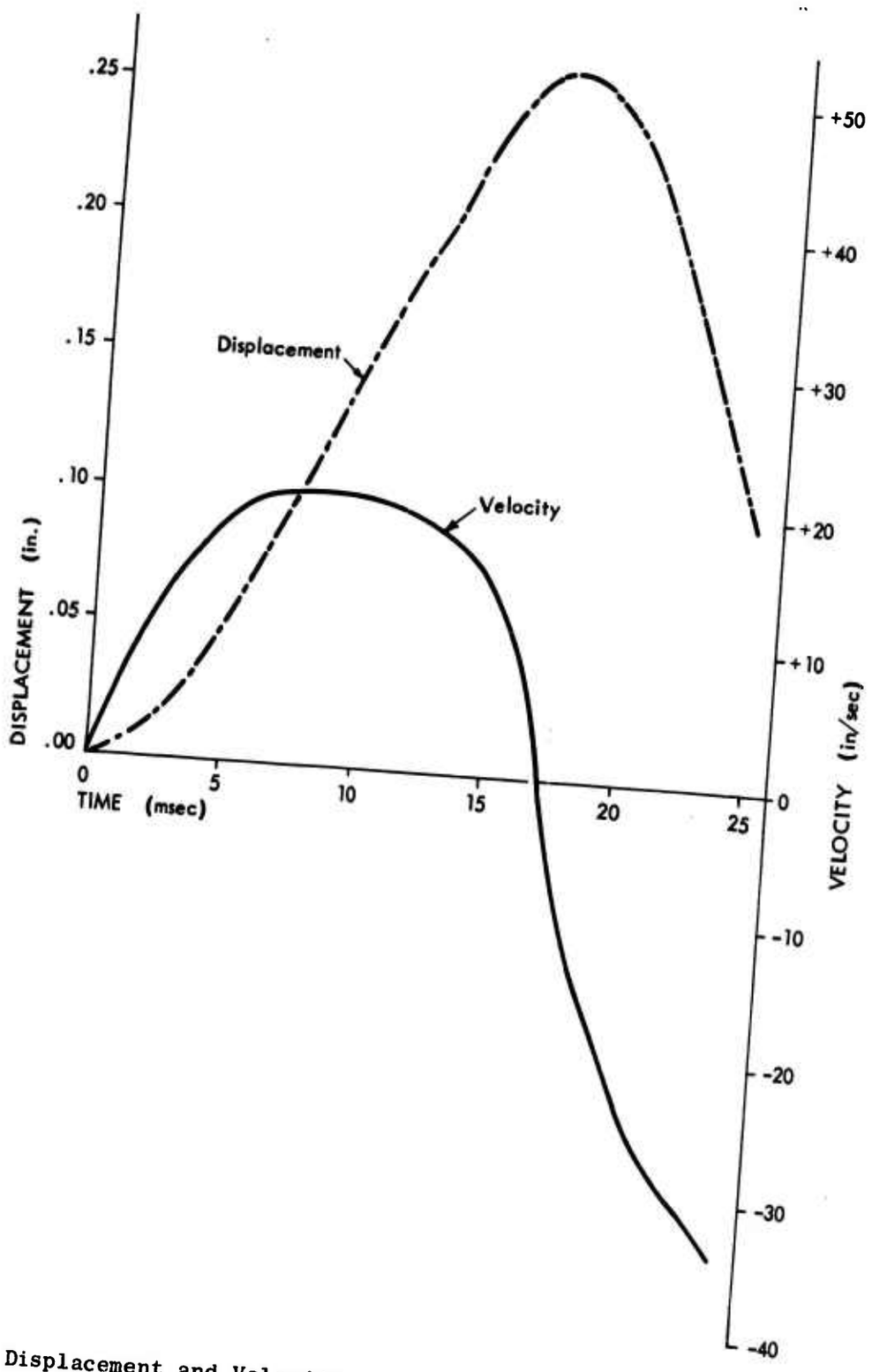

Fig. 4-30. Displacement and Velocity vs Time for Wall with Doorway (Node 360)

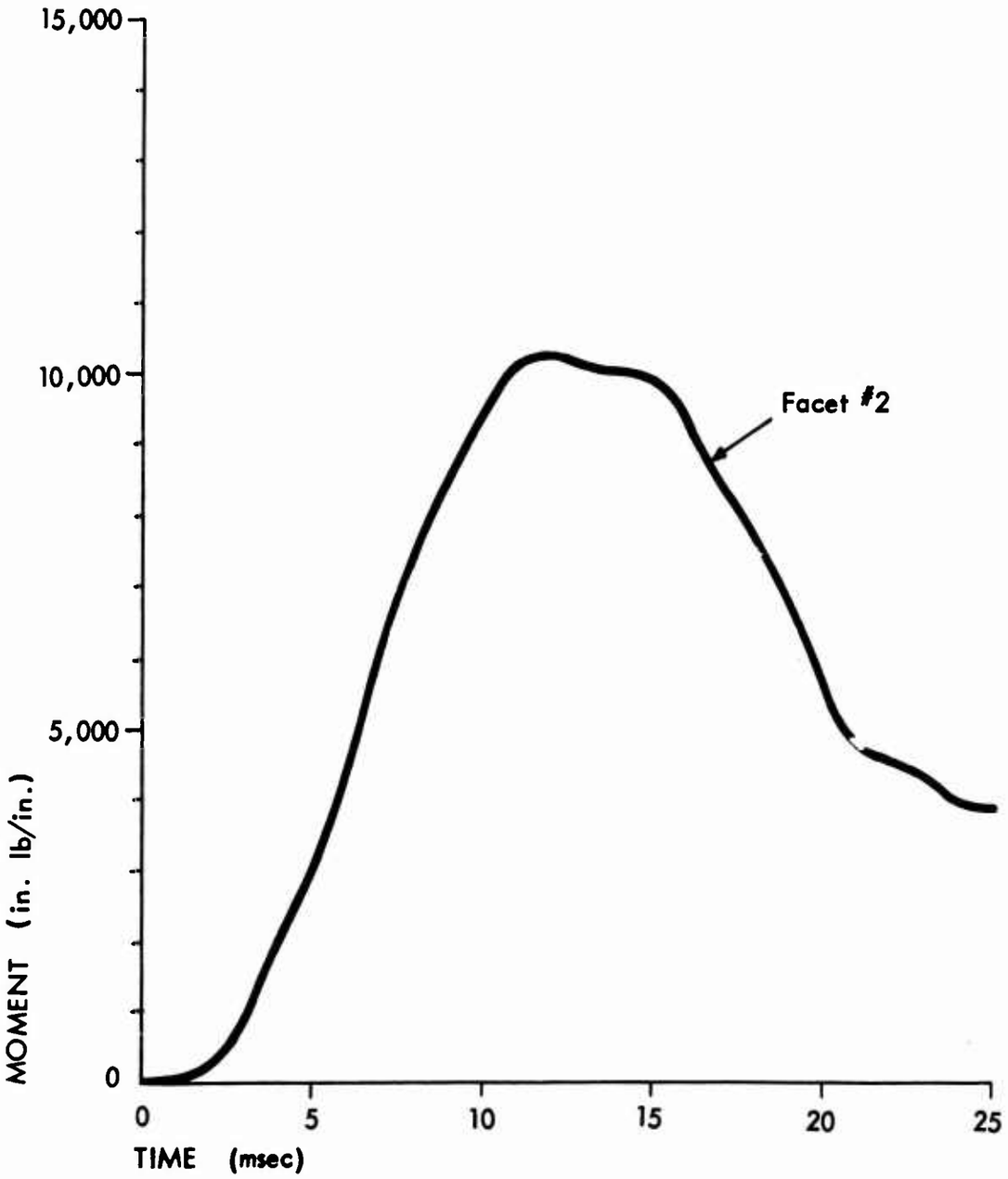

Fig. 4-31. Stress vs Time for Wall with Doorway

Section 5

LOADING AND STRUCTURAL RESPONSE OF WALL PANELS SUMMARY OF PROGRESS TO DATE

NONREINFORCED BRITTLE MATERIALS

During the past three years, a large part of the shock tunnel program has been concentrated on nonbearing nonreinforced brick panels. We are confident from our test results that the prediction capability for the performance of brick walls under blast loading can be extended to other configurations and support conditions.

To date, we have predicted the performance of — and tested to verify our predictions — a number of 8-ft x 12-ft panels, including three simple-beam support panels (8-in. and 12-in. thick without openings, and 8-in. thick with a 3-ft wide doorway) and an 8-in. thick simple plate support panel without openings. Successful response predictions for panels with door and window openings were made by using loading information (from tests with nonfailing configurations) in the SAMIS computer code. Although most predictions and tests were made for the simple beam support configuration, our success with this (and the simple plate support configuration as well) make us confident that equally successful predictions could be made for the performance of pin-fixed or fixed-fixed configurations. For such untested configurations we feel that only a minimum number of tests would have to be made, principally to verify predicted response for each configuration.

For these nonreinforced walls, only two major questions appear to remain: whether walls of other brittle (masonry) materials (e.g., cinder block and clay tile) behave in a manner similar to that of the brick walls tested; and what significant changes in response — if any — might be expected for load bearing or multi-story curtain walls in which the walls are subjected to initial vertical loads prior to — and during — interaction of the walls with a shock wave. The current research efforts are being directed toward answering these questions.

The desirability of having concentrated our efforts in the past on walls of brittle materials was confirmed in the analysis of NFSS structures which showed conclusively that walls of these brittle materials (brick, clay tile, concrete block, and nonreinforced concrete) predominate.

One of the important observations made during the program (and one which is generally confirmed by other observers) is the relatively large scatter in observed failure loadings due to the large statistical variations among walls and material properties. Predictions for a great number of walls* – which would be needed in casualty studies, for example – must take into account these statistical variations.

The authors of this report believe that effort should be made to collect and study the great amount of data existing on the static strength of a large variety of walls. This effort should result in a reasonable probability distribution (for different classes of masonry from different parts of the country) for the static strengths of a variety of walls. With such information, and with our ability to predict the performance of walls in any configuration (with or without openings) and with any support configuration, it is anticipated that reasonable predictions (in a statistical sense) can be made for a great number of walls in a variety of configurations.

Typical of the kind of predictions that could be made is that shown in Fig. 5-1 which is based on the assumption that the distribution of all our beam data represents a reasonable approximation to the strengths of brick wall materials. The figure is for an 8-ft x 12-ft x 8-in. nonreinforced brick wall without openings, simply supported on top and bottom, and subjected to a step-

---

* It should be noted here that on a large-scale prediction or the prediction of a large number of walls, the emphasis must be on the expected performance, not on the concept of design allowable as used in typical engineering projects. For example, the URS series of brick beams exhibits a mean tensile strength in flexural tests of about 200 psi which implies a minimum stress of about 50 psi. With a minimum stress of 50 psi, one is not surprised to find a design allowable in the building code of 20 to 25 psi in tension. Thus, the URS test data has been consistent with that of other researchers.

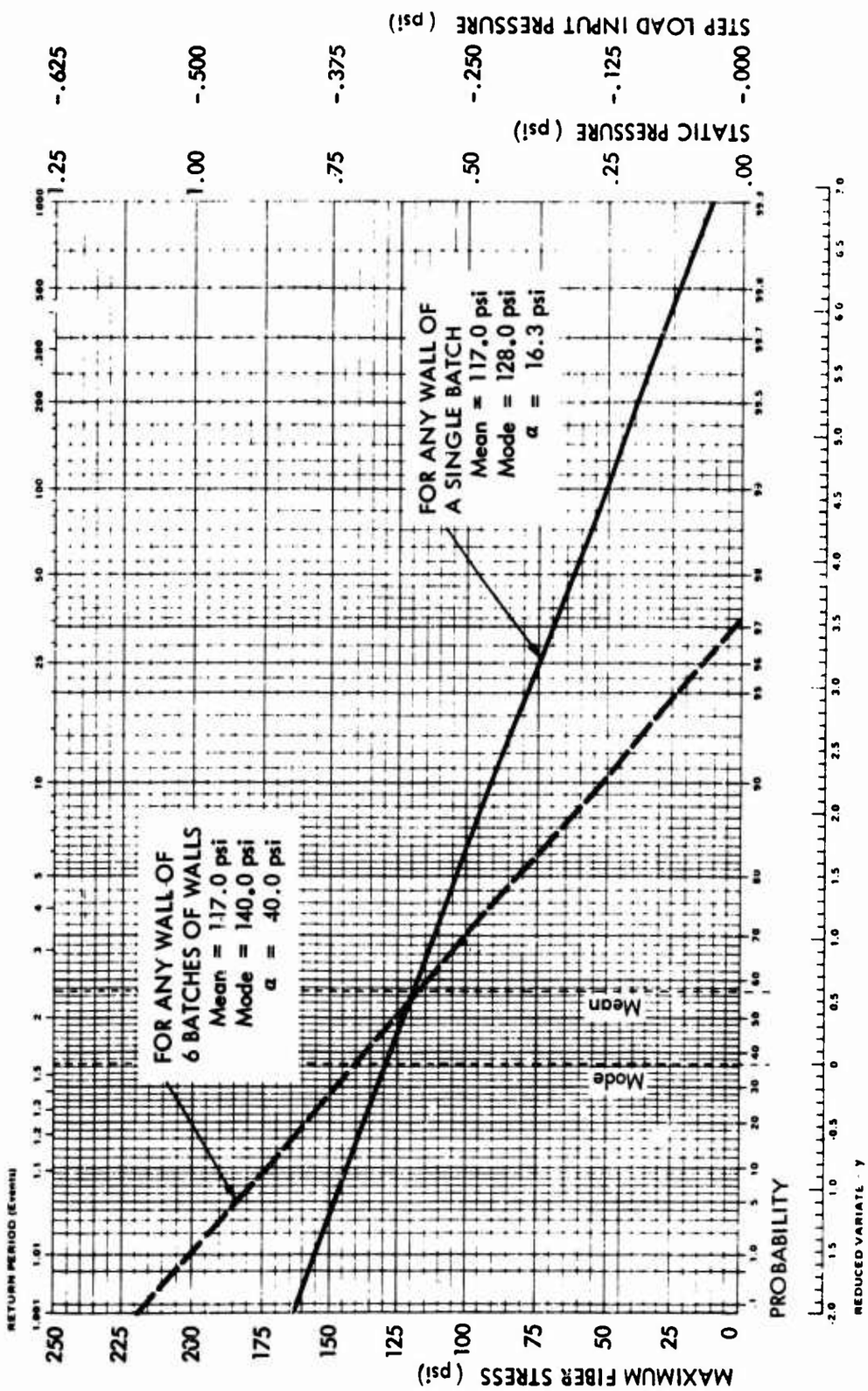

Fig. 5-1. Predicted Strength Distribution for 8-ft x 12-ft x 8-in. Brick Wall Panel

loading of long duration (i.e., over 25 msec) not unlike a blast load of long duration on a large building.

By referring to the statistical theory of Appendix B, the information could be extended to other support and loading conditions, for example, in the manner shown in Fig. 5-2, a type of plot that gives insight into the influence of support conditions and load form upon the strength (probability of failure) or in the manner shown in Fig. 5-3, where reflected overpressure can be compared to fiber stress.

For more complex wall forms, such as walls with doorways, changes of failure distribution are expected for a number of reasons. Among the major reasons is the change in loading functions (Fig. 5-4) which changes displacements (Fig. 5-5) and reduces fiber stress at the same incident overpressure level (Fig. 5-6). From this some increase in fracture overpressure can be expected.

A second important reason to expect changes in failure distribution illustrates the importance of understanding the probabilistic implications of the statistical information on wall and material properties. A wall with a doorway contains less brick than one without a doorway, and hence there is a lower probability that the wall contains a flaw. That is, because there is less material at a given stress level in the wall with a doorway there should be a lower probability of its failure. Fig. 5-6 is an approximation of the strength distribution one might expect for an 8-ft x 12-ft x 8-in. brick wall with a 3-ft x 8-ft doorway.

It should be appreciated that before prediction curves for either simple or complex configurations are prepared, all available test data from the literature should be compiled and analyzed to derive a better understanding of the distribution of wall and material properties. It is conceivable that regional differences or differences based on mortar types would be found which could alter wall and material properties in a significant way (more scatter or different distributions).

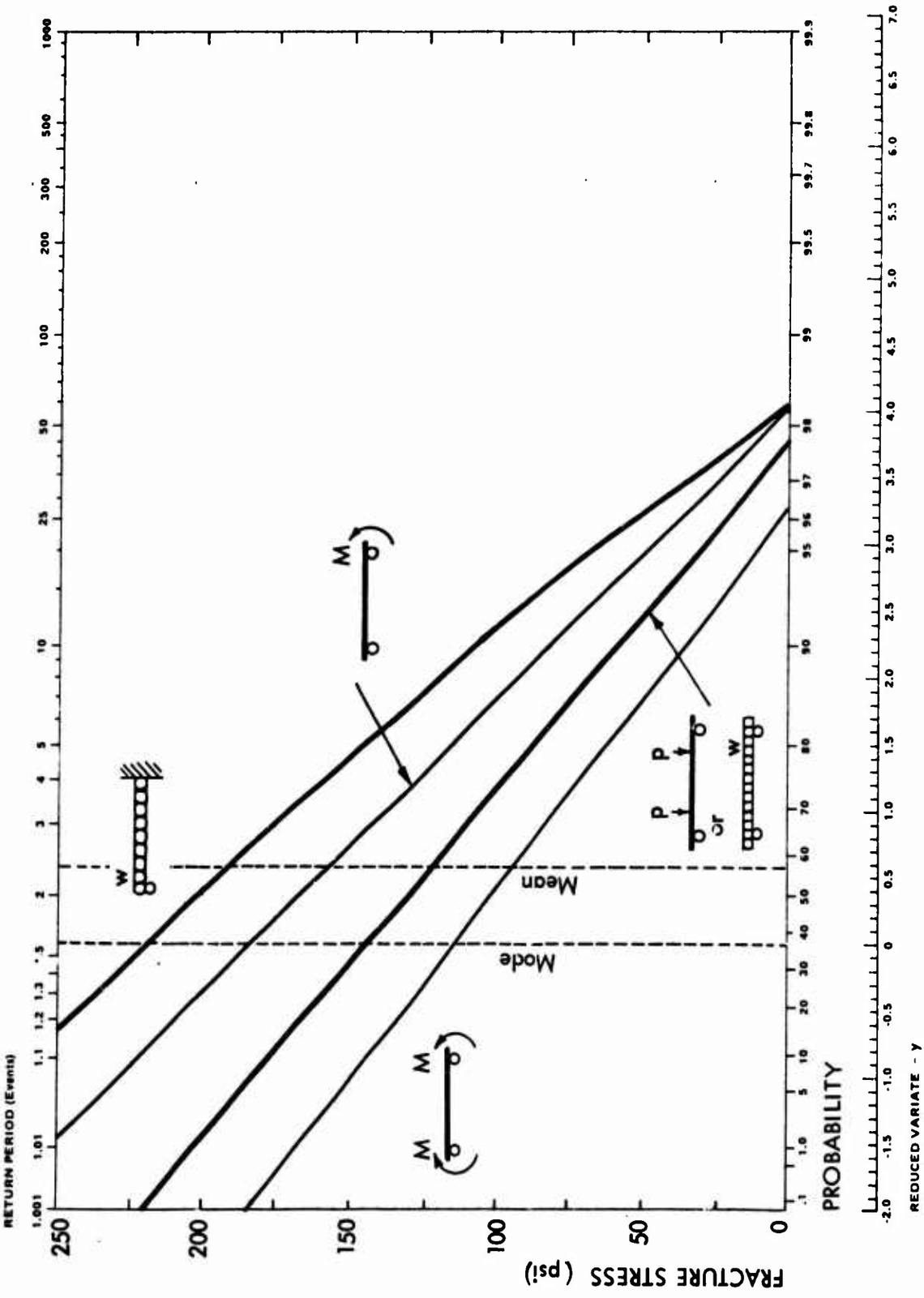

Fig. 5-2. Extreme Probability Plot of Fracture for 8-ft x 12-ft x 8-in. Walls with Various Loadings and Support Conditions

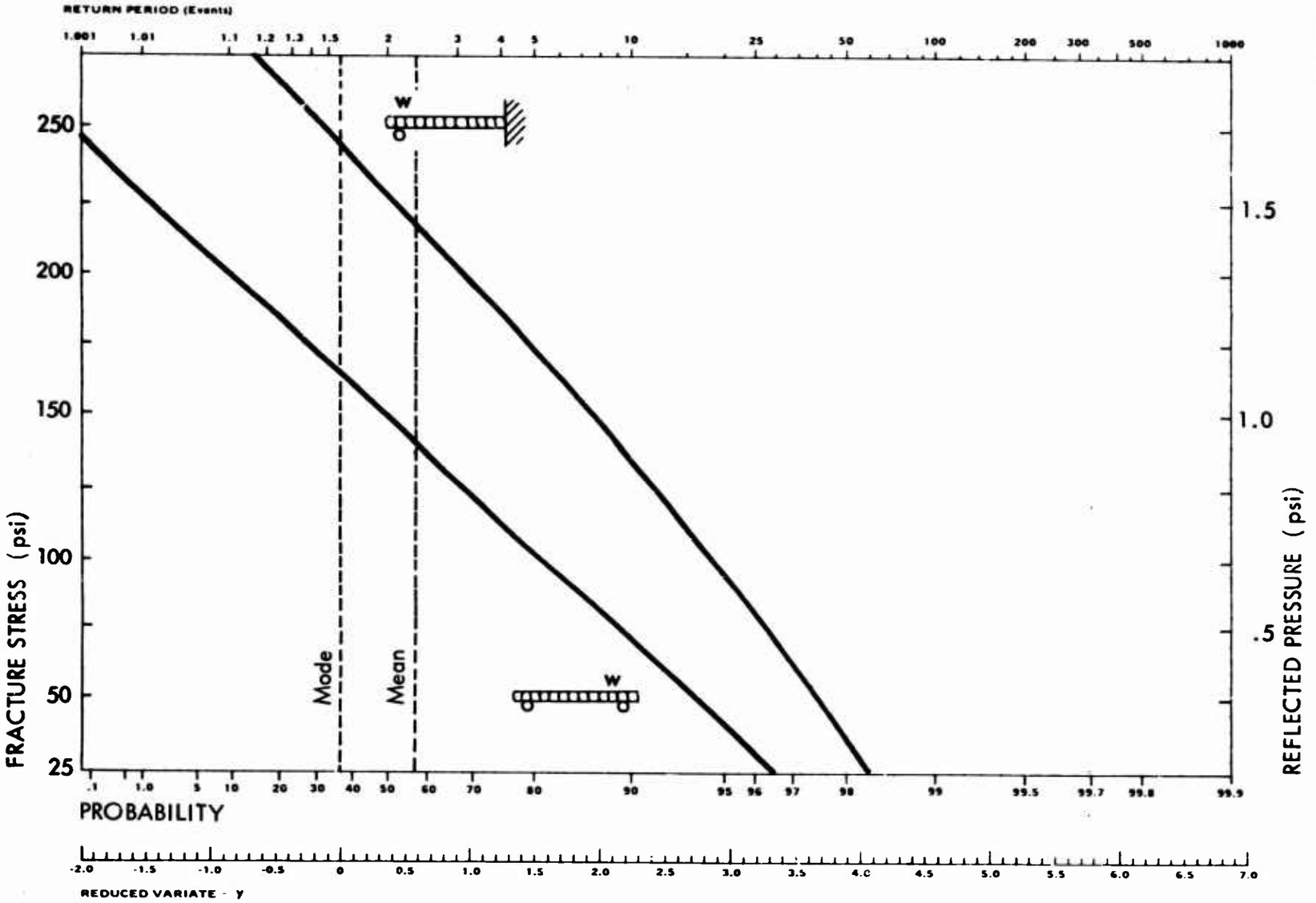

Fig. 5-3. Extreme Probability Plot of Fracture for 8-ft x 12-ft x 8-in. Walls with Various Support Conditions and a 3-ft x 8-ft Doorway

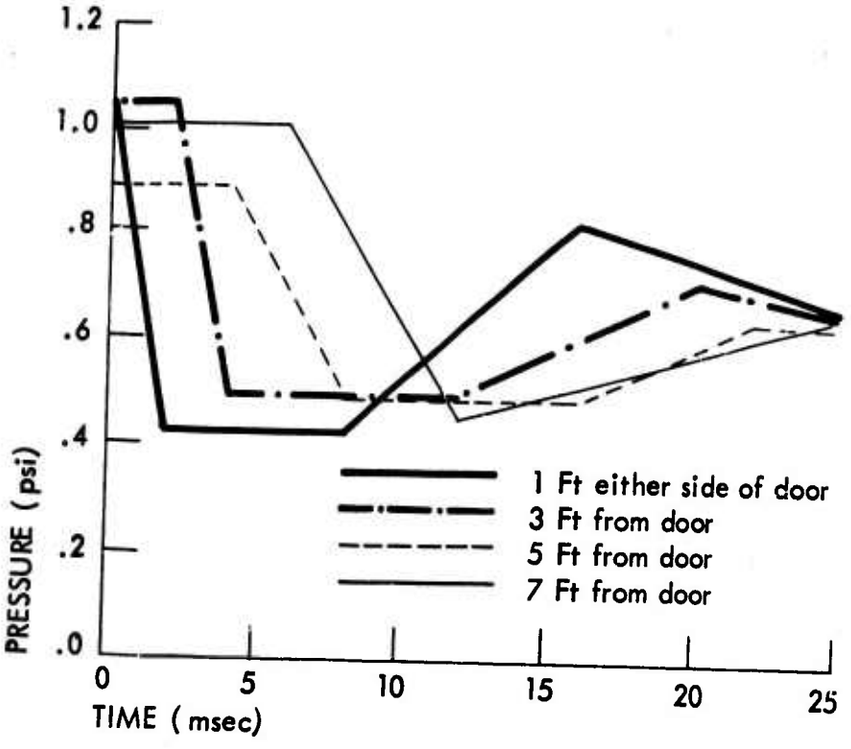

Fig. 5-4. Wall Loads

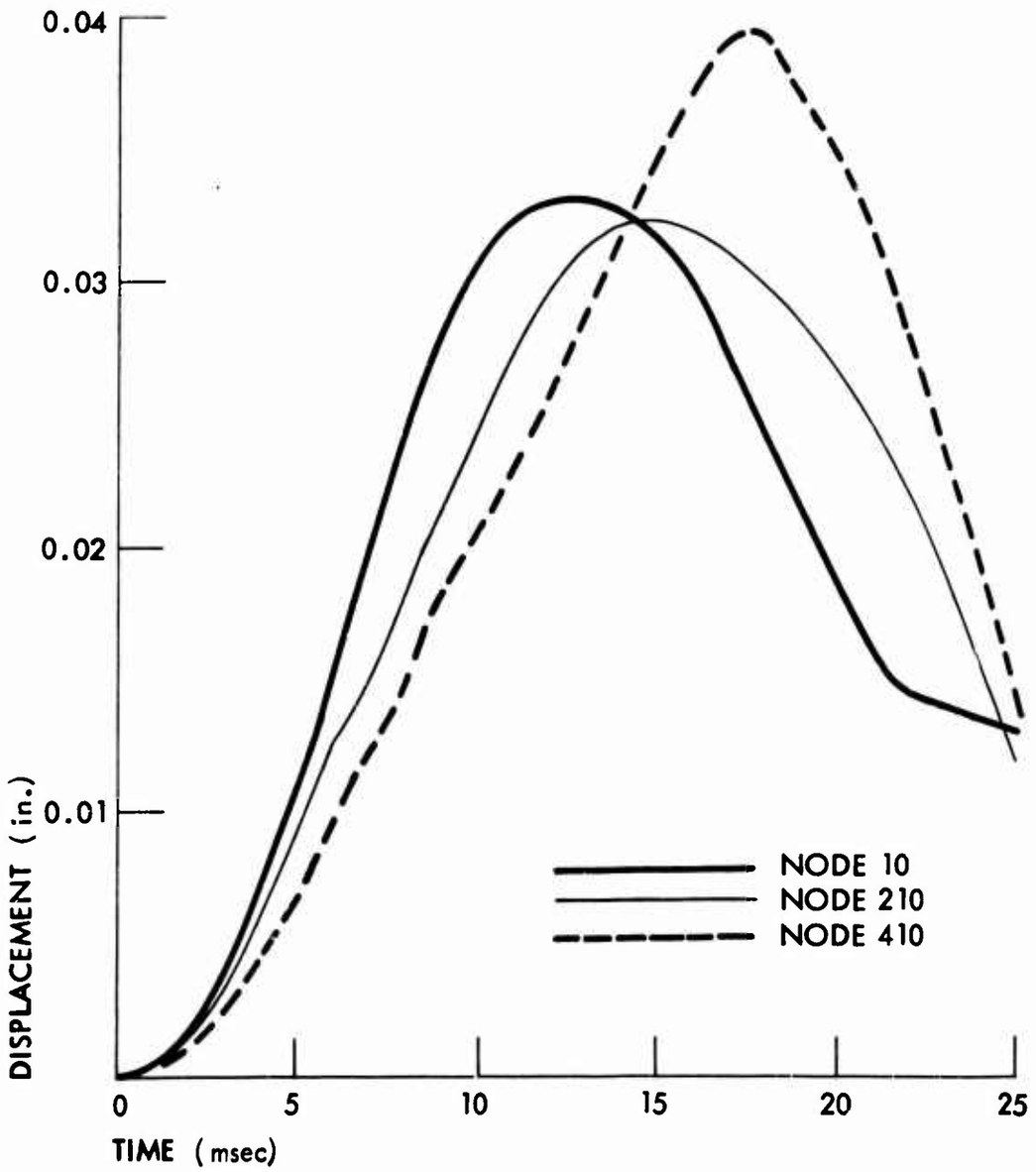

Fig. 5-5. Displacement vs Time

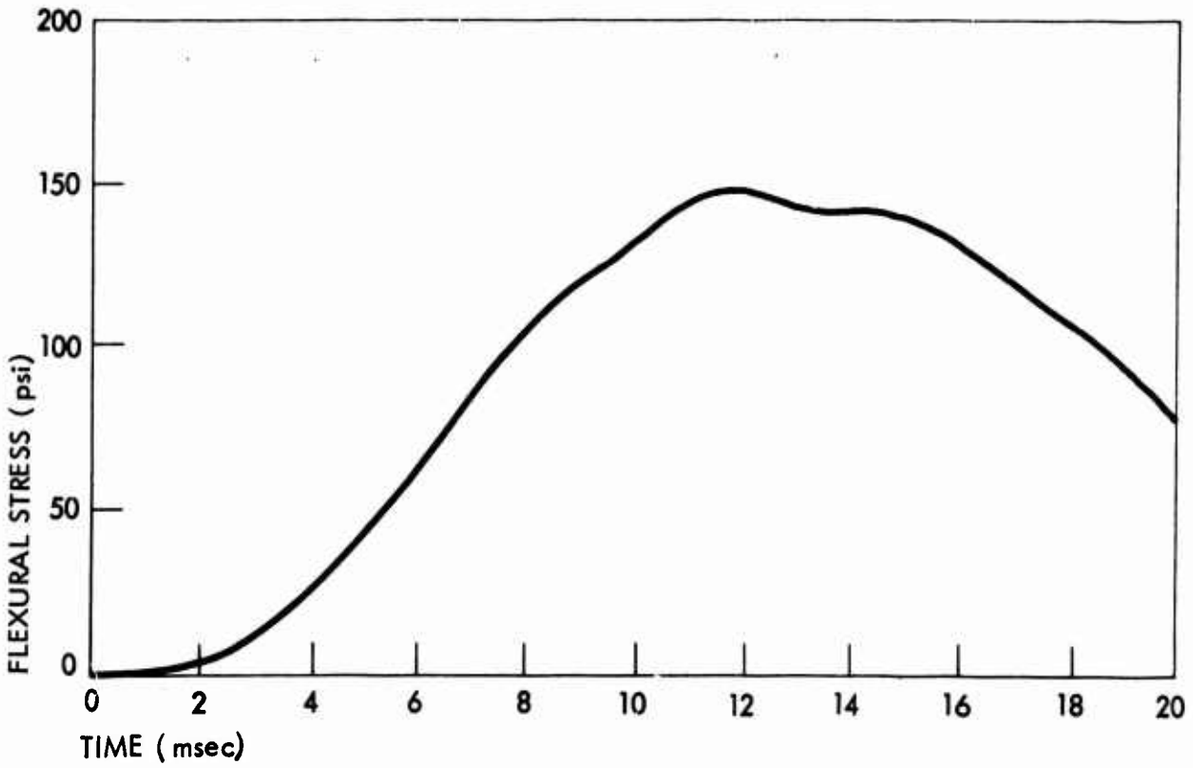

Fig. 5-6. Doorway Wall Panel Stress Area of Node 10

OTHER WALL TYPES

Many tests have been performed on interior timber-stud partitions. To date none of these partitions have contained openings, but it is felt that by extending the analytical and experimental techniques developed for walls of brittle materials, the program for timber stud walls with openings should become limited and inexpensive.

It appears that major emphasis in the future should be on reinforced concrete walls, both precast and in place.

Section 6

REFERENCES

1. Hill, E. L., et al., Structural Characteristics of NFSS Buildings, Vols. I - IV, Research Triangle Institute, Final Report OU-237, Durham, North Carolina, February 1967.

2. Wilton, C. W., B. L. Gabrielsen, J. Edmunds, and S. Bechtel, Loading and Structural Response of Wall Panels, URS Report No. 709-4, URS Research Company., Contract DAHC20-67-C-0136, November 1969.

3. Wiehle, C. K., and J. L. Bockholt, Existing Structures Evaluation, Part I: Walls, Stanford Research Institute, Palo Alto, California, November 1968.

4. Willoughby, A. B., C. W. Wilton, B. L. Gabrielsen, and J. V. Zaccor, A Study of Loading, Structural Response, and Debris Characteristics of Wall Panels, URS 680-5, URS Research Co., Contract 11618(6300A-250), July 1969.

5. Gumbel, E. J., Theory of Extremes, Columbia University Press, New York, 1958.

6. Weibull, W., A Statistical Theory of the Strength of Materials, Handling No. 151, Engineering Academy, General Lithographic Library, Stockholm, Sweden, 1939.

7. Tucker, John, Jr., "Statistical Theory of the Effect of Dimensions and of Method of Loading Upon the Modulus of Rupture of Beams," Proc. ASTM, Vol. 41, 1941.

8. Fishburn, C. C., Effect of Mortar Properties on Strength of Masonry, National Bureau of Standards Monograph 36, November 20, 1961.


BLANK PAGE

Appendix A
THE URS SHOCK TUNNEL

Presented in this Appendix is a brief description of the URS shock tunnel facility including a discussion of the operating concept, a description of the instrumentation, test hardware and support equipment and the results of calibration tests performed at the facility.

DESCRIPTION

The shock tunnel is located at the URS Research Company's field laboratory in the San Francisco Bay Area, near the north end of the Golden Gate Bridge. This laboratory is underground, in a former coastal defense gun emplacement complex, and contains approximately 23,000 sq ft of floor space, which is divided into shops, instrumentation rooms, a wave tank, explosives magazines, and the shock tunnel facility. A cutaway view of this laboratory is shown in Fig. A-1.

The shock tunnel occupies approximately 8,000 sq ft of this laboratory and is shown in Figs. A-2 and A-3. It is rectangular in cross section, 163 ft long, and has walls of reinforced concrete, varying from 3 to 12 ft in thickness. The first 63 ft of the tunnel contains the compression chamber and has an 8- by 8.5-ft cross section. The remaining tunnel expands, in an 8-ft long transition section, to a 92-ft long 8- by 12-ft chamber.

The Compression Chamber

The compression chamber is a 3/8-in. thick, 7-ft 8-in.-diameter steel tube, 63 ft long, with a 1/2-in.-thick domed end closure. The space between the tube shell and the concrete wall of the tunnel has been filled with foamed-in-place rigid urethane foam This foam provides a continuous elastic support around and along the entire tube to prevent tube collapse, supplies the necessary hold-down strength, and provides a large amount of damping on the tube to

Fig. A-1. Cutaway View of the URS Physical and Engineering Sciences Field Laboratory

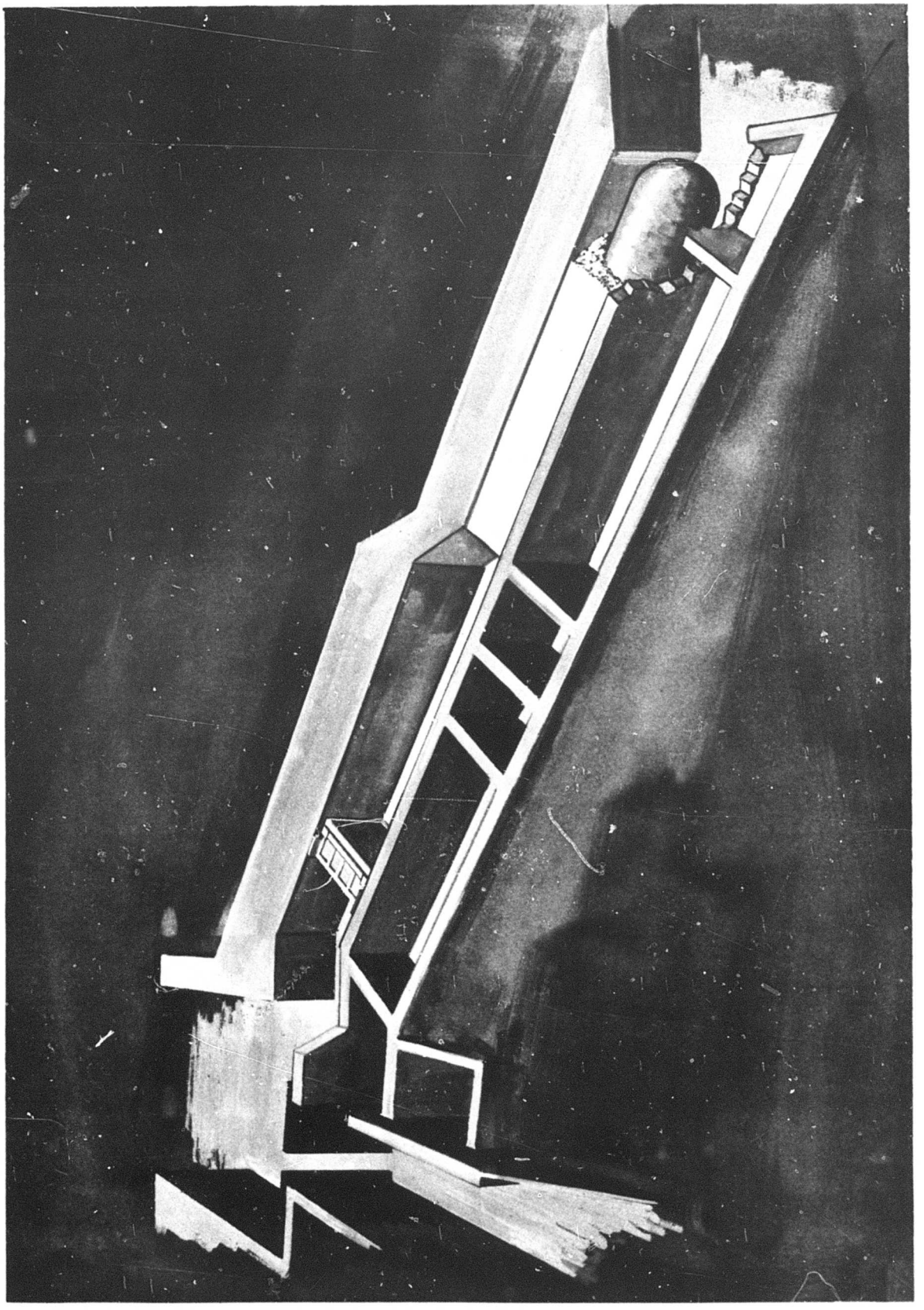

Fig. A-2. Cutaway View of the Shock Tunnel Facility

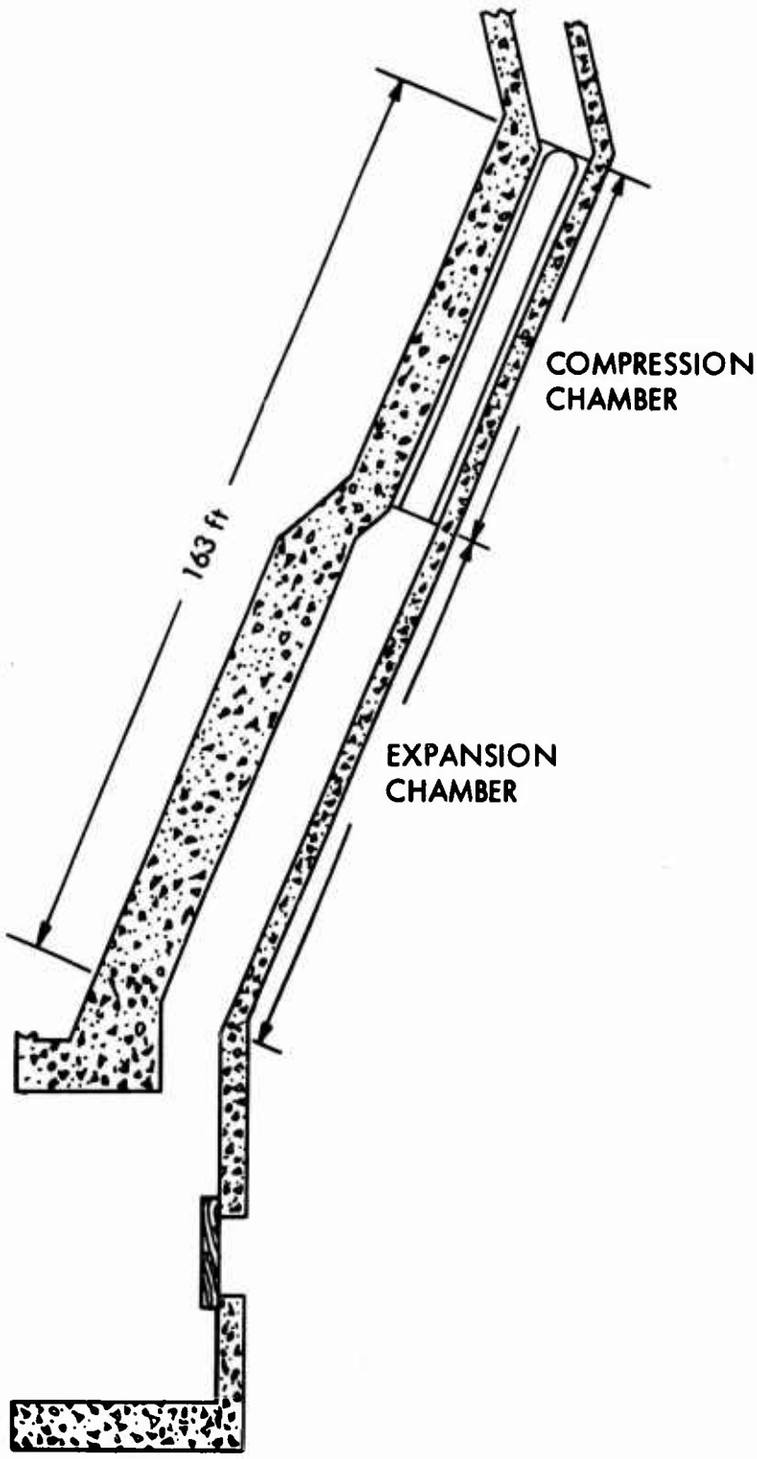

Fig. A-3. Plan of Shock Tunnel

facilitate making pressure measurements on the walls of the tube. As a further side benefit, it reduces noise and vibration throughout the facility. A thin steel collar has been installed around the mouth of the tube to protect the foam from air blast, and a 24-in.-diameter accessway with a blast door has been installed in the domed end of the tube. The purpose of this door is to allow access to the compression chamber for installing the explosive charges after the tunnel is blocked with a test specimen, and to provide ventilation in the tunnel.

The Expansion Chamber

The expansion chamber is approximately 100 ft long and for the majority of its length has an 8-1/2- by 12-ft cross section, the 12-ft dimension being horizontal.

Test specimen mounting positions have been installed in the expansion chamber between 70 and 80 ft from the mouth of the compression tube. One of these locations is illustrated in Fig. A-4, a cutaway view of the shock chamber, which shows a brick wall and support frame in place in the tube. A more complete explanation of the support hardware is given below.

Operating Concept

The tunnel is operated as a shock tube by means of the volume detonation technique, with Primacord as the explosive material. In this mode of operation, the Primacord is distributed uniformly throughout a section of the compression chamber portion of the tunnel. On detonation of the Primacord (which proceeds at a rate of about 20,000 ft/sec), a quasi-static pressure is built up very rapidly throughout the entire compression chamber. The expansion of this high-pressure gas into the remaining part of the tunnel generates the desired shock wave.

Unlike conventional compressed-gas shock tubes, it is not necessary to separate the compression chamber from the expansion chamber with a frangible diaphragm. The detonation of the Primacord is sufficiently rapid that the

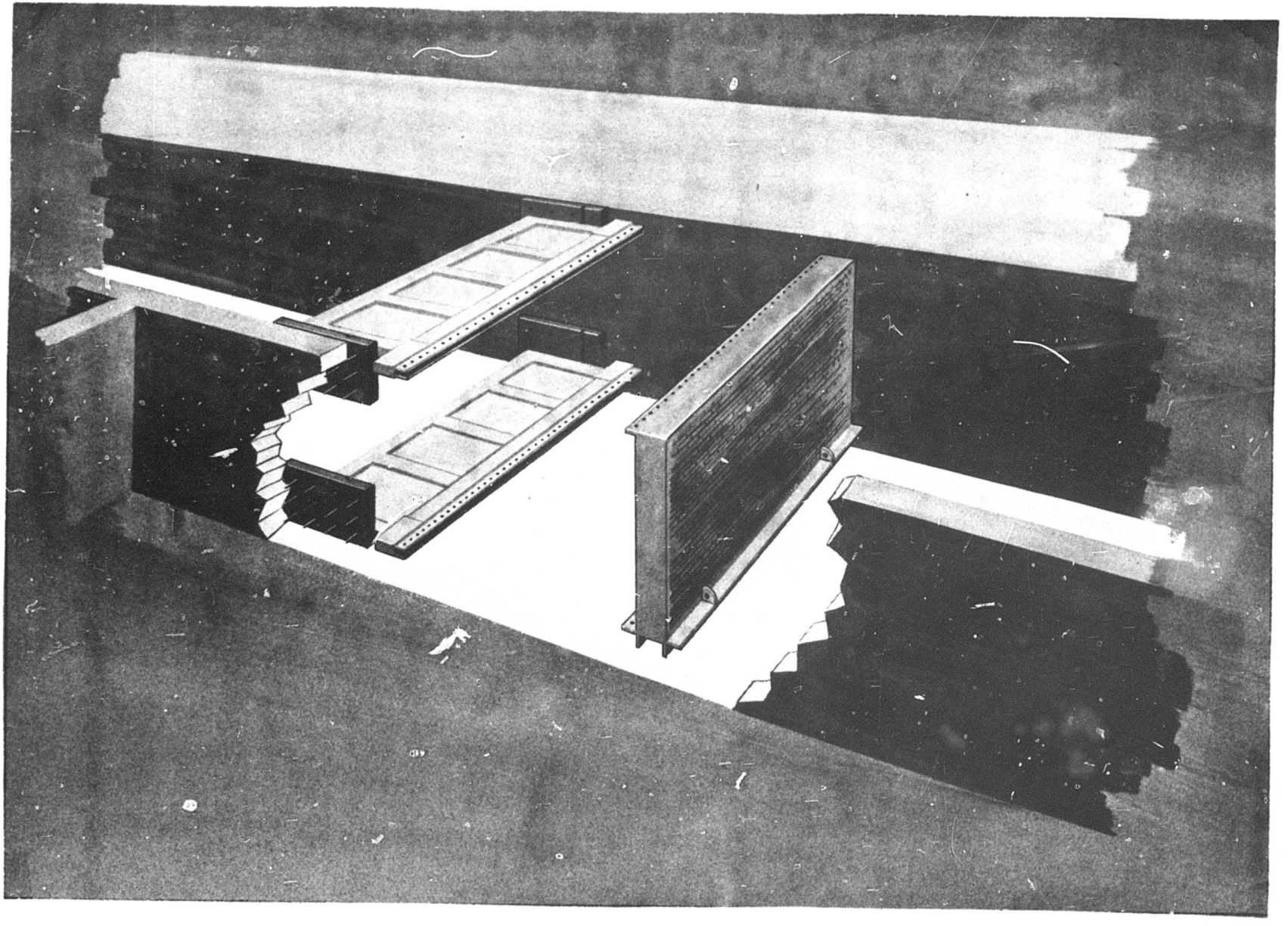

Fig. A-4. Cutaway View of Shock Tunnel Showing Test Panel and Simple Beam Support Condition Hardware

pressure buildup in the compression chamber is affected very little by the small amount of the overall volume during the buildup process.

Test Section Hardware

Because of the requirements of the various programs carried out in the tunnel, the test section hardware now includes: nonfailing walls (see Fig. A-5), which can be arranged with a variety of openings simulating doorway and window openings and which can be instrumented in many places; vertical plate girders, which can provide all around support to test walls (see Fig. A-6); and a plate girder support location with which a variety of simulated rooms can be set up ranging in length from 4 ft to 15 ft. The tunnel has also been equipped with a variety of viewing ports to facilitate motion picture recordings of wall failures and the effects of shock flows.

Shock Tunnel Instrumentation

The shock tunnel instrumentation includes: air blast gages mounted in the tunnel wall for monitoring the input loading wave; load cells for measuring the load transferred from a test specimen to its support frame during the loading cycle; strain gage and air pressure instrumentation for the test specimens; and high-speed cameras in blast-protected mounts for recording the response of the test specimen.

A block diagram of the instrumentation system is presented in Fig. A-7.

SHOCK TUNNEL CAPABILITIES

When first put into operation, the shock tunnel was calibrated by conducting approximately 50 tests in which variables of charge density, charge location, charge length, method of detonation, and tunnel geometry (both open and closed) were investigated. Additional calibration data were acquired during the course of the many test programs conducted in the shock tunnel.

The results of these tests are briefly summarized below:

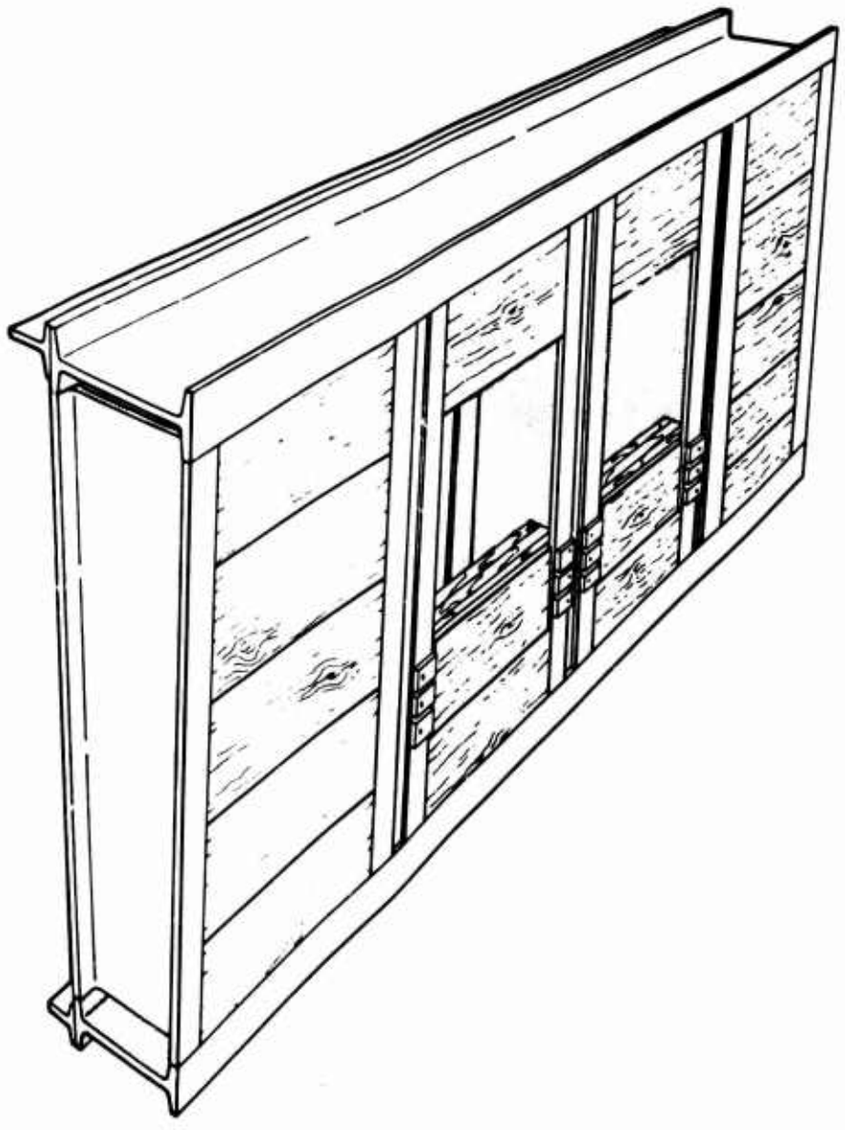

Fig. A-5. Sketch of Nonfailing Wall

Fig. A-6. Cutaway View of Shock Tunnel Showing Test Panel and Simple Plate Support Condition Hardware

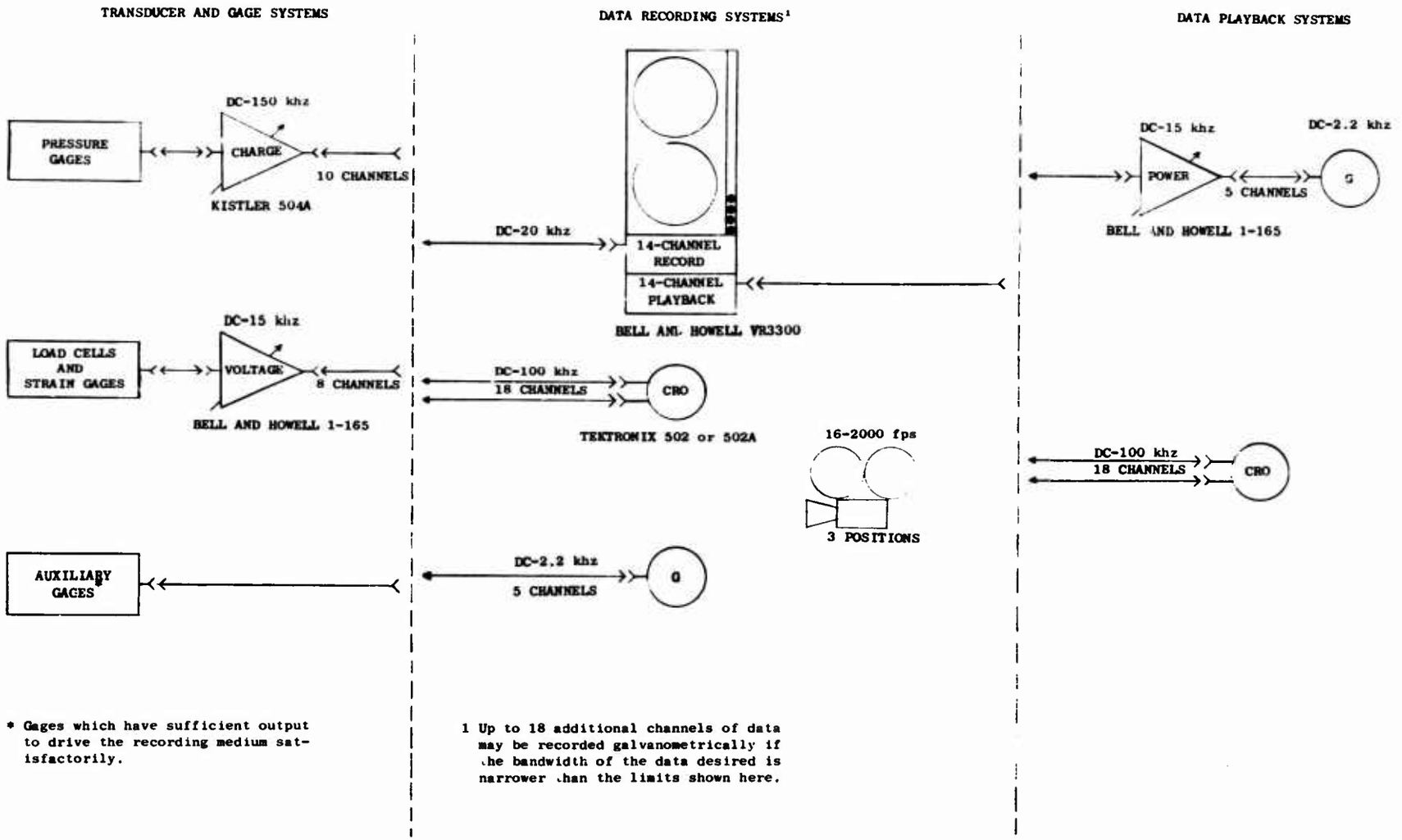

Fig. A-7. Block Diagram of Data Recording and Playback Options

- The pulse shapes and peak overpressures obtained from the same charge density and charge arrangement are reproducible.*

- Shock overpressures increase with increasing charge density. For example, the two-strand charges tested (approximately 0.0125 lb/ft) which varied in length from 40 to 60 ft, yielded a peak incident overpressure of 3.7 psi at the test section location, while an eight-strand charge (approximately 0.05 lb/ft) yielded a peak incident overpressure of 9 psi.

- The pulse shape varies with charge arrangement. For example, when the Primacord strands are placed together at the center of the tube, a classical shock wave is obtained. When the strands are separated and spread out in the tube, shapes that are essentially flat-topped are obtained.

- Pulse durations increase with increase in charge length, with typical durations approximately 40 to 60 msec for a 40-ft charge, and 80 to 100 msec for a 60-ft charge, for both the classical and flat-topped pulse shapes. The duration of the flat-topped portion of the latter pulses ranged from 30 to 50 msec (see Fig. A-8).

- Some minor variations in pressure are observed across the shock tunnel cross section.

Mean values of incident shock front overpressure as a function of the number of strands of Primacord used on an individual test are shown in Fig. A-9. Statistical analyses of shock front data from numerous tests indicated that instrumentation variability to be expected from a single test is quite low (95 percent of all readings should fall within 10 percent of a mean value). Additional analyses indicated that 95 percent limits on the variation from the mean values of incident shock front pressures from test to test range from about 20 percent for experiments with 3, 4, and 6 strands of Primacord to about 30 percent for 2 and 2-1/2 strand experiments.

* By reproducible, it is meant that statistically (see Ref. 4) the shot-to-shot pressures are reproducible.

Fig. A-9. Sample Data From Four-Strand Open-Tunnel Test

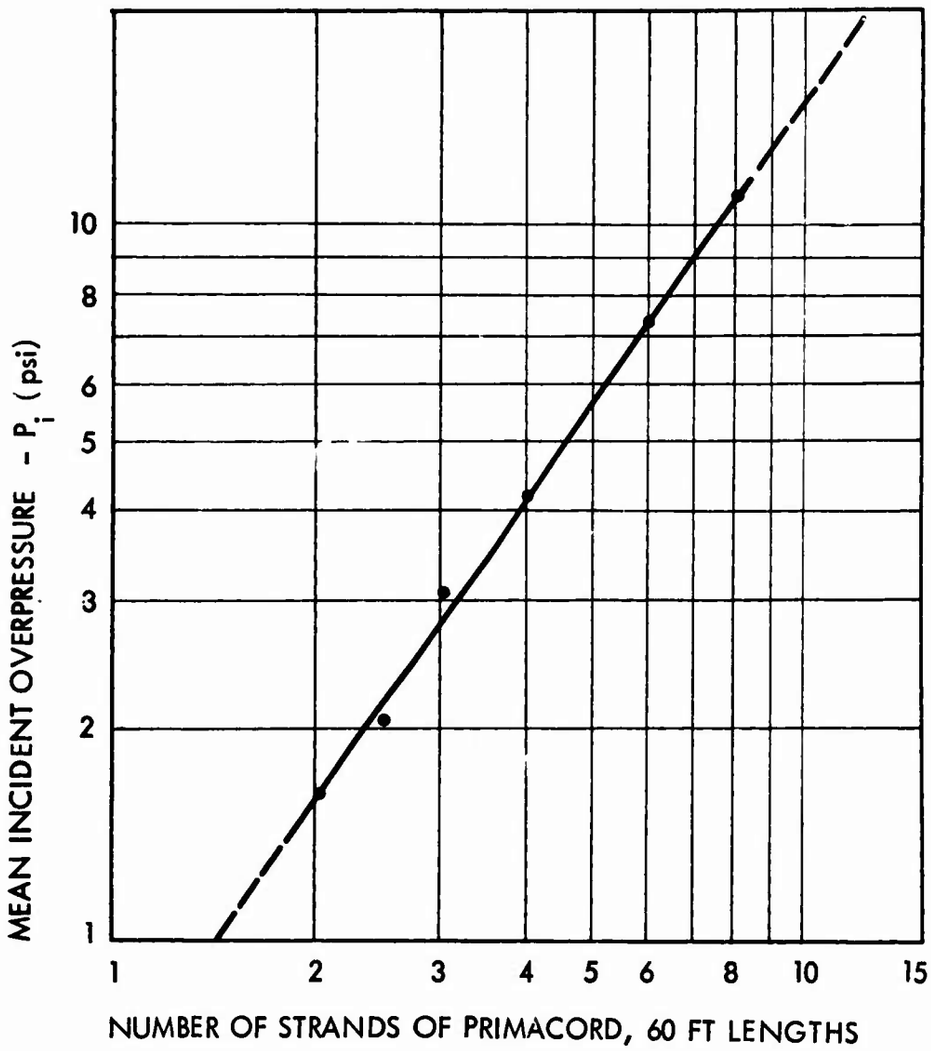

Fig. A-9. Shock-Front Magnitudes of Incident Overpressure Waves as a Function of the Number of Parallel Strands of Primacord Detonated Simultaneously in the Compression Chamber


BLANK PAGE

Appendix B

BRITTLE STRUCTURES — DYNAMIC FAILURE AND STATISTICAL THEORY

This appendix is the culmination of three years of study and observations of the dynamic failure of brittle materials. Not all facets of the work are as yet rigorously proved, but are often inferred from data reported by URS and other researchers. Much work is still required and the development of this failure theory will continue.

The first part of this appendix, development of low-level-fatigue models, was reported in detail in Ref. 2 and expanded here to include a crack-sensitive continuum model. The statistical failure theory was originally presented in Ref. 4 and has been somewhat expanded and tailored for a more complete failure theory.

LOW-LEVEL-FATIGUE MODEL

This portion of the analysis and theory was motivated by the desire to understand the apparent strength increase of brittle materials under dynamic loading. Strength increase values on the order of 25 percent are encountered and recommended in the literature and have been considered to be reasonable for design purposes. It therefore seemed appropriate to develop a more rigorous theoretical basis for pairing a given strength increase with a given dynamic load. Such a theory, combined with the work on the size effects on brittle material behavior, could lead to the development of a more complete failure theory.

Analysis

First, we will set up a few problems in theoretical mechanics whose results will be of value in later development of low-level-fatigue models. It is felt that separating the classical mechanics work from the newer concepts will simplify the model development.

MODEL I

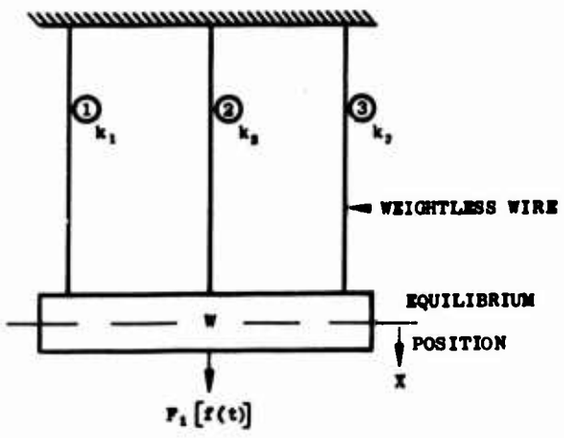

Let

$k_1 = k_2 = k_3 = k$

W = weight

$F_1[f(t)]$ = forcing function

g = gravity

ω = frequency in rad/sec

T = period in sec

and

δ_{st} = W/3k (in.)

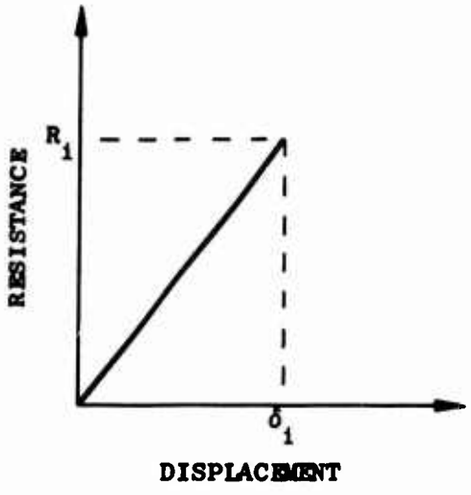

CONSTITUTIVE CHARACTER

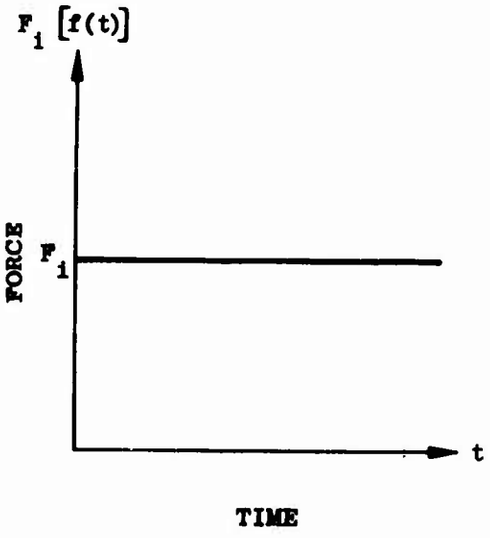

LOAD

One can write

$$\frac{W}{g}\ddot{x} + 3k\,x = F_1$$

which has a solution of the form

$$x = \frac{F_1}{3k}(1 - \cos \omega t)$$

where

$$\omega^2 = \frac{3k\,g}{W} \qquad \text{and} \qquad T = \frac{2\pi}{\omega} \qquad \text{(plotted in Fig. B-1)}$$

MODEL II

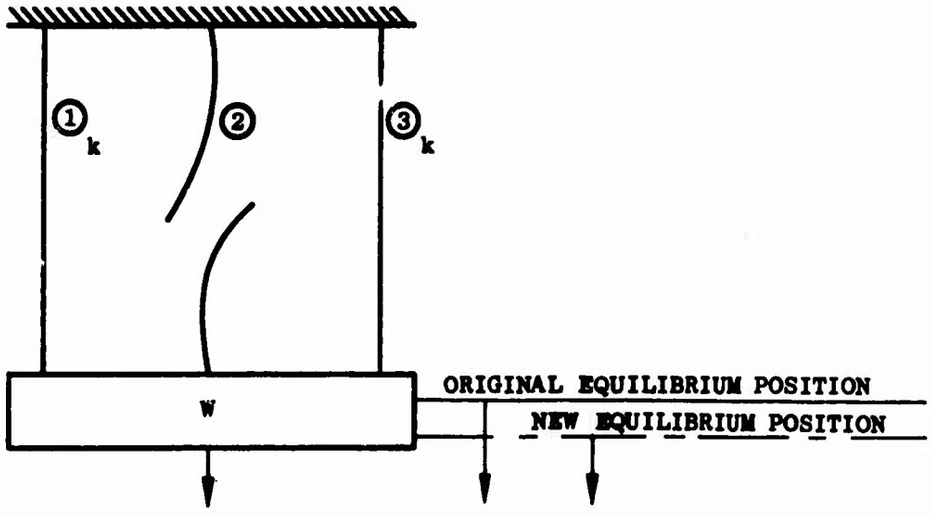

Assume that wire 2 breaks at t = T/2, therefore

$$x - \eta = \frac{W}{6}$$

and

$$\dot{x} = \dot{\eta}$$

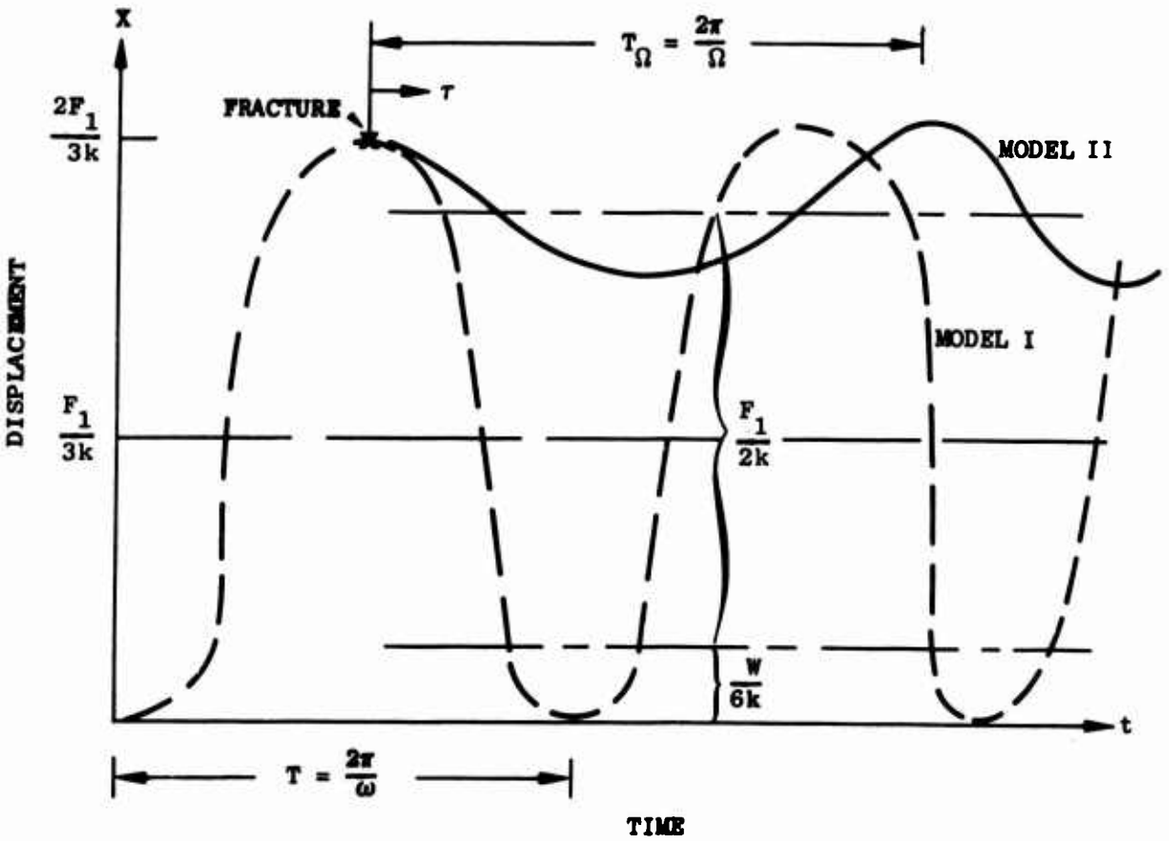

Fig. B-1. Response of Models I and II

then for $\tau \geq t - T/2$, it follows that

$$\frac{W}{g}\ddot{\eta} + 2k = F_1[f(\tau)]$$

with

$$\eta_{(\tau=0)} = \frac{2F_1}{3k} - \frac{W}{6k}$$

and

$$\dot{\eta}_{(\tau=0)} = 0$$

which has a solution of the form

$$\eta = \left(\frac{F_1}{6k} - \frac{W}{6k}\right)\cos\ \Omega\ \tau + \frac{F_1}{2k}$$

or

$$x = \left(\frac{F_1}{2k} + \frac{W}{6k}\right) + \left(\frac{F_1}{6k} - \frac{W}{6k}\right)\cos\ \Omega\ \tau$$

where

$$\Omega = \sqrt{\frac{2kg}{W}} \qquad \text{and} \qquad T_\Omega = \frac{2\pi}{\Omega}$$

and is shown as a dashed line in Fig. B-1.

We observe that the maximum displacement for both Model I and Model II is the same, but the Model II period is greater, i.e., $T_\Omega = \sqrt{3/2}\ T$, and that the equilibrium position has shifted to $x = W/6k$.

Model III

As in Model II, we will assume that the center wire has fractured, but we will assume that it fractured at T/4. Hence, at

$$t = \frac{\pi}{2\omega} \text{ , } x = \frac{F_1}{k} \text{ , and } \dot{x} = \frac{F_1 \omega}{3k}$$

or at $\tau = 0$, where $\tau \geq t = T/4$

$$\dot{\eta} = \frac{F_1 \omega}{3k}$$

and

$$\eta = \frac{F_1}{3k} - \frac{W}{6k}$$

which has an equation of motion of

$$\eta = \frac{F_1}{\sqrt{6}\ k} \sin \Omega \tau - \left(\frac{F_1}{6k} + \frac{W}{6k} \right) \cos \Omega \tau + \frac{F_1}{2k}$$

or

$$x = \frac{F_1}{2k} + \frac{W}{6k} - \frac{\sqrt{7F_1^2 + F_1 W}}{6K} \cos (\Omega \tau - \Theta)$$

where

$$\Omega = \sqrt{\frac{2kg}{W}}$$

and

$$\Theta = \arctan \left[\frac{-\sqrt{6}\ F_1}{F_1 + W} \right]$$

This is plotted in Fig. B-2 in a manner similar to Fig. B-1; that is, it shows Model I response (solid) and Model III response (dotted). In this figure we observe that once again the equilibrium position is shifted and that the period $T_\Omega > T$ as before, but this time the maximum deflection is increased beyond that indicated by Model I and is also greater than Model II.

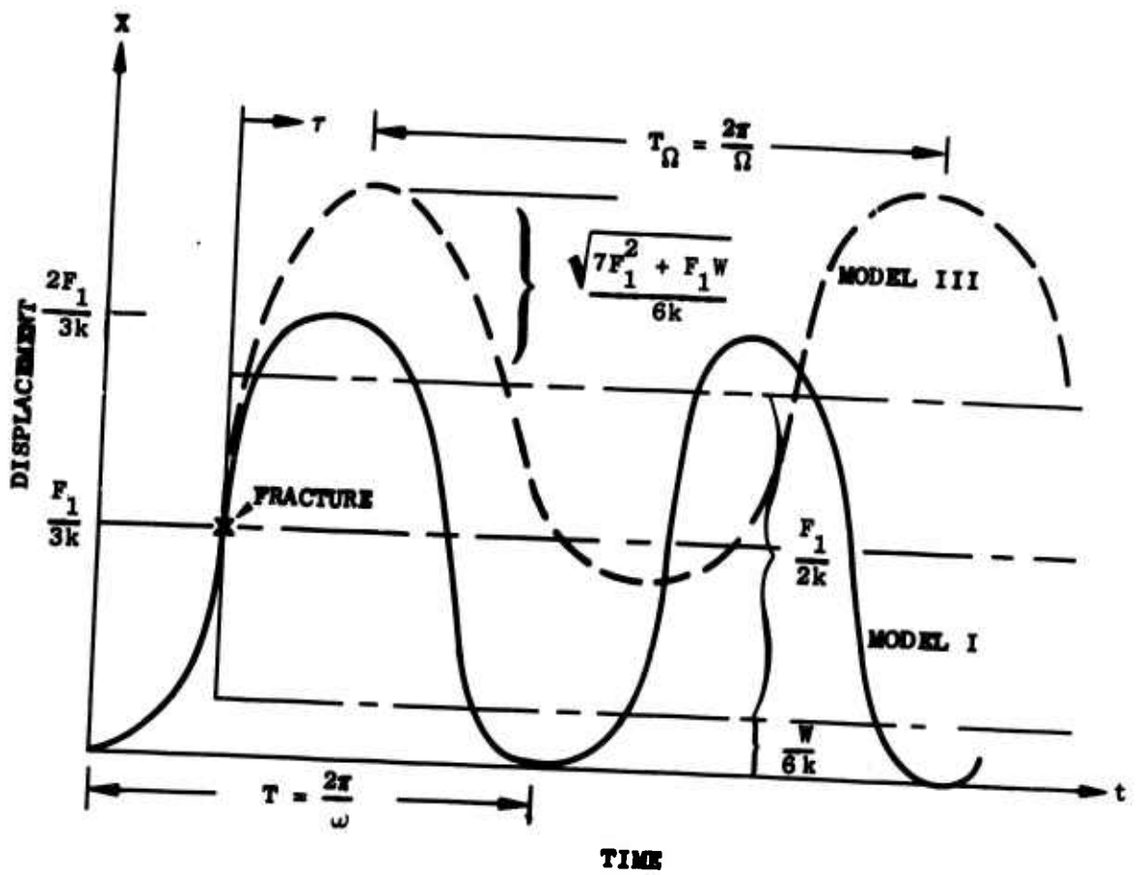

Fig. B-2. Response of Models I and III

With this background we may now proceed with the task of developing a low-level-fatigue model.

Consider the foregoing three-wire system made up of two different wire strength combinations:

Case I Let $R_1 = R_3 = 2R_2 = R$,

then the static resistance function is as shown below.

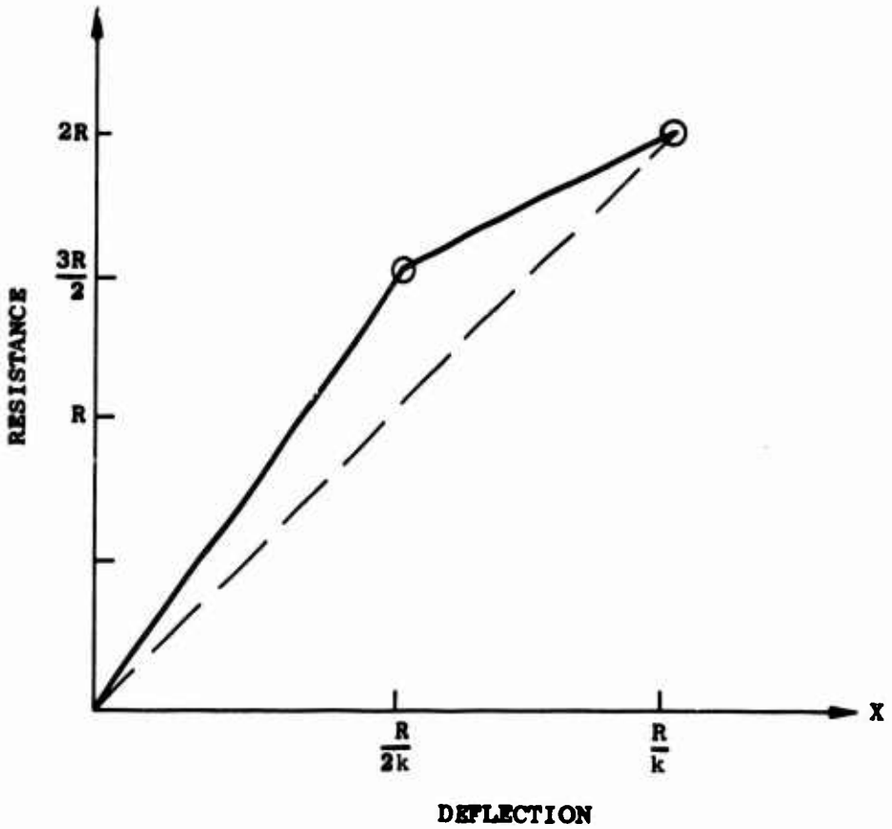

To construct the foregoing resistance function, one first visualizes loading the system very slowly to $F_1 = 3R/2$; that is, each wire has R/2 stress. At this time, the center wire fractures, and we continue loading until $F_1 = 2R$, the remaining wires (1) and (3) fracture, and the system collapses.

Case II Let $R_1 = R_3 = \frac{2}{3} R$ and $R_2 = \frac{R}{2}$

such that

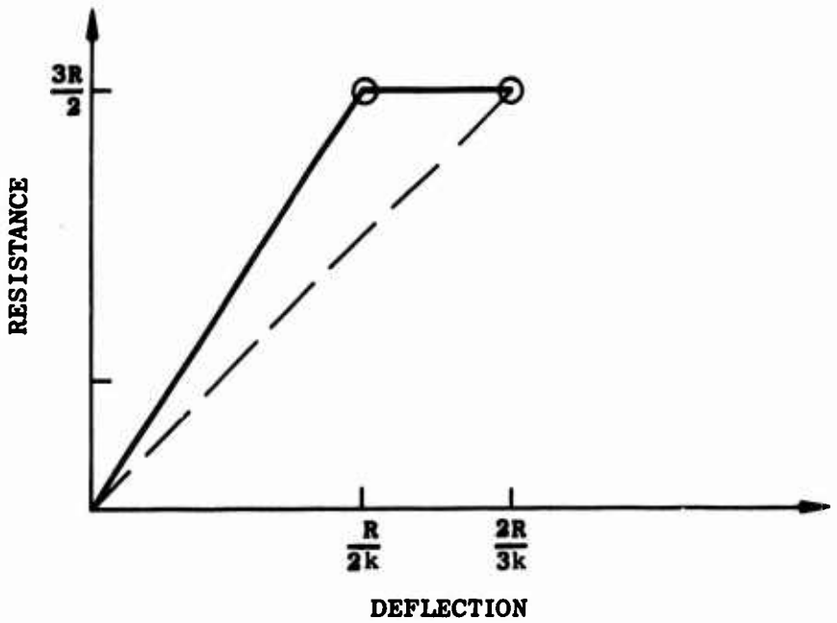

In Case II, we observe that if F_1 (static) = 3R/2, the center wire (2) fractures as before, but there is inadequate reserve resistance, and the displacement continues without an increase in load to complete failure (collapse).

With some mathematical models developed and two structural systems selected, these ideas can now be combined.

Test Case I

Let

$$F_1[f(t)] = \frac{3}{4} R,$$

a step function. Then one can write for $t \geq 0$

$$x = \frac{F}{3K} (1 - \cos \omega t)$$

or

$$x = \frac{R}{4k} (1 - \cos \omega t)$$

where

$$\omega^2 = \frac{3k}{M}$$

which yields a maximum response of

$$x_{max} = \frac{R}{2k} \quad \text{at} \quad \omega t = \pi \quad \text{or} \quad t = \frac{T}{2}$$

From resistance function for this model we observe that the center wire (2) just fractures; hence for $t > T/2$

$$x = \left(\frac{F_1}{2k} + \frac{W}{6k}\right) + \left(\frac{F_1}{6k} - \frac{W}{6k}\right) \cos \Omega \tau$$

where

$$F_1 = \frac{3}{4} R$$

and

$$\Omega^2 = \frac{2k}{M}$$

For simplicity let us assume that the weight $W = R/2$ and the resistance functions are for the reserve above the dead load W.

It then follows that

$$x = \frac{R}{k}\left(\frac{11}{24} + \frac{1}{24} \cos \Omega \tau\right)$$

which is illustrated below.

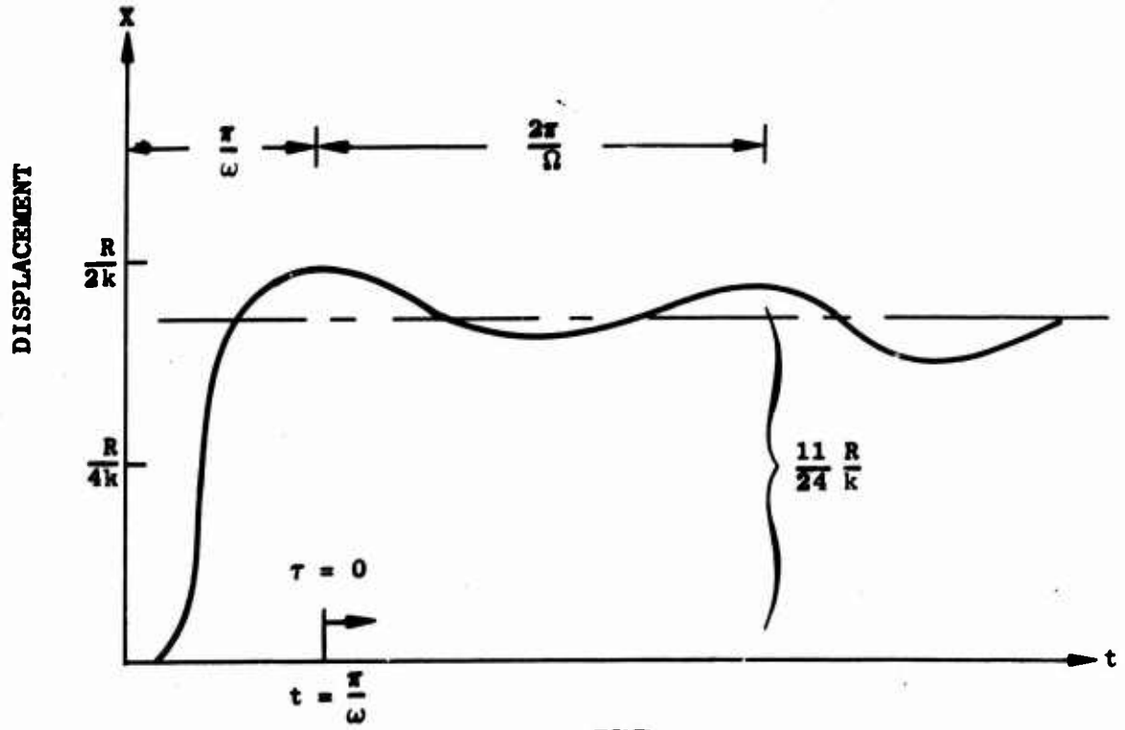

It is interesting to observe that the foregoing response is the same for either material, Case I or Case II. However, the residual structures are quite different; that is, both of them follow the dotted curves on their respective resistance functions, each having a stiffness 2k. However, Case I has a strength of 2R and Case II a strength of 3/2R.

Another observation of interest is that for the Case II structure one would judge from the static case that if a failure starts the entire structure would fail; however, this is not the case at all in the dynamic situation. Hence, we have our first look at a case of low-level-fatigue developing.

To pursue this example a bit further, we could once again apply a force $F_1[f(t)] = 3/4$ R as a step function and not harm the residual Case I structure since it has a residual strength of 2R and a stiffness of 2k; however, a second application of this load would indeed destroy the Case II system. Hence, its fatigue life is two cycles for this loading.

Next, let us look at the case where F_1 = 3/2 R, or (statically) the level that just breaks a wire in Case I and causes failure in Case II. Letting

$$F_1[f(t)] = \frac{3}{2} R \text{ for } t \geq 0$$

$$= 0 \quad \text{for } t < 0$$

we can write

$$x = \frac{R}{2k} (1 - \cos \omega t)$$

which plots as shown below and causes failure at t = T/4 or $\omega t = \pi/2$ of the middle wire.

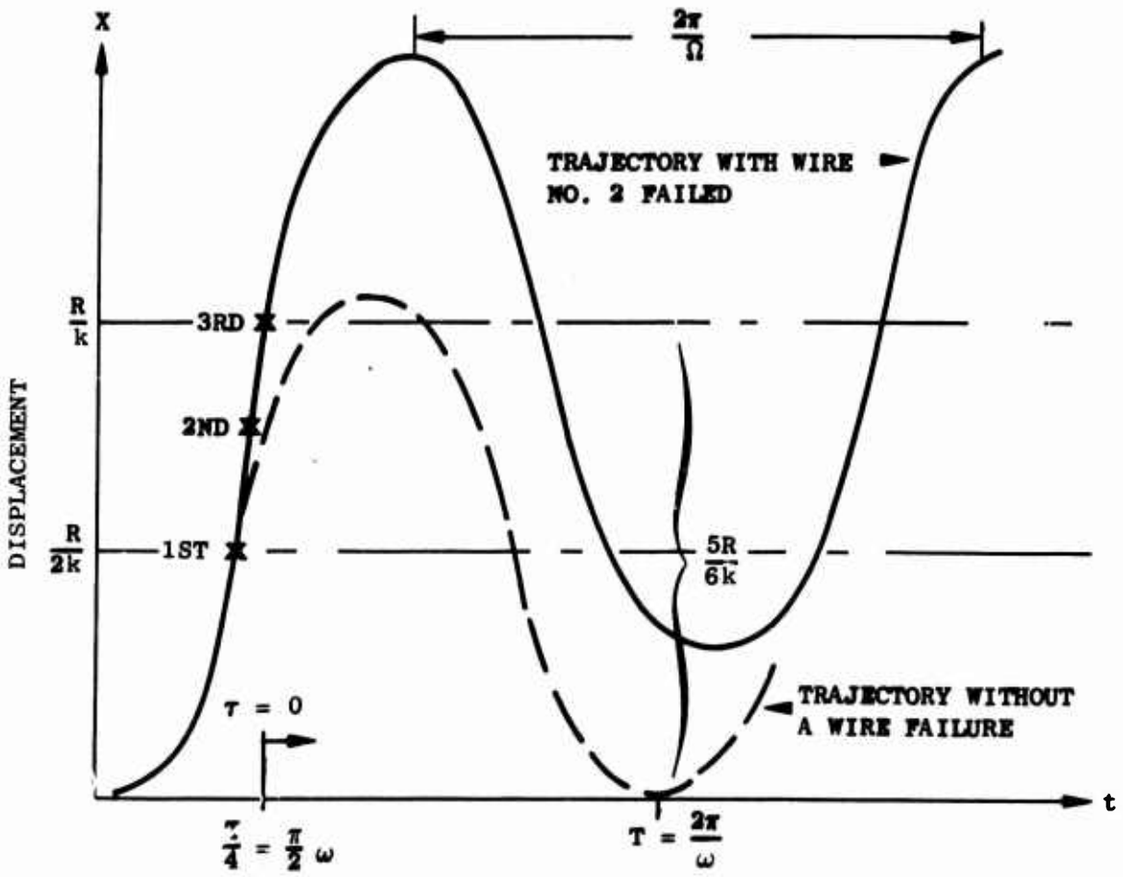

After fracture, one can write

$$x = \frac{F_1}{2k} + \frac{W}{6k} + \frac{\sqrt{7F_1^2 + F_1 W}}{6k} \cos(\Omega \tau - \alpha)$$

and

$$\alpha = \arctan\left[\frac{-\sqrt{6}\, F_1}{F_1 + W}\right]$$

or

$$x = \frac{5R}{6k} - \frac{4.06R}{6k} \cos(\Omega \tau + 61.4 \text{ deg})$$

for $t \geq T/4 = \pi/2 = \omega t$.

From the foregoing example we see that a load of $F_1 = 3/2R$ will indeed fracture the entire system for either Case I or Case II. For Case I, when $x = R/k$, all the wires are fractured and the entire system will fail (point labeled "3rd"). For Case II, when $x = 2R/3k$ (point labeled "2nd"), the entire system will fail.

Discussion

The foregoing models are aimed at developing some insight into low-level fatigue and dynamic response of systems.

Low-level fatigue is of particular interest to structural engineers in the design and construction of brittle structures, especially with regard to dynamic loads like earthquakes or, in our particular case, blast damage. It is easy, from just the two simple problems presented, to visualize a load that would fail the Case II system and not harm the Case I system. From

this one can easily visualize how a building could sustain unobserved damage during one loading (quake and blast) and have different performance characteristics for the next loading event.

These examples also allow us to study load transmission to support structures. Let us consider these examples redesigned to measure reactions.

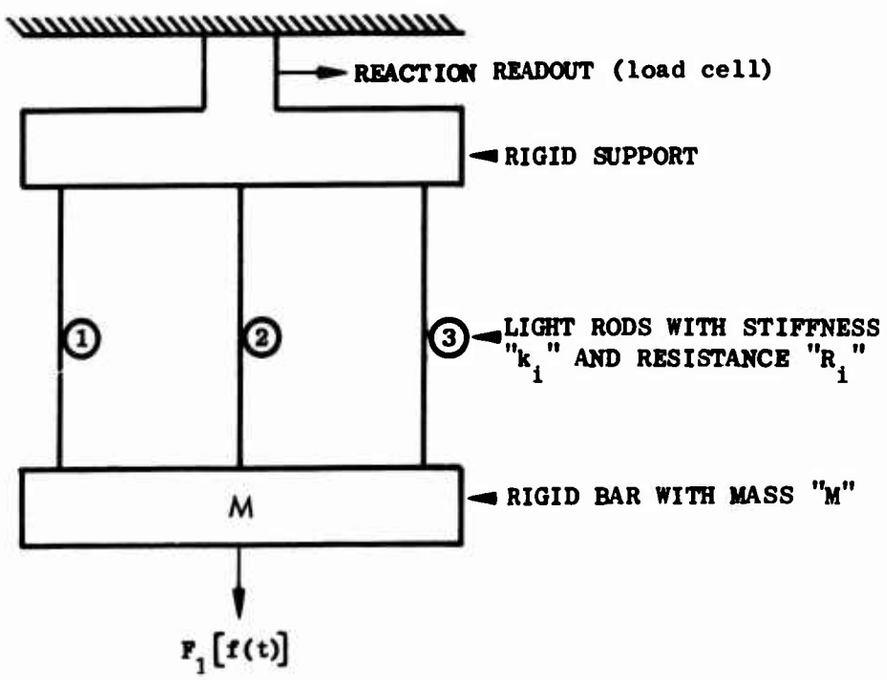

In this problem, if

$$T\omega = \frac{2\pi}{\omega} = 20 \text{ msec}$$

then

$$T_{\Omega} = \frac{2\pi}{\Omega} = 24.5 \text{ msec}$$

The center wire (2) would then fracture in 5 msec for F_1 = 2/3 R, the second example considered. For the Case I, structural system failure takes place at x = R/k, or at t = 7.87 msec, just 2.87 msec later. For the Case II structural system, failure occurs at x = 2/3 (R/k) and occurs just 1.02 msec later, or at 6.02 msec.

The observation of importance here is that the Δt increment between wire failures becomes less and less as the applied force is increased, such that the apparent reaction approaches the summation of strengths as the applied load $F_1[f(t)]$ approaches infinity. Hence one could redraw the load deflection (resistance functions) as follows.

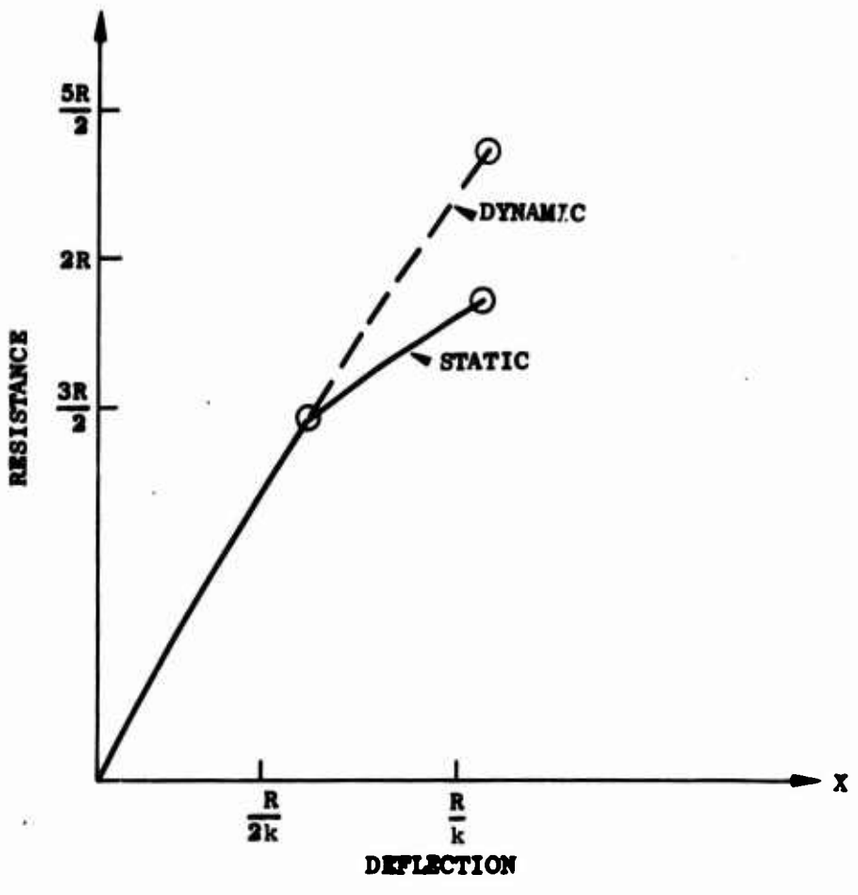

CASE I

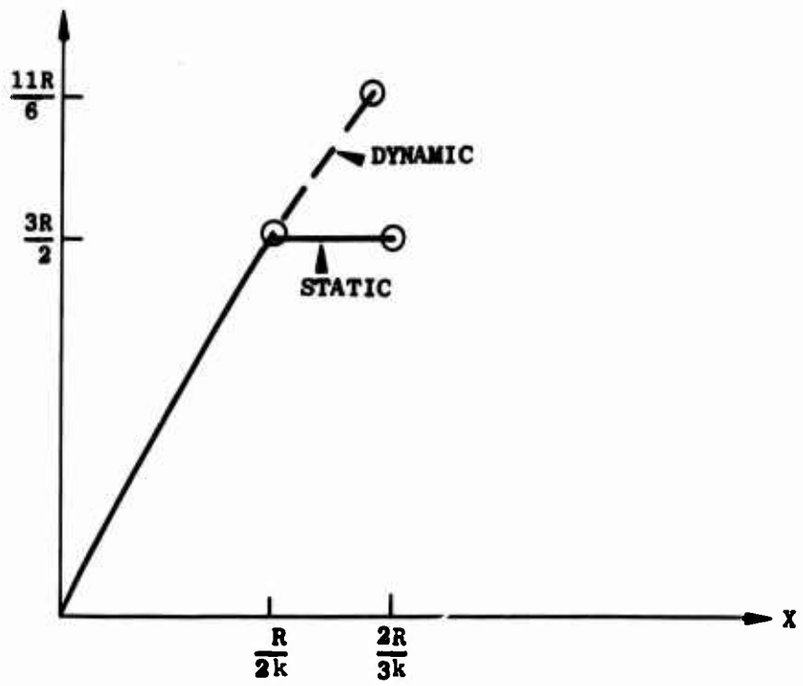

CASE II

Obviously the ultimate dynamic strength is approached asymptotically as the applied load approaches infinity, i.e., all failures occur at the "same" time. Since there is little experimental evidence concerning the effect of overload magnitude, the following exponential form is assumed as a reasonable approximation.

Let

R_s = the static resistance

R_D = tne dynamic resistance (maximum possible)

$\overline{F}$ = the force $F_1[f(t)]$ that just fractures the system (assume a step loading)

α = constant based on test data, assumed 1 for now.

and

$$R_o = R_s + (R_D - R_s)\,[1 - \alpha \exp(-\lambda)]$$

where

$$\lambda = \beta\left(\frac{F_1}{\bar{F}} - 1\right) \text{ for } F_1 \geq \bar{F}$$

where β is a constant, based on test data, assumed 1 for now.

For example, in our Case I system

$$R_s = 2R, \text{ and } R_D = \frac{5}{2} R$$

Let

$$F_1\,[f(t)] = 2\bar{F}$$

then

$$R_o = 2R + \frac{R}{2}\,[1 - \exp\,(-1)]$$

or

$$R_o = 2.21\ R \text{ or } 88.5\%\ R_D.$$

Then for the Case II system,

$$R_s = \frac{3}{2} R,\ R_D = \frac{11}{6} R$$

Let

$$F_1[f(t)] = 2\bar{F}$$

then

$$R_o = \frac{3}{2} R + \frac{R}{3} \left[1 - \exp(-1)\right]$$

or

$$R_o = 1.66R \text{ or } 90.5\% R_D.$$

The next phase of the effort is to extend this methodology to a crack-sensitive continuum.

Crack-Sensitive Continuum Model

Based on the rather thorough and detailed development for the discrete case, it is possible to present a proposed model for the continuum case.

The illustrative model for the continuum follows from the discrete case and is shown below:

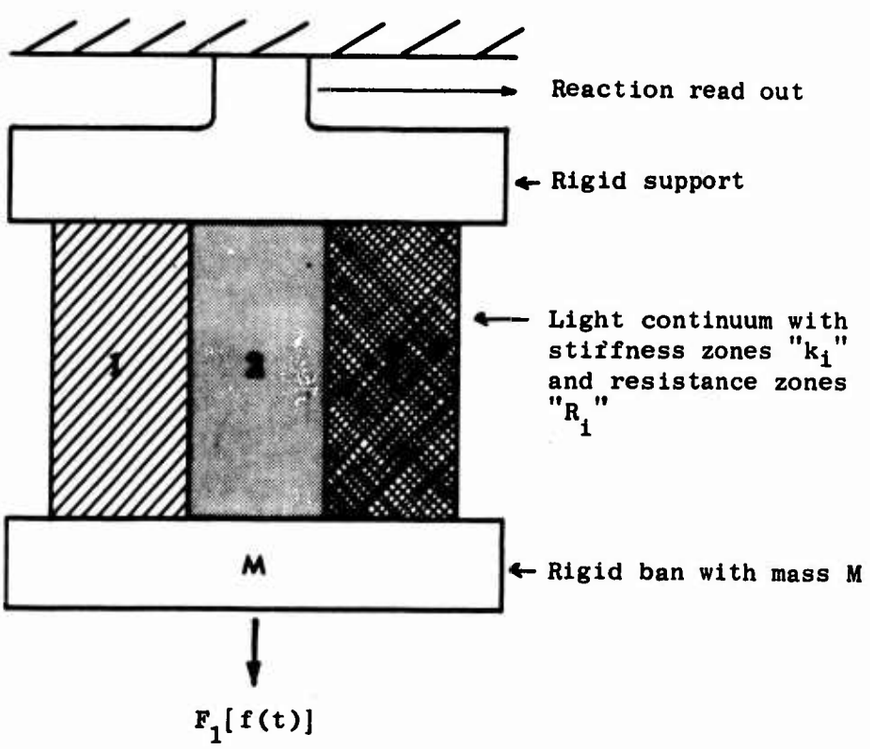

Let us assume a material such that the resistances of Zones 1 and 3 are equal to 2/3R, Zone 2 is R/2 and $k_1 = k_2 = k_3 = k$, such that the static and dynamic strengths appear as in the sketch below (from our discrete work). These characteristics are the same as for the second material considered in the discrete case and similar to classical brittle materials. That is, the static limit is controlled by the "weakest element or zone" and the upper or dynamic bound lies at some higher value. Two problems now remain: first, how does the transition from dynamic to static take place, and secondly, where is this dynamic value? First, we will theorize about the transition zone and we will tackle the upper bound problem, i.e., the dynamic strength.

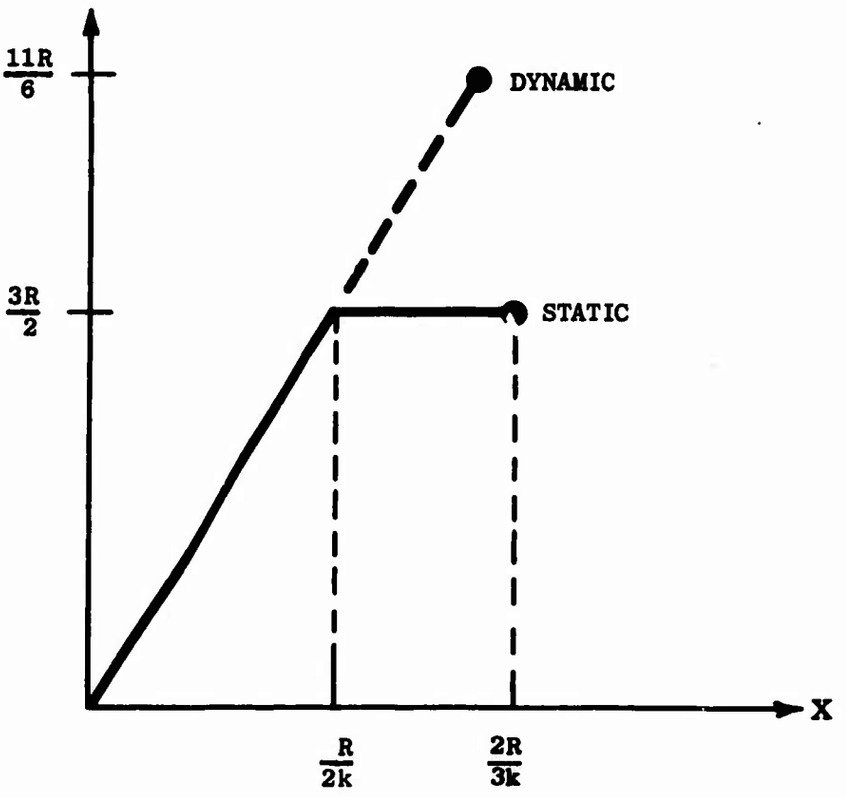

As for the discrete zone case we will assume an exponential form of transition as before:

Let

R_s = static resistance

R_D = dynamic resistance

$\bar{F}$ = the step load F_1 $[f(t)]$ that just fractures the system

and

$$R_o = R_s + (R_D - R_s)[1 - \alpha \exp(-\Lambda)]$$

where $-\Lambda$ will have to include a measure of crack sensitivity.

Further, let us assume a Λ of the form

$$\Lambda = \beta \left(\frac{F_1}{\bar{F}} - 1 \right) \left(\frac{L_c/V_c}{T/2 - t_s} \right) \text{ for } F_1 > \bar{F}$$

$$\Lambda = 0 \text{ for } F_1 \leq \bar{F}$$

(Note: the limit on $F_1 \rightarrow \bar{F}$ is $\equiv 0$)
where

L_c is the length of a crack

V_c is the crack propagation velocity or

$$V_c = \frac{1}{2} \sqrt{E/\rho}$$

E is the modulus of elasticity

ρ is the mass density

t_s is the time to failure if the system fractured at the static strength level

α & β are data-based constants as before and assumed to be unity

Recall from earlier work that the time to any set displacement can be found by

$$\cos \omega t = 1 - X_t \frac{k}{F_1}$$

for a step function load equal to F_1, or, in a more convenient form,

$$t = \frac{1}{\omega} \cos^{-1} \left[1 - X_t \frac{k}{F_1} \right]$$

where $\omega = \sqrt{k/M}$ and X_t is the displacement of interest.

For example, if $F_1 = \bar{F}$ and $X_t = 2\bar{F}/k$ (the peak displacement), we find

$$t_s = \frac{\pi}{\omega} = \frac{T}{2} \text{ and } R_o = R_s$$

Before working an example problem, let us discuss a bit further the term

$$1 - \exp \left[- \left(\frac{F_1}{\bar{F}} - 1 \right) \left(\frac{L_c/V_c}{T/2 - t_s} \right) \right] \text{ for } F_1 > \bar{F}$$

Of course, we assume that $F_1 > \bar{F}$, that is, a crack will start.

We note that the term

$$\frac{L_c/V_c}{T/2 - t_s}$$

is a measure of the time to completely fracture (L_c/V_c) and the time $T/2 - t_s$ available for fracturing. Hence, if $R_s/2 \leq F_1 \leq R_D/2$ and the term

$$\frac{L_c/V_c}{T/2 - t_s} \geq \frac{1}{2}$$

there is a possibility of partial fracture and not complete failure on the first half period of oscillation; however, with the step-like loading, failure will indeed occur on later oscillations and the R_o response computed by the formula is certainly the upper bound value.

Continuing with our example, we see that if $F_1 < (11/12)R$, we may have a partial fracture, i.e., a case of low-level fatigue in a continuum if $(L_c/V_c)/(T/2 - t_s) \geq 1/2$. Note that the 1/2 enters this inequality because the fracturing can continue on both temporal sides of peak displacement, not just one side as in the discrete wire model. Another observation is that $2\left[(L_c/V_c)/(T/2 - t_s)\right]$ is an estimate of the portion of the number fractured.

To complete the example let us assume

$$R_s = \frac{3}{2} R$$

$$R_D = \frac{11}{6} R,$$

$$\frac{L_c/V_c}{T/2 - t_s} = 1$$

and $F_1 = 2\bar{F}$. Then the expected response

$$R_o = 1.66\ R \text{ or } 90.5\%\ R_D$$

as in the earlier discrete model (Case II). Since $2\bar{F} = 3/2R$ is greater than 11/12R, the system would completely fail.

To this point, we have been mainly concerned with the formulation of a mathematical function to describe the transition domain for dynamic response between a static resistance R_s and a dynamic upper bound resistance R_D.

Since crack-sensitive brittle materials are highly size sensitive--that is, the static resistance R_s depends on the size of specimen--we need a method of calculating the static strength. In addition, a method of estimating the upper bound R_D would be desirable. To treat this problem we turn to a statistical failure theory.

STATISTICAL FAILURE THEORY

This effort considers in some detail the problem of material strength variability. Brittle materials, such as brick, inherently have a great deal of scatter in material properties. For example, in the compressive strengths as determined from compression tests, a plus or minus 50 percent scatter is not rare. This random behavior does not preclude the use of these materials or the prediction of their performance, but it does make the problem more complicated. Statistical techniques represent one of the most promising approaches for understanding brittle structural behavior because these methods permit meaningful statements about the expected performance despite the variability, such as the distributions of R_S and R_D.

As a first step in using this approach, the data generated in the static testing of twenty-two brick beams* from six separate batches of beams will be considered.

The experimental data points from this small number of samples plot in a rather well-behaved manner on extreme probability paper (Fig. B-3). This is not surprising since the "extreme" type of performance is typical of brittle materials. Failure is often propagated by flaws, and the distribution of flaws is often considered to be extreme (Refs. 5 and 6). The reason the distribution of the "largest flaws" is of interest is that it determines the distribution of "smallest strengths," i.e., failure which, for the purpose of this section, is defined as the occurrence of the first crack.

The model of the beam to describe this brittle material response will be constructed of eight segments. The analysis of the model will first consider the probability of failure of the beam for the various loading conditions, such as shown in Fig. B-4.

---

* The static test program is described in Appendix B, Ref. 4.

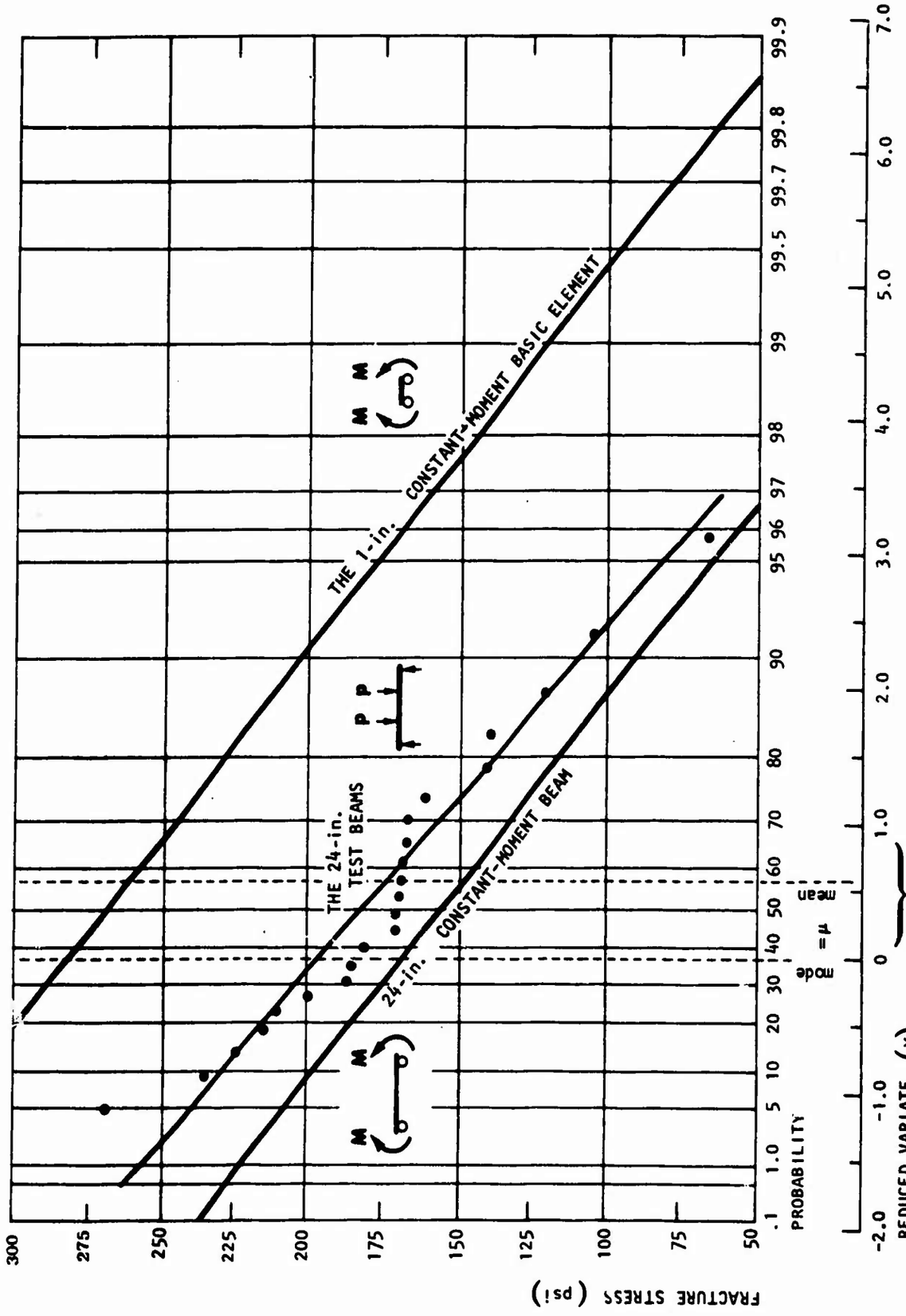

Fig. B-3. Extreme Probability Plots of Flexural Fracture Stress for Various Beams

709-11

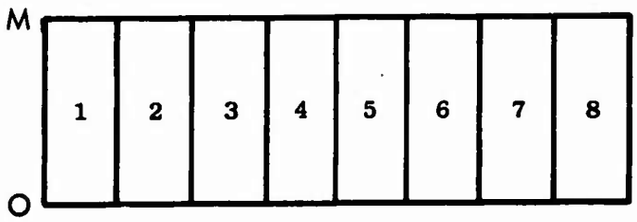

Case 1: UNIFORM MOMENT

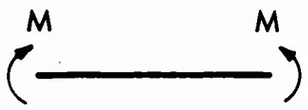

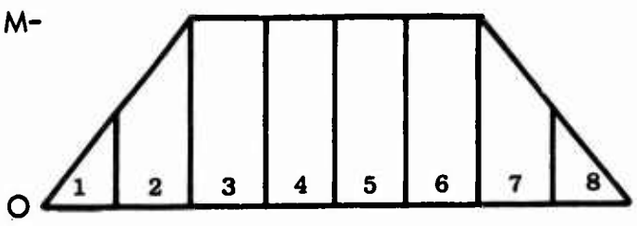

Case 2: 1/4-POINT LOADING

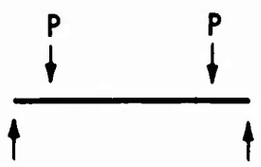

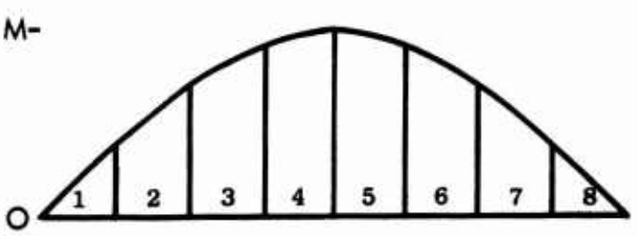

Case 3: UNIFORM LOAD

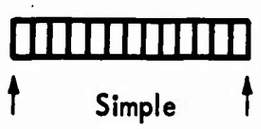

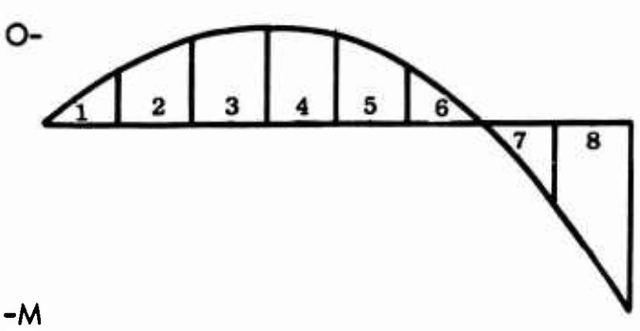

Case 4: UNIFORM LOAD

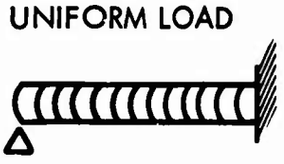

Fig. B-4. Typical Loading Cases and Moment Diagrams

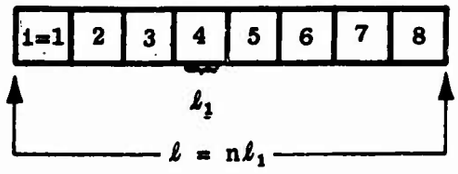

It will be noted that for all cases except Case 1 the different segments of the beam have different stress levels; however, all beams have the same maximum stress. For example, if the maximum stress is 100 psi in Case 2, segments 3, 4, 5, and 6 have a probability of failure of 0.075 (from Fig. B-3) and segment 8 has a probability of failure $P_f = 0.014$ (assuming $\sigma = 25$ psi).

The overall probability of failure of at least one segment of the beam, P_f, can be obtained by considering basic probability theory.

Let P_{si} be the probability of the i^{th} element not failing. Then

$$P_f = 1 - \prod_{i=1}^{n} P_{si}$$

Referring back to Fig. B-3, one can see that the data, limited as they are, conform reasonably well to the extreme value theory (Ref. 5), where the probability of success P_{si} (i.e., not failing) of a test on elemental beam is

$$P_{si} = e^{-e^{+y_i}}$$

where

$$y = \frac{1}{\alpha}(x-\mu)$$

and α is a measure of the dispersion (scatter), μ is the modal value, and x is the x^{th} observation, or stress, on the x^{th} element. For example, in Fig. B-3 it can be seen that $\mu = 195$ psi and $\alpha = 40.85$ psi for the test beams.

The probability of an "n" element beam not failing can now be written as

$$P_s = \prod_{i=1}^{n} P_{si}$$

$$= \prod_{i=1}^{n} e^{-e^{+y_i}}$$

$$= \prod_{i=1}^{n} e^{-e^{+\frac{1}{\alpha}(x_i-\mu)}}$$

and the probability of it failing is

$$P_f = 1 - P_s$$

The foregoing also can be written as

$$P_f = 1 - P_s = 1 - e^{-\left[\sum_{i=1}^{n} e^{\frac{1}{\alpha}(x_i-\mu)}\right]}$$

To put this into a more tractable form for moment diagrams of various shapes, it is convenient to introduce a new reduced variate $\bar{y}$.

Then let it be assumed that P_s for the ensemble of segments is of the form

$$P_s = e^{-e^{+\bar{y}}}$$

where $\bar{y}$ is some as yet undetermined reduced variate. It then follows that

$$e^{-e^{+\bar{y}}} = e^{-\sum_{i=1}^{n} e^{\frac{1}{\alpha}(x_i-\mu)}}$$

or

$$e^{+\bar{y}} = \sum_{i=1}^{n} e^{\frac{1}{\alpha}(x_i-\mu)}$$

and

$$\bar{y} = -\frac{\mu}{\alpha} + \log_e\left(\sum_{i=1}^{n} e^{\frac{1}{\alpha}(x_i)}\right)$$

since μ and α are constant for all elements.

This is the general form of $\bar{y}$ for any moment (stress) system on an "n" element beam.

For convenience one could determine the distribution of a 1-in. (or unit-length) element from the basic 24-in. test specimen. To do this we simply ask what values must μ and α be in a 1-in. element to yield a modal value of 195 psi and an α of 40.85 psi in the test specimen. Mathematically we need the values of μ and α in

$$\bar{y} = \frac{-\mu}{\alpha} + \log_e\left(\sum_{i=1}^{n} e^{\frac{1}{\alpha}x_i}\right)$$

where n = 24 to fit the data plot shown in Fig. B-3.

A more tractable form of the above equation for numerical (computer) computation is

$$\bar{y} = -\frac{\mu}{\alpha} + \log_e\left(\sum_{i=1}^{n} e^{\frac{\sigma_1}{\alpha} f_i}\right)$$

where

σ_1 is the maximum flexural stress in the beam and

f_i is in percentages of the maximum flexural stress.

This yields, for example, in the 24-in. test specimen

$\mu = 282$, and

$\alpha = 36$ for the 1-in. beam segment.

Using the distribution of the "unit length," one can make an integral approximation which may be more convenient for other moment (stress) shapes. It follows that

$$\bar{y} = -\frac{\mu}{\alpha} + \log_e\left(\sum_{i=1}^{n} e^{x_i/\alpha}\right)$$

can be written

$$\bar{y} \approx -\frac{\mu}{\alpha} + \log_e \int_0^{\ell} e^{x_i(\ell)/\alpha}\, d\ell$$

Recall that $x_i(\ell)$ is the stress in the outer fiber of the i^{th} element and only the absolute value of x_i is of interest. If

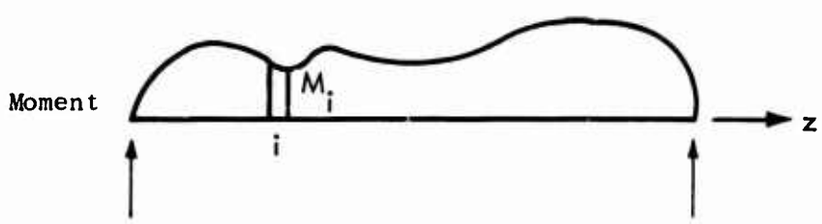

then it follows that

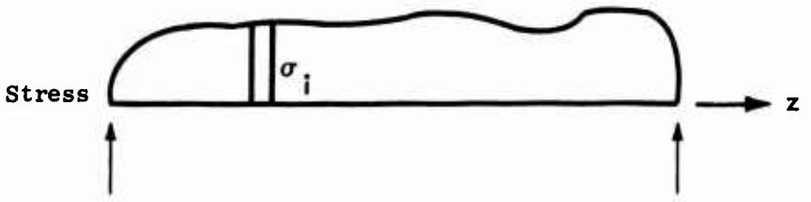

where

$$x_i = |\sigma_1 \ f(z)|$$

$$\bar{y} = -\frac{\mu}{\alpha} + \log \int_0^{\ell} e^{\left|\frac{\sigma_1}{\alpha} f(z)\right|} dz$$

This function is plotted in Fig. B-5 for a number of different cases.

Several observations can be made from this simple exercise; for example, from conventional mechanics the same strength would be predicted for all beams since the maximum fiber stress is the same. However, using the statistical element approach, it can be seen that only <u>one</u> element of the pin-fixed beam is at maximum stress while <u>all</u> elements of the constant-moment beam are at maximum stress, which increases the probability of failure at any particular stress level. In fact, the modal (most frequent) strength for a constant-moment is 168 psi, while for the uniformly varying moment it is 270 psi. Similarly, the statistical means are 147 psi vs 235 psi. The pin-fixed case can thus be considered statistically to be about 1.6 times as strong as the constant-moment case.

Another important observation is that the distribution is no longer the same. That is, no longer is a straight line obtained on the extreme probability paper. From this it can be deduced that a moderately different probability distribution of failures will result from different loadings (moment) of the beam. That is, if a beam is loaded uniformly to a maximum fiber stress of σ_1,

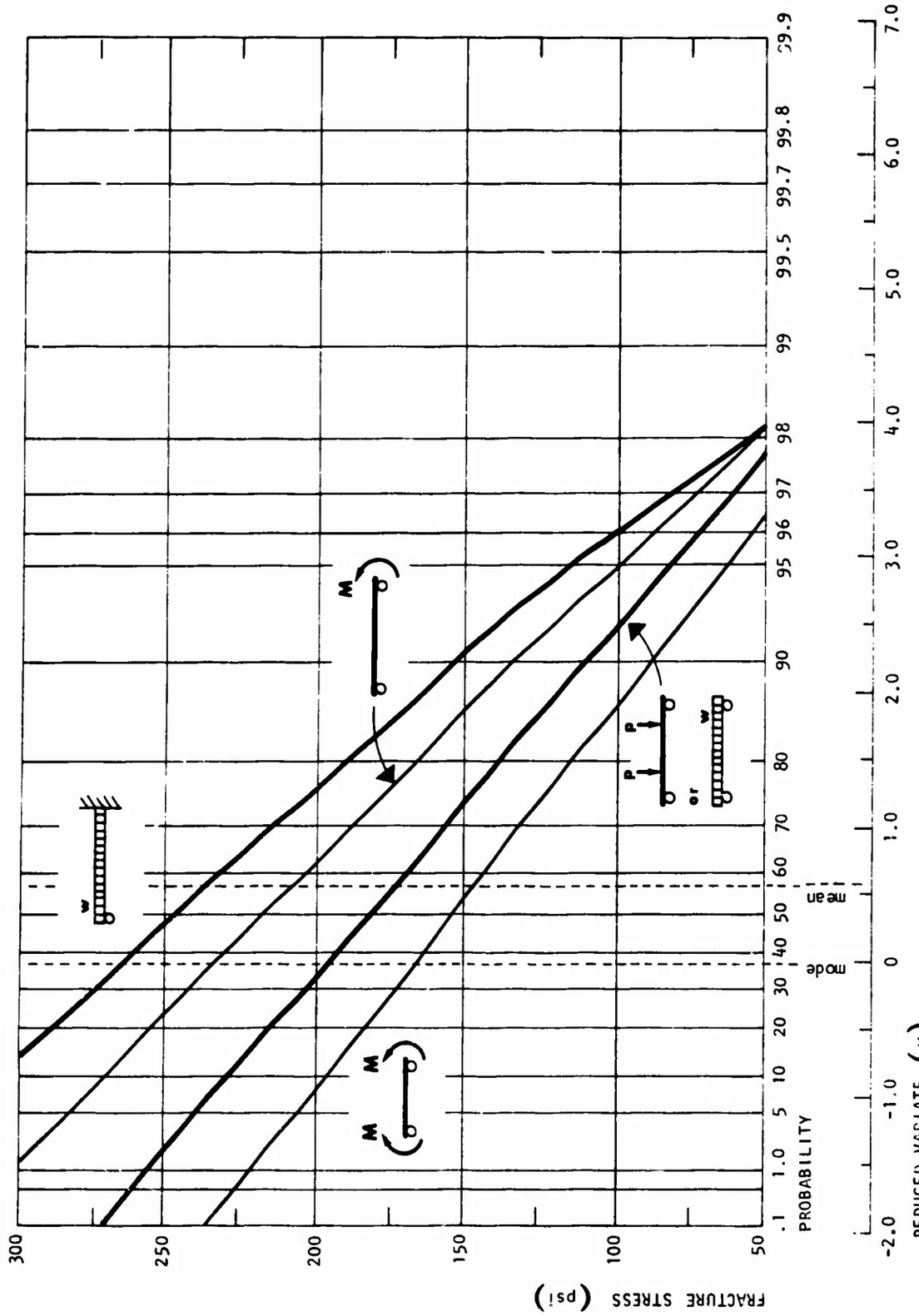

Fig. B-5. Extreme Probability Plot of Fracture for 24-in. Beams with Various Loadings

or with a concentrated load to a maximum stress of σ_1, different probabilities of failure exist and different statistical laws govern.

Having developed a basic statistical theory of failure for brittle (brick) beams, it is now possible to extend this work to wide beams. The theory of failure, as presented in the preceding work, is based on flaws (the distribution of largest flaw), after Weibull (Ref. 6). This approach contends that once a "basic element" fails, the structure has failed. Hence, the work was not limited to beams of any specific length, but confined to the basic width b_j (approximately 8 in.) to eliminate the need for modifying the theory. In other words, by using the width of the test beams as the "basic element" width, the failure of an element did indeed induce failure. The question at hand is: Can we extend this thinking to wider beams, plates, etc?

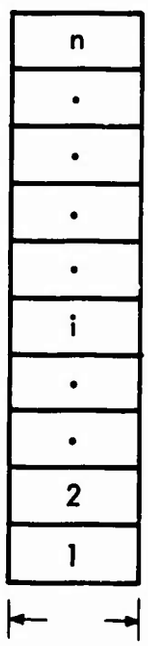

The theory states that for an n-element beam of width b_j, the probability of failure can be stated as follows (also see p. B-28).

$$P_f = 1 - \prod_{i=1}^{n} P_{si}$$

or

$$P_s = \prod_{i=1}^{n} P_{si}$$

where P_{si} is the probability of the i^{th} element not failing at its particular stress level.

Following this course of logic, and desiring to consider a beam of m elements in width, we may write

$$P_f = 1 - \left[\prod_{i=1}^{n} P_{si}\right]^m$$

This approach shifts the distribution of failure stress to lower and lower values as m and n increase in size, but maintains the same variance or scatter; see probability distributions below.

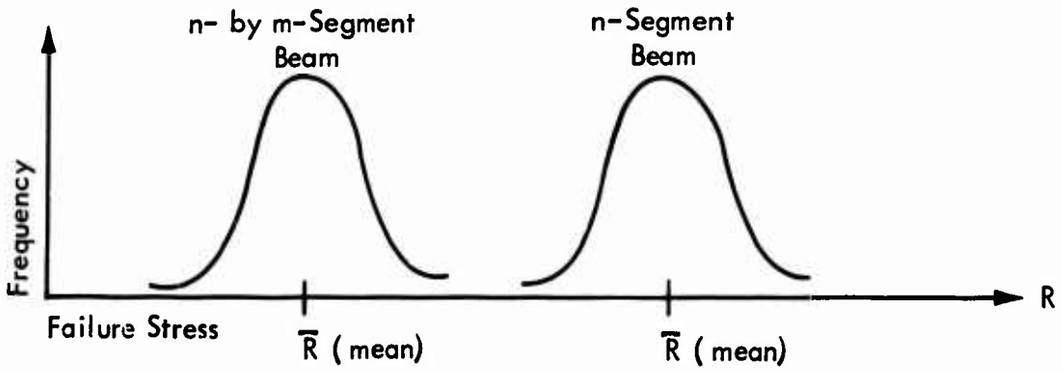

For example, if we look at Fig. B-3, we see that the modal failure stress for a "basic 1-in. element"* is μ = 282 and α = 36. For the n = 24 beam (about 8-1/4 by 8-1/4 by 24 in.), under constant stress we find μ = 168 and α = 36. Based on the "flaw theory" formulation, one would obtain the same answer for a beam of n = 1 and m = 24, or a beam 8-1/4 in. deep by 198 in. wide and 1 in. long, or for n = 8 and m = 3, which is 8-1/4 in. by 24-3/4 in. by 8 in. long.

Let us assume that the m beams are entirely independent; i.e., they are constructed separately and greased on adjoining surfaces.

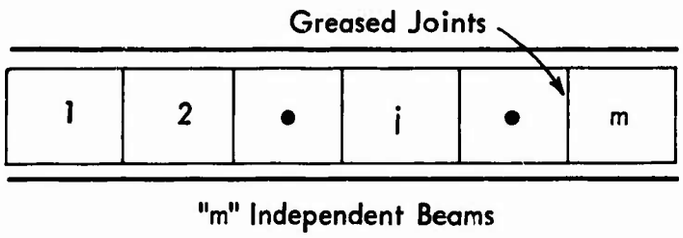

* The basic element is approximately 8-1/4 by 8-1/4 by 1 in.

Now we define failure as the failure of all of the m beams. This is a parallel* system where the expected strength is the summation of the expected strengths, i.e., the summation of random variables.

If R_j is the strength of the j^{th} element, $E[\cdot]$ the expectation, and $Var[\cdot]$ the variance, then

$$E[R] = \sum_{j=1}^{m} E\left[R_j\right]$$

and

$$Var[R] = \sum_{j=1}^{m} Var\left[R_j\right]$$

and, for our special case where R_j is an identically distributed random variable

$$E[R] = m\, E\left[R_j\right]$$

$$Var[R] = m\, Var\left[R_j\right]$$

This parallel-system approach maintains the same central value and increases the variance.

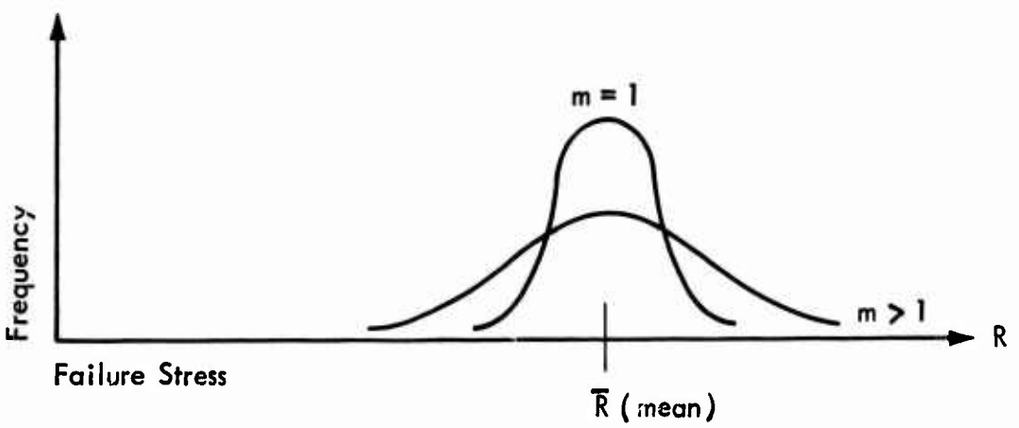

* This theory was expounded by John Tucker, Jr., in Ref. 7.

From the earlier work on low-level fatigue, one would expect that the response of a brittle structure to a dynamic load would lie somewhere between the Flaw Theory and the Parallel Theory. Hence, we must now formulate a theory or procedure to establish the failure strength if it is between the two established theories.

Let

$$\left[p = P \text{ Complete Failure} \mid \text{The } i^{th} \text{ element has failed}\right]$$

and

$$q = 1 - p$$

Then, if p = 1, the Flaw Theory prevails; if p = 0, the Parallel System theory prevails. Between these domains must lie the "truth," i.e., the distribution p lies toward the Flaw Theory line from the Parallel System line (see Fig. B-6).

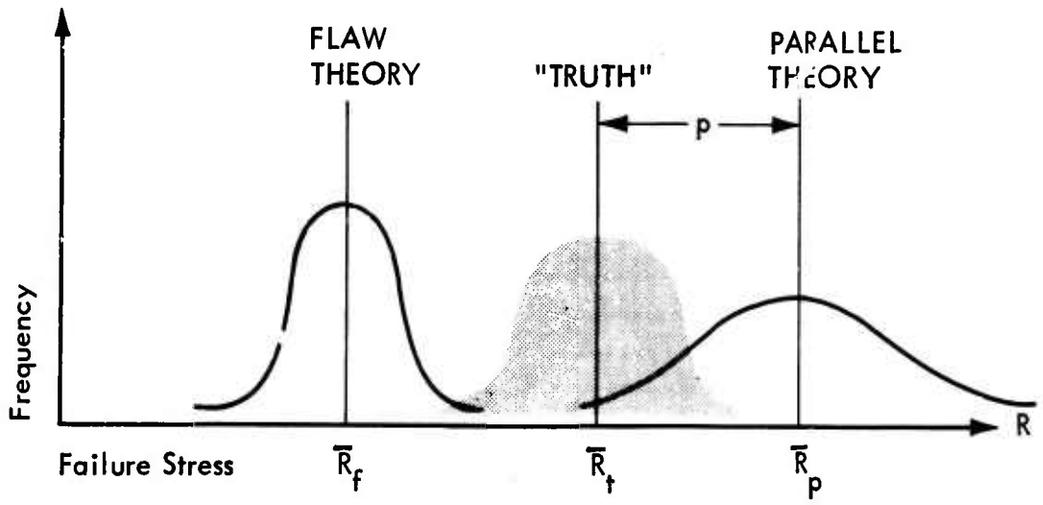

Fig. B-6. "Flaw Theory" and "Parallel Theory" for Wide Beams

At this point, of course, it would be ideal to have (1) a series of statically tested wide beams to verify the static theory and give us a measure of the crack propagation to failure and flaw theory, and (2) some dynamic small beam tests to check the dynamic results and theory.

GENERAL BRITTLE FAILURE THEORY

In this section, the low-level-fatigue ideas of the first section are combined with the statistical ideas of the third section to create a reasonably complete failure theory.

From the continuum section, the proposed observed resistance was of the form

$$R_o = R_s + (R_D - R_s)\left[1 - \alpha \exp(-\Lambda)\right]$$

where

R_o is the observed resistance

R_s is the static resistance

R_D is the dynamic resistance (maximum)

$$\Lambda = \beta\left(\frac{F_1}{\bar{F}} - 1\right)\left(\frac{L_c/V_c}{T/2 - t_s}\right) \text{ for } F_1 > \bar{F}$$

$$\Lambda = 0 \text{ for } F_1 \leq \bar{F}$$

and α and β are constants chosen as 1 for the discussion, modifiable by actual test data.

The equation can be rewritten into a more convenient form as

$$R_o = R_s e^{-\Lambda} + R_D (1 - e^{-\Lambda});$$

then recall that

$$0 \leq e^{-\Lambda} \leq 1.$$

Hence, let

$$p = e^{-\Lambda}$$

and

$$q = 1 - p$$

$$= 1 - e^{-\Lambda}$$

where p is the probability that Flaw Theory dominates and q is the probability that the Parallel System dominates the failure.

Therefore,

$$R_o = pR_s + qR_D$$

If one now assumes that R_s and R_D are random variables (an obvious "truth"), we may write:

$$E\left[R_o\right] = p\ E\left[R_s\right] + q\ E\left[R_D\right]$$

and

$$\text{Var}\left[R_o\right] = p^2\ \text{Var}\left[R_s\right] + q^2\ \text{Var}\left[R_D\right] + 2pq\ \text{Cov}\left[R_s, R_D\right]$$

where

$$\text{Cov}\left[R_s, R_D\right] = \rho \left\{\text{Var}\left[R_s\right]\ \text{Var}\left[R_D\right]\right\}^{1/2}$$

and the correlation coefficient ρ is

$$-1 \leq \rho \leq 1,$$

and in our work it is suspected that $\rho = 1.0$ since R_s and R_D are for the same element. If, indeed, $\rho = 1$ we may then write

$$\text{Var}\left[R_o\right] = \left[p\ \text{Var}\left[R_s\right]^{1/2} + q\ \text{Var}\left[R_D\right]^{1/2}\right]^2$$

or

$$\text{Std. Dev.}\left[R_o\right] = p\ \text{Std. Dev.}\left[R_s\right] + q\ \text{Std. Dev.}\left[R_D\right]$$

$$S_{R_o} = p\ S_{R_s} + q\ S_{R_D}$$

To illustrate the use of the formulas and the theory, let us consider the test panels used in the experimental portion of the program. In this section we will develop the predicted behavior; a more complete data-theory correlation will be presented later.

From Ref. 4 (Appendices A and B), one finds that for an 8-in. by 24-in. test beam

$$\bar{x} = 175$$

$$\alpha = 36$$

for the constant moment case. Note that the data from which the above figures are derived consisted of data from six test series; hence, one might assume that the variance for a single series is one-sixth (1/6) or

$$\bar{x} = 175 \text{ psi}$$

$$\alpha = 15 \text{ psi}$$

which is also in line with the variability indicated by the Bureau of Standards in their tests series (Ref. 8).

If we were to consider our basic element 1 in. wide by 8 in. thick by 24 in. long, we would obtain a strength distribution defined by

$$\mu = 241 \text{ psi}$$

$$\alpha = 16.3$$

which may be a reasonable approximation to the upper bound dynamic strength for a test beam of 8 by 8 by 24 in. or the static strength of 1 by 8 by 24 in. test beam if constructable.

Assuming that the 1-by 8-by 24-in. beam is the basic element, we could build the static and dynamic probability distributions for the 8-ft by 12-ft URS test beam wall.

The static strength "R_s" is derived from the theory of flaws as the summation of n times m basic elements when n = 4 and m = 144, or

$$\mu = 128 \text{ psi}$$

$$\alpha = 16.3$$

which is plotted in Fig. B-7. The results are not unreasonable when compared to other large specimen test data, such as the P.C.A. and N.B.S. Further, the typical failure strength of 50 psi given in many building codes (such as UBC), which provides an allowable of 20 to 25 psi for design, certainly seems reasonable for this work.

To establish the dynamic upper-bound based on the foregoing assumptions of the 1 by 8 by 24 in. basic element, with

$$\mu = 241$$

and

$$\alpha = 16.3$$

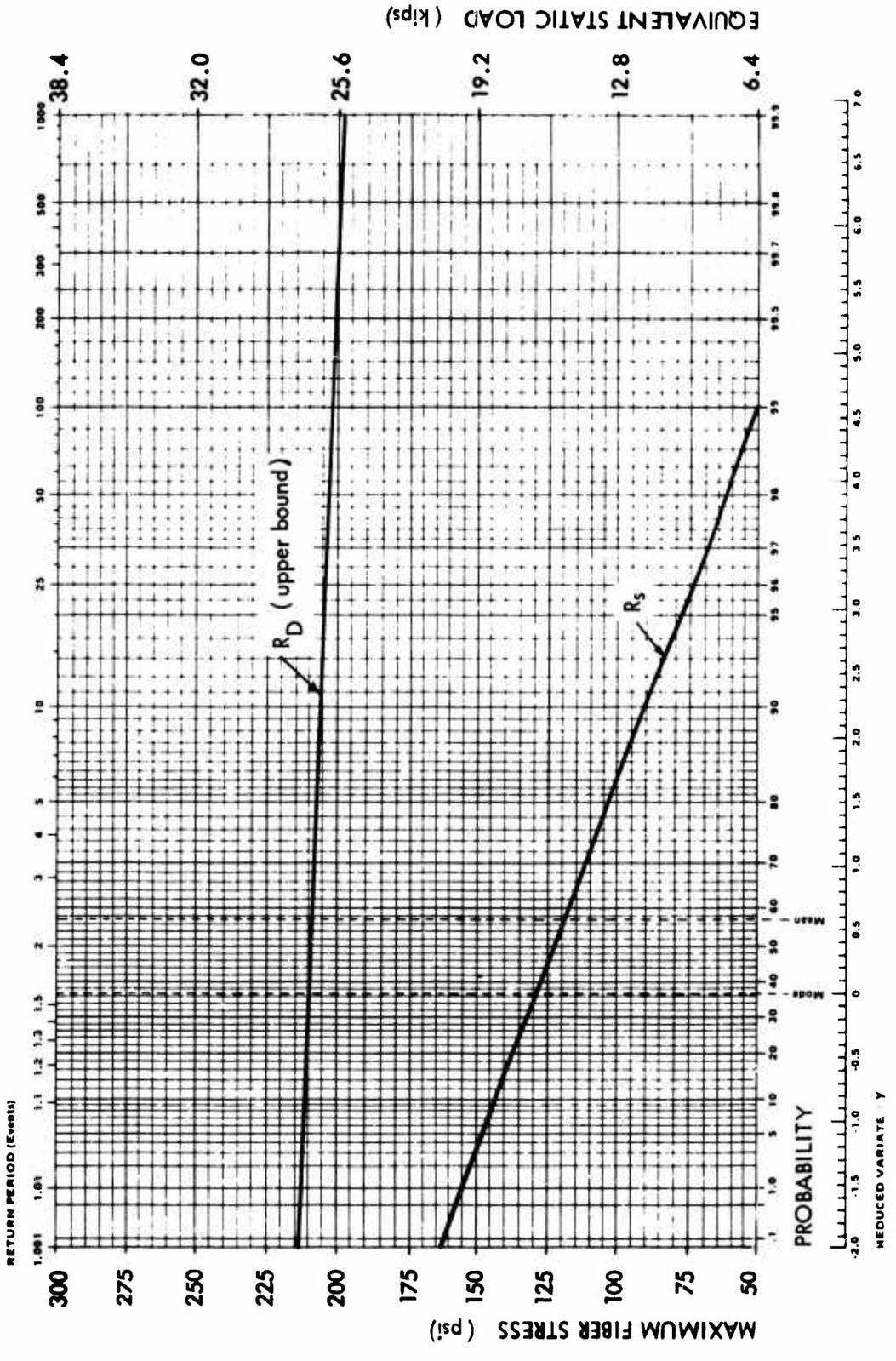

Fig. B-7. Plot of R_S and R_D of Flaw Theory

we next construct the basic beam of the wall on a 1-by 8-by 96-in. beam which has the following properties:

$$\mu = 218 \text{ psi}$$

$$\alpha = 16.3 \text{ psi}$$

$$\bar{x} = 209 \text{ psi}$$

The wall is made up of m (m = 144) parallel, identically distributed beams. The dynamic theory of failure proposes that the upper-bound resistance of the wall is the summation of m independent beam resistances R_i:

$$R_D = \sum_{i=1}^{m} R_i$$

such that

$$E\left[R_D\right] = m\, E\left[R_i\right]$$

and

$$\text{Var}\left[R_D\right] = m\, \text{Var}\left[R_i\right]$$

If the resistance R_i is interpreted as the total load a basic beam element can support, we can write

$$R_i = p\ell$$

where p is the applied load in psi and ℓ is the length in inches (we have used a 1-in. width of beam).

It follows, from basic mechanics, that

$$\sigma = \frac{p\ell^2}{8} \cdot \frac{C}{I}$$

or

$$p = k\sigma$$

where

$$k = \frac{8I}{C\ell^2}$$

Since σ is a random variable, the strength of the beam element in flexure tests, we may write

$$E[p] = k\ E[\sigma]$$

and

$$Var[p] = k^2\ Var[\sigma]$$

It follows that one may now write the resistance of the beam in terms of the stress in the form

$$E\left[R_i\right] = k\ell\ E\left[\sigma\right]$$

and

$$Var\left[R_i\right] = k^2\ell^2\ Var\left[\sigma\right]$$

which means the dynamic resistance of the entire wall is of the form

$$E[R] = mk\ell\ E[\sigma]$$

and

$$Var[R] = mk^2\ell^2\ Var[\sigma]$$

The resistance of the wall, of course, can be expressed in terms of the apparent dynamic fiber stress because

$$\sigma_D = \frac{R_D}{K}$$

where

$$K = mk\ell,$$

which reduces the dynamic stress random variable to the following:

$$E\left[\sigma_D\right] = E\left[\sigma\right]$$

and

$$Var\left[\sigma_D\right] = \frac{1}{m} Var\left[\sigma\right]$$

For our particular example, the basic beam element stress distribution is given by

$$E[\sigma] = 209 \text{ psi}$$

$$\mu = 218 \text{ psi}$$

$$\alpha = 16.3 \text{ psi}$$

Hence, we may approximate the dynamic stress distribution by

$$E\left[\sigma_D\right] = 209 \text{ psi}$$

and

$$\alpha_D = \frac{16.3}{\sqrt{m}} = 1.36 \text{ psi for } m = 144.$$

This distribution is plotted on the graph of Fig. B-7 as R_D upper bound in terms of stress and equivalent applied static load.

Proceeding with the example for illustrative purposes, we have

$$E\left[R_o\right] = p\ E\left[R_s\right] + q\ E\left[R_D\right]$$

and

$$S_{R_o} = p\ S_{R_s} + q\ S_{R_D}$$

where

$$E\left[R_s\right] = 118 \text{ psi}$$

$$E\left[R_D\right] = 209 \text{ psi}$$

$$S_{R_s} = 16.3 \text{ psi}$$

$$S_{R_D} = 1.36 \text{ psi}$$

and

$$p = e^{-\Lambda} \text{ and } 1 - p = q$$

since

$$\Lambda = \left(\frac{F_1}{\bar{F}} - 1\right)\left(\frac{L_c/V_c}{T/2 - t_s}\right)$$

where, as before, F_1 is the applied load and $\bar{F}$ is an applied load just sufficient to cause fracture;

$$L_c = 12 \text{ ft}$$

$$V_c = 1/2\sqrt{\frac{E}{\rho_c}}$$

where $E = 1 \times 10^6$ psi

and ρ_c = 0.0208 lbs $sec^2/in.^2 ft^2$

and T = 34 msec from computer analyses (see Section 4) and experimental results.

Table B-1 is illustrated in Fig. B-8; both show the mean value $\left(E\left[R_o\right]\right)$ plus the 95 percent upper and lower bounds. The curve may be interpreted as follows: if a structure were loaded with a load four times as great as that required to just break the wall $(\bar{F})$, the structure would respond as if it had material properties $\bar{x}$ = 172 psi and S_x = 7.1 psi, which is 1.47 times as strong as the static case, a significant increase. The upper and lower bound curves are plotted assuming that probability distribution remains extremal in form. Hence, the upper bound is established using the distribution of maximum extremes and the lower bound using the minimum distribution of the extremes.

The implications of the foregoing work are rather interesting and far-reaching. Perhaps one of the most interesting and intuitively pleasing is that there is, indeed, an upper bound dynamic resistance for a particular structure. Further, an upper bound strength distribution is reached, which is more meaningful. Another item that is interesting, but disturbing, is the reduction of variability as the dynamic load is reached. One must recall that the plot is of the apparent stress at dynamic failure, and in the derivation the variance of the total load was n times as large as that of a single element. Another thing one must keep in mind is the fact that if we have a large enough number of parallel elements and the failure resistance is the summation of all m resistances, the total resistance will be identically the average for large m.

From the foregoing we can conclude that for flaw sensitive brittle materials subjected to dynamic loads:

1. The smaller the variability under static conditions, the smaller the gap between static and dynamic behavior.
2. The greater the number of possible parallel elements in a system the greater the gap between static and dynamic strength.

3. A large specimen of a flaw sensitive material is going to present the experimenter with a much greater difference in load between static and dynamic cases than smaller specimens. In fact, if a flaw sensitive material is sufficiently homogeneous to make very small specimens, there should be a size where the static and dynamic resistances are identical.

4. On the practical side, the understanding of this phenomenon (if the theory proves correct) will allow the experimenter to infer his upper bound for a particular experiment and plan accordingly.